Year : 2020

Novel antibody-based therapeutic approaches for redirecting T cell effector functions towards tumors expressing CD248 (TEM1)

Fierle Julie Katrin

UNIL | Université de Lausanne

Faculté de biologie
et de médecine

Département d'Oncologie Fondamentale

Novel antibody-based therapeutic approaches for redirecting T cell effector functions towards tumors expressing CD248 (TEM1)

Thèse de doctorat ès sciences de la vie (PhD)

présentée à la

Faculté de biologie et de médecine
de l'Université de Lausanne

par

Julie Katrin FIERLE

M.Sc. in Molecular Medicine
Albert-Ludwigs University Freiburg, Germany

Jury

Prof. Werner Held	Président
Prof. George Coukos	Directeur de thèse
Dr. Steven M. Dunn	Co-directeur de thèse
Prof. Oliver Hartley	Expert
Dr. Christine A. Power	Experte

Lausanne, 2020

Imprimatur

Vu le rapport présenté par le jury d'examen, composé de

Président·e	Monsieur	Prof.	Werner	**Held**
Directeur·trice de thèse	Monsieur	Prof.	George	**Coukos**
Co-directeur·trice	Monsieur	Dr	Steven M.	**Dunn**
Expert·e·s	Monsieur	Prof.	Oliver	**Hartley**
	Madame	Dre	Christine A.	**Power**

le Conseil de Faculté autorise l'impression de la thèse de

Madame Julie Katrin Fierle

Master of science, Université Albert Ludwigs, Allemagne

intitulée

Novel antibody-based therapeutic approaches for redirecting T cell effector functions towards tumors expressing CD248 (TEM1)

Lausanne, le 5 mars 2020

pour le Doyen
de la Faculté de biologie et de médecine

Prof. Niko GELDNER
Directeur de l'Ecole Doctorale

Acknowledgements

First and foremost, I would like to thank **Dr. Steven Dunn** for the support and guidance throughout the last 4.5 years. Taking on the challenge of being the first PhD student of the newly founded lab and seeing my project grow from initial discovery to *in vivo* testing has been an invaluable experience. I am very grateful for all that I have learned from you throughout these years. Thank you very much for the trust you put in me, for giving me the freedom to work in my own way and for always having my back! The last years have been an incredible learning experience, ultimately allowing me to grow into an independent scientist.

I would also like to express my deep gratitude to **Prof. George Coukos**, who gave me the opportunity to pursue my PhD in this exciting scientific environment. You are a truly inspiring person and exceptional scientist and I have the utmost respect for what you have created in Lausanne. Thank you very much for providing the framework and guidance that enabled this project.

In addition, I would like to acknowledge my PhD jury, with my committee representative and president, **Prof. Werner Held,** and the experts **Dr. Christine Power** and **Prof. Oliver Hartley**. Thank you very much for taking the time to read and assess my thesis manuscript, for traveling to Lausanne for my private thesis defense and especially for the stimulating discussion we had during and after my presentation.

Importantly, I would like to thank my colleagues from the L-AbCore team, who supported me throughout my PhD and without whom a lot of the presented work would not have been possible. Thank you all for your help, for countless funny coffee and lunch breaks and for the great team spirit that has made my PhD a truly enjoyable experience. But first of all, thank you for your constant encouragement and companionship throughout these years!

I will start with **Mariastella deTiani**. Thank you so much for all your help in the last years. Without you, I would not have been able to test half of the constructs that we have made and I would not have arrived at this point. I am incredibly grateful that I could always rely on you. Not only are you the heart and soul of the lab, you are also one of the kindest and most patient people I have had the pleasure to meet.

Special thanks also go to **Johan Abram**, who joined the lab at the same time as I did and who greatly contributed to my settling into the lab and into Lausanne. Thank you for being my partner-in-crime for the first years of my PhD and for all the helpful scientific and technical discussions. You have always been my go-to person for all kinds of advice, ranging from lab-related topics to sustainability and outdoor activities. Merci beaucoup!

I would also like to thank **Matteo Brioschi**, without whom I would not have been able to test my molecules *in vivo*. I am also very grateful for all the proteins that you expressed and/or purified for me. Besides your remarkable skill with the mice, I also admire the sense of calm and optimism you bring into every situation. Also, a big thank you to **Vasileios Atsaves** for all the interesting discussions we have had since you joined the team. I greatly admire your dedication and perseverance, especially when it comes to personal development and challenging old habits. Thank you for encouraging me to believe in myself and to step out of my comfort zone.

Abstract

Over the last two decades, the options for treating cancer have been revolutionized by the rapidly expanding field of human immunotherapy, and the innate potential of T cells to target, attack and control malignant cell growth is now widely accepted. Some of the most powerful immunotherapeutic strategies rely on the retargeting of T cells via antibody-derived recognition domains. For instance, these can be embedded in a synthetic chimeric antigen receptor (CAR), combining an antibody-derived targeting domain, typically a single-chain variable fragment (scFv), and intracellular signaling domains derived from the T cell receptor (TCR) complex and various co-stimulatory molecules. Another approach for harnessing the cytotoxic potential of T cells involves the use of bispecific antibody-derived molecules comprising a tumor-targeting moiety together with an associated 'bridging' anti-CD3 recognition domain. Both strategies have been applied successfully to treat hematological malignances, but achieving equivalent objective efficacy against solid tumors remains challenging, in part because of a relative absence of truly tumor-restricted antigen targets.

Tumor endothelial marker 1 (TEM1, Endosialin) has been proposed as a marker of neo-vasculature in embryonic and cancerous tissues. Due to its upregulation in the stroma and vasculature of many solid tumors and absence in healthy adult tissues, TEM1 represents an attractive tumor-associated antigen.

This thesis presents the *de novo* isolation and functional characterization of a diverse panel of fully human scFv binders targeting TEM1 from a naïve phage display antibody library. To accelerate antibody discovery, we have developed and validated a novel approach that integrates SpyCatcher/SpyTag covalent tag fusion technology into our phage display selection and screening workflows. Moreover, we have made significant progress towards the development of a powerful phenotypic selection strategy capable of flagging *directly* those scFvs in a library that possess cell-based CAR-activity. Using these approaches, we have identified several defined scFv candidates with distinct biophysical properties that recognize different domains of TEM1, and which have subsequently been investigated as targeting moieties for both CARs and soluble T cell engagers. In this latter context, both anti-CD3 and anti-TEM1 domains have been incorporated into a stable, trivalent bridging molecule (termed 'TriloBiTE') that permits either bivalent or biparatopic recognition of TEM1 on the surface of target cells.

Among our panel of novel antibodies, two lead candidates specifically redirect human T cells to TEM1 expressing target cells, both as CARs and as bispecific T cell engaging mediators, leading to the secretion of effector cytokines and lysis of tumor cells. From our investigations of these anti-TEM1 scFvs, target affinity and epitope location have emerged as two key parameters impacting on TEM1-directed T cell retargeting. Encouragingly, preliminary *in vivo* data for one of our candidate clones formatted as a soluble TriloBiTE suggests an ability to suppress TEM1$^+$ tumor establishment and growth, paving the road for further, more detailed investigations.

In summary, my thesis highlights two technological advances for the *de novo* discovery of functional antibody moieties and presents a first proof-of-principle for the immunotherapeutic targeting of TEM1.

Résumé

Au cours des deux dernières décennies, les options pour le traitement du cancer ont été révolutionnées par le domaine en pleine expansion de l'immunothérapie humaine. Parmi les stratégies immunothérapeutiques les plus puissantes, certaines se concentrent sur la redirection des lymphocytes T grâce à des domaines de reconnaissance dérivés d'anticorps. Ces domaines peuvent être intégrés dans un récepteur antigénique chimérique (CAR) synthétique, combinant un domaine de ciblage dérivé d'un anticorps, des domaines de signalisation intracellulaire dérivés du complexe du récepteur des lymphocytes T (TCR) et des diverses molécules de costimulation. Une autre approche pour exploiter le potentiel cytotoxique des cellules T implique l'utilisation de molécules bispécifiques dérivées d'anticorps. Ces dernières associent un fragment ciblant la tumeur à un domaine de reconnaissance anti-CD3. Les deux stratégies ont été appliquées avec succès pour traiter des tumeurs malignes hématologiques, mais il reste difficile d'obtenir une efficacité équivalente contre les tumeurs solides, en partie à cause de la rareté des cibles antigéniques véritablement limitées aux tumeurs. Dans ce contexte, le « tumor endothelial marker 1 » (TEM1, Endosialin) a été proposé comme marqueur de la néovasculature dans les tissus embryonnaires et cancéreux. En raison de son expression dans le stroma et le système vasculaire de nombreuses tumeurs solides et de son absence dans les tissus adultes sains, TEM1 représente un antigène tumoral attractif.

Cette thèse présente l'isolement *de novo* et la caractérisation fonctionnelle d'un panel varié de molécules scFvs entièrement humains ciblant TEM1, à partir d'une librairie d'anticorps naïfs sélectionnée par phage display. Pour accélérer la découverte d'anticorps, nous avons développé et validé une nouvelle approche qui intègre la technologie de fusion covalente de l'interaction SpyCatcher/SpyTag dans notre processus de sélection et de screening par phage display. De plus, nous avons fait des progrès significatifs vers le développement d'une stratégie de sélection phénotypique puissante capable d'identifier directement les scFv qui possèdent une activité dans le format CAR. En utilisant ces nouvelles méthodologies, nous avons identifié plusieurs candidats scFvs avec des propriétés biophysiques distinctes qui reconnaissent différents épitopes de TEM1. Ces scFvs candidats ont été étudiés en tant que composants de molécules CARs et en tant que médiateurs bispécifiques de cellules T. Dans ce dernier cas, les domaines anti-CD3 et anti-TEM1 ont été incorporés dans une molécule trivalente stable (appelée « TriloBiTE ») qui permet la reconnaissance bivalente ou biparatopique de TEM1 à la surface des cellules cibles.

Parmi nos nouveaux anticorps, deux candidats principaux redirigent spécifiquement les cellules T humaines vers des cellules cibles exprimant TEM1, à la fois comme CAR et comme TriloBiTE, aboutissant à la sécrétion de cytokines effectrices et à la lyse des cellules tumorales. Nos recherches sur ces scFvs anti-TEM1 ont permis d'établir que l'affinité avec la cible et la localisation de l'épitope sont deux paramètres clés qui ont un impact sur le reciblage des cellules T vers TEM1. De plus, les données *in vivo* préliminaires pour un de nos clones candidat formaté en TriloBiTE suggèrent une capacité à supprimer l'établissement et la croissance des tumeurs TEM1^{+}, ouvrant la voie à des investigations plus détaillées.

En résumé, ma thèse met en évidence deux avancées technologiques pour la découverte *de novo* de fragments d'anticorps fonctionnels et présente une première preuve de principe pour le ciblage immunothérapeutique de TEM1.

Table of Contents

List of Figures

List of Tables

List of Supplementary Figures

List of abbreviations

ACT	adoptive cell transfer
ADC	antibody-drug conjugate
ALL	acute lymphoblastic leukemia
APCs	antigen presenting cells
APC	allophycocyanin
AUC	area under the curve
BCMA	B cell maturation antigen
BCR	B cell receptor
BiTE	bispecific T cell engager
C	constant
CAF	cancer-associated fibroblast
CAR	chimeric antigen receptor
CD	cluster of differentiation
CDR	complementarity-determining region
CEA	carcinoembryonic antigen
CFU	colony-forming unit
CRS	cytokine release syndrome
CS03	cell screening round 3
CTLA4	cytotoxic T lymphocyte antigen 4
CTLD	c-type lectin domain
DAPI	4',6-Diamidino-2-phenylindole
DC	dendritic cell
dCI	direct capture and immobilization
DSF	differential scanning fluorimetry
E:T	effector-to-target cell ratio
ECD	extracellular domain
ECM	extracellular matrix
EGF	epidermal growth factor

ELISA	enzyme-linked immunosorbent assay
EpCAM	epithelial cell adhesion molecule
ER	endoplasmic reticulum
Fab	fragment, antigen binding
FACS	fluorescence activated cell sorting
FBS	fetal bovine serum
Fc	fragment, crystallizable
FcRn	neonatal Fc receptor
FDA	Food and Drug Administration
FL	full-length
GAPDH	glyceraldehyde-3-phosphate-dehydrogenase
GFP	green fluorescent protein
H	heavy
HC	heavy chain
HIF	hypoxia-inducible factor
HLA	human leukocyte antigen
HRP	horseradish peroxidase
HSC	hematopoietic stem cells
IDO	indoleamine 2,3-dioxygenase
IFN-γ	interferon-γ
Ig	immunoglobulin
IHC	immunohistochemistry
IL	interleukin
IMAC	ion affinity chromatography
IPTG	Isopropyl-β-D-thiogalactopyranoside
ITAM	tyrosine-based activation motifs
KO	knock-out
L	light
LC	light chain
LDH	lactate dehydrogenase

mAb	monoclonal antibody
MDSC	myeloid-derived suppressor cells
meso	mesothelin
MFI	median fluorescence intensity
MHC	major histocompatibility complex
MMAE	monomethyl auristatin E
MW	molecular weight
NF-κB	nuclear factor κB
NFAT	nuclear factor of activated T cells
NGS	next-generation sequencing
NIR	near-infrared imaging
NK	natural killer
NSG	NOD/SCID/IL-2Rγ KO
NT	non-transduced
ORF	open reading frame
PBMCs	peripheral blood mono-nucleated cells
PBS	phosphate-buffered saline
PCR	polymerase chain reaction
PD02	phage display round 2
PD1	programmed death 1
PDGFR-β	platelet-derived growth factor receptor β
PE	phycoerythrin
PET	positron emission tomography
PFA	paraformaldehyde
PK	pharmacokinetics
PMA	phorbol myristate acetate
PSMA	prostate-specific membrane antigen
RSS	recombination signal sequence
RT	room temperature
scFv	single-chain variable fragment

SDS-PAGE	sodium dodecyl sulfate polyacrylamide gel electrophoresis
SEC	size-exclusion chromatography
SMAC	supra-molecular activation complex
SPR	surface plasmon resonance
SpyC	SpyCatcher
SpyT	SpyTag
TAA	tumor-associated antigen
TCR	T cell receptor
TEM1	tumor endothelial marker-1
TEM1(Δn)	N-terminally truncated fragment of TEM1
TGF-β	transforming growth factor β
TILs	tumor infiltrating lymphocytes
TM	transmembrane
TME	tumor microenvironment
TNF-α	tumor necrosis factor-α
T_{reg}	regulatory T cell
TriloBiTE/tB	Tri-lobed bi-directional T cell engager
TRUCK	T cells redirected for universal cytokine-mediated killing
V	variable
VEGF	vascular endothelial growth factor

Chapter 1   Introduction

1.1   The immune system

The human immune system comprises a variety of cells and molecules which together defend the body against infectious agents and their toxins. Most of the cells of the immune system, called white blood cells, or leukocytes, derive from the lymphoid and myeloid lineages of pluripotent stem cells, which in turn derive from the hematopoietic stem cells (HSCs) in the bone marrow. Once mature, they migrate to peripheral tissues or circulate through the bloodstream or the lymphatic system, constantly monitoring for invading pathogens and abnormal cells.

1.1.1   Innate and adaptive immunity

The immune system can be divided into two main components, the innate and the adaptive immune system (reviewed extensively in Janeway's Immunobiology, 9th edition[1]). The innate immune system continuously defends the body against invading pathogens and is indispensable for the initiation of the adaptive immune response. The first line of defense is provided by anatomical barriers, such as the skin and mucosal surfaces of the oral cavity and gastrointestinal tract. Once pathogenic microbes penetrate this physical barrier and invade the underlying tissue, other components of the innate immune system are activated, such as the complement system, which plays a major role in the defense against invading bacteria[2]. Furthermore, cellular components of the innate immune system, such as macrophages, dendritic cells, and granulocytes, are rapidly activated to engulf and destroy invading microorganisms and induce inflammation[1].

Besides the non-specific innate immune system, the adaptive immune system enables highly specific responses to a vast array of proteinaceous and non-proteinaceous, usually polymeric molecules termed antigens. These highly specific lymphocytes, which comprise T cells and B cells, possess highly variable receptors that allow the recognition of virtually any foreign antigen[3,4]. Another important feature of the adaptive immune system is the generation of long-lasting immunological memory, conferring protective immunity against recurring infection[1]. For both B and T lymphocytes, antigen recognition through the antigen receptor (B cell receptor (BCR) or T cell receptor (TCR), respectively) induces activation and differentiation into so-called 'effector' and 'memory' lymphocytes. Antigen binding to the BCR causes B cells to proliferate and differentiate into effector cells, termed plasma cells. These plasma cells produce and secrete large quantities of antibodies, which circulate through blood and tissue fluids[5].

Similarly, T cells are endowed with a T cell receptor (TCR), which recognizes foreign antigens and, upon activation, induces the proliferation and differentiation of T cells into various effector subtypes. There are two main types of T cells. CD8 T cells, also known as cytotoxic T cells, which are characterized by the expression of the cluster of differentiation (CD) 8 co-receptor on their surface. Their main role is to kill abnormal or infected cells bearing foreign antigens, as further detailed below. The other key population of T cells, commonly referred to as helper T cells, express CD4 co-receptor on their surface and produce secreted cytokines and other signals that modulate the response of other cell types[3,6].

1.1.2 Antigen recognition by T cells

Each antigen receptor recognizes a specific antigenic determinant, or epitope, of any given antigen's molecular structure. The TCR recognizes a foreign or aberrant peptide epitope, which is presented by glycoproteins of the major histocompatibility complex (MHC) family on the surface of the body's cells[1,7]. There are two classes of MHC molecules, class I and class II. Both form a peptide-binding groove to display antigenic peptides, but they differ in their domain structure, peptide binding properties and in their expression pattern[8].

MHC class I molecules are encoded by three genes (HLA-A, HLA-B and HLA-C in humans), which are all highly polymorphic, and are recognized by CD8^{+} cytotoxic T cells. MHC class I molecules are expressed by almost all nucleated cells and present peptides derived from endogenously expressed and processed 'self' and foreign antigens, such as are present following viral infections[8,9]. In this way, they enable cytotoxic T cells to detect and eliminate infected or otherwise abnormal cells. Additionally, MHC class I molecules can present exogenous extracellular peptides through a process termed cross-presentation[10].

In contrast, MHC class II molecules are normally only expressed by antigen presenting cells (APCs), such as dendritic cells, macrophages and B lymphocytes, which take up and present circulating extracellular foreign agents and macromolecules[8,11]. The resulting processed antigens are recognized by CD4^{+} T cells, which upon activation release cytokines, which can enhance and modulate the effector functions of APCs and other cell types. Similar to MHC class I, class II molecules are encoded by three highly polymorphic genes (HLA-DR, HLA-DQ and HLA-DP in humans), with hundreds of different alleles found in the human population[12]. This MHC polymorphism enables the presentation of a vast variety of different peptides and determines each individuals discrete 'self' immune 'peptidome'[13]. Importantly, an extensive T cell sorting and selection process that takes place in the thymus ensures that the TCR repertoire is restricted to recognize specific endogenous MHC alleles and tuned to make weak binding contacts with the MHC molecule and any 'self' bound peptide antigens[14].

Following recognition of cognate peptide:MHC complexes by the TCR, proteins in the T cell membrane are actively rearranged to form an immunological synapse at the interface of the two interacting cell types[15-17]. The immunological synapse is crucial for enabling productive TCR signaling and is organized into distinct areas, the supra-molecular activation complexes (SMACs)[18]. At the center of the SMAC (cSMAC), the TCR and CD4/8 co-receptors cluster together with T cell co-stimulatory molecules, such as CD28. In a peripheral region of the synapse, the so-called pSMAC, cell adhesion molecules such as the T cell integrin lymphocyte function-associated antigen 1 (LFA-1) reinforce the cell-cell interaction by binding to intercellular adhesion molecule 1 (ICAM-1) on the APC. Larger molecules, such as the transmembrane tyrosine phosphatase CD45 are confined to the distal edges of the interface (dSMAC)[18].

In addition to peptide:MHC recognition and TCR signaling, co-stimulatory signaling is required for full T cell activation, which typically takes place in secondary lymphoid organs, such as lymph nodes.[19] (Fig. 1.1). This so-called two-signal model[20] was proposed following the discovery of the co-stimulatory molecule CD28, which interacts with B7-1/2 (CD86/CD80) on the surface of an APC in order to fully activate a naïve T cell[21]. Without co-stimulation, activated T cells will go into anergy, a state of growth arrest and relative unresponsiveness[22]. Besides CD28, many other receptors can provide co-stimulation, such as 4-1BB, OX40 and CD40L. Similarly, co-inhibitory receptors are essential to attenuate T cell responses, induce tolerance towards self-antigens, and protect tissues from excess T cell induced damage. Key among these are cytotoxic

T lymphocyte antigen 4 (CTLA4), which displaces CD28 from its ligand B7-1/2, and programmed death PD1. Together, co-stimulatory and co-inhibitory receptors modulate TCR signaling and T cell function[19].
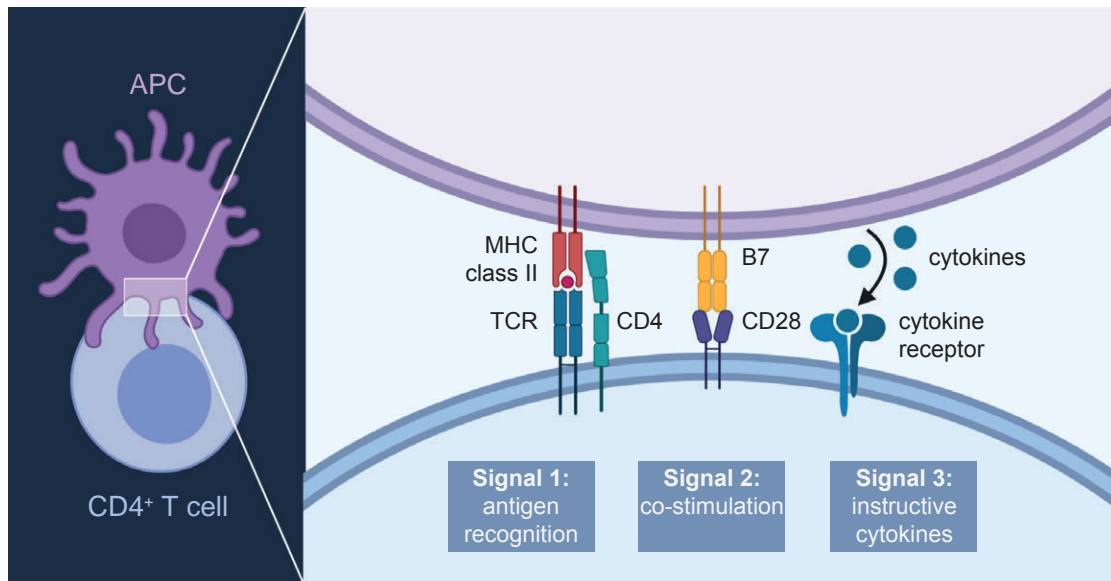
Figure 1.1. Productive T cell activation requires three different signals.

Signal 1 is delivered upon antigen recognition by the TCR. Co-stimulatory receptors such as CD28 mediate signal 2 upon ligand binding. Signal 3 involves instructive cytokines produced by primed antigen presenting cells (APCs) and directs T cell differentiation.

1.1.3   T cell receptor structure and signaling

The TCR is composed of two separate polypeptide chains, the TCR α and β chains, which are linked through a disulfide bond. The genes encoding the TCR chains are closely related to immunoglobulins and their structure resembles a membrane-bound fragment, antigen binding (Fab) domain, but, in contrast to antibodies, they are never secreted[1]. The majority of T cells express an α:β heterodimeric TCR, but some cells bear alternative γ:δ TCRs, whose functions are still being investigated[23].

Both TCR chains contain an N-terminal variable (V) region, which is primarily involved in antigen recognition, and a constant (C) region, followed by a transmembrane and short cytoplasmic domain. While the variable TCR α/β chains confer antigen specificity, they are required to associate with other molecules in order to transmit the information of antigen recognition to the cytosol. These signaling molecules are part of the CD3 complex, which comprises a CD3$\delta\varepsilon$ heterodimer, which associates with the TCR α chain, and a CD3$\gamma\varepsilon$ heterodimer, which interacts with the TCR β chain (Fig. 1.2). Moreover, the CD3ζ chain, which forms a homodimer, associates with the TCR chains[24,25]. The assembly of the resulting TCR complex relies mainly on charge interactions between positively charged amino acids in the TCRα/β transmembrane (TM) regions, and negatively charged residues in the CD3 TM domains.[26] Cell surface expression of the TCR requires the assembly of the whole TCR complex including all signaling components[25].
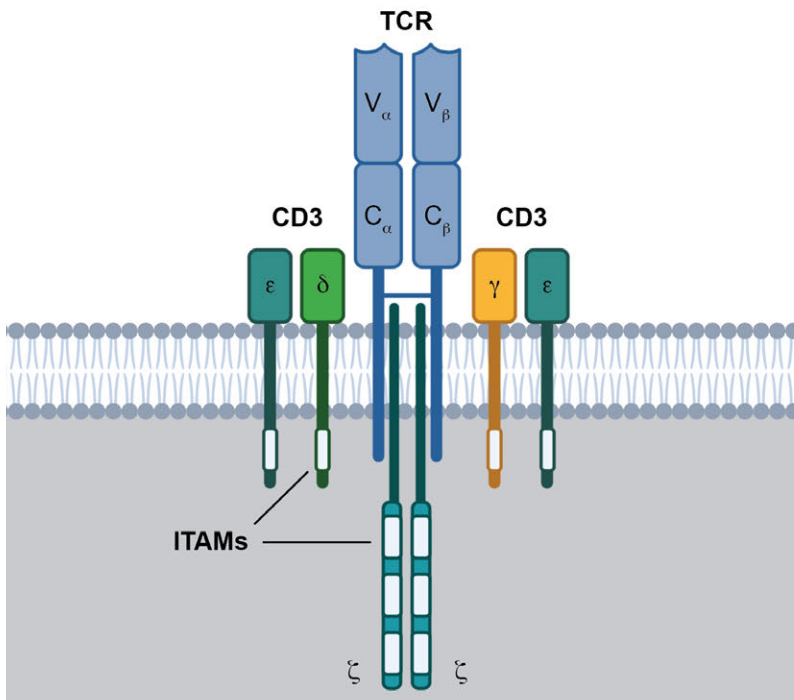
Figure 1.2. Composition of the TCR complex.

The antigen-specific TCR α and β chains associate with the CD3 ε/δ and CD3 γ/ε heterodimers, as well as the CD3 ζ chains to form the TCR complex. The CD3 chains contain intracellular ITAM domains, which transmit the TCR signal to the cytosol.

Upon antigen binding, immunoreceptor tyrosine-based activation motifs (ITAMs) in the cytoplasmic domains of the CD3γ, δ, ε and ζ chains become phosphorylated at two tyrosines, respectively. This initial phosphorylation of ITAMs is executed by the Src-family kinase Lck, which is associated with the cytoplasmic domains of CD4 and CD8[27]. Furthermore, the interaction through the co-receptors helps to stabilize the TCR – peptide:MHC interaction in order for signal transduction to occur. These initial phosphorylation events allow the recruitment of intracellular kinases containing tandem SH2-domains, such as ZAP-70 (ζ-chain-associated protein), which in turn are phosphorylated and activated[28] (Fig. 1.3). Further downstream of the TCR signaling cascade, ZAP-70 recruits and phosphorylates a number of adaptor proteins, such as linker of activated T cells (LAT) and SLP-76 (SH2 domain containing leukocyte protein of 76 kDa)[29,30]. Moreover, PI 3-kinase is activated, generating phosphatidyl-inositol triphosphate (PIP$_3$) at the inner membrane, which then together with the adaptor proteins mentioned above, recruits phospholipase C-γ (PLC-γ). PLC-γ then cleaves the membrane lipid PIP$_2$, generating membrane-bound diacylglycerol (DAG) and the cytosolic messenger inositol 1,4,5-triphosphate (IP$_3$), which triggers the opening of calcium channels in the endoplasmic reticulum (ER) membrane and in the plasma membrane, causing a Ca^{2+} influx into the cytosol[31].

Among other effects, the cytoplasmic Ca^{2+} influx mediates activation of transcription factors of the nuclear factor of activated T cells (NFAT) family[32] (Fig. 1.3). Specifically, Ca^{2+} is bound by calmodulin, which subsequently binds and activates the serine/threonine phosphatase calcineurin, leading to the dephosphorylation of NFAT. While phosphate groups usually mask the nuclear localization signal of NFAT, dephosphorylation causes NFAT to enter the nucleus, where it acts on the transcription of many genes

involved in T cell function. For instance, it activates the expression of interleukin-2 (IL-2)[32]. Furthermore, the membrane-conferred mediator DAG induces the activation of Ras and the mitogen-activated protein kinase (MAPK) cascade, as well as the activation of protein kinase C-θ (PKC-θ). These pathways lead to the activation of the transcription factors AP-1 and NF-κB, which both contribute to the control of T cell effector functions[27].

Finally, other consequences of TCR signaling are the upregulation of metabolic pathways via the serine/threonine kinase Akt, as well as enhanced integrin-mediated cell adhesion and reorganization of the cytoskeleton[28].
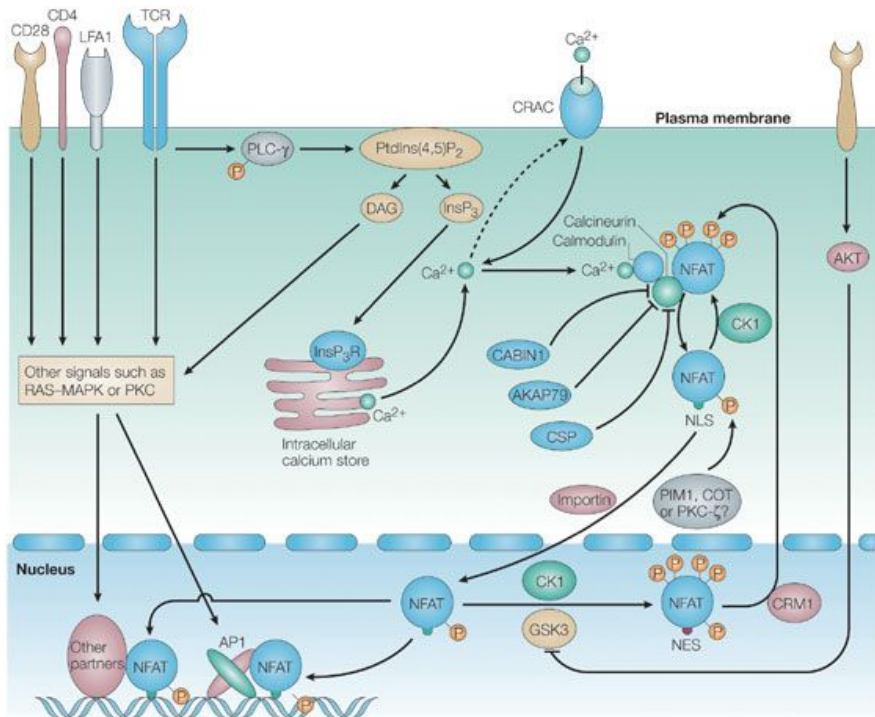
Figure 1.3. NFAT signaling in activated T cells.

Early TCR signaling induces a Ca^{2+} influx, which activates transcription factors of the NFAT family. Figure adapted from Macian, F. *Nat Rev Immunol*, **5**(6), 472–484 (2005)[32].

1.1.4   T cell effector functions

Recognition of a specific peptide:MHC complex by the TCR is only the first step in the activation of a naïve T cell. Effective expansion and survival however require two additional signals: (i) a co-stimulatory signal (signal 2) provided by the same APC (i.e. via CD28 – B7.1/2) and (ii) cytokines (signal 3), which direct the differentiation of the naïve T cell into a specialized T cell subset[1] (see Fig. 1.1). This first antigen encounter and T cell priming typically takes place in peripheral lymph nodes. The primary cytokine produced by activated naïve T cells is IL-2, which induces accelerated cell cycling and proliferation[33]. Along with the production of IL-2, antigen encounter with appropriate co-stimulation induces the expression of CD25, the α chain of the IL-2 receptor, which upon association with the β and γ chains creates a heterodimeric receptor with greatly increased affinity compared to the β/γ IL-2 receptor expressed by naïve T cells[34]. Naïve T cells

activated in this way therefore undergo clonal expansion and during this process also differentiate into the different effector subtypes, a process that is primarily driven by the cytokine milieu. A key feature of effector T cells is their independence from co-stimulation, enabling for instance the killing of any cell infected with a virus and presenting viral peptides on MHC I molecules[1].

CD8 T cells are predisposed to differentiate into cytotoxic effector cells, whose key feature is the ability to recognize and destroy abnormal cells. Upon antigen recognition, CD8 effector cells release cytotoxic granules selectively at the immunological synapse. Biochemical conditions, particularly the pH, within the granules prevent the action of the cytotoxins stored in these granules, mainly perforin and granzyme, but they become active once released[35-37]. Perforin forms pores in the plasma membrane of the target cell, allowing the delivery of granzymes[38]. Granzymes are proteases which induce apoptosis of the target cell, both by cleaving caspases and by causing mitochondrial damage[39]. Additionally, CD8 T cells express membrane-bound death signals such as Fas ligand, which can induce apoptosis of target cells expressing Fas[40,41]. Moreover, activated cytotoxic T cells release cytokines such as interferon-γ (IFN-γ) and tumor necrosis factor-α (TNF-α). IFN-γ stimulates antigen presentation on MHC class I molecules, activates macrophages and inhibits viral replication. TNF-α also activates macrophages and can induce apoptosis in cells expressing TNF receptor-I[42].

In contrast, CD4 T cells can differentiate into several effector subtypes, primarily dictated by fate-specifying cytokines provided by APCs and other innate immune cells[43]. The different CD4 effector subtypes are specialized to enhance the effector functions of other cells in order to eliminate a specific class of pathogens[43]. For instance, T_H1 cells secrete IFN-γ, which improves the eradication of intracellular pathogens by macrophages[44].

In summary, upon peptide:MHC recognition, the predominant effector function of CD8 T cells is the lysis of abnormal or virally infected cells, whereas CD4 T cells mainly carry out regulatory functions, instructing other immune cells via cytokines. However, it has been shown that certain CD4 T cell subsets can also exert cytotoxic effector functions[45]. The following section introduces another key player of the adaptive immune system, the B cells.

1.1.5 B cell activation and effector functions

Like T cells, B cells have the capacity to recognize a vast array of different antigens. In B cells, the antigen-binding proteins are called immunoglobulins and any given B cell produces immunoglobulins of a single specificity[1]. The activation and clonal expansion of B cells occurs upon antigen recognition by the BCR, a membrane-bound form of immunoglobulin.

Similar to the TCR, the antigen-specific BCR associates with invariant signaling molecules, in this case Igα and Igβ. These single-chain proteins form a disulfide-linked heterodimer and associate with the heavy chains of the BCR via hydrophilic interactions[46]. The association with the Igα:Igβ dimer enables the transport of the BCR to the cell surface and provides the ITAM-containing cytoplasmic domains necessary for signal transduction[1,46]. Cross-linking of BCR via a multivalent antigen activates the ITAM-associated Src-family kinases Fyn, Blk and Lyn, which phosphorylate tyrosine residues in the ITAMs. An SH2-domain containing tyrosine kinase, Syk, is recruited to the phosphorylated ITAMs and initiates a signaling cascade involving the scaffold protein SLP-65 as well as PLP-γ and its products DAG and IP$_3$. Antigen-dependent BCR signaling is

further enhanced by engagement and clustering of the B-cell co-receptor, a complex formed by the cell-surface proteins CD19, CD21 and CD81[1,47].

Ultimately, the BCR signaling pathway leads to increased survival, metabolic changes and a rearrangement of the actin cytoskeleton to create an immune synapse. In B cells, the immune synapse mainly serves to facilitate antigen uptake for subsequent presentation on MHC class II molecules[48]. Subsequently, activated B cells undergo clonal expansion and differentiate into plasma cells, which secrete large quantities of soluble antibodies[49].

1.1.6 Antibody structure and function

Secreted IgG antibodies are structurally depicted as Y-shaped proteins with a molecular weight of of approximately 150 kDa. The structure of an antibody is shown in Figure 1.4. Antibodies combine several functionalities: Principal amongst these is the recognition of a variety of antigens through specific (and often high-affinity) binding mediated by the terminal regions of each 'arm'. Other related functions are concerned with the activation of immune 'effector' functions, leading to the neutralization and elimination of the bound antigen. Additional elements in the antibody structure actively promote the persistence of the molecule within the circulation. The two 'arms' of the molecule represent the extremely variable, or V region, which allows the recognition of virtually any antigen, whether a small molecule (a hapten) or a large conformation epitope of a protein. The binding strength of one arm to its target dictates the 'affinity' of the molecule, while the combined binding strength conferred by both arms acting in concert is referred to as 'avidity'. The remaining constant, or C region domains are conserved for a given antibody class and are responsible for eliciting and controlling the strength of the associated immune effector functions and for governing the circulating half-life of the antibody. The most abundant class of antibodies, the IgG, consists of four polypeptide chains, two identical heavy chains (HC) of approximately 50 kDa, and two identical light chains (LC) of around 25 kDa (Fig. 1.4)[50-54]. There are two types of light chains, termed λ and κ, which are represented in different ratios in different species. In humans, the average ratio of κ to λ light chains is 2:1, but in mice it is 20:1[55]. The two heavy chains are linked by disulfide bonds in the 'hinge' region of the molecule, and each heavy chain is similarly linked through a disulfide to a light chain. Historically, proteases were used to study the antibody structure and the resulting nomenclature is still being used today. For instance, papain cuts the antibody into three different fragments, two antigen-binding fragments (Fab) and one readily crystallizable fragment (Fc)[50,51,53,54]. This enzyme cleaves in the hinge region of the antibody, a flexible stretch of amino acids that allows a certain range of motion of each Fab arm in order to allow the simultaneous binding of two antigens.

Both heavy and light chains are composed of compactly folded immunoglobulin (Ig) domains, which show strong homology on the sequence- and on the structural level[56]. While heavy chains consist of four such Ig domains, the smaller light chains contain only two Ig domains. In both cases, the N-terminal Ig domain bears highly variable regions and is therefore termed variable (V) domain[56]. The V domains of heavy (HC) and light chains (LC) combined correspond to the antigen-binding V region of the antibody and they can be isolated genetically and linked synthetically to generate a single-chain variable fragment (scFv)[57]. In contrast, the constant domains of heavy and light chains make up the C region[1,52]. For the heavy chain, which contains three C domains, these are numbered CH1, CH2 and CH3 from the N- to C-terminus (Fig. 1.4), with CH2 and CH3 forming the Fc region. The constant region of the heavy chain defines the class, and/or isotype, and therefore the effector function of an antibody[1,55]. There are five major classes, IgM, IgD, IgG, IgA and IgE, with

IgG being further classified into four subclasses (i.e. IgG1, 2, 3 and 4), all conferring different structural and immunological properties[55].

Each Ig structural domain is composed of two β sheets, each built from several β strands, which are tightly packed together and stabilized by a disulfide bond. V and C domains share this immunoglobulin fold, but the V domains are slightly larger and contain additional β strands[52,56].
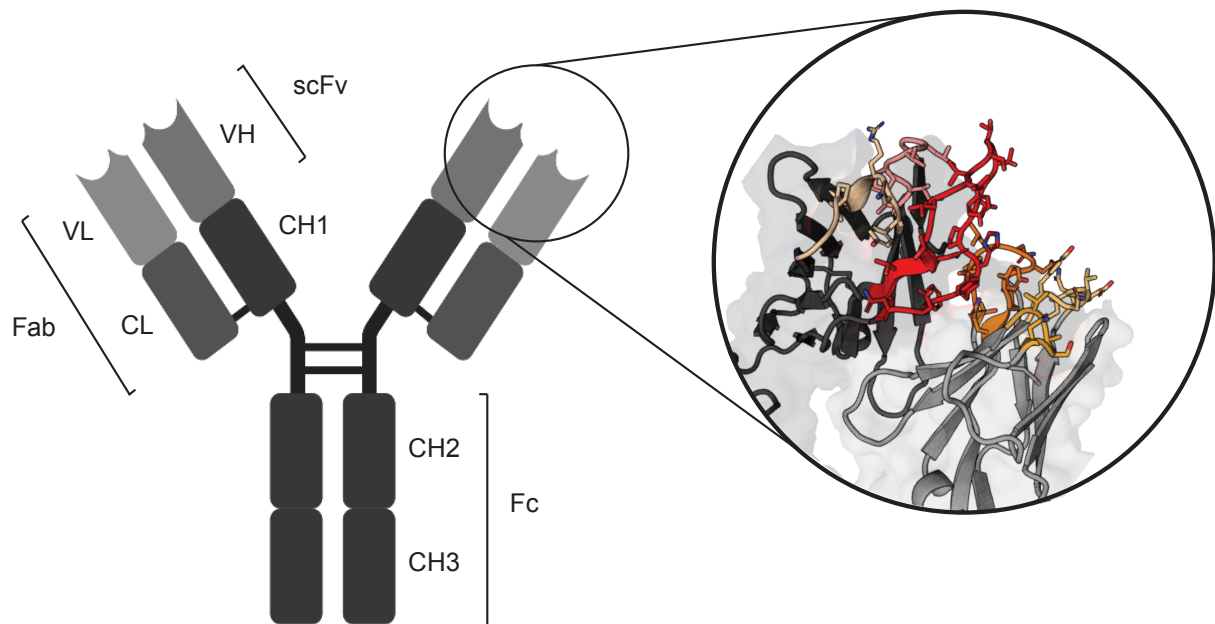
Figure 1.4. The structure of an IgG antibody.

Schematic representation illustrating the structure of an IgG antibody. The molecular structure of the variable region of an exemplary human antibody is shown (PDB accession 4JHW, chain H and L), with the CDR loops highlighted in colors, and side chains shown in stick representation. The protruding red loop corresponds to the HC CDR3, the lighter hued loops correspond to HC CDR 1 and 2. CDR loops of the light chain are colored in orange. Fab, fragment, antigen-binding; VL, variable light; CL, constant light; VH, variable heavy; CH1-3, constant heavy 1-3; scFv, single-chain variable fragment; Fc, fragment, crystallizable.

Importantly, each mature structural V domain contains three hypervariable regions, which are separated by four framework regions. These hypervariable regions, which are termed complementarity-determining regions (CDRs), form protruding loops at the edge of the Ig fold and define the antigen specificity of the antibody. Each antigen-binding site is thus composed of six CDR loops, three from the heavy chain and three from the light chain, which collectively contribute to antigen recognition (Fig. 1.4). However, not all CDRs have to directly engage in the antibody paratope (the amino acid residues responsible for binding the epitope), but rather help to orient those residues that do interact with the epitope[55,58].

1.1.7 Antibody and TCR diversity

The vast repertoire of immunoglobulins and TCRs represents the underlying principle of adaptive immunity, enabling the recognition of any antigen encountered. Several sequential gene rearrangement and splicing processes are required to realize this potential.

Firstly, combinatorial diversity is created by somatic recombination of gene segments encoding the variable regions of heavy and light chains (V_H and V_L) or the variable regions of the TCR α and β chains (V_α and V_β)[59]. The mature V_L and V_α regions are encoded by the splicing of two different gene segments, V (variable) and J (joining), while V_H and V_β regions contain an additional D (diversity) gene segment spliced between the V and J elements. Both TCR and antibody genetic loci contain clusters of genes encoding each of the V, (D), and J repertoire segments which are randomly, yet sequentially, recombined during lymphocyte development in a process called V(D)J recombination[60]. Subsequently, the rearranged variable domains are spliced to constant domain exons. Whereas the CDR1 and CDR2 domains are encoded directly in the germline V gene segment, the hypervariable CDR3 loops arise as a consequence of junctional V(D)J recombination[59,60].

Antibody and TCR V(D)J recombination is mediated by the RAG recombinase (encoded by the recombination-activating genes 1 and 2), which recognizes and cleaves specific recombination signal sequences (RSSs) that flank each V, D, and J segment[61,62]. An RSS consists of a conserved heptamer and nonamer sequence, which are separated by a non-conserved spacer of either 12 or 23 base pairs. According to the 12/23 rule, a gene segment followed by an RSS with a 12bp-spacer can only be joined with a segment proceeded by an RSS containing a 23bp-spacer[61]. This ensures that each V segment can only be joined to a D segment, or in the LC (α) loci to a J segment. The RAG recombinase is only expressed in developing lymphocytes and induces a double-strand break in the DNA, which is then re-sealed by non-homologous end joining (NHEJ) while looping out the RSSs and redundant gene segments[60,62,63]. The formation of the so-called coding joint is prone to nucleotide insertions or deletions, further increasing the sequence variability of the rearranged V region CDR3s. Occasionally, the DNA is nicked in the region between gene segments rather than at the precise end. In this case, single-stranded DNA overhangs can occur, are filled with new nucleotides, the so-called palindromic 'P nucleotides', by the DNA repair machinery. Alternatively, the DNA can be nicked resulting in blunt ends, in which case non-templated 'N nucleotides' can be added randomly by the enzyme terminal dideoxy transferase (TdT) before re-ligation[64]. This insertion of N nucleotides can result in ultra-long CDR3 loops, which usually occurs only in the HC, as the TdT gene is only expressed at earlier stages of B cell development/Ig gene rearrangement.

The final dimension to the generation of diversity is achieved by the pairing of HC (β) and LC (α) chains in order to create a functional antibody (TCR). As lymphocyte precursors can undergo several rounds of cell division before LC (α) rearrangement, each HC (β) can be clonally paired with different LCs (α chains)[55,59].

Generally, the affinity of naïve/new B cell antibody molecules created by VDJ recombination is relatively low. However, after initial antigen encounter, the rearranged Ig loci are further diversified by the enzyme-driven introduction of mutations into the rearranged variable domains in a process termed somatic hypermutation[65,66]. In the event of beneficial affinity-improving mutations, the resulting B cells will undergo clonal expansion[55,59]. This iterative 'affinity maturation' process of continuous mutation and selection drives the generation of antibodies with affinity constants (KDs) typically in the picomolar to low nanomolar range. The mutation process is primarily driven by activation-induced cytidine deamidase (AID), an enzyme that is

exclusively expressed in germinal center B cells[67-69]. In actively transcribed regions, such as the Ig loci, the DNA is temporarily unwound and opened, allowing AID to deamidate cytosine residues, thereby converting them to uracil[70]. The resulting lesion is subsequently repaired by the mismatch repair and the base-excision repair pathways, using error-prone DNA polymerases[71]. These mutagenic processes do not occur at the TCR loci and their affinities are determined solely by V(D)J recombination.

Additionally, AID initiates so-called class or isotype 'switching' by rearranging the genes in the C_H locus[69,72,73]. The C_H locus contains a series of different C regions, which correspond to the different antibody isotypes and which are fused to the VDJ segment by mRNA splicing. Naïve B cells initially express the HC isotypes μ or δ and thus express IgM or IgD immunoglobulins as cell surface receptors. Each of the C genes is preceded by a repetitive intronic switch region, which lead to RNA polymerase stalling, enabling AID and other enzymes to attack the DNA. The resulting double-strand break is repaired by non-homologous recombination, excising intervening sequences[72]. The choice of isotype for class switching is primarily determined by the cytokine milieu, with different cytokines enhancing the transcription of different C isotypes[74,75]. Class switching to IgG isotypes yields the principle, secreted form of Ig present in peripheral blood.

1.1.8   Antibody engineering and phage display

Their ability to recognize virtually any given target make antibodies an extremely valuable tool for numerous therapeutic and diagnostic applications. Moreover, since the structure and function of the different domains of the antibody are well characterized, they can be engineered to generate customized antibodies with the desired properties. Another key feature of the antibody molecule is its outstanding diversity, with the naïve antibody repertoire comprising at least 10^{11}-10^{12} unique antibody clones[76-78]. Many efforts have thus focused on controlling and directing the output of this vast immunological repertoire, predominantly with the aim of identifying an antibody specific for a given antigen. In principle, this can be achieved via two different strategies: (i) the immunization of host animals, and (ii) the generation and *in vitro* selection of combinatorial antibody libraries[79,80].

Depending on the desired outcome, native combinatorial immune libraries can either be constructed from the immune repertoires of pre-exposed (or diseased) donors, or of non-immunized healthy individuals[79,81-83]. Harvested variable domain repertoires may derive from all or selected isotypes, whether naïve (IgM/D) or affinity matured/class-switched (IgG/A/E). In addition, synthetic and semi-synthetic libraries can be created by rational and controlled gene synthesis technologies, allowing a precise choice of V domain frameworks and CDR length/diversity. While antigen biased, or immune libraries may prove useful for the rapid isolation of high-affinity binders to the immunogen, these need to be regenerated for each antigen target of choice. Highly diverse naive (or 'one pot') libraries, on the other hand, can, in principle harbor binders to a broad diversity of different antigens and are powerful reusable tools for the *in vitro* isolation of fully human antibodies. Such naïve libraries are built by isolating mRNA from bulk peripherally circulating CD19$^+$ B cells, and amplifying collectively the VH and VL regions by polymerase chain reaction (PCR)[84]. These VH and VL chains are then randomly combined, often in scFv format, to generate large renewable libraries, typically exceeding $1x10^{10}$ distinct entities. Although well validated for antibody discovery applications, a concern of such approaches is the loss of the original B cell clone VH/VL Fv domain pairing. In B cells, the heavy and light chains of an antibody have undergone several rounds of selection and editing in order to eliminate combinations that bind to self-molecules or that are structurally unstable[85]. However, as Fv formation through VH/VL pairing is highly degenerate, artificial combinatorial libraries create many novel variants

capable of breaking such native immune tolerance, which allows the isolation of fully human antibodies that recognize therapeutically important human target antigens[86].
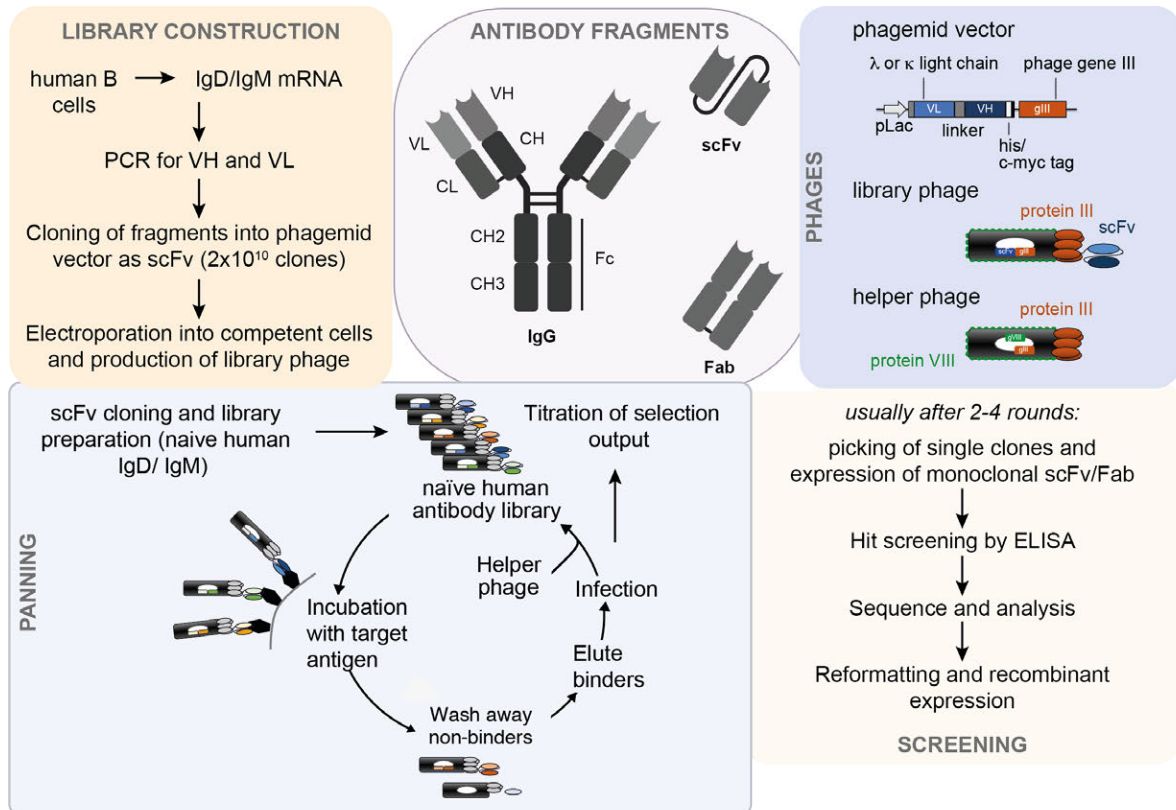
Figure 1.5. Antibody Phage Display.

Schematic overview of the phage display methodology as it was used in this thesis.

The underlying principle of binder selection from a diverse antibody library is the linkage of phenotype and genotype. Each member of the library must be packaged in a way that allows its phenotypic (expressed) selection while retaining the encoding genetic information. The most widely used strategy to achieve this uses filamentous M13 bacteriophage as the packaging unit. Filamentous phage combines the robust display of antibody variants on individual phage particles with efficient packaging of the corresponding genetic information, and highly amplifiable replication in bacterial host cells[87,88] (Fig. 1.5). Phage display libraries usually utilize Fab or scFv fragments (see Fig 1.4 and 1.5), as these can be adequately expressed and folded in prokaryotic host cells. The latter scFv fragments comprise the VH and VL domain joined by a suitable linker and are produced from a monocistronic vector, typically a so-called phagemid, which contains a phage origin of replication. Fab vectors differ in that a bicistronic vector is required for the separate expression of VHCH and VLCL chains, which then assemble into the Fab. The entire combinatorial library repertoire of VH and VL domains is sampled in a phagemid vector system[89,90], which permits the fusion of the scFv or Fab (via one chain) to a structural capsid protein of the bacteriophage, usually the major coat protein pVIII or the minor coat protein pIII[91,92].

The helical pIII protein contains 406 residues and accumulates in the periplasm of the prokaryotic host cell[93,94]. After assembly of the phage particles, an average of four pIII copies are located at the tip of the phage. The N-terminus of pIII bind to the F-pili of *E.coli* and is thus indispensable for the infectivity of the phage[95]. Phages with scFv/Fab domains fused to each of their pIII proteins would therefore not be able to replicate. To solve this problem, a helper phage system is used where the helper phage contains the genetic information for native pIII, so that ultimately the assembled phages retain some native pIII for infectivity and display a single antibody-linked pIII molecule (on average)[89].

The resulting phage population can then be screened for binding to an immobilized antigen in a process referred to as 'panning' or 'selection' (Fig. 1.5). In this process, phages are incubated with immobilized antigen in several consecutive selection rounds, and only antigen-binding phages are retained and replicated. At the end of this process, antibodies expressed by single clones are screened for antigen binding, typically by enzyme-linked immunosorbent assay (ELISA) and sequenced, as further detailed throughout chapter 2.

As an alternative to phage, many other display technologies have been developed, such as yeast display, ribosome display and mammalian display[96-98]. All of these technologies have their own unique advantages, but phage display remains the most versatile and most widely used method for selecting antibodies from *in vitro* combinatorial libraries. Importantly, display technologies have led to the development of a number of therapeutic antibodies. Among them, the anti-TNF-α antibody adalimumab (Humira) is the first fully human phage display-derived antibody to be approved for clinical use, and it is also the best-selling drug (by revenue) world-wide[99].

Besides their use as antagonists or agonists of therapeutically or otherwise relevant targets, antibodies can be engineered to deliver enhanced or novel effector functionality. For instance, antibodies can deliver toxic 'payloads' to cancerous lesions[100], or their unique antigen-binding properties can be employed to redirect T cell effector functions for the treatment of cancer, as will be discussed in the next section.

1.2   Cancer Immunotherapy

1.2.1   Anti-tumor immunity

Cancer remains one of the leading causes of death worldwide and the second-leading cause of death in Switzerland, with an incidence of 120.7 cases per 100.000 inhabitants in 2018[101]. The underlying principle of the disease is the progressive transformation of normal cells into malignant cells, driven by a series of genetic and epigenetic alterations. Despite being an extremely heterogeneous disease, six original hallmarks have been defined that are common to most if not all human cancers: (i) self-sufficient proliferation, (ii) insensitivity to growth suppressors, (iii) evasion of apoptosis, (iv) replicative immortality, (v) sustained angiogenesis, and (vi) invasion and metastasis[102]. These common traits of cancer cells have later been extended to include (vii) reprogramming of cellular metabolism, and (viii) immune evasion[103]. Tremendous effort has been undertaken to correct or counterbalance any of these hallmark traits. In light of the extreme potency of the immune system and especially T cells to detect and eliminate aberrant cells, this section will focus on the concept of immune evasion and on strategies aiming to boost anti-tumor immunity.

Under physiological conditions, cells and tissues are subjected to constant immune surveillance and both the innate and the adaptive immune system contribute to the eradication of abnormal cells[104]. The accumulation of mutations by tumor cells leads to the expression of tumor antigens, which, if intracellular, can be processed and presented on the surface of MHC class I molecules and recognized by T cells as 'foreign'. Additional antigens may be considered as tumor 'associated' if their expression levels or regulation deviate markedly from those same antigens found in healthy cells, leading to a differential cell presentation profile. Tumor antigens can thus be loosely classified into: (i) cell type-specific differentiation markers, (ii) tumor associated antigens such as cancer-testis antigens or onco-viral proteins, and (iii) neo-antigens arising from mutated endogenous proteins which have been shown to lead to spontaneous T cell responses in patients[105]. Non-proteinaceous tumor antigen candidates such as aberrant glycosyl or glycolipid (or related) core structures on tumor cell glycoproteins or membranes also represent an additional class of tumor 'signature' molecules[106-108].

The mounting of an effective anti-tumor immune response, a process that has been referred to as the Cancer-Immunity Cycle, requires a series of discrete cellular events[109,110]. Firstly, dendritic cells (DCs) must capture, process and present tumor antigens. At this stage, in order to promote immunity rather than tolerance to tumor antigens, DCs have to receive additional activation/maturation signals, such as proinflammatory cytokines[111]. Next, DCs have to process the captured antigens and present them on MHC class II molecules, or, via cross-presentation, on MHC class I[11,112]. These antigen-loaded DCs then must migrate to secondary lymphoid organs and initiate effector T cell responses by presenting tumor antigens along with adequate co-stimulatory signals. Importantly, DCs lacking an immunogenic maturation signal will predominately induce tolerance by promoting the differentiation of regulatory T cells (T_{reg})[113]. Activated effector T cells subsequently need to migrate to the tumor tissue and infiltrate the tumor bed, where they must recognize and kill their cancer targets. Ultimately, the lysis of tumor cells releases additional tumor antigens, thereby further driving the cancer immunity cycle[109,110].

However, despite their presence in many solid tumors, such tumor infiltrating lymphocytes (TILs) are often dysfunctional and incapable of tumor eradication, in part because the tumors adapt by eliminating cells expressing T cell targets, a process that is referred to as 'immune editing'[114]. Furthermore, the tumor microenvironment (TME) is often highly immunosuppressive, with several mechanisms contributing actively to prevent an effective anti-tumor T cell response. One common mechanism of immune evasion is the downregulation of MHC class I molecules by tumor cells to avoid recognition by T cells[115]. Alternatively, tumor cells may express inhibitory cell surface molecules, such as PD-L1 or PD-L2, which bind to PD-1 on the surface of activated T cells and promote T cell exhaustion or anergy[116]. Other mechanisms of immune evasion involve the secretion of immunosuppressive metabolic enzymes, such as indoleamine 2,3-dioxygenase (IDO) and arginase, which inhibit T cell function via amino acid deprivation[117,118].

Additionally, tumors often trigger the local accumulation of T_{reg} cells and other suppressive immune cells, such as myeloid-derived suppressor cells (MDSC) and cancer-associated fibroblasts (CAFs), which release inhibitory factors such as transforming growth factor β (TGF-β)[119,120]. The tumor microenvironment also plays a crucial role in promoting local immunosuppression. For instance, endothelial cells in the tumor bed may downregulate adhesion molecules to prevent tumor homing by T cells, a mechanism that is, in part, mediated by vascular endothelial growth factor (VEGF)[121].

1.2.2 Cancer immunotherapy

These inhibitory mechanisms, however, also present opportunities for therapeutic intervention and so a number of strategies have been developed to harness the potential of T cells to recognize and eliminate cancer cells, including, for example, therapeutic cancer vaccines, which aim to boost the cancer-immunity cycle[110]. Early vaccination attempts have mainly focused on shared tumor peptide antigens, such as the melanocyte differentiation antigen gp-100[122] or the cancer-testis antigen MAGE-A3[123]. These trials have often shown only limited efficacy, in part due to a poor understanding of appropriate peptide delivery and limited DC activation/maturation[109]. With technological breakthroughs enabling the wide use of next-generation sequencing (NGS) to comprehensively map the 'mutanome', that is the entirety of somatic mutations in a given tumor sample, new and personalized vaccination strategies are currently being explored. Pre-clinical studies revealed that a substantial fraction of predicted neo-epitopes were immunogenic and could be employed successfully in synthetic RNA- or long peptide vaccines, eliciting productive CD4 and CD8 T cell responses[124,125]. Based on these results, a number of first-in-human clinical trials have attempted to manufacture personalized tumor vaccines on the basis of each melanoma patient's individual mutational profile and predicted neo-epitope landscape[126,127]. Promising results, including indications of immunogenicity of the predicted neo-epitopes, and first clinical responses have now encouraged further investigations of personalized vaccines, especially in combination with other immunotherapeutic strategies, such as checkpoint blockade.

Under physiological conditions, co-inhibitory signals, or immune checkpoints, play a key role in preventing autoimmunity and excessive tissue damage during T cell responses. Similarly, tumor cells commonly exploit and hijack these inhibitory ligands and receptors as a mechanism of immune resistance[128,129]. They therefore present an ideal opportunity for therapeutic intervention, and antagonistic antibodies blocking two of the key checkpoints, CTLA-4 and PD1, are now approved and marketed drugs. The CTLA-4 checkpoint is expressed early on activated T cells and acts as an antagonist of the co-stimulatory receptor CD28, both by outcompeting CD28 in binding its ligands B7.1 (CD80) and B7.2 (CD86) and by transmitting inhibitory signals[130,131]. Consequently, the amplitude of a T cell response is dampened and excessive T cell activation prevented[132]. This led to the rationale that blockade of CTLA-4 action could boost endogenous anti-tumor immune responses[133]. In fact, ipilimumab, an antagonistic anti-CTLA-4 antibody, was the first therapeutic agent to mediate a survival benefit for patients with metastatic melanoma, and was approved by the US Food and Drug Administration (FDA) in 2010[134]. However, due to the unleashing of T cell effector functions, CTLA-4 blockade is often accompanied by severe immune-mediated toxicities[135]. While CTLA-4 acts within the timeframe of T cell priming, other checkpoints regulate inflammatory responses in peripheral tissues. Key among these is PD1, which is upregulated by activated T cells and interacts with ligands such as PDL1 (also known as B7-H1), which in turn are induced in peripheral tissues by inflammatory cytokines, such as IFN-γ[136]. As a consequence, T cell activity and tissue damage are controlled and autoimmunity is prevented[137,138]. The same mechanism comes into play in the tumor microenvironment, where tumor and stroma cells commonly express PDL1 to suppress T cell effector functions[128]. Like CTLA4, PD1 is also highly expressed on T_{reg} cells, but here enhances their proliferation, which further contributes to immunosuppression[139]. In addition, chronic antigen exposure has been shown to induce persistent PD1 expression, rendering antigen-specific T cells exhausted or anergic[140]. Therefore, there is a strong rationale for therapeutic targeting of the PD1-PDL1 axis, and eight blocking antibodies have been approved to date, targeting several tumor indications.

Another strategy to enhance anti-tumor immunity is the adoptive transfer of large numbers of anti-tumor T cells (adoptive cell therapy; ACT). It is widely accepted that TILs can recognize tumor antigens, especially neo-antigens, and mediate productive immune responses, although those are frequently suppressed. Therefore, protocols have been developed to rapidly expand TILs from resected tumor material (up to 10^{11}) and re-infuse them into the patient in large numbers[141]. Additionally, the expanded lymphocytes can be selected for tumor recognition and effector functions; as a result of the expansion protocol, they become activated *in vitro*. Early studies have demonstrated that ACT using autologous TILs could induce tumor regression in patients with metastatic melanoma, but the infused cells were short-lived and did not persist in the patients[142]. This obstacle was in part overcome by the introduction of preparative lymphodepletion prior to ACT[143]. Since then, a number of studies have shown solid objective response rates of around 50 % to ACT with autologous TILs in melanoma patients[141,143-145]. Strikingly, a subset of patients displayed durable and long-term remission[145]. However, although TILs can also be expanded from other tumor types, only melanoma TILs show robust and consistent anti-tumor reactivity. A possible explanation for this phenomenon is the high rate of non-synonymous mutations in melanoma compared to other cancer types[146]. In fact, several studies have identified cancer-specific mutations in melanoma samples that were recognized by autologous TILs inducing complete cancer regression[147,148]. Current efforts therefore focus on the identification of neo-epitopes and neo-epitope-reactive TILs[147,148].

Given the often limited endogenous immune response to cancer (neo)antigens and the disappointing outcome of TIL-transfer in most cancer types, genetic engineering of autologous T cells represents an attractive alternative to elicit anti-tumor immunity.

1.2.3   T cell engineering and chimeric antigen receptors

In order to redirect antigen specificity, T cells can be equipped with transgenic TCRs or with chimeric antigen receptors (CARs), synthetic immune receptors combining an extracellular recognition domain with intracellular signaling domains (Fig. 1.6).

TCRs and CARs typically recognize fundamentally different antigens. TCRs recognize peptides derived from the intracellular proteome, which are presented on MHC molecules. A key requirement for T cell therapy with a transgenic TCR is therefore the expression of cognate antigenic peptides by tumor cells and their presentation on the tumor cell surface in the correct (cognate) MHC class I context recognized by the TCR. Once these requirements are met, TCRs are intrinsically highly sensitive and therefore represent attractive tools for redirecting T cell specificity. The first transgenic TCR tested in the clinic was directed against an HLA-A2 restricted peptide derived from the melanocyte differentiation marker gp100[149]. Initial results were rather modest and so attempts have been undertaken to increase the affinity of the TCR for cancer targets, which is typically lower than the affinity of TCRs recognizing viral targets (low micromolar vs. nanomolar range)[150]. Trials using T cells equipped with affinity-engineered TCRs have indeed improved the clinical response rate, but have also led to substantial on-target off-tumor toxicities (including side effects such as vitiligo, due to the elimination of normal gp100-containing melanocytes)[151]. The fatal neuro- and cardiotoxicities observed with TCR-based therapies directed against the cancer-testis antigen MAGE-A3 further revealed the risks inherent with engineered transgenic TCRs[152,153]. Whilst native TCRs undergo stringent selection via thymic processes, engineered molecules may acquire undesirable activation threshold affinities for closely related native peptide antigens on healthy tissues, resulting in severe toxicities. This is exacerbated by the TCR having 'built in' cross-reactive potential to many peptidic antigens[154,152,155]. Leveraging engineered TCRs for

therapeutic ACT therefore presents significant safety challenges, although an affinity-enhanced TCR recognizing the cancer-testis antigen NY-ESO-1 has recently shown clinical efficacy and is being evaluated in a late-stage clinical trial[156]. Other current efforts aim at developing neo-vasculature-specific TCR therapies with native (thymically 'approved') TCRs that would be expected to have higher natural affinities and more potent anti-tumor activities[157,158]. Conceptual disadvantages of TCR-based therapies are the restriction of any given TCR therapeutic to patients possessing the requisite cognate MHC haplotype.

In contrast to TCRs, CARs recognize unprocessed cell surface antigens which thus enables MHC-independent tumor cell targeting[159]. Early CARs combined an antigen-binding domain, usually an scFv, with an intracellular signaling domain derived from the CD3ζ chain (Fig. 1.6).
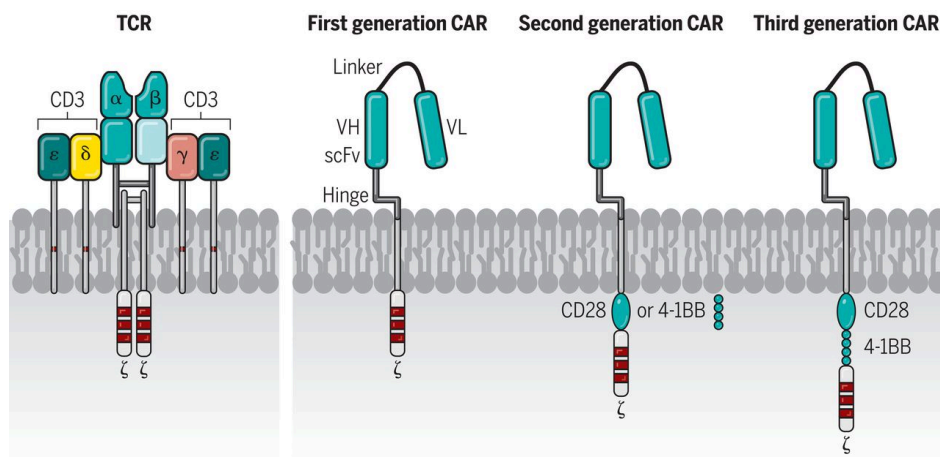
Figure 1.6. T cell engineering with transgenic TCRs vs. the various CAR generations.

T cells can be equipped with transgenic T cell receptors (TCRs, left), or chimeric antigen receptors (CARs, right) to redirect antigen specificity. CAR constructs link an extracellular antigen recognition domain, usually a single-chain variable fragment (scFv), with intracellular signaling domains derived from the TCR/CD3 complex. 1st-generation CAR designs only contain a CD3ζ signaling domain, while 2nd- and 3rd-generation CARs encompass one or more additional co-stimulatory domains in addition to CD3ζ. VH, variable heavy; VL, variable light. Adapted from June, C. H. *Science* 359, 1361-1365 (2018)[160].

Since clinical trials with these first-generation CARs produced disappointing results, with rapid clearance/inactivation of the adoptively transferred cells [161,162], second-generation CARs were engineered to include an additional co-stimulatory domain derived from CD28, 4-1BB or OX40, with the intention of promoting the maintenance of T cell effector functions together with durable proliferation and expansion[162-164]. Similarly, third-generation CAR designs include two or more consecutive co-stimulatory domains and aim to further refine and optimize these desirable properties[160]. Recently, fourth-generation CAR T cells, termed TRUCKs, have been engineered to express both a CAR and to secrete activating mediators, such as pro-inflammatory cytokines[165]. A key attraction of the CAR paradigm is the independence from antigen presentation on MHC. This circumvents one of the most common mechanisms of immune evasion, namely, the downregulation of MHC-associated antigen presentation[115], but also necessitates a requirement for suitable tumor cell surface bound targets.

The potential of CAR-T cell therapy is best exemplified for the CD19 antigen, a B cell differentiation marker and part of the B cell co-receptor that is restricted to the B cell lineage[166]. CD19 represents a nearly ideal

target with its high expression levels in B cell malignancies and restriction to the B cell lineage, the loss of which is tolerable. Clinical trials with second-generation CARs directed against CD19 have shown tremendous success in the treatment of B cell leukemia with a majority of patients initially achieving apparent remission[167-170]. In the case of CD19, on-target off-tumor T cell activity is tolerable, since the resulting B cell aplasia can be treated with intravenous immunoglobulin[170]. However, the severe cytokine release syndrome (CRS) observed in some patients poses a challenge to the therapeutic administration of CAR-T cells and requires careful monitoring and management of immune-related toxicities[167,171]. Further, cerebral edema has been reported as an unexpected neurological complication possibly due to endothelial damage[167,172].

Beyond CD19, CAR-T cells directed against other B cell targets such as B cell maturation antigen (BCMA) or CD22 have shown potent anti-tumor activity in early clinical trials[173,174]. Targeting solid tumors, on the other hand, has proven more difficult, partly due to insufficient tissue penetration and a potentially immunosuppressive tumor microenvironment[175]. Early-phase trials involving CARs specific for mesothelin, carcinoembryonic antigen (CEA) and GD2 ganglioside have only generated minimal clinical responses[160,176]. Attempts to target ERBB2/HER2 or CEACAM5 have led to severe on-target off-tumor toxicities, highlighting another hurdle that is frequently encountered with target antigens being insufficiently restricted to tumor cells[177,178]. Many proposed cell surface markers currently under immunotherapeutic investigation are shared antigens that are also often expressed on normal healthy tissues to varying extents. Therefore, strategies to enhance tumor selectivity are a priority in the field, and some of them will be discussed in the next section, along with other considerations for the engineering of CARs.

1.2.4 Current challenges and structural considerations for CAR-T cell engineering

The CAR constructs currently used in clinical trials have mostly been designed empirically, based on what is understood from TCR signaling and T cell activation. Despite their tremendous success in treating patients with B cell malignancies, a number of obstacles have thus far prevented the extension of CAR-T cell therapy to other tumor types. Some of these obstacles could be tackled by improving the molecular design strategies for CAR engineering.

One of the clinical challenges emerging for CD19 CAR-T cell therapy is the development of resistance. Resistance mainly occurs through two distinct mechanisms: (i) downregulation or mutation of CD19, analogous to antigenic escape as a common mechanism of immune evasion[179], and (ii) failure of the CAR-T cells to proliferate and persist *in vivo*[180]. Another major challenge for the treatment of solid tumors is the discrimination of tumor cells from normal cells, since many of the proposed targets are not exclusively expressed in the tumor tissue. In light of the fatal toxicities observed with some T cell-based therapies directed against non-exclusive tumor antigens, the choice of target antigen is of paramount importance[177]. Hence, molecules that are expressed during development, but are absent in normal healthy adult tissues, such as ROR1 and GD2, represent attractive candidates[181,182].

Another possibility, which can also be applied to prevent resistance, is the implementation of a 'two-signal' system, which, in analogy to co-stimulation during T cell activation, ensures that the T cell is only activated in the appropriate context. To achieve this, a dual-receptor strategy has been proposed, where the primary CD3ζ and the secondary CD28/4-1BB signaling domains are split between two separate CAR constructs recognizing two different antigens[183-185]. However, the signaling of the CD3ζ-bearing CAR might have to be tightly controlled in order to avoid activation in the presence of single-positive cells[184]. Alternatively,

transcriptional circuits based on a synthetic Notch (SynNotch) receptor system have been designed to achieve conditional expression of the CAR only in the presence of tumor cells[186,187]. A different variant of a 'two-signal' system involves an inhibitory signaling receptor to mitigate T cell activation in the presence of normal cells[188]. For instance, an inhibitory secondary CAR has been designed by combining the endodomain of PD1 or CTLA4 with a recognition domain directed against PSMA, which inhibited T cell activation in the presence of PSMA-expressing cells[188]. Here, the choice of ligand to deliver the negative signal is a critical issue.

Other tumor antigens are expressed at low density and therefore pose the problem of sensitivity rather than selectivity. While CD19 is estimated to be expressed in abundance, with around 10'000 copies per cell, alternative targets such as ROR1 are likely expressed two- to five-fold lower[189]. A study using an anti-CD20 CAR suggested that ~200 CD20 molecules per cell were the minimum threshold for lytic activity, whereas efficient cytokine production required around ten-fold higher antigen density[190]. These activation thresholds may differ from antigen to antigen, and additionally depend on T cell intrinsic factors, such as the involvement of co-receptors and endogenous TCR/CD3 clusters. The clustering of TCRs with multiple ITAM domains and co-receptors has evolved to ensure a high level of signal amplification upon physiological TCR signaling, which can respond to as few as ~10 target pMHC on the cell surface (e.g. NY-ESO1:HLA-A2)[191,192]. It remains to be seen whether CARs can be engineered to exploit or recapitulate this degree of sensitivity, or indeed, whether this is desirable from a targeting specificity perspective. In contrast to natural TCRs, the targeting scFvs of CARs often have relatively high affinities. For some targets, e.g. ROR1, it has been shown that the potency of CAR-T cells increases with increasing targeting affinity[193]. On the other hand, other studies have described an avidity threshold for both CARs and TCRs, above which T cell effector functions plateau or even decrease[194,195]. These observations are in line with the 'serial triggering' model, which suggests improved T cell activation upon serial engagement of multiple TCRs by the same peptide:MHC[196].

Another key aspect of T cell activation and cytotoxicity is the formation of an immunological synapse. The structure of the TCR – peptide:MHC interaction dictates the distance of T cell and APC, and is estimated to be around 15 nm[189]. This close interaction excludes the bulky membrane-located phosphatases CD45 and CD148 from the synapse, which otherwise attenuate T cell signaling[197,198]. A similarly close interaction may be necessary for efficient CAR signaling. The spatial distance between a CAR-T cell and its target is mainly influenced be the relative location of the target epitope and by the spacer domain between the scFv and the membrane. There are several reports of improved T cell activation when the same epitope is expressed closer to the membrane[199-201]. Moreover, it has been shown that the CAR spacer domain can be tailored for optimal CAR signaling depending on the epitope location[193,202].

In summary, the optimal binding properties of a targeting scFv towards a given target antigen cannot (yet) be reliably predicted or modelled. Even when a candidate scFv recognizes its target in solution, it may not necessarily confer potent T cell activation in the context of a surface-bound CAR. Therefore, the development of unbiased screening approaches to directly select scFvs on the basis of their ability to induce T cell activation may provide an efficient path for the development of new and improved CARs. Ideally, such screening platforms would not only sample large libraries of potential binders, but also include different linker/spacer designs to account for steric constraints imposed by the epitope location. Chapters 4 and 5 discuss these challenges in further detail, and present a high-throughput approach for the cell-based selection of binders with the desired functional properties.

1.2.5 Bispecific antibodies for cancer immunotherapy: molecular formats

Redirecting T cell effector functions via CARs generally requires genetic engineering of autologous T cells for each patient. An alternative, yet analogous approach, has been developed using bispecific antibodies (biAbs) which simultaneously engage a tumor cell and a T cell, thereby redirecting T cell activity and stimulating a polyclonal T cell response[203,204]. Specifically, antibody-derived '*engager*' molecules can physically link tumor cells via a cell-surface antigen, and T cells, usually via CD3 (Fig. 1.7). By this approach, MHC restriction can be bypassed and T cells are activated through TCR/CD3 complexes irrespective of individual TCR specificities. By bridging tumor and T cell, the engager molecule creates an artificial immune synapse and induces the release of perforin and granzymes, ultimately leading to target cell lysis[205] and tumor regression[206]. Importantly, T cell activation and killing via bispecific engagers can occur in the absence of formal co-stimulation[207,208]. It has been established that dual binding by both engager arms is required for synapse formation and target cell lysis[209]. In this way, bystander cells that do not express the chosen tumor-associated antigen, are spared. Furthermore, it has been shown that T cells activated with a bispecific T cell engager (BiTE) are capable of serial killing of multiple tumor cells providing the BiTE is present[210]. Hence, such T cell engaging bispecifics represent an attractive class of molecules for therapeutic development, especially given their potential as 'off-the-shelf' soluble drugs.
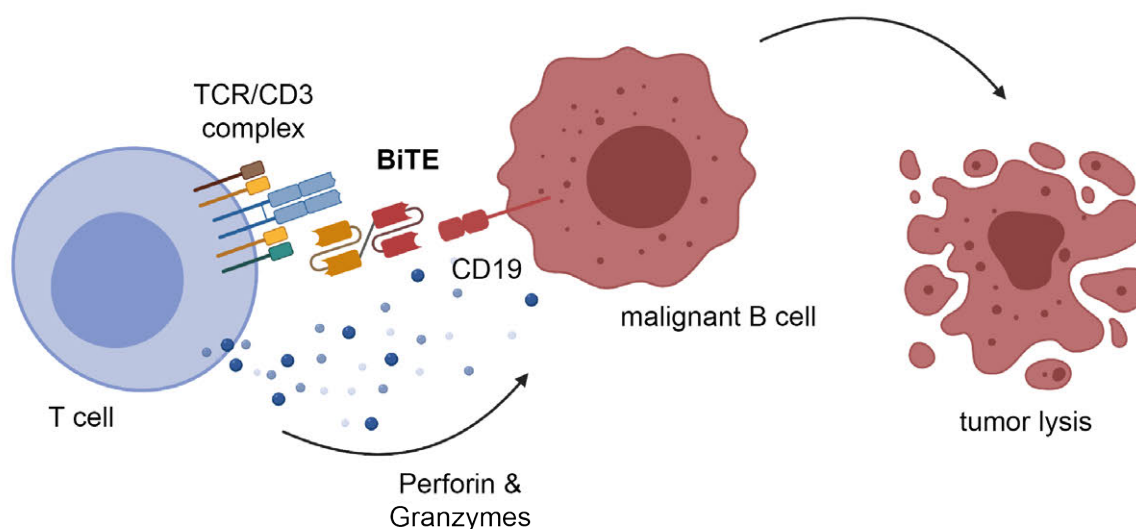
Figure 1.7. Bispecific T cell engagers redirect T cells to target malignant cells.

T cell engaging bispecifics simultaneously bind a tumor-associated antigen, here CD19, and CD3 expressed by T cells. This cross-linking creates an immune synapse, leading to the secretion of lytic granules and ultimately to tumor cell lysis. A classical tandem BiTE is depicted as an exemplary molecule. TCR, T cell receptor; BiTE, bispecific T cell engager.

To this end, over 100 different bispecific antibody formats with different structural and functional properties have been designed, with more than 20 being commercialized in the context of proprietary technology platforms[211-213]. Conceptually, these formats can be classified into (i) fragment-based; (ii) symmetric IgG-based; and (iii) asymmetric IgG-based formats[212] (Fig 1.8).
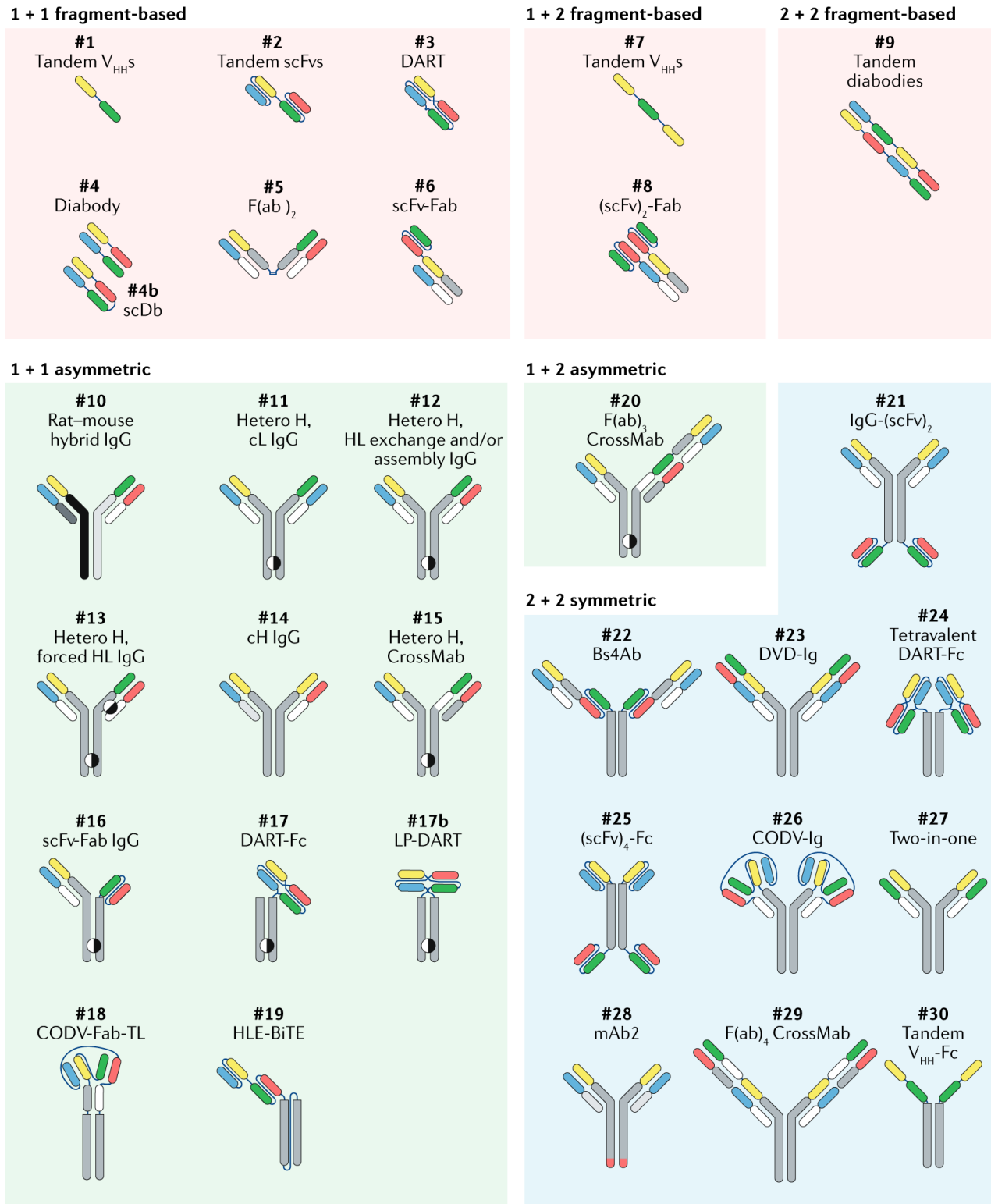
Figure 1.8. Overview of a selection of bispecific antibody formats.

Bispecific antibody (biAb) formats can be categorized into fragment-based, asymmetric IgG-based and symmetric IgG-based. Exemplary platforms mentioned in the text are #2 bispecific T cell engager (BiTE), #10 rat-mouse hybrid TrioMab, #11 and #12 knobs-into-holes technology, #23 dual variable domain (DVD)-Ig. Antibody domains are depicted as follows: orange, variable heavy (H) chain specificity 1; green, variable H chain specificity 2; blue, variable light (L) chain specificity 1; red, variable L chain specificity 2; grey, H chain constant region; white, L chain constant region; light grey, alternative L chain constant region; format #10: dark grey and black, rat L chain and immunoglobulin G2b (IgG2b) H chain; and white and light grey, mouse L chain and IgG2a H chain. cH common heavy; cL, common light; HLE, half-life extended; scDb, single-chain diabody; scFv, single-chain variable fragment; VHH, heavy chain-only variable domain. Figure adapted from Labrijn, A. F. *Nat Rev Drug Discov* **18**, 585–608 (2019)[212].

Fragment-based formats rely on the simple combination of antigen-binding domains, usually scFvs or Fabs, in the absence of a Fc region (Fig. 1.8). The most prominent example for this class of bispecifics are classical BiTEs which combine an anti-CD3 scFv with an scFv specific for a tumor-associated antigen, connected via a short peptide linker[204] (Fig. 1.8). Blinatumomab, an anti-CD19 BiTE, is the first and currently only FDA-approved T cell engager, demonstrating an impressive complete response rate of 43 % in a phase II/III trial for the treatment of relapsed/ refractory B cell acute lymphoblastic leukemia (ALL)[214,215]. BiTEs and other fragment-based bispecifics are often small (~55 kDa for tandem scFv-based BiTEs) and lack an Fc domain, which, due to the lack of neonatal Fc receptor (FcRn)-mediated recycling, substantially decreases their plasma half-life[203,216]. Moreover, due to their deviation from the natural antibody structure, fragment-based bispecifics can have issues with expression yields, stability and aggregation, requiring challenges for downstream processing and formulation during manufacturing[217]. On the other hand, the modular design of such molecules is highly attractive as it permits the incorporation of additional domains for increased valency or additional functionality[218].

Bispecific formats retaining the native IgG architecture (biAbs) benefit from the unique stability and long half-life of antibody molecules, but generating bispecific IgG comes with another challenge: the chain-association (pairing) issue. Theoretically, co-expression of two different heavy and light chains could yield 10 different molecules, of which only one would correspond to the desired HC/LC combination[219]. A number of strategies have been developed in order to circumvent this issue (Fig. 1.8). For instance, HC constant domains have been engineered for preferential heterodimerization[220-222]. Here, the "knobs-into-holes" technology has been pioneering, generating complementary structures between the two heterodimeric HCs, which were subsequently paired with common light chains[222,223].

Similarly, strategies have been designed to ensure correct heavy and light chain pairing[224-226]. An early solution to this problem was the combination of two HC/LC pairs with different species origin, i.e. rat and mouse[225]. More recently, orthogonal Fab interfaces have been designed to favor correct pairing[224]. Furthermore, purification strategies have been adapted to selectively enrich for the intended asymmetric molecule, for instance by modulating protein A binding of the two HCs[225]. Alternatively, the two specificities can be assembled on the protein level, for example by controlled Fab-arm exchange[227,228]. The resulting asymmetric formats closely resemble natural antibodies and are therefore usually restricted to functionally monovalent (1 + 1) targeting.

Alternative design strategies bypass the chain-association issue by integrating both specificities in one HC/LC pair, i.e. by appending scFv or Fab fragments to a full antibody structure[229] (Fig. 1.8). The resulting symmetric molecules still resemble natural IgG molecules, but differ in size and molecular architecture, which can lead to stability or solubility issues[212]. Formats with appended domains, such as the DVD-Ig, may nominally comprise bivalent antigen-binding domains, but due to the close proximity of the domains, it is not always apparent whether such designs translate into functional bivalency[212,229].

This plethora of bispecific antibody formats is reflected in the global clinical development arena, which currently encompasses over 85 bispecific antibody molecules, half of which are T cell redirecting antibodies for cancer therapy[212].

1.2.6 Design parameters impacting on the potency of soluble T cell engagers

The efficiency of simultaneous antigen engagement is critically impacted by a number of design parameters, such as binding strength (affinity/avidity), epitope location and format architecture. For instance, small fragment-based formats, such as BiTEs, have been shown to mediate more efficient linking of tumor and target cells, which is reflected by the ability of blinatumomab to induce cytotoxicity at much lower effector-to-target ratios than a full-length biAb[230]. On a different note, Fc-deficient molecules such as blinatumomab are rapidly cleared from the circulation and therefore have to be administered by continuous infusion[216]. Despite increasing half-life, a native Fc part can also mediate unwanted binding to Fcγ receptors on healthy cells. In the case of the CD3 x EpCAM bispecific catumaxomab, this behavior has led to severe T cell-mediated hepatotoxicity[231]. Moreover, the presence of a functional native Fc part seems to dampen therapeutic activity of CD3-engaging biAbs *in vivo*[232]. As a consequence, all CD3-targeting biAbs that are currently under clinical evaluation have engineered Fc domains, ideally abrogating FcγR and C1q interaction, but retaining FcRn binding[233,234]. Independent of the presence of an Fc domain, format architecture and relative paratope orientation have a key impact on simultaneous target binding and therapeutic activity[229,235].

Similarly, the choice of antigen-binding domain for both T cell targeting and tumor recognition is of paramount importance for the potency of T cell engager molecules. Most published T cell engagers utilize CD3ε-binding units derived from the same murine antibody clones, often a variant of OKT3[236]. Depending on the technology platform, this clone has usually been humanized, affinity matured and/or engineered to reduce immunogenicity[212]. While T cell engager variants with high CD3 affinity can induce more potent cytotoxicity *in vitro*, such molecules show unfavorable biodistribution and pharmacokinetics, since they can accumulate in T cell-dense tissues[237,238]. Generally, monovalent CD3-binding is favored over bivalent CD3 engagement in order to balance tumor-specific T cell activation and tumor-independent 'tonic' activation mediated by CD3 crosslinking[212,237,238]. Besides T cell retargeting, natural killer (NK) cells are emerging as anti-tumor effector cells that can be recruited by a bispecific activating mediator, usually via CD16A[239,240].

Efficient recognition of the tumor cell is critical for specificity and therapeutic activity and largely depends on the characteristics of the binding antibody domain and the molecular properties of the antigen itself. For some targets, such as CEA, CD33 and HER2, effective T cell engagement seems to depend on antigen expression levels[241-243]. Other targets, such as prostate-specific membrane antigen (PSMA) show no such obvious correlation[244]. Further complexity is provided by the affinity and binding kinetics of the tumor-targeting entity. In this context, increasing the avidity by bivalent tumor binding has been shown to enhance potency and selectivity of T cell engagers[242,245]. The latter is especially important when the tumor-associated antigen is not truly tumor restricted, but expressed at lower levels on healthy tissues. A good example for such a case is HER2. Here, it has been suggested that utilizing a bivalent biAb with lower monovalent affinity for HER2 specifically redirects T cells to HER2-overexpressing tumor cells while sparing normal cells expressing HER2 at low density[245]. Besides expression levels, other properties of the antigen can impact on biAb activity, such as its mobility in the membrane[246] and the size of its extracellular domain[247]. Targeting either a smaller antigen or a more membrane-proximal epitope has proven beneficial for efficient T cell engagement[247,248]. Presumably, bringing both cell types into close proximity allows optimal synapse formation and thus potent cytotoxic activity.

In summary, while various molecular formats have been developed for soluble T cell engagers, defined rules for the design of effective molecules are lacking. At this point, targeting domains and molecular formats still

have to be validated empirically in order to identify an effective combination of tumor binding and T cell retargeting domains.

1.2.7   T cell engaging bispecifics in clinical development

Following the encouraging results achieved with blinatumomab, a number of T cell engagers are currently being evaluated in the clinic, with the majority of molecules aiming to treat hematological malignancies. Most of these molecules are directed against a conserved set of well-validated targets, including CD19, CD29, CD33, CD38, CD123 and BCMA[212]. The bispecifics currently in the pipeline are however not redundant, since they utilize different molecular formats, which are likely to reveal differential safety and efficacy profiles.

Clinical experience with blinatumomab has revealed a number of adverse events with T cell engagers directed against B cells. As expected, B cell aplasia accompanies a successful anti-leukemia response and some cases of acute cytokine release syndrome have been reported[211]. Although potentially life-threatening, this condition can often be managed with immune-suppressing interventions[249]. Further, neurotoxicity ranging from dizziness to convulsions and delirium has been observed in 10-20 % of the patients treated with blinatumomab[203]. In these cases, the very short half-life of this molecule has proven advantageous in mitigating severe side effects.

Besides hematological malignancies, a number of biAbs directed against solid tumors are currently under clinical evaluation[212]. Again, the majority of these molecules target well-established antigens, such as HER2, epidermal growth factor receptor (EGFR) vIII, PSMA and epithelial cell adhesion molecule (EpCAM). However, the often immunosuppressive TME, irregular tumor vasculature and insufficient tumor penetration represent major hurdles for sufficient T cell recruitment and engagement. Another complication is the presence of low-levels of these antigens in healthy tissues. On-target, off-tumor toxicities are therefore a major concern, especially since pre-clinical safety studies in rodents are often complicated by altered or absent cross-reactivity of the lead candidate towards the equivalent murine antigens and/or effector T cells.

Based on knowledge gained with blinatumomab and other clinical-stage bispecifics, multiple phase I and II trials are currently underway exploring combinations of T cell engaging bispecifics with other treatments, such as immune checkpoint inhibitors[212]. Alternatively, formats containing three or more specificities are being explored. For instance, trispecific NK cell engagers (TriKEs) combining CD133 x CD16 with an IL-15 cross-linker are being tested in a phase I trial[250]. Another strategy aims to simultaneously engage CD3 and CD28 on T cells in addition to a tumor antigen in order to increase the potency of anti-tumor cytotoxicity[251]. The pending results from the host of ongoing clinical trials with T cell engaging bispecifics will undoubtedly contribute to our understanding of this class of molecules and their therapeutic potential. Finally, it is anticipated that conceptual and technical advances will continue to improve tumor targeting with bispecific antibody-based engager molecules in order to generate a wider therapeutic impact.

1.3 Tumor endothelial marker 1 and the tumor microenvironment

1.3.1 The tumor microenvironment

Solid tumors are complex organ-like structures, with several cell types contributing to the formation of a favorable tumor microenvironment (TME). In addition to cancer cells, fibroblasts and the extracellular matrix (ECM) they produce, blood vessels, lymphocytes and myeloid cells all contribute to the tumor tissue[252]. A critical step in the formation of tumors is the induction of neo-angiogenesis, that is, the sprouting of new blood vessels, to ensure a steady supply of nutrients and oxygen[253]. In contrast to physiological neo-angiogenesis, the resulting tumor vasculature appears disorganized, with tortuous, dilated and collapsed capillaries[254]. Vascular immaturity and incomplete pericyte coverage and function leads to vessel instability and increased permeability[255,256]. Furthermore, the uncontrolled growth of cancer cells within a tissue can compress and collapse tumor vessels, causing inadequate perfusion[257]. Together, these vascular abnormalities lead to aberrant permeability and hypoxia in parts of the tumor tissue, which favors the selection of more aggressive tumor cells and impedes the anti-tumor capacity of immune cells[254,257].

Moreover, observations of tumor-specific immune cells co-existing with proliferating tumor cells has shaped the concept of immune privilege, a situation where the TME actively suppresses T cell activity. In fact, in many cancer types, (cytotoxic) T cells are excluded from the direct vicinity of cancer cells[258], preventing any anti-tumor cytotoxicity and strongly limiting the potential of immunotherapeutic intervention. Key cell types directing the exclusion of T cells are cancer-associated fibroblasts (CAFs), myeloid-derived suppressor cells (MDSCs) and tumor-associated macrophages (TAMs)[259-261]. For instance, reactive nitrogen species produced by MDSCs can post-translationally modify chemokines like CCL2, which in their modified form still attract monocytes, but not T cells[262]. In addition, the tumor vasculature also contributes by preventing T cell extravasation into the TME, while allowing other immune cells to migrate[175]. Mechanistic insights into this phenomenon came from studies comparing immune-infiltrated vs. immune-excluded tumors. Motz et al. described that immune-excluded tumors express the apoptosis signal FasL, leading to apoptosis of CD8$^+$ T cells, but not T$_{reg}$ cells, which up-regulate the apoptosis inhibitor c-FLIP, leading to the selective exclusion of CD8 T cells from the TME[263].

There are many more mechanisms of immunosuppression by the TME. However, the examples above illustrate that the tumor stroma is a specialized tissue adapted to support the uncontrolled proliferation of cancer cells. Further, tumor neo-vasculature is structurally and functionally different from normal vasculature. Given their crucial role in supporting tumorigenesis, both the tumor stroma and the neo-vasculature represent attractive targets for diagnosis and therapeutic intervention. Thus, many efforts have focused on identifying specific markers of tumor stroma and vasculature.

1.3.2 Tumor endothelial marker 1 (TEM1/ Endosialin/ CD248): expression pattern

TEM1, also known as endosialin or CD248, is a transmembrane glycoprotein which was first described as a surface marker of human embryonic fibroblasts and tumor endothelium[264,265]. Later on, high-resolution analysis of a range of human cancers revealed that TEM1 is not expressed by endothelial cells, but rather by pericytes, myofibroblasts and smooth muscle cells within the tumor vasculature[266-271]. TEM1 is upregulated in various human cancer types including colorectal cancer[265,272], breast cancer[273,274] and malignant brain tumors, such as glioblastoma[270,275]. Unlike in carcinomas, where TEM1 expression is restricted to the

perivascular area, human sarcomas express TEM1 in both malignant and stromal cells. Indeed, 81 % of clinical sarcoma specimens were shown to be positive for TEM1, with all sarcoma subtypes being represented[271,276].

Today, TEM1/endosialin is considered to be restricted to activated cells of the mesenchymal lineage, both during embryonic development and malignant growth[268,277,271,275]. For instance, in lymphoid tissues, pericytes and fibroblasts were found to express TEM1 during tissue development, but not in the adult, except for situations of intense tissue remodeling[278]. Moreover, TEM1 expression was detected during wound healing, where TEM1^{+} stromal cells were shown to promote angiogenesis and re-epithelialization[279]. In healthy adults, TEM1 expression is largely undetectable except for tissues with active angiogenesis, i.e. regenerating wound tissue, the corpus luteum and the stromal compartment of the endometrium[265,280,281]. Moreover, one study reported TEM1 expression on a subset of human, but not murine naïve CD8^{+} T cells, where it had an anti-proliferative effect[282]. Finally, TEM1 was detected on human mesenchymal stem cells in the bone marrow[283].

Besides cancer, TEM1 may play a role in fibrotic diseases, such as rheumatoid arthritis[284], chronic kidney disease[285], liver fibrosis[286] and idiopathic pulmonary fibrosis[287]. In these conditions, TEM1 seems to contribute to pathogenic processes, since TEM1 knock-out (KO) mice developed less severe fibrotic phenotypes, for instance reduced synovial hyperplasia and inflammation in models of rheumatoid arthritis[284]. This unique expression pattern makes TEM1 an oncofetal protein with potential both as a biomarker and as a therapeutic target.

1.3.3   Structure and function of TEM1

Structurally, TEM1 is a single-pass transmembrane protein of 757 amino acids with a predicted molecular mass of 80.9 kDa[267,288]. The large extracellular region consists of five separate domains, a c-type lectin domain followed by a sushi-like domain and three EGF repeats, and is separated from the membrane by a heavily O-glycosylated sialomucin stalk[288] (Fig. 1.9). The extensive post-translational glycosylation substantially increases the molecular weight from the predicted 80.9 kDa for the theoretical polypeptide to 165 kDa in the mature form[264]. Intracellularly, the short cytoplasmic domain contains a putative PDZ binding domain, which can act as adaptor molecule for the assembly of signaling complexes[284,289]. The N-terminal 360 residues bear sequence homology with thrombomodulin/CD141 (39 %) and the complement receptor C1qRp (33 %)[288], which may give some indications regarding the biological function of TEM1, which to date has not been fully elucidated.
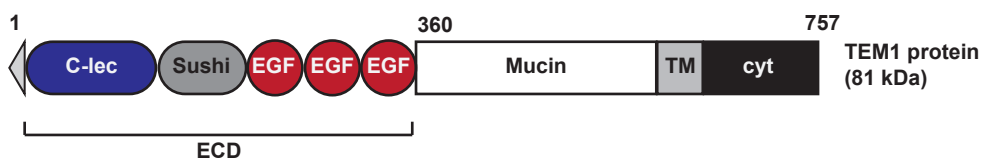
Figure 1.9. Domain structure of human TEM1/endosialin/CD248.
The extracellular domain (ECD) of TEM1 is composed of a c-type lectin domain (C-lec), a Sushi-like domain, and three epidermal growth factor (EGF) repeats. The ECD is extended from the membrane via a heavily O-glycosylated sialomucin stalk. TM, transmembrane domain; cyt, cytoplasmic domain. The N-terminal triangle represents the signal peptide. Figure adapted from Christian S. *J Biol Chem*, **276**(10), 7408–7414 (2001)[288].

However, its selective expression on pericytes and fibroblasts during active angiogenesis suggests a potential role in (tumor) angiogenesis. TEM1 KO animals develop normally, with no apparent defects in vascularization and wound healing[290]. However, while subcutaneous tumor growth was not affected by the lack of TEM1, orthotopically implanted tumors showed impaired tumor growth and reduced invasiveness in TEM1 KO mice[290]. These findings indicate that TEM1 might play a pro-tumorigenic role within an intact tumor microenvironment, possibly during tumor angiogenesis.

In line with this hypothesis, an increase in TEM1 expression was observed under hypoxia, mediated by the transcription factor HIF-2α (hypoxia-inducible factor)[291]. Confirmed binding partners of TEM1 encompass components of the ECM, such as collagen type I and IV, as well as fibronectin[292]. Consequently, TEM1 expression was shown to enhance cell adhesion to fibronectin and migration through matrigel[292]. In addition, TEM1 as well as CLEC14A and CD93, both expressed on endothelial cells, bind to Multimerin-2 (MMRN2), an endothelial selective ECM protein implicated in angiogenesis and tumor progression[293]. Recognizing distinct sites on MMRN2, CLEC14A and TEM1 can bind simultaneously at the interface between endothelium and pericytes and blocking of the CLEC14A – MMRN2 interaction had anti-angiogenic and anti-tumor effects[293]. These interactions indicate a role for TEM1 in the cross-talk between pericytes and endothelial cells, which communicate through the common basement membrane and via paracrine signaling to ensure the survival and maturation of blood vessels[294].

Platelet-derived growth factor receptor-β (PDGFR-β) signaling is crucial for the survival and proliferation of pericytes and is induced by PDGF-$\beta\beta$ secreted by endothelial cells. In the absence of TEM1, the pro-proliferative effect of PDGF-$\beta\beta$ is attenuated, despite intact PDGFR-β expression and autophosphorylation[295]. TEM1 might therefore influence signaling components downstream of PDGFR-β[295]. However, although the proliferation of pericytes is essential for sprouting angiogenesis, loss of endosialin did not have any significant impact on pericyte recruitment and vessel sprouting in the developing murine retina[296].

In the context of tumor progression, TEM1 was found to promote spontaneous metastasis[297]. Similar to previous findings, Viski and colleagues found no structural differences in the tumor stroma of wild-type vs. TEM1 KO mice. However, TEM1-expressing pericytes actively promoted tumor cell intravasation in a cell contact-dependent manner. Furthermore, they described a correlation of upregulated TEM1 in primary human breast cancer samples with increased metastatic potential and poorer survival[297].

Together, these findings suggest that TEM1 plays a role in pericyte – endothelial cell interaction and vascular patterning. In cancer, TEM1 acts as a pro-tumorigenic factor of the TME, facilitating metastatic dissemination and possibly tumor angiogenesis. Although further investigations are required to decipher the complex role of TEM1 under physiological and pathological conditions, both its expression pattern and potential pro-tumorigenic role make TEM1 an interesting target for therapeutic intervention.

1.3.4   TEM1 as a drug target

Based on the tumor-restricted expression pattern and frequency of TEM1 upregulation in the tumor stroma, a number of studies have started to explore TEM1 as a drug target in cancer.

A humanized monoclonal antibody targeting TEM1, ontuxizumab (MORAb-004), was shown to target TEM1 on pericytes, resulting in dysfunctional tumor microvasculature and impaired tumor growth[298]. Following these encouraging pre-clinical results, ontuxizumab has entered clinical evaluation. A first-in-human phase I

study in patients with treatment-refractory solid tumors revealed promising pharmacokinetics, preliminary anti-tumor activity and, importantly, a good safety profile[299]. Subsequently, a randomized, placebo-controlled phase II study confirmed that ontuxizumab is well tolerated, but generated no objective response in chemo-refractory metastatic colorectal cancer[300]. Similarly, efficacy as a single-agent was low in metastatic melanoma patients[301]. Lastly, ontuxizumab was evaluated for the treatment of pediatric solid tumors and soft tissue sarcoma, but showed no enhanced activity over chemotherapy[302,303].

In order to increase the therapeutic effect of TEM1-targeting with monoclonal antibodies, antibody-drug conjugates (ADC) are being explored as an alternative strategy. This class of therapeutics is manufactured by conjugating the antibody with two to four highly potent small molecule toxins, often targeting microtubules, using a covalent linker that is stable in plasma but cleaved once internalized. An anti-TEM1 ADC using monomethyl auristatin E (MMAE) demonstrated high specificity and durable anti-tumor efficacy in a pre-clinical model, as did another antibody conjugated to a duocarmycin derivative[304,305].

Besides ontuxizumab (MORAb-004), a fully human anti-TEM scFv binder, has been isolated from a human scFv library by yeast display and formatted as an scFv-Fc fusion protein[306]. The convenient human/murine cross-reactivity of this molecule, termed scFc78, has enabled bio-distribution studies evaluating both the specificity of the antibody and the feasibility of tumor imaging using TEM1 as a biomarker. These tumor imaging studies have revealed the potential of this molecule as a vascular tumor theranostic using radioactive conjugates, and as a tool for near-infrared imaging[307,308]. Moreover, scFc78 was used to further evaluate TEM1 expression in paraffin-embedded clinical sarcoma specimens, which confirmed TEM1 expression in 96 % of human sarcomas[309]. This study also demonstrated the potential of immunotoxin-based therapy for sarcoma using the scFv fragment fused to a protein toxin[309].

Finally, a proof-of-principle study evaluated the potential of TEM1 as a target antigen for cancer immunotherapy[310]. Specifically, TEM1 cDNA was fused to a minimal fragment of tetanus toxoid in order to vaccinate immunocompetent mice. Prophylactic vaccination elicited $CD8^+/CD4^+$ T cell responses and delayed tumor formation in different murine tumor models. Similarly, therapeutic vaccination led to reduced vascularity, increased tumor infiltration and T cell responses against TEM1 as well as other murine antigens, ultimately reducing the progression of established tumors. Importantly, physiological processes such as wound healing and reproduction were not impeded[310].

In summary, TEM1 is widely expressed during pathogenic neo-angiogenesis of various human cancers. Additionally, it represents an excellent tumor-associated antigen in human sarcoma, an often aggressive disease with limited therapeutic options. Furthermore, a number of pre-clinical and early clinical studies established the feasibility of therapeutic targeting of TEM1 without severe adverse effects. Therefore, TEM1 represents an interesting new target for cancer therapy, in particular using novel immunotherapeutic paradigms such as CARs and bispecific T cell engagers. Exploring the potential of immunotherapeutic targeting of TEM1 will be the main focus of this work, as presented in detail in the next section.

Aims and Objectives

This thesis originates at the interface of antibody discovery and cancer immunotherapy. It aims to accomplish the following four main objectives:

Exploring and validating the functional utility of SpyCatcher/SpyTag covalent fusion tag technology for *de novo* antibody discovery.

The production and purification of soluble recombinant antigen represents an early bottleneck in the isolation of antibody binders using *in vitro* library selection approaches such as phage display. Aiming to overcome this bottleneck and accelerate antibody discovery, chapter 2 presents the broad utility of the SpyCatcher/SpyTag covalent fusion system for the direct capture and immobilization of soluble antigens for phage display selection and screening procedures.

De novo discovery of novel fully human scFv binders targeting TEM1.

Building on the direct capture and immobilization technology described in chapter 2, chapter 3 focuses on the isolation and functional validation of novel fully human scFv binders targeting different epitopes on the extracellular domains of TEM1. The resulting diverse panel of scFv antibodies encompasses attractive candidates for the development of various therapeutic and diagnostic applications.

Redirecting human T cells towards TEM1-expressing target cells.

Due to its upregulation in the stroma and vasculature of many solid tumors and relative absence in healthy adult tissues, TEM1 has been discussed as an interesting tumor-associated antigen. Although several studies have proposed TEM1 as a cancer biomarker and target for antibody-drug conjugates, no T cell redirecting therapies aiming at TEM1 have been published to date. Therefore, employing the novel anti-TEM1 scFv binders described in chapter 3, chapter 4 presents a proof-of-concept for the immunotherapeutic targeting of TEM1, using both soluble T cell engagers and CAR-T cells. Moreover, the development and validation of a new trivalent T cell engager format, termed 'TriloBiTE', is highlighted.

Development of a phenotypic screening platform for the direct identification of functional CARs among large candidate libraries.

Both clinical efficacy and safety of CAR-T cell therapy strongly depend on the choice of targeting moiety for the synthetic immune receptor. In addition, clones that function as soluble antibodies do not always efficiently redirect T cells in the context of a CAR. Aiming to overcome this problem and bypass several labor-intensive screening steps in the typical CAR discovery cascade, we are working towards a powerful phenotypic screening strategy to select functional scFv binders directly in the CAR format. Progress in this direction is the topic of chapter 5.

Chapter 2   Integrating   SpyCatcher/SpyTag covalent fusion technology into phage display workflows for rapid antibody discovery.

ScFv clones isolated in this chapter appear in subsequent chapters under the following nomenclature: HS06, 1C1; HS07, 3B6; MS03, 2B11; HS201, 38B7; HS202, 40O3; P4, hP4.

Authors and affiliations:

Julie K. **Fierle**[1], Johan Abram-Saliba[1], Matteo Brioschi[1], Mariastella deTiani[1], George Coukos[1,2,3] and Steven M. Dunn[1,2]

[1] Ludwig Center for Cancer Research of the University of Lausanne, Lausanne, Switzerland.
[2] Department of Oncology, Hospital of the University of Lausanne (CHUV), Lausanne, Switzerland.
[3] Ovarian Cancer Research Center, Perelman School of Medicine, University of Pennsylvania, Philadelphia, USA.

Author contributions:

SMD, JKF and JAS conceived and designed the experiments. JKF, MdT, JAS, MB and SMD performed the experiments. JKF, JAS, MB, MdT and SMD analyzed the data. JKF, SMD and GC wrote/reviewed the manuscript.

2.1   Abstract

An early bottleneck in the rapid isolation of new antibody fragment binders using *in vitro* library approaches is the inertia encountered in acquiring and preparing soluble antigen fragments. In this report, we describe a simple, yet powerful strategy that exploits the properties of the SpyCatcher/SpyTag (SpyC/SpyT) covalent interaction to improve substantially the speed and efficiency in obtaining functional antibody clones of interest. We demonstrate that SpyC has broad utility as a protein-fusion tag partner in a eukaryotic expression/secretion context, retaining its functionality and permitting the direct, selective capture and immobilization of soluble antigen fusions using solid phase media coated with a synthetic modified SpyT peptide reagent. In addition, we show that the expressed SpyC-antigen format is highly compatible with downstream antibody phage display selection and screening procedures, requiring minimal post-expression handling with no sample modifications. To illustrate the potential of the approach, we have isolated several fully human germline scFvs that selectively recognize therapeutically relevant native cell surface tumor antigens in various *in vitro* cell-based assay contexts.

2.2   Introduction

Over the past 20 years display technologies have become established as robust and powerful approaches for the *in vitro* isolation of protein and nucleic acid-based ligands with utility for both clinical and non-clinical applications[311-313]. However, despite considerable advances in library construction and binder enrichment strategies, certain aspects of display-based discovery technologies remain inefficient and potentially rate limiting. Among these is the need to generate recombinant, functionally immobilized antigens or antigen-fragments to sustain the needs of multiple *in vitro* selection and screening activities. Usually, antigen material is provided chromatographically purified, often with oligo-histidine or IgG Fc affinity tags present. In this format, it can be passively adsorbed directly to plastic well or tube surfaces, or biotinylated to permit essentially stable binding to streptavidin-coated matrices. The latter allows for significantly greater flexibility with regard to selection procedures and for this reason is generally favored.

Biotinylation of antigens can be carried out using either chemical or enzyme-catalyzed approaches[314,315], however these procedures often require antigen-specific optimization and, together with the requirement for purified protein, represent a significant inertia for rapid and multiple-throughput library selection projects. Approaches to circumvent this bottleneck have sought to exploit the native prokaryotic biotinylation apparatus, such that fusion of antigens to the biotin carboxyl carrier protein (BCCP) or to minimal biotin acceptor peptides (BAPs) have become established approaches for the *in vivo* production of naturally biotinylated recombinant molecules in *E. coli*[316,317]. Eukaryotic cells co-transfected with both BAP-tagged antigens and bacterial biotin ligase (BirA), and supplied with exogenous biotin have likewise been shown to efficiently produce biotin-BAP-antigen fusions in both the cytosolic and secreted compartments[318-321].

Despite its apparent attraction for display technology workflows, *in vivo* biotinylation is still subject to certain process drawbacks. Key among these are variable and inconsistent levels of biotinylation, inefficient biotinylation of proteins secreted to the media from bacterial hosts, and the hydrophobic character of biotin which could, in principle, lead to a reduction in the solubility of certain proteins and promote undesirable aggregation.

Alternative possibilities for direct antigen production and capture are provided by the classical protein fusion tags such as glutathione *S*-transferase[322], carbohydrate polymer-binding proteins[323-325], and the Fc fragment of IgG[326,327]. However, although matrix-based purification (including bead capture) using these tag systems is well established, they each suffer from shortcomings and potential incompatibilities with library display and selection workflows. Common reported issues relate to the size of the tag itself (26 kDa for GST; 40 kDa for maltose binding protein, MBP; 50 kDa for dimerizing Fc) and to the aggregation of fusion proteins due to oxidation-induced oligomerization (GST)[328]. Similarly, certain engineered enzyme fusion tags, despite their potential for direct stable covalent capture via catalytic cycle trapping, are typically large (e.g. 34 kDa for Halotag7) which may explain why they have not been widely adopted for display technologies[19-21].

Decisions regarding the production of complex protein antigens can heavily influence the outcome of *in vitro* antibody and antibody-fragment discovery projects. Whereas reagent or 'tool' binders intended for use in denatured protein assays (e.g. immunoblots) can often be successfully isolated by using arrays of synthetic peptides, such molecules frequently fail to recognize native antigens on cells that generally present folded spatial or discontinuous surface epitopes rather than linear peptides. Reported strategies that seek to

produce antigens in a high-throughput generic manner often fail to replicate adequately the structural characteristics of many native antigens, often due to the absence of eukaryotic post-translational and/or redox modifications important for conformational folding and/or function[329]. In this regard, we opted to investigate the recently reported SpyCatcher/SpyTag (SpyC/SpyT) ligand pair, which, in common with Halotag, results in an irreversible covalent bond between the interacting partners[330,331]. Unlike Halotag however, SpyC/SpyT is a 'split' protein system which, following association, is stabilized via the formation of an unusual side-chain amide bond. The reaction is reported as being rapid and insensitive to media, buffer composition, detergents, pH, temperature, and oxidation status, and with no requirement for metal ion addition[331]. Additionally, the relatively small size of the SpyC domain (~12.5 kDa) could be considered advantageous for phage panning with a reduced likelihood of propagating tag-directed 'background' binders.

Here we report the utility of SpyC/SpyT as a convenient and robust capture tool for the acceleration of antibody fragment discovery by phage display.

2.3   Results

2.3.1   Preliminary evaluation of *E. coli* for the production and secretion of mammalian extracellular protein domains fused to Spycatcher

We initially sought to confirm that the CnaB2-derived SpyC domain could function as an effective C-terminal fusion partner under typical prokaryotic expression conditions and, importantly, that the desired fusions could be secreted to the media at levels sufficient to allow subsequent solid-phase capture and enrichment. To avoid potential steric interference between the upstream protein of interest and the SpyC tag, we chose to include the majority of the parental CnaB2 N-terminal amino acid sequence, and incorporated tandem epitope tags as an additional spacer moiety (pSTEVe6, Supplementary Fig. 2.1). For solid-phase immobilization, we synthesized a biotinylated minimal SpyT (bSpyT) peptide with an additional tetra-peptide 'linker' extension and a C-terminal lysine-biotin to allow a pre-coating of streptavidin-coated beads or plate wells (Fig. 2.1a).

As experimental test 'antigens' we first selected extracellular domain components (ECDs) of the human CD3 complex assembled in a single chain format, and a series of corresponding anti-CD3 scFv antibody fragments. CD3-SpyC fusions, expressed and secreted by *E. coli* TG1 cells, could be captured specifically on bSpyT-loaded streptavidin coated beads and plate wells (Supplementary Fig. 2.1). Importantly, soluble CD3$\varepsilon\delta$ and CD3$\varepsilon\gamma$ SpyC-fusions were bound by UCHT1, an anti-CD3 mAb known to interact with a non-conserved epitope found only in CD3 heterodimers and not in misfolded or monomeric CD3ε (Supplementary Fig. 2.1)[332,333]. Similarly, the anti-CD3 scFv-SpyC fusions, expressed and captured on a bSpyT-coated surface, were shown to retain their expected T cell activating functionality (Supplementary Fig. 2.1).

Collectively, these observations suggested that the direct capture and immobilization (dCI) of SpyC-protein fusions from clarified bacterial media is efficient and that fused antigens can retain their functional structure.
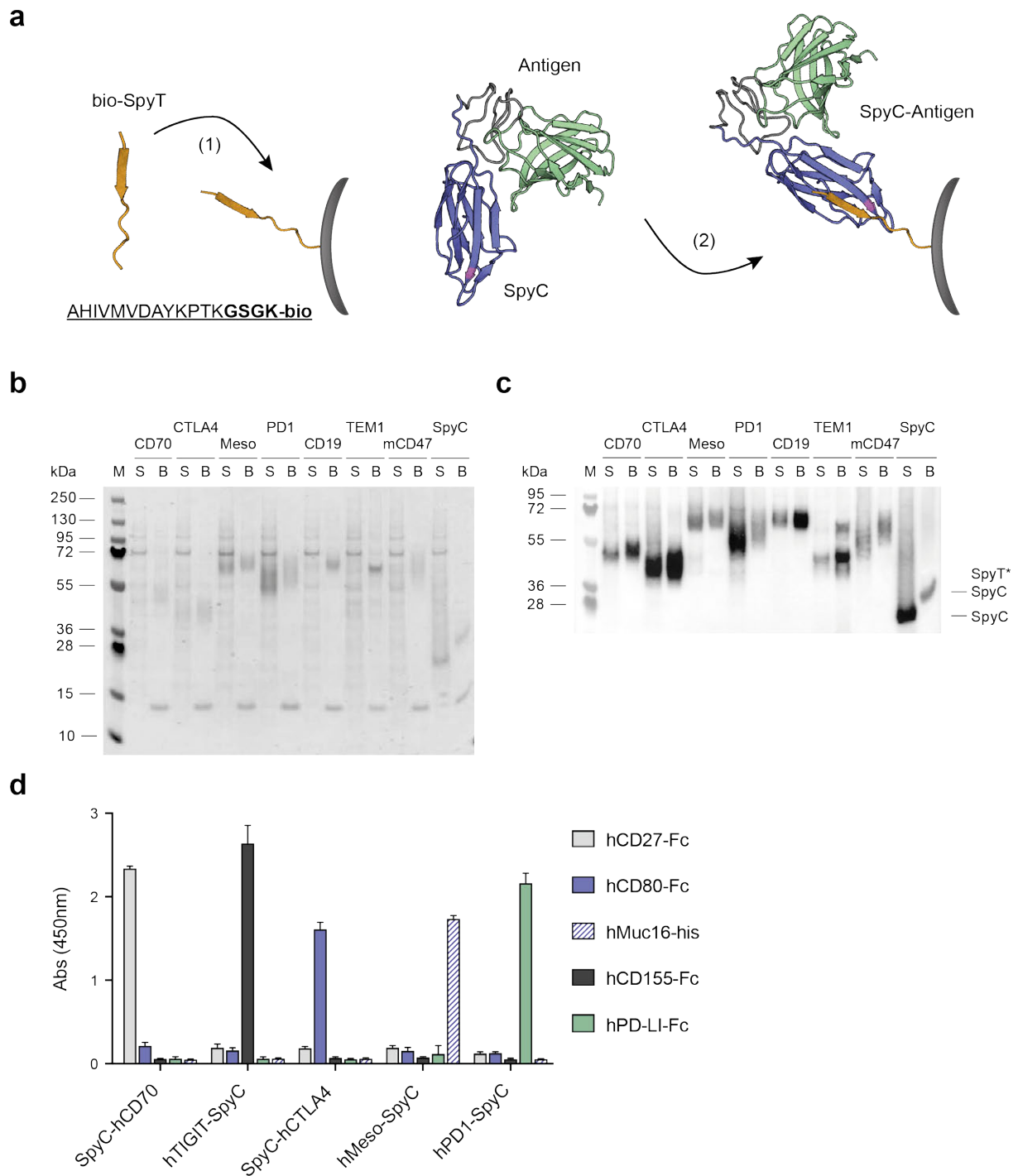
Figure 2.1. Production and functional evaluation of mammalian extracellular antigen-SpyCatcher fusions.

(**a**) Schematic representation of the direct capture and immobilization (dCI) of SpyC-antigens via surface-bound bio-SpyT. (**b, c**) Mammalian cell expression and direct capture of representative SpyC-antigen fusions (see Table 2.1) on bSpyT-loaded magnetic beads. (**b**) Coomassie-stained SDS-PAGE (reducing). The insert-less pSTEVe49 vector cassette expresses the free HA-tagged SpyC (far right). (**c**) Anti-HA tag ECL Western staining of recombinant SpyC-antigens expressed in HEK culture supernatants ('S'), and following selective covalent enrichment on SpyT beads ('B'). Covalent immobilization to SpyT on the beads results in a shift to a higher MW corresponding to the mass of the peptide adduct. Samples were run on separate gels and interspersed with irrelevant samples, but were processed in parallel. Full-length gel and blot images can be found in Supplementary Figure 2.2. (**d**) ELISA illustrating functional recognition of selected immobilized dCI SpyC-antigens by cognate recombinant ligands.

Antigen ECD	Key Architecture	PTM	MW/pI	Vector	Expression	Capture
SpyC	β; FBR; IgS	-	12.5/4.6	e49	✓	✓
CD3εδ	β; IgC	2 N-gly (δ)	21.5/4.6	e20	✓	✓
CD3γε	β; IgC	2 N-gly (γ)	22.7/5.0	e20	✓	✓
EpCAM	α/β; Thy1	3 N-gly	27.3/5.6	e38	✓	x
				e49	✓	✓
TEM8	α/β; VWFA	3 N-gly	33.1/5.4	e38	✓	x
TEM8 (*nSP*/cΔ)	α/β; VWFA	2 N-gly	23.3/5.3	e38	✓	✓
TEM1 (cΔ)	α/β; CTL; Sus; EGFLc	~4 O-gly	37.6/4.6	e20	✓	✓
TEM1 (cΔ) *	α/β; CTL; Sus; EGFLc	~9 O-gly	49.4/4.6	e20	✓	✓
TEM1 (nΔ)	Mucin-like domain	~15 O-gly	14.0/7.2	e49	✓	✓
CEACAM1	β; IgV, IgC	~20 N-gly	31.8/4.7	e38	✓	✓
CEACAM5 (CEA)	β; IgV, IgC	~28 N-gly	32.3/5.6	e38	✓	✓
CEACAM6	β; IgV, IgC	~12 N-gly	31.4/5.1	e38	✓	✓
CD70	β/coil ‡; TNF-L	2 N-gly	17.4/8.9	e38	✓ (weak)	✓ (weak)
				e49	✓	✓
Mesothelin	α; ATR	3 N-gly	34.3/5.0	e38	✓	✓
ROR1	β/coil ‡; IgC; Krn; Frz	4 N-gly	42.5/5.4	e38	✓	✓
ROR2	β/coil ‡; IgC, Krn, Frz	3 N-gly	41.5/6.2	e38	x	x
TNFR2	β/coil; tnfr-cr	4 O-,2 N-gly	25.3/7.0	e38	✓	✓
CD19	β/coil; IgC	5 N-gly	29.8/7.2	e38	x	x
				e49	✓	✓
BCMA	β/turn; tnfr-cr		5.9/7.6	e38	✓	✓
CTLA4	β; IgV	2 N-gly	13.5/4.6	e38	✓	✓
				e49	✓	✓
PD1	β; IgV	4 N-gly	16.3/8.8	e38	✓	✓
Tigit	β; IgV	2 N-gly	13.2/4.8	e38	✓	✓
TIM3	β; IgV	1 O-,1 N-gly	20.2/6.6	e38	✓	✓
TIM1	β; IgV; mucin stalk	x O-,4 N-gly	29.1/7.0	e38	✓ (*Het*)	✓ (*Het*)
				e49	✓ (*Het*)	✓ (*Het*)
HER2-CTF611	N/A (peptide)	1 N-gly	4.7/4.4	e38	✓	✓
PSMA	α/β; PA; pM28	10 N-gly	79.5/6.4	e49	x	x
SIRPα	β; IgV		12.9/8.0	e38	✓	✓
SIRPα *	β; IgV	2 N-gly	12.9/9.0	e38	✓	✓
CD47	β; IgV	5 N-gly	13.5/5.4	e20	x	x
				e38	✓	*NT*
CD47 *	β; IgV	6 N-gly	13.7/5.1	e20	✓	✓
FRα			25.1/8.3	e38	✓ (weak)	x
LAG-3	β; IgV, IgC		46.1/9.5	e38	✓ (weak)	x
EGFRvIII	β; RLD; FL; GFR4	8 N-gly	38.3/6.5	e38	✓	✓

Table 2.1. Antigen ECD fragments evaluated as SpyC fusions and selected physical characteristics.

Unless otherwise indicated, the recombinant ECDs are human and terminate proximal to a TM domain/GPI anchor. Indicated *potential* post-translational modifications are derived from curated UniprotKB features and predictive O-glycosylation tools (NetOGlyc 4.0 Server).[334] Fusions were assessed for both expression and bead-capture by SDS-PAGE and anti-HA tag ECL Western blotting. Domain folds and motifs: FBR, fibronectin binding repeat; IgS, Ig-superfamily; thy1, thyroglobulin-like type 1; IgV, Ig-like V-type; IgC, Ig-like C2-type; VWFA, Von Willebrand factor type A; CTL, C-type lectin-like; Sus, Sushi; EGFLc, EGF-like calcium binding; ATR, ARM-type repeats; Krn, kringle; Frz, Frizzled; TNF-L, Tumor Necrosis Factor-like; tnfr-cr, TNFR cysteine rich repeats; PA, protease associated; pM28, peptidase M28; RLD, Receptor L-domain; FL, furin-like cysteine-rich; GFR4, growth factor receptor 4 domain. * murine sequence; ‡ prediction by PSIPRED v3.3; *nSP*, native signal peptide; cΔ, ECD truncation with C-terminal (membrane proximal) deletion; nΔ, ECD truncation with N-terminal (membrane distal) deletion; *Het*, expression and/or capture product appears very heterogeneous by SDS-PAGE; *NT*, not tested.

2.3.2 Pipeline production of SpyC-antigens for antibody phage display using a small-scale mammalian expression system

Following our validation studies in *E. coli*, we next constructed vector cassettes (pSTEVe20/38/49; Supplementary Fig. 2.1) appropriate for use in a mammalian transient expression system based on the HEK293-6E host cell line. We selected a diverse test panel of mammalian membrane protein ECD fragments representing established and prospective therapeutic target antigens for solid and hematological malignancies, and differing in size, charge and structural complexity (Table 2.1). Antigens were fused N- or C-terminally to SpyC and targeted to the secretory pathway by appending to a common synthetic signal peptide. From SDS-PAGE and Western blotting of supernatants from 2 ml cultures we were able to show that 30 of the 32 antigen fragments (93 %) could be expressed as fusions and secreted, and that of these, 26 (81 %) could be directly captured from media supernatants on bSpyT-loaded magnetic beads for subsequent phage display experiments (Table 2.1, Fig. 2.1b, c, d and Supplementary Fig. 2.1). Encouragingly, a sub-panel of dCI SpyC-fused antigens were shown to retain specific recognition for their well-described physiologically relevant ligands (Fig. 2.1d), confirming that SpyC-fusions, expressed and secreted from mammalian host cell lines, can retain native structural characteristics.

2.3.3 dCI SpyC-fusion antigens represent suitable targets for scFv antibody discovery by phage display

We next sought to evaluate how dCI SpyC-fusion antigens performed in scFv phage display experiments alongside a classical purified antigen. We therefore expressed an ECD fragment of human tumor endothelial marker 1 (TEM1, CD248, Endosialin; N-terminal mature 353 residues) in HEK cells and purified the protein by Ni-NTA chromatography. The protein was subsequently biotinylated enzymatically, quality-controlled by band-shift gel assay, and dialyzed into PBS prior to its immobilization onto streptavidin magnetic beads. In parallel, we produced SpyC fusions in HEK cell culture media for dCI using truncated h/mTEM1 ECDs (N-terminal mature 353 and 460 residues respectively). Using large, fully human and essentially germline naïve scFv libraries (CHV101_DMκ and CHV101_DMλ), we applied two rounds of phage display selection against the three bead-immobilized antigens. An examination of selection metrics (Table 2.2) suggested strong enrichment for binders at round 2 using both antigen formats, resulting in significant ELISA-positive hit frequencies for both lambda and kappa libraries. Random sequencing of only modest numbers of re-arrayed hits (30 for the combined h/mTEM1-SpyC panel and 41 for the hTEM1-bio) revealed considerable clonal diversity within the h/mTEM1-SpyC panel with ~83 % of clones being represented by a unique sequence. This compares favorably with the number of 'uniques' identified from the hTEM1-bio sequencing (~90 %, data not shown). Interestingly, three of these clone sequences (Fig. 2.2) were also found to occur in the hTEM1-bio panel, suggesting that the two antigen formats present shared or equivalent epitopes. Further, all hit clones emerging from the dCI TEM1-SpyC outputs also recognized the corresponding full length ECDs of human and mouse TEM1 (668 and 680 mature ECD residues respectively) that were produced in a rodent cell line (CHO) and purified via Ni-NTA chromatography. Importantly, the relative binding activities of these clones towards the human and murine TEM1-SpyC antigens appeared to be broadly conserved for the corresponding classically produced antigens (Fig. 2.2). Taken together, the data demonstrates that an arbitrary selection of diverse unique hit clones isolated by panning against SpyC-formatted TEM1 antigens can recognise TEM1 produced and purified using traditional procedures, implying that a substantial level of structural 'equivalence' is preserved between the SpyC-fusion and traditional antigen formats.

	LIBRARY	hTEM1-bio		hTEM1-SpyC		mTEM1-SpyC	
		λ	κ	λ	κ	λ	κ
R1	Input (phage; CFU)	7.4×10^{12}	5.3×10^{12}	7.4×10^{12}	5.3×10^{12}	7.4×10^{12}	5.3×10^{12}
	Output (CFU)	1.4×10^{6}	1.1×10^{6}	5.6×10^{5}	6.3×10^{5}	4.4×10^{5}	3.2×10^{5}
R2	Input (phage; CFU)	1.6×10^{11}	1.2×10^{11}	1.2×10^{11}	1.4×10^{11}	2.4×10^{11}	1.9×10^{11}
	Output (CFU)	2.3×10^{9}	1.7×10^{9}	3.0×10^{9}	2.6×10^{9}	5.3×10^{9}	4.1×10^{9}
	*Enrichment Factor**	**7.6×10^{4}**	**6.8×10^{4}**	**3.3×10^{5}**	**1.6×10^{5}**	**3.7×10^{5}**	**3.6×10^{5}**
R2	ELISA hit rate (%)[‡]	43	25	56	42	68	44

Table 2.2. Panning metrics and hit-rates of phage display selections against TEM1.

R1 and R2 input and output panning metrics illustrating respective library enrichments and primary ELISA hit-rates for both TEM1-bio and TEM1-SpyC antigens. CFU, colony-forming units; * (R2 Output/Input)/(R1 output/input), [‡] signal threshold > 5x background.

Clone ID	Panning antigen	# Seqs[†]	ELISA antigen				Library
			hTEM1 (SpyC)	mTEM1 (SpyC)	hTEM1 (L)	mTEM1 (L)	
HS01	hTEM1-SpyC	1					λ
HS02	hTEM1-SpyC	1					λ
HS03	hTEM1-SpyC	1					λ
HS04	hTEM1-SpyC	1					λ
HS05	**hTEM1-SpyC**	**1**					λ
HS06	**hTEM1-SpyC**	**1**					λ
(HB01)	*hTEM1-bio*	*1*					λ
HS07	hTEM1-SpyC	1					κ
HS08	hTEM1-SpyC	1					κ
HS09	hTEM1-SpyC	1					κ
HS10	**hTEM1-SpyC**	**2**					κ
HS11	**hTEM1-SpyC**	**1**					κ
(HB02)	*hTEM1-bio*	*1*					κ
HS12	hTEM1-SpyC	1					κ
MS01	mTEM1-SpyC	1					κ
MS02	mTEM1-SpyC	3					λ
MS03	**mTEM1-SpyC**	**3**					λ
(HB03)	*hTEM1-bio*	*1*					λ
MS04	mTEM1-SpyC	1					λ
MS05	mTEM1-SpyC	1					λ
MS06	mTEM1-SpyC	1					λ
MS07	mTEM1-SpyC	1					λ
MS08	mTEM1-SpyC	1					λ
MS09	mTEM1-SpyC	1					κ
MS10	mTEM1-SpyC	1					κ
MS11	mTEM1-SpyC	1					κ
MS12	mTEM1-SpyC	1					κ
MS13	mTEM1-SpyC	1					κ

Figure 2.2. Phage display versus TEM1 antigen format.

Raw ELISA profiling data for 30 randomly selected scFv hit clones isolated from the dCl h/mTEM1-SpyC antigen panning experiments. Bar length reflects the relative ELISA signal strengths for human and murine TEM1-SpyC and recombinant, CHO-cell derived and purified TEM1 full-length ECD antigens (L). ELISAs were conducted separately and independently for the TEM1-SpyC and TEM1 (L) antigens. Identical clone sequences obtained from 21 randomly picked hTEM1-bio R2 ELISA hits are shaded. SpyC antigens were captured via dCl on prepared streptavidin-bSpyT plate well surfaces whereas purified recombinant TEM1 (L) was immobilized on plate wells by passive adsorption.

Importantly, very few enriched clones were found to recognize the SpyC domain (<5 % of screened clones isolated against h/mTEM1) indicating that, despite being of bacterial origin, the small SpyC domain does not appear to be excessively immuno-dominant when using naïve, native content antibody libraries. Supplementary Table 2.1 summarizes the frequencies of clones binding isolated SpyC in screened outputs from several SpyC-fusion phage panning experiments conducted without active SpyC deselection (i.e. subtraction).

In addition to traditional plate-based ELISA screening, we also employed crude SpyC-antigen supernatants in bead-based multiplexed assays with the aim of acquiring higher information content for selection outputs. Fluorescently barcoded streptavidin bead multiplexes, pre-loaded with four to six distinct dCI SpyC antigens were used to screen phage display output clone supernatants for specific and/or cross-reactive antigen binding. By incorporating the dCI methodology into a 'no wash' direct read 384-well protocol on an iQue Screener Plus instrument (IntelliCyte), we were able to greatly accelerate primary output specificity screening (Supplementary Fig. 2.3). Furthermore, we were able to use this approach to successfully identify improved affinity matured clone sequences enriched against the same cognate dCI SpyC-antigen in a high-stringency phage display selection experiment (Supplementary Fig. 2.3).

2.3.4 Secreted SpyC-antigen fusions support the isolation of scFvs that recognize native endogenous cell epitopes and have downstream functional utility

To investigate whether scFvs isolated against dCI SpyC-fusions could recognize endogenous cognate antigens on appropriate target cells, we reformatted three representative anti-TEM1 clones as scFv-Fc (IgG1) fusions alongside a previously described anti-TEM1 antibody, sc78[335]. All of the clones expressed well in our transient HEK293-6E system (100-200 mg/l) and, following purification by Protein A affinity chromatography, all antibodies were seen to stain HEK293T cells transfected with full-length hTEM1, as well as several cell lines previously established as positive for endogenous TEM1, but not lines negative for TEM1 (Fig. 2.3a). One clone, HS06, showed clear preference for recognition of the human A673 and SK-N-AS TEM1+ lines with significantly reduced binding to the 2H11 and TC1 TEM1+ murine lines. During downstream characterization of HS06, we were also able to confirm that SpyC fusions have convenient and practical utility for affinity determination using surface plasmon resonance (SPR). The simple addition of free bSpyT peptide to crude HEK expression supernatant containing secreted hTEM1-SpyC, followed by rapid buffer exchange via spin column, allowed the efficient capture of the resultant covalent complex on a streptavidin-coupled Biacore chip. Rapid single-cycle kinetic binding data obtained for purified monovalent H06 scFv yielded a modest double-digit nanomolar affinity (Fig. 2.3b), characteristic of many antibody clones isolated from natural germline repertoires that have not undergone somatic hyper-mutation and clonal expansion. Encouragingly, reference KD data obtained using a commonly employed anti-Fc capture step to immobilize HS06 scFv-Fc as the 'ligand', a full-length (FL) recombinant hTEM1 ECD 'analyte', and multi-cycle kinetics, were shown to be comparable (Supplementary Fig. 2.4). To explore whether primary scFv hits arising from SpyC-fusion panning were suitable for subsequent entry into classical lead optimization experiments, we mutated the HS06 scFv by error-prone PCR to generate a library of ~10^9 variants and panned this library sequentially against both immobilized mTEM1-bio and hTEM1-bio in order to select for increased-affinity variants with h/mTEM1 cross-reactivity. A strongly enriching clone (HS06mut) containing a single VH CDR3 amino acid substitution was recovered and its affinity determined using both hTEM1-SpyC and purified full-length hTEM1 ECD.

a

TEM1 binding (anti-Fc-Alexa647)

b

HS06_VH_CDR3

CASL**T**SYYGDPTGFDYW

$K_D \approx 68$ nM

HS06mut_VH_CDR3

CASL**I**SYYGDPTGFDYW

$K_D \approx 1$ nM

time (sec)

c

time (sec)
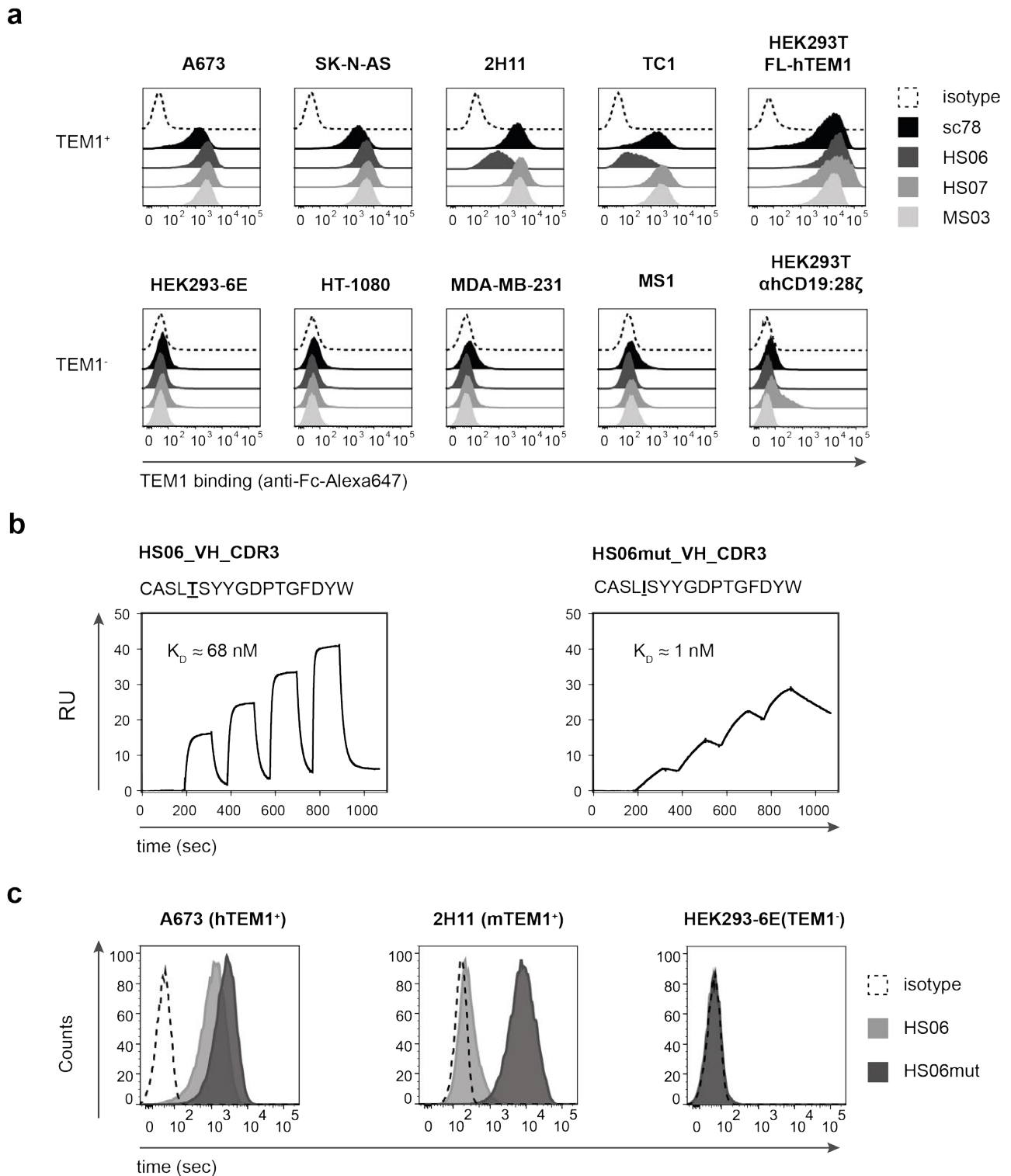
Figure 2.3. Characterization of anti-TEM1 clones isolated by dCl SpyC-antigen selection.

(**a**) Binding of reformatted and purified scFv-Fc (hIgG1) clones (2 μg/ml) to human and murine cell lines. A673, human Ewing's sarcoma; SK-N-AS, human neuroblastoma; 2H11, murine tumor vascular endothelium; TC1, murine lung adenocarcinoma; HEK293-6E, human embryonic kidney; HT-1080, human fibrosarcoma; MDA-MB-231, human mammary carcinoma; MS1, murine pancreatic islet endothelium. Additionally, binding of anti-TEM1 scFv-Fc clones to HEK293T cells transiently transfected with native FL-hTEM1 and an irrelevant surface protein (αhCD19:28ζ CAR) control is also shown. (**b**) SPR monovalent affinity determination of parental clone HS06 (left) and an affinity-matured variant, HS06mut (right). hTEM1-SpyC has been used as the immobilized ligand and monovalent HS06/HS06mut monovalent BiTE as the soluble analyte, with concentration ranges of 100, 50, 25, 12.5 and 0 nM for HS06, and 5, 2.5, 1.25, 0.625 and 0 nM for HS06mut. (**c**) Binding of HS06mut variant scFv-Fc (0.1 μg/ml) to endogenous human (A673) and murine (2H11) TEM1+ cell lines.

Remarkably, this single point mutation was shown not only to confer a ~70 to 80-fold improvement in raw KD towards human TEM1 in both formats (Fig. 2.3b and Supplementary Fig. 2.4), but also to possess appreciable cross-reactivity to mTEM1 (Fig. 2.3c). Taken together, our data validates TEM1-SpyC as a flexible reagent for the isolation and early characterization of functional anti-TEM1 molecules using highly streamlined dCI methodology.

We subsequently sought to demonstrate that SpyC-fusion antigens would be suitable for more challenging discovery projects; for example, the isolation of scFvs intended to neutralize specific receptor-ligand interactions. To investigate this, we chose the murine signal regulatory protein alpha (SIRPα):CD47 interaction as a test case. After confirming the correct folding and efficient capture of the mCD47 ECD SpyC-fusion, we panned the libraries against bead-captured mCD47-SpyC and then screened the resultant binder clones by dCI competition ELISA to identify scFvs that specifically blocked the interaction between dCI mCD47-SpyC and an Fc-fused version of the CD47 ligand, SIRPα. Encouragingly, scFv clones with neutralizing activity could be readily isolated from the CHV101_DM libraries and, following reformatting to murine IgG2a, a representative candidate (MS115) was further characterized alongside two neutralizing rodent hybridoma mAbs[336]. Clone MS115 was shown to compete effectively with the binding of SIRPα for CD47-SpyC and to retain its neutralization activity using a His-tagged and purified mCD47 antigen sourced from a commercial vendor (Supplementary Fig. 2.5). Critically, MS115 recognized endogenous mCD47 present on a murine tumor cell line but did not stain the corresponding knock-out (Supplementary Fig. 2.5). Hence, dCI SpyC-antigen selection and screening is compatible with the rapid isolation of target-selective neutralizing antibodies.

2.3.5 dCI SpyC-antigens are suitable targets for the selection of functional scFv warheads for immunotherapy applications

Aside from classical antibody targeting applications, scFv 'warheads' have also demonstrated considerable utility in recruiting and re-directing the exquisitely potent killing functions of cytotoxic T cells towards tumor-associated cell-surface targets. The two principle therapeutic paradigms, namely chimeric antigen receptors (CARs) and soluble bispecific 'engagers', both facilitate T cell-mediated killing by 'bridging' target and T effector cells followed by the transmission of activation signals from intracellular CD3 and co-receptor signaling components. We therefore sought to evaluate the utility of the dCI SpyC-antigen format for the rapid discovery of functional CAR scFv 'warhead' panels. To this end, we chose the mature ECD of human mesothelin as a relevant immunotherapeutic target[337,338]. Following panning of the CHV101_DM libraries against dCI mesothelin-SpyC, and the subsequent identification of binder clones in both dCI mesothelin-SpyC primary ELISA and secondary flow cytometry assays, six scFvs of interest were reformatted into a generic 2nd generation CAR comprising a CD28 spacer, transmembrane (TM) domain and cytosolic domain fused to CD3ζ immunoreceptor tyrosine-based activation motif (ITAM) signaling elements. The resultant CAR panel was transfected into an engineered Jurkat reporter cell line to assess CAR-mediated NFAT activation in response to target cell lines known to express endogenous cell surface mesothelin. All six clones were shown to trigger a strong induction of CD3 ITAM-mediated NFAT signaling in the presence of mesothelin-expressing H-226 tumor cells (Fig. 2.4a). The magnitude of these signals compared favorably with those observed for a control CAR armed with the clinically validated murine anti-CD19 FMC63 scFv in the presence of CD19-expressing Raji cells, and with a published anti-mesothelin human scFv (P4)[339,340].

a
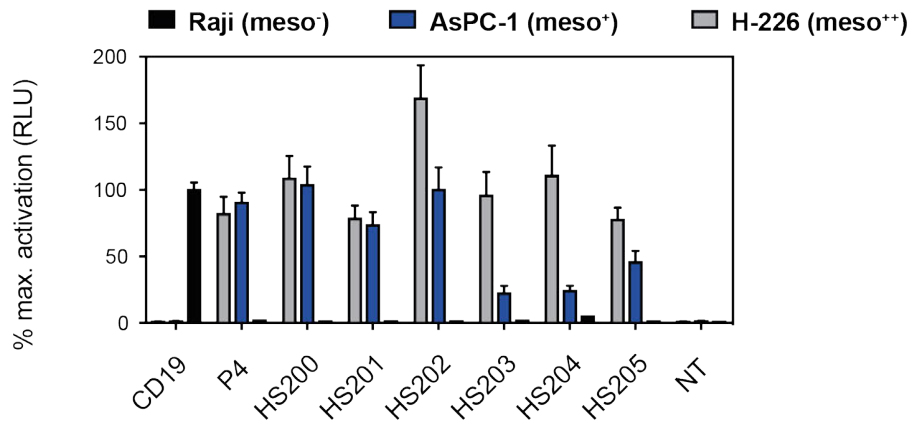
b
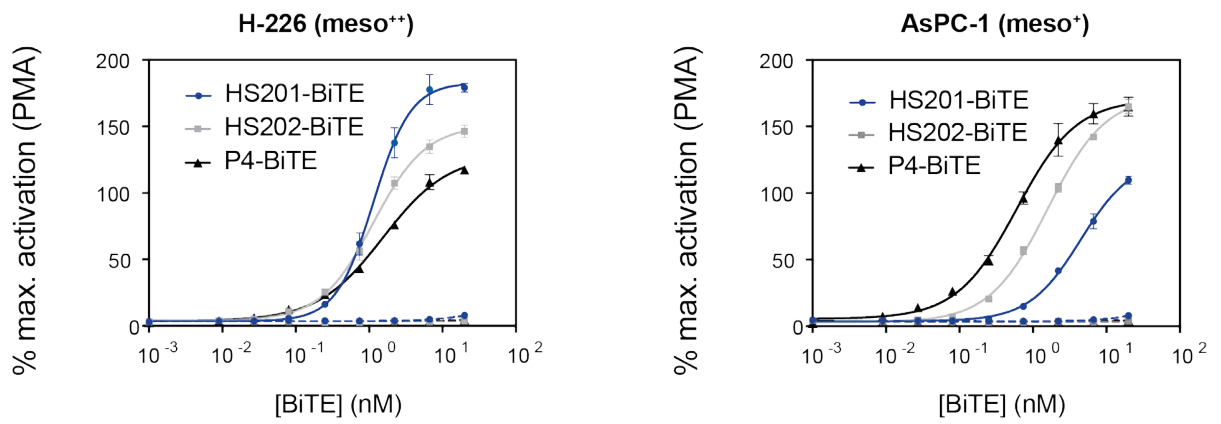
c
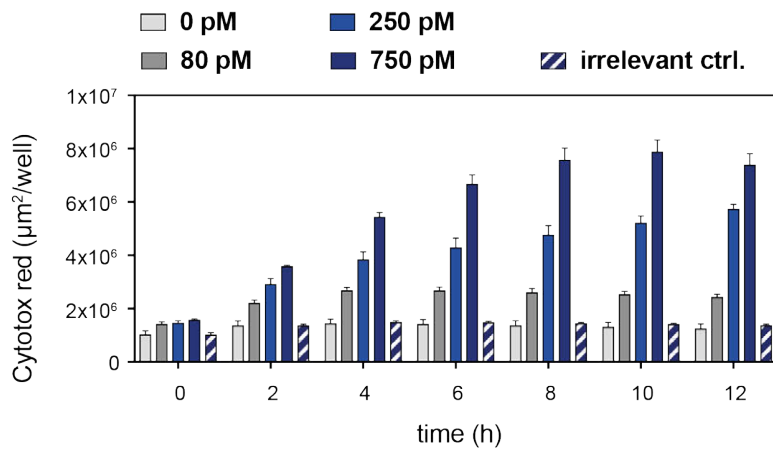
d
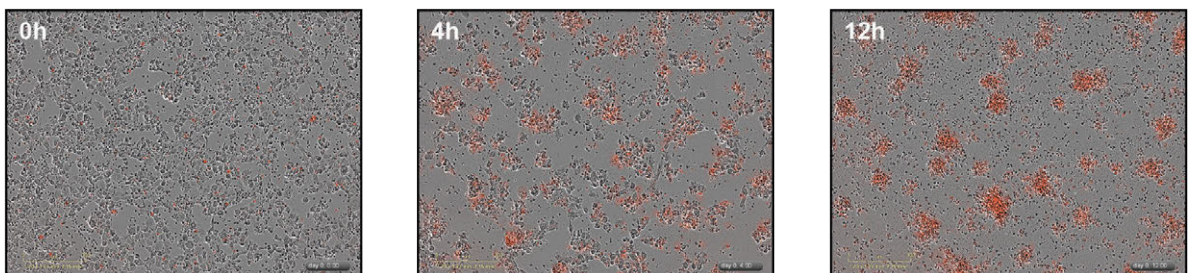
Figure 2.4. Functional target cell engagement by anti-mesothelin scFvs isolated from dCI selection experiments.

(a) Induction of NFAT-driven expression of luciferase in Jurkat reporter cells transduced with anti-mesothelin CARs employing different scFv clones. Luciferase activity was measured after 24h of co-culture with mesothelin expressing target cells (H-226, AsPC-1) or meso-negative Raji B cells. CD19 and P4 CARs are included as positive controls for CD19 and mesothelin respectively. NT, non-transformed control. (b) Induction of NFAT-driven expression of luciferase in Jurkat reporter cells in the presence of H-226 (left), and AsPC-1 (right) target cells and soluble T cell engagers. Dashed lines represent baseline stimulation in the presence of engager molecule and HEK293-6E mesothelin-negative cells. (c) Mesothelin specific T cell engager constructed from clone HS201 redirects primary human CD8+ T cells to kill H-226 tumor target cells. Image-based acquisition of Cytotox Red fluorescence reports the extent and real-time kinetics of killing. Baseline killing was determined against irrelevant meso-negative A673 cells using 750 pM engager. (d) Time-dependent killing of H-226 cells in the presence of 2nM HS201 engager by primary human T cells (Pan-T purified; 14 days post isolation). Dead cell clusters emit red fluorescence.

In the presence of AsPC-1 tumor cells, which are known to express lower levels of surface mesothelin, three of the six clones yielded substantially less NFAT reporter activation, probably reflecting the relatively modest monovalent affinities of these primary non-optimized scFv binders (data not shown).

To explore further the potential of the anti-mesothelin clones originating from the SpyC dCI selections, we constructed soluble T cell engagers from two of the novel scFvs showing promising CAR signaling activity, together with P4. Unlike classical BiTEs which employ two monovalent scFvs linked in tandem[203], our final molecules were bivalent for the anti-mesothelin warheads and monovalent for a humanized anti-CD3. Similar to the CAR format, the three resulting T cell engagers were shown to trigger potent NFAT-mediated activation of the Jurkat reporter line in a cell target and dose-dependent manner (Fig. 2.4b). Interestingly, while the HS201 and HS202 clone engagers displayed similar activation kinetics to the P4 benchmark clone against H-226 meso-high cells, clear differences in sensitivity were evident against meso-moderate AsPC-1 cells, with the HS201 engager being the most discriminatory. Extending the study to cell killing confirmed that this experimental T cell engager molecule could efficiently redirect primary human T cells to kill H-226 tumor cells *in vitro* in a time and concentration dependent manner (Fig. 2.4c, d). Collectively, the results indicate that our dCI procedure using small scale, SpyC-fusion supernatants can be employed successfully for the rapid and cost-effective isolation of functional scFv 'warheads' for a range of potential applications, including cancer immunotherapy.

2.4   Discussion

In the current study, we sought to develop a minimal, cost-effective and generic solution to native mammalian cell-surface antigen production that could be easily integrated into a typical scFv antibody phage-display discovery workflow. With this in mind, we decided to evaluate the reportedly robust and irreversibly associating SpyC/SpyT ligand pair in combination with a widely used human cell-line protein production host using modular episomal expression vector tools.

To-date, the SpyC/SpyT interaction has been reported principally in the context of defined molecular assembly and imaging applications[341-344,345]. Following the elucidation of the original 2-component system, the inventors further engineered the SpyC module to function as an effective uncoupled peptide ligase for head-to-tail oligomerization of proteins of interest tagged with both SpyT and a partner peptide (SpyK) containing the corresponding reactive lysine[346]. However, to the best of our knowledge, the evaluation of

SpyC/SpyT as a practical tool for antibody phage display-based molecular discovery applications has so far not been reported.

In this work, we synthesized chemically a SpyT peptide with a biotin handle to allow the controlled pre-coating of immobilized streptavidin matrices with a high molar density of SpyT ligand to favor avid surface capture of SpyC-fusion proteins present in crude media supernatants. Although more cost-effective and efficient than expressing and purifying large stocks of recombinant biotinylated SpyC protein, a principle concern was that the use of the larger bacterial SpyC component for the antigen fusion partner would prove incompatible with efficient expression and/or secretion from cellular hosts. However, we observed that a codon-optimized SpyC sequence preceded by an immunoglobulin signal peptide was exported efficiently by HEK293-6E cells. Our subsequent findings confirm that the SpyC module tolerates fusion to many diverse mammalian cell-surface extracellular fragments/domains, and retains its functional integrity (as shown by efficient and selective capture on SpyT-surfaces) following its secretion by HEK293 cells in either an N- or C-terminal fusion orientation (Fig. 2.1 and Table 2.1). By employing an optimized transient transfection protocol and a high-productivity HEK293 cell line, sufficient SpyC-antigen fusion material can be generated from small culture volumes to support multiple parallel and diverse discovery activities comprising several dCI selection and screening rounds.

Interestingly, our broader observations demonstrate that even poorly expressing fusions can yield successful outcomes. For example, the secreted concentration of murine CD47-SpyC was estimated by ECL-Western analysis to be in the region of only 1 μg/ml and below our limit of detection for visible SDS-PAGE dye staining in crude expression media. However, SpyT-bead enrichment from 2 ml of media proved adequate for efficient and robust phage-display clone enrichment, mirroring the selection performance of SpyC-antigens expressing at far higher levels and allowing the isolation of functional clones (Supplementary Fig. 2.5).

Collectively, our scFv phage display screening data gathered to-date suggests that the bacterial SpyC tag sequence is only modestly immunogenic as a fusion partner using our IgM/IgD-derived libraries — even in the absence of a typical solid-phase deselection step (Supplementary Table 2.1). Conveniently, SpyC has an additional advantage for display applications in that a single point mutation destroys its capability to form the covalent iso-peptide bond with SpyT[331]. Hence, purified SpyC(mut) can presumably be employed as an effective soluble library subtraction reagent or can be exploited in its fusion form as a soluble competitor during off-rate selections.

In principle, we would anticipate that SpyC/SpyT dCI methodology could be readily integrated into any binder discovery platform that employs a solid-phase capture for enrichment, for example ribosome display, as well as phage display using non-immunoglobulin or synthetic library scaffolds. It could also be adapted for approaches that enrich for binders using flow cytometry-based sorting of particles, for example yeast, mammalian, bacterial and aptamer particle display technologies. For these cases, SpyC-antigen expression supernatants could be directly 'charged' with synthetic SpyT conjugates containing either biotin or appropriate bright dye adducts prior to incubation with library particles and sorting. Finally, the direct interfacing of dCI from small-scale cultures with automated magnetic bead handling would support applications requiring high-throughput scaling of selections[347].

In conclusion, we have extensively tested the practical utility of SpyC/SpyT and shown it to be an attractive and convenient tagging/immobilization tool for *de novo* antibody hit-discovery selection, screening and

characterization, circumventing the classical requirement for traditional antigen purification/processing. We have confirmed its general compatibility with i) mammalian soluble expression and secretion, and ii) the direct capture and immobilization of fusion antigens from crude cell media. The provision of covalent anchorage for antigen targets by SpyC/SpyT dCl, such that surface complexes can survive the prolonged incubations and extensive washing steps typically applied during stringent selection protocols, has permitted the successful isolation of several functional antibody candidates recognizing diverse therapeutic targets.

2.5 Materials and Methods

2.5.1 Molecular biology, protein expression and phage display

Prokaryotic expression and secretion of SpyC-fusion proteins

The nucleotide sequence of the CnaB2-derived SpyCatcher (SpyC) domain was synthesized (GeneArt, Thermo Fisher Scientific) with reference to the sequence of Genbank accession: JQ478411.1 (amino acids 28-136) and cloned into a pUC119-derived prokaryotic expression vector (pSTEVe16) containing a periplasmic secretion signal. The protein of interest was cloned N-terminal to the SpyC domain, separated by tandem myc/his or HA/his epitope tags. The amino acid sequences of the extracellular region of the human CD3ϵ,δ and γ chains were obtained from UniProtKB (http://www.uniprot.org/)[348] and assembled as single-chain heterodimers using a 28 amino acid flexible spacer. The amino acid sequences of anti-CD3 antibody variable domains were extracted from the following published patents: UCHT1 (US8519100), OKT3 (Blinatumomab; WO2005052004), Pasotuxizumab (WO2008119567A2), Solitomab (US8076459B2), Foralumab (US 20060177896A1). A murine CD3-specific scFv was constructed from the sequenced 145-2C11 hamster mAb.[349] Genes were synthesized in scFv format and cloned into pSTEVe16.

E. coli TG1 cells (Lucigen, #60502) were electroporated with the relevant plasmids and grown overnight on agar prepared with 2TY medium supplemented with 2 % glucose and 100 µg/ml ampicillin (2TYAG). Colonies were inoculated into 96-well plates containing 2TYAG and cultures were grown overnight at 30 °C. For protein expression, 4 µl of overnight culture was used to inoculate 170 µl Terrific Broth (TB) containing 0.1 % glucose and 100 µg/ml ampicillin. The cultures were grown in 96-well PP U-form microplates (Greiner, #650201) with shaking at 30 °C for 3-4 h until reaching an OD600 of 0.6. Protein expression was induced by adding 20 µl per well of 1 mM Isopropyl-β-D-thiogalactopyranoside (IPTG; Merck, #420322) to achieve a final concentration of 100 µM. Expression was allowed to continue for 16-18 h at 30 °C with shaking at 750 rpm, 70% humidity before harvesting of media for subsequent analysis.

Eukaryotic protein expression and purification

Extracellular domain (ECD) fragments of human and mouse membrane antigens were synthesized (GeneArt, Thermo Fisher Scientific) based on sequences and predicted topologies obtained from UniprotKB. Gene fragments were fused N- or C-terminally to vector-encoded SpyC housed in pTT-based mammalian episomal expression vectors.[350] All vectors contained an identical semi-synthetic signal peptide (pSTEVe20/38/49 constructs). Selected scFv candidates were typically either sub-cloned into a pTT-based vector containing a vector-encoded human IgG1 constant region to produce scFv-Fc fusion proteins, reformatted into modular

pTT-based IgG heavy and light chain vectors for co-transfection and production of assembled IgGs, or fused to anti-CD3 UCHT1 domains to generate secreted T cell engagers.

Recombinant protein was produced using the mammalian HEK293-6E/pTT transient expression system (National Research Council of Canada; obtained under licence). HEK293-6E cells were grown in Freestyle F17 medium (Thermo Fisher Scientific, #A13835) containing 4 mM GlutaMAX (Life Technologies, #35050061), 0.1 % Pluronic® F-68 (Life Technologies, #24040032) and 25 µg/mL G418 (Life Technologies, #10131019) at 37 °C, 5 % CO2 and 120 rpm. For transfection, the DNA was mixed with FectoPRO (Polyplus, #116-010) transfection reagent in F17 medium without supplements, according to the manufacturer's instructions. After five days of protein expression, cultures were subjected to low speed centrifugation and the media collected. Samples could be used immediately for direct capture and immobilization (dCI) experiments or snap-frozen and stored at -80 °C until required.

ScFv-Fc fusions and IgG molecules were purified from clarified expression media using a HiTrap™ MabSelect column (GE Healthcare, #11003494), followed by extensive dialysis against phosphate-buffered saline (PBS). His-tagged T cell engagers were purified by IMAC chromatography using a HisTrap™ Excel column (GE Healthcare, #17-3712-05). The peak monomer fractions were pooled and buffer-exchanged into PBS using a Superdex 200 Increase 10/300 GL preparatory grade column (GE Healthcare, #28-9909-44). The 6xhis-tagged variants of human or murine TEM1 ECD containing a C-terminal biotinylation sequence were purified using a HisTrap™ excel column followed by site-directed enzymatic biotinylation using purified BirA.[351] Following confirmation of biotinylation by avidin gel shift assay,[352] the proteins were buffer exchanged into PBS supplemented with 0.1% BSA and stored at -80 °C.

Transient transfection of HEK293T cells with the FL-hTEM1 cDNA ORF (extracted from Genbank RefSeq NM_020404.3) and an irrelevant membrane-localised control ORF (anti-hCD19 2nd generation CAR construct) utilized the pTagGFP2-N CMV promotor vector (Evrogen, #FP192). Briefly, HEK293T cells were detached and plated in 6-well plates at 10^6 cells/well in a volume of 4 ml. Recombinant plasmid DNA (4 µg) was combined with 400 ml serum-free DMEM and 6 ml Turbofect reagent (Life Technologies, #R0532), and incubated for 20 min at RT before being added dropwise to the plated cells. Transfected cells were maintained at 37 °C, 5% CO_2 under a humidified atmosphere for 48 h.

<u>Direct capture and immobilization (dCI) of secreted SpyC-fusion proteins for downstream library selections</u>

For solid-phase immobilization of SpyC-fused antigens, we synthesized a C-terminally biotinylated SpyT peptide (bSpyT) with a 4-amino acid 'spacer' extension (>90% purity; Protein and Peptide Chemistry facility, UNIL). Streptavidin-conjugated magnetic beads (80 µl; M-280 Dynabeads; Life Technologies, #11206D) were suspended in 1 ml of PBS containing 1 µM of bSpyT peptide and incubated overnight at 4 °C or 1 h at room temperature (RT) with gentle rotation. After 3x 1 ml wash steps in PBST (PBS + 0.1 % Tween-20) and 1x 1 ml wash step in PBS, the coated beads could be stored at 4 °C until required or incubated directly with 2 ml of SpyC-fusion expression supernatant for 2 h with gentle rotation at RT. The antigen-coated beads were washed 4x with PBST and 1x in PBS and generally used immediately for dCI evaluation and phage display experiments.

Selection of human germline scFvs by phage display using SpyC-fusion proteins

All phage display selections were carried out using two large, fully human scFv libraries (CHV101_DMκ and CHV101_DMλ; SMD, unpublished) constructed from the peripheral blood of 120 healthy volunteer donors (Service de Transfusion, Epalinges, Switzerland). Briefly, IgD/IgM VH, and Vκ/Vλ domain repertoires were amplified from cDNA prepared from mRNA affinity-purified from enriched $CD19^+$ cells, using a newly designed primer panel. Amplicons were pooled, purified and cloned sequentially (Vκ/Vλ followed by VH) into the gIII display cassette of a newly designed phagemid vector (pCHV101; SMD, unpublished). A bacterial library of ~$2x10^{10}$ colonies was generated following electroporation into *E. coli* TG1 cells. Phage library rescue was performed according to standard published procedures and single-use phage aliquots were stored in a stabilization buffer at - 80 °C.

Streptavidin magnetic beads pre-coated with bSpyT and coated with SpyC-antigens (or coated directly with purified and biotinylated h/mTEM1 ECD) were used as solid-phase targets for phage display selections. The scFv phage libraries were first blocked with PBST containing 2% skimmed milk, 1% BSA for 30 min at RT, and then incubated for 30 min with streptavidin beads coated only with SpyC domain to subtract ('de-select') non-specific or SpyC-specific binders. Subsequently, blocked and de-selected phage particles were transferred to tubes containing similarly blocked SpyC-antigen beads, and incubation was continued at RT for 1 h. Non-binding phage were removed by 5x 1 ml washes with PBST followed by 1x 1 ml PBS. Typically, the stringency of selection was increased at the second round by transferring the 5x 1ml PBST washed beads into a Falcon tube containing 50 ml PBST and allowing lower affinity phage to passively dissociate over 20 min prior to rapid magnetic capture and final washing with 1ml 1x PBS. Bound phage were eluted from the beads with 200 μl of 20 μg/ml trypsin (Sigma Aldrich, #T1426) in PBS for 30 min at 37 °C (stationary). Eluted phage were allowed to infect minimal medium-grown *E. coli* TG1 cells grown to an OD600 of 0.4-0.5 in 10 ml of 2TY medium supplemented with 2 % glucose (2TYG) for 1 h at 37 °C (stationary). The infected cells were collected by centrifugation at 4000 rpm (RT), re-suspended in 3 ml 2TYG, and plated on 2TYAG agar with incubation at 30 °C for 18-20 h. Colonies were scraped from plates and the cells stored frozen in 2TYG containing 15 % glycerol pending further rounds of phage rescue and selection. Phage rescue between rounds was performed according to standard protocols using M13KO7 helper phage (Life Technologies, #18311019) added at a MOI of 5:1. Secreted phage were collected and purified by two rounds of PEG/NaCl precipitation according to standard protocols, and stored as frozen, single-use aliquots in a stabilization buffer.

Clones were cultured for primary screening by picking individual colonies into 2TYAG liquid medium, growing until turbid and then inoculating cells into supplemented TB medium for the induction of protein expression as described above.

Affinity maturation of anti-TEM1 clone candidates

Selected scFv clones were subjected to random mutagenesis across the whole scFv, using error-prone PCR with the Diversify PCR random mutagenesis kit (Takara, #630703). The scFv was amplified in one, two or three subsequent rounds of PCR with 25 cycles in the presence of 640 μM MnSO4 and 40 μM dGTP in order to generate variants with low, intermediate and high mutational load. Mutated scFv library DNA was cloned into pCHV101 and electroporated into *E. coli* TG1 cells to generate libraries of ~10^9 colonies. Phage particles displaying the mutagenized scFv libraries were rescued and PEG/NaCl-precipitated before being used in high-stringency affinity maturation selections against either purified bio-TEM1 ('classical' approach) or TEM1-SpyC

(dCI approach). In order to enrich for high-affinity, cross-reactive binders towards both human and murine TEM1 ECD, the first round of selection was performed against bead-immobilized bio-hTEM1 and the second round against bio-mTEM1. Both rounds included competition ('off-rate selection') with 200 nM free unlabelled antigen and an extended high-volume washing step of 50 ml PBST (30 min for R1 and overnight for R2). For the dCI approach, employed using the SpyC-hTEM1(Δn) fusion target, R1 beads were loaded with HEK expression supernatant diluted 1:10 in PBS with stringent washing following phage binding (6x 1 ml PBST, 2x 50 ml PBST (20 min), 1x 1 ml PBS). For R2, the expression supernatant was diluted further (1:50) and the stringency increased with an additional 2x 50 ml PBST (20 min) washes. For all experiments, random colonies were picked from the R2 selection output and sequenced to assess clone integrity and diversity prior to the initiation of screening.

2.5.2   Biophysical and biochemical protein characterization

SDS-PAGE and Western Blotting

To elute bound protein, SpyC-antigen coated beads were re-suspended in 1x LDS buffer (NuPAGE; Life Technologies, #NP0007) with 10 % reducing agent (NuPAGE; Life Technologies, #NP0009) and boiled at 95 °C for 10 min. The beads were pelleted by centrifugation and the eluted protein fraction was separated on a Novex 4-12% Bis-Tris Gel (Life Technologies, #NP0321) for 38 min at 200 V. Separated protein fractions were visualized by Coomassie Blue staining (InstantBlue; Expedeon, #ISB1L) or transferred to nitrocellulose membranes (iBlot2; Thermo Fisher Scientific, #IB23001). After blocking with 5 % milk/ PBST, the membranes were incubated with an HRP-conjugated anti-HA tag antibody (Thermo Fisher Scientific, #PA1-29751), diluted 1:1000 in PBS containing 1 % BSA. Membranes were washed four times in PBST and HA-tagged protein was detected with an enhanced chemi-luminescent (ECL) HRP substrate (Thermo Fisher Scientific, #34080), followed by image acquisition using a Fusion FX imaging system (Vilber).

Surface plasmon resonance (SPR)

SPR analysis was performed on a Biacore T200 instrument (GE Healthcare). Experiments involving TEM1-SpyC ligand immobilization used a Series S SA sensor chip (GE Healthcare, #BR-1005-31). Briefly, 1 ml of crude TEM1-SpyC expression media was incubated with 1 μM of bSpyT at RT for 2 h with gentle rotation. The resulting covalent TEM1-SpyC:bSpyT complex was separated from free bSpyT by buffer-exchange into 1x filtered Biacore running buffer (HBS-EP+; 0.01 M HEPES, 0.15 M NaCl, 0.05% Surfactant P20, 3mM EDTA, pH 7.4; GE Healthcare, #BR-1006-69) using a spin column with a 10 KDa cut-off (Vivaspin 6; GE Healthcare, # 28932296). The biotinylated TEM1-SpyC ligand complex was immobilized on the SA chip at a density of 150 RU. For kinetic analysis, analytes were diluted into running buffer and injections/dissociations carried out at 30 μl/min with data collected in Single Cycle Kinetics mode. For Fc-capture experiments, 10000 RU of AffiniPure Goat Anti-Human IgG (Jackson ImmunoResearch, #109-005-098) were immobilized on a CM5 Series S sensor chip (GE Healthcare, #BR-1005-30) by amine coupling according to the manufacturer's instructions. Anti-TEM1 scFv-Fc molecules were captured at a target density of 100 RU and analytes were injected and dissociated at 30 μl/min with data acquired in Multiple Cycle Kinetics mode. Surfaces were regenerated between cycles/experiments by injecting 10 mM glycine-HCl, pH 1.5 for 30 s. Corrections for bulk shift and refractive index changes were performed by subtracting the signal of a reference flow cell from the active cell.

2.5.3   Binder characterization and screening assays

Enzyme-linked immunosorbent assay (ELISA)

For screening of scFv clones (and variant molecules) by dCI SpyC-antigen ELISA, wash steps were performed using 300 µl PBST dispensed from a BioTek 405 automatic plate washer. Nunc Maxisorp 96-well plates (Thermo Fisher Scientific, #442404) were coated with 100 µl of 10 µg/ml Neutravidin (Life Technologies, #31000) in PBS over-night at 4 °C, washed 3x with PBST and incubated with 100 µl of 1 µM bSpyT peptide in PBS for 1 h at RT with gentle agitation. After blocking in 5 % skimmed milk/PBST for 1 h, wells were washed 3x with PBST and 100 µl SpyC-antigen expression supernatants (typically diluted 1:10 in PBST + 1 % BSA for mammalian expression, or blocking buffer for bacterial expression) were added to allow covalent capture by the bound bSpyT. Incubation was at RT for 1.5 h. Wells were washed 4x with PBST and 100 µl blocked scFv culture supernatants added. Wells were washed 4x with PBST and binders were detected using a primary recombinant anti-myc tag antibody (derived from parental mAb clone 9E10, in-house) and a horseradish peroxidase (HRP) conjugated goat anti-mouse IgG antibody (Sigma Aldrich, #A9917). The colorimetric read-out was developed with TMB substrate reagent (Biolegend, #34029) and stabilized with 2N sulfuric acid. Absorbance was measured at 450 nm and 620 nm on a BioTek Synergy plate reader. ELISAs were performed in parallel against both cognate antigen-SpyC and non-fused SpyC in order to eliminate hits to the latter.

CD3-SpyC single-chain heterodimers were detected using 1 µg/ml of a murine anti-hCD3 antibody (clone UCHT1, Thermo Fisher Scientific, #MA1-80044) followed by a HRP-conjugated anti-HA tag antibody (Thermo Fisher Scientific, #PA1-29751; diluted 1:5000), or with UCHT1-scFv displaying phage particles revealed using an M13 antibody HRP conjugate (Sigma Aldrich, cat. 27-9421-01). For evaluation of cognate ligand binding to captured SpyC-antigens, purified bivalent hFc(IgG1)-fusions (hCD27, hCD80, hCD155, hPD-L1) or his-tagged monomer (hMuc16) were purchased from R&D Systems. Ligands were diluted to 2 µg/ml in PBST + 1% BSA and incubated for 1 h at RT. After washing, bound Fc-fusions and bound Muc16 were detected with goat anti-human IgG Fc polyclonal HRP conjugate (Sino Biologicals, #SSA001; 1:5000 dilution) or anti-His tag HRP conjugate (Genscript, #A00612; 1:1000 dilution) using TMB as substrate.

Multiplexed bead-based no-wash screening assay using SpyC-fusion proteins

For screening of scFv clones by mix-and-read bead multiplex assay, SpyC-fused antigens in expression supernatants were covalently captured on fluorescently barcoded streptavidin-coated beads (Spherotech yellow beads, #SVFB-2552-6K) using the dCI protocol described above. The antigen-coated bulk bead populations were combined and blocked in assay buffer (PBS/2%BSA/0.1% PBST/2mM EDTA/0.02% sodium azide) for 30 min on ice. Multiplexed beads (10 µl) were added to wells of a 96-well plate, followed by an equal volume of scFv-containing *E. coli* TG1 expression supernatants diluted 1:5 or 1:10 in assay buffer. After incubating on ice for 30 min, bound scFvs were detected by subsequent addition of 10 µl of an iFluor647-conjugated anti-his tag antibody (GenScript, #A01802-100) at a final dilution of 1:200 in assay buffer. Following a further 20 min incubation on ice, the sample plate was read directly on an Intellicyt iQue TM Screener PLUS instrument (10 s sampling; 1 µl/s). Bead populations displaying different immobilized SpyC-antigens were resolved by their respective barcoding fluorescence intensity (FITC), and scFv binding to each population was assessed by iFluor647-mediated median fluorescence intensity (MFI). Data analysis was performed using Forecyt software (Intellicyt).

mCD47:mSIRPα competition ELISA screening

96-well ELISA plates were coated as described above with Neutravidin, bSpyT and mCD47-SpyC. Alternatively, plates were coated directly with 0.5 μg/ml commercially available his-tagged mCD47 (Sino Biologicals, #57231-M08H-50). Pre-blocked scFv expression supernatants (100 μl) were added to each well immediately followed by 100 μl of diluted HEK expression supernatant containing recombinant mSIRPα-Fc (hIgG1) fusion produced by transient transfection. Appropriate dilutions of mCD47-SpyC and mSIRPα-Fc that yielded signals within the linear part of the response curve were determined previously by chequerboard ELISA titration. Following incubation for 1 h, the bound mSIRPα-Fc levels were determined by colorimetric detection with goat anti-human IgG Fc polyclonal HRP conjugate (Sino Biologicals, #SSA001; 1:5000 dilution) using TMB as substrate. Neutralizing scFv clones were reformatted as murine IgG2a and purified. Their mCD47:mSIRPα-blocking activity was confirmed in ELISA titration experiments alongside commercially available benchmark rodent mAbs (kindly provided by Irving Weissman lab, Stanford). All competitors were titrated in a 3-fold dilution series starting at 2.5 μg/ml and mixed 1:1 v/v (200 μl final) with in-house produced mSIRPα-Fc HEK supernatant before addition to the plate. After 1 h of incubation, binding of mSIRPα-Fc to plate-bound mCD47 was revealed by goat anti-human IgG HRP-conjugated antibody (Sino Biologicals, #SSA001; 1:5000 dilution) followed by the addition of TMB substrate for colorimetric detection.

2.5.4   Cell assays

Cell culture

A-673 (ATCC CRL-1598), 2H11 (ATCC CRL-2163), MS1 (ATCC CRL-2279) and HT-1080 (ATCC CCL-121) cells were maintained in Dulbecco's modified Eagle's medium (DMEM) supplemented with GlutaMAX and 10 % fetal bovine serum (FBS). SK-N-AS (ATCC CRL-2137) and TC1 (ATCC CRL-2934) cells were additionally supplemented with 0.1 mM non-essential amino acids (Gibco, Life Technologies, #11140050). HEK293T (ATCC CRL-11268) cells were cultured in DMEM, 10% FBS and 100 U/ml penicillin/streptomycin (Gibco, Life Technologies, #15140122). MDA-MB-231 (ATCC HTB-26), NCI-H226 (ATCC CRL-5826), AsPC-1 (ATCC CRL-1682), Raji (ATCC CCL-86), A-20 (ATCC TIB-208), A-20_CD47KO (kindly provided by Irving Weissman lab, Stanford) and Jurkat NFAT Lucia cells (Invivogen, #jktl-nfat) cells were cultured in RPMI-1640 Glutamax (Life Technologies, #61870010) containing 10% FBS. A-20 cells were additionally supplemented with 0.05 mM 2-β-mercaptoethanol and Jurkat Lucia cells were maintained under selective pressure using 100 μg/ml zeocin (Invivogen, #ant-zn-1). All cells were maintained at 37°C, 5% CO_2 in a humidified incubator and the absence of mycoplasma from all cell lines was confirmed by regular testing (GATC service).

Peripheral blood mono-nucleated cells (PBMCs) were isolated from fresh buffy coats by density centrifugation using Lymphoprep (Axonlab, #1114545). T cells were subsequently extracted by magnetic separation using a human pan-T cell isolation kit (Miltenyi Biotec, #130-096-535) and stimulated with human T cell activator CD3/CD28 beads (Life Technologies, #11161D) and 50 RU IL-2 (Peprotech, #200-02-50UG) for 5 days. After the removal of the beads, primary T cells were further expanded with IL-7 and IL-15 (Miltenyi Biotec, #130-095-367 and #130-095-765) for a further 5-10 days.

Flow cytometry

Adherent cells were detached using 10 mM EDTA, counted and resuspended in fresh, complete culture medium. All subsequent steps were performed on ice. For each sample, 0.5×10^6 cells were first blocked in FACS buffer (5 % FBS in PBS) and then incubated for 1 h with test antibody (typically 1-2 μg/ml) or expression

supernatant diluted in FACS buffer. After washing three times with FACS buffer, the following secondary antibodies were added: Alexa Fluor 647 AffiniPure Goat Anti-Human IgG (Jackson Immunoresearch, #109-605-098, 1:200 dilution) or Alexa Fluor 647 anti-mouse IgG (Life Technologies, #A-21236, dilution 1:50). Secondary antibodies were incubated for 30 min and the cells were washed again three times. Immediately before data acquisition, dead cells were stained with 4',6-Diamidino-2-phenylindole (DAPI, 1:2000 dilution). Data was acquired using an LSR-II flow cytometer equipped with FACSDIVA software (BD Biosciences). Data analysis and plotting were carried out using FlowJo v10 (FlowJo LLC).

Lentiviral transduction of Jurkat NFAT Lucia cells

Sequences encoding human anti-mesothelin scFvs or an anti-CD19 scFv (FMC63; extracted from Sequence 2, patent US7446179) were linked to a spacer/hinge, transmembrane region and intracellular costimulatory domain derived from the hCD28 costimulatory domain, and to an intracellular hCD3ζ signaling domain. The resulting 2nd generation CAR cassettes were appended to an in-frame monomeric green fluorescent protein ORF (TagGFP2, Evrogen) and cloned into a modified pRRL lentiviral vector (Origin: Didier Trono lab, EPFL). Virus was produced by transient transfection of HEK293T cells using pCMVR8.74 and pMD2.G plasmids for packaging (Origin: Didier Trono lab, EPFL) and Turbofect transfection reagent (Life Technologies, #R0532). Virus-containing supernatant was harvested after 48 h, concentrated by ultracentrifugation and added directly to 5×10^5 Jurkat NFAT Lucia cells. Transduced cells were expanded for 10-14 days before performing functional assays.

Jurkat NFAT activation reporter cell assays

For CAR and soluble engager assays designed to measure ITAM-mediated 'Signal 1' activation responses, 5×10^4 target cells were seeded in 96-well plates and allowed to attach for 20 h. Subsequently, 10^5 Jurkat NFAT Lucia reporter cells were added to each well. For activation assays using T cell engager molecules, molecules were added in 3-fold serial dilutions, starting from 20 nM. Phorbol myristate acetate (PMA)/ionomycin was included as a positive response control. After 24 h of co-culture, the supernatants were collected and mixed with an equal volume of QUANTI-Luc luciferase substrate (Invivogen, #rep-qlc-1). Luminescence was measured immediately using a BioTec H1MFG Synergy plate reader. For functional analysis of anti-CD3 scFv-SpyC fusions, TG1 *E. coli* expression supernatants were added to Neutravidin/bSpyT-coated 96-well Maxisorp plates and incubated for 2 h at RT to allow covalent capture of fusions. After washing (5x PBST, 2x PBS), Jurkat Lucia reporter cells were added and secreted luciferase determined as above.

Primary T cell cytotoxicity assay

Specific target cell killing was assessed using real-time kinetic cell imaging (Incucyte system, Essen Bioscience). Target and control cells (1.5×10^4) were seeded in 96-well plates prior to the start of the experiment. When approximately 30 % confluency was observed, soluble T cell engager molecules were added as 3-fold serial dilutions, starting from 20 nM. Positive control test wells were treated with 1 % Triton X-100. Primary human T cells prepared and expanded as described above were added to the plates (10^5 per well) to obtain an E:T ratio of approximately 5:1. Cytotox Red reagent (Essen Bioscience, #4632) was added to a final dilution of 1:4000, and resultant cell death was monitored as an increase in fluorescence over time.

2.6 Supplementary Information
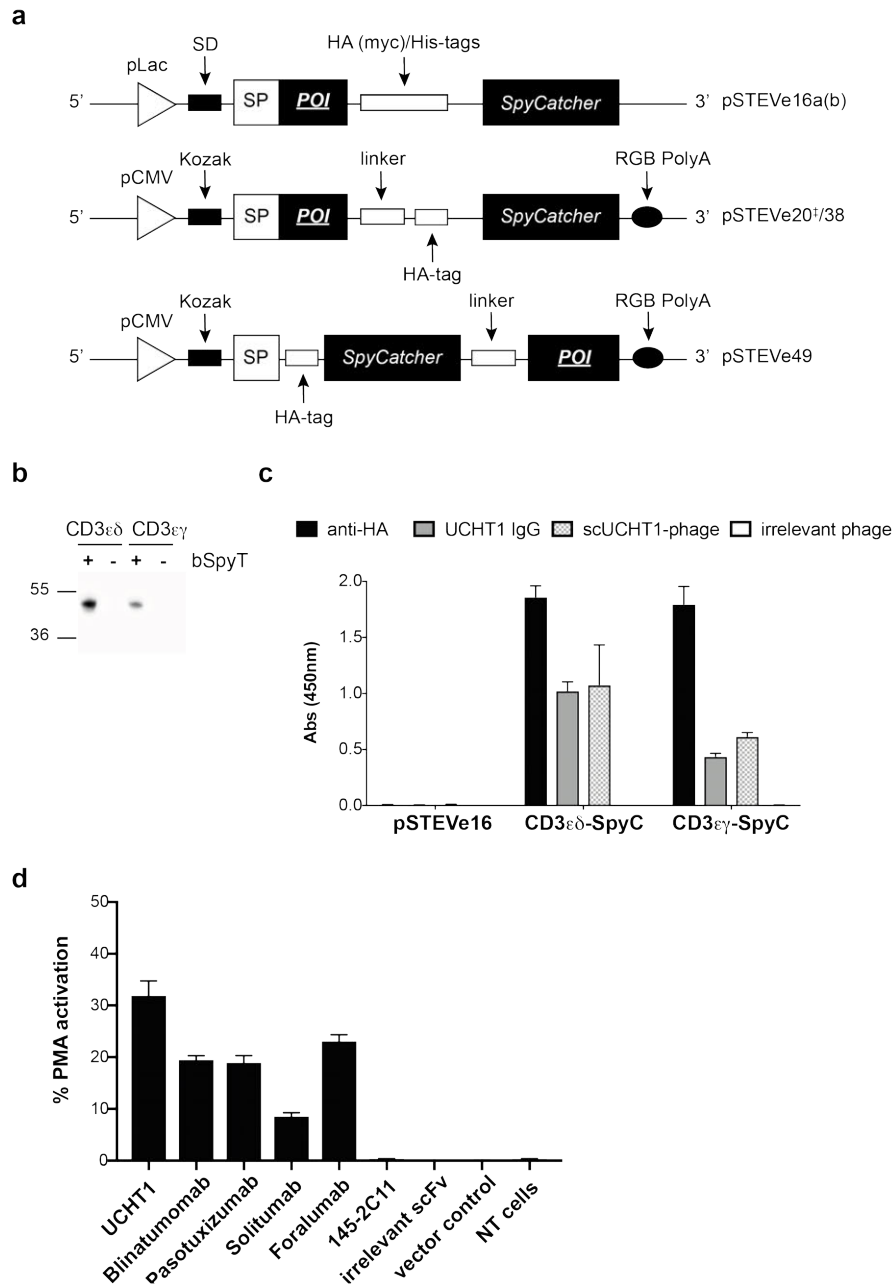
Supplementary Figure 2.1. Production and functional evaluation of mammalian antigen-SpyC fusions.

(**a**) Prokaryotic and eukaryotic expression vector cassettes used for the production of SpyC-fused proteins. SP, signal peptide; POI, protein of interest, ‡pSTEVe20 is an earlier variant of pSTEVe38 comprising the original non-codon optimized SpyC sequence and a histidine-tag; (**b**) The expression and secretion of single-chain hCD3 heterodimer-SpyC fusions in *E. coli* TG1 using vector pSTEVe16. Bead capture from culture supernatants is dependent on the presence of SpyT on the beads (Western blot detection of intact fusion protein via anti-HA tag ECL). (**c**) Secreted CD3-SpyC heterodimers were directly captured from bacterial media using plate wells pre-coated with Neutravidin and bSpyT, and detected by anti-HA tag and UCHT1 (as both IgG and as a scFv-phage reagent. (**d**) Functionality of a panel of anti-CD3 scFv-SpyC fusions (parental IgG names retained) expressed and secreted from *E. coli*. Fusions captured on Neutravidin/SpyT coated assay plates retain the functional ability to cross-link native human cell surface CD3 and stimulate NFAT-driven secretion of luciferase from a Jurkat NFAT reporter cell line. The anti-murine CD3 clone, 145-2C11, does not recognize hCD3 and was included as an additional negative control. NT, non-transformed; PMA, phorbol myristate acetate.
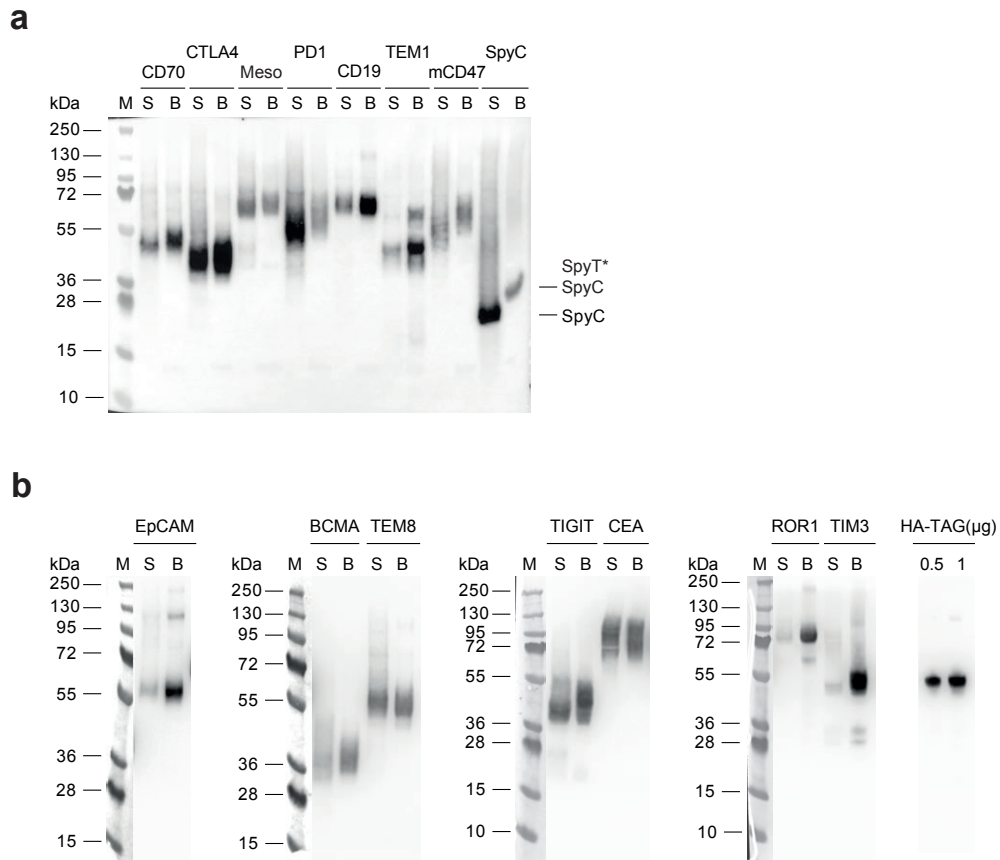
Supplementary Figure 2.2. Full Western Blot analysis of captured SpyC-antigens.

(**a**) Full-sized anti-HA tag Western Blot image corresponding to Fig. 2.1c. Representative SpyC-antigens were expressed in HEK293-6E cells and directly captured from the expression supernatant ('S') onto bSpyT-loaded magnetic beads ('B'). Covalent immobilization to SpyT on the beads results in a shift to a higher MW corresponding to the mass of the peptide adduct. (**b**) Additional SpyC-antigens that were captured and analyzed as described above. Samples were run on separate gels in the presence of additional undisclosed samples and controls, but were processed in parallel. Only relevant lanes of full-sized images are shown with their respective size marker.

a

b
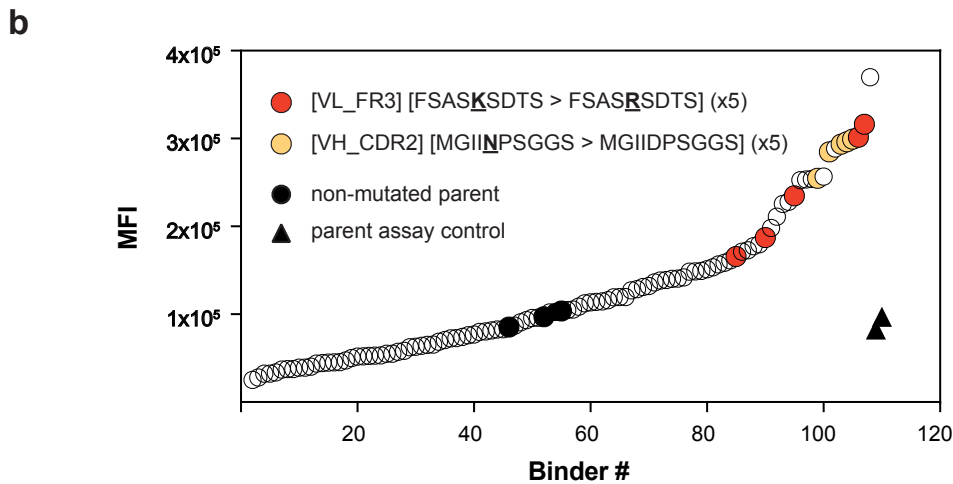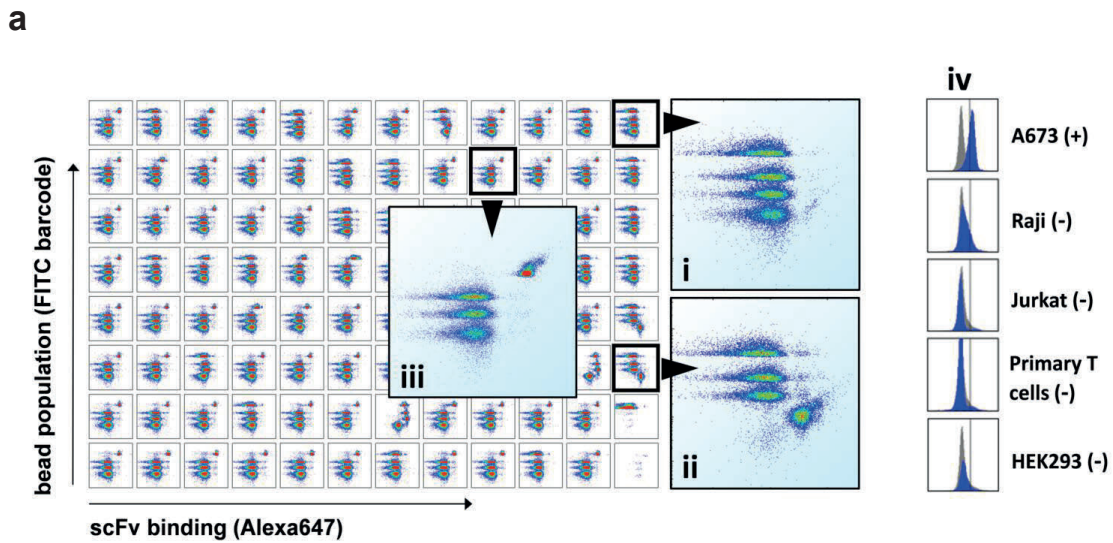
Supplementary Figure 2.3. Multiplexed bead-based primary screening of scFv clone supernatants from hTEM1(Δn) R2 selection outputs.

(**a**) Barcoded streptavidin beads were pre-loaded with bSpyT prior to dCI of the respective antigens from HEK expression supernatants. The resulting 4-plex comprises (from top/brightest): hTEM1(Δn)-SpyC, mTEM1(Δn)-SpyC, SpyC-domain only, hEGFRvIII-SpyC. Expanded panels: (i) irrelevant scFv supernatant (negative control); (ii) scFv specific for EGFRvIII (positive control); (iii) representative screening 'hit' (HS301) selective for hTEM1(Δn); (iv) binding profile of purified HS301 scFv-Fc towards endogenous TEM1^{+} (A673) and TEM1^{-} cell lines (isotype staining control as grey curve). (**b**) Bead-based multiplex MFI distribution plot of binders to SpyC-hTEM1(Δn) coated beads obtained following error-prone mutagenesis of the HS301 parental clone and two stringent dCI selection rounds against SpyC-hTEM1(Δn). Hit threshold was set at 5x background with no binding to mesothelin-SpyC or control SpyC coated beads. Multiple occurrences of enriched point-mutated variants of interest clustering at significantly higher MFI values than the parent are indicated. MFI, median fluorescence intensity.
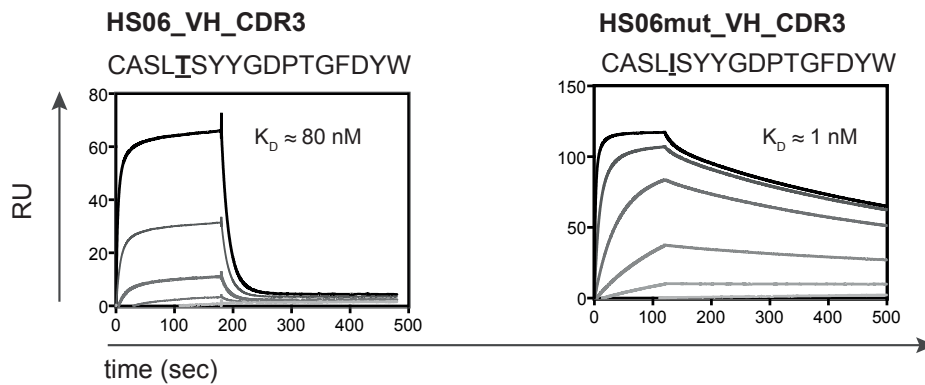
Supplementary Figure 2.4. SPR affinity measurement of clone HS06 and a matured variant HS06mut.

SPR monovalent affinity determination of parental clone HS06 (*left*) and an affinity-matured variant, HS06mut (*right*), using HS06/HS06mut scFv-Fc as the immobilized ligand. Soluble hTEM1-FL analyte concentration ranges were 100, 50, 25, 12.5 and 0 nM for HS06, and 5, 2.5, 1.25, 0.625 and 0 nM for HS06mut. hTEM1-FL, full-length human TEM1 ECD (NS0 cells; R&D Systems, #7855-CD-050).
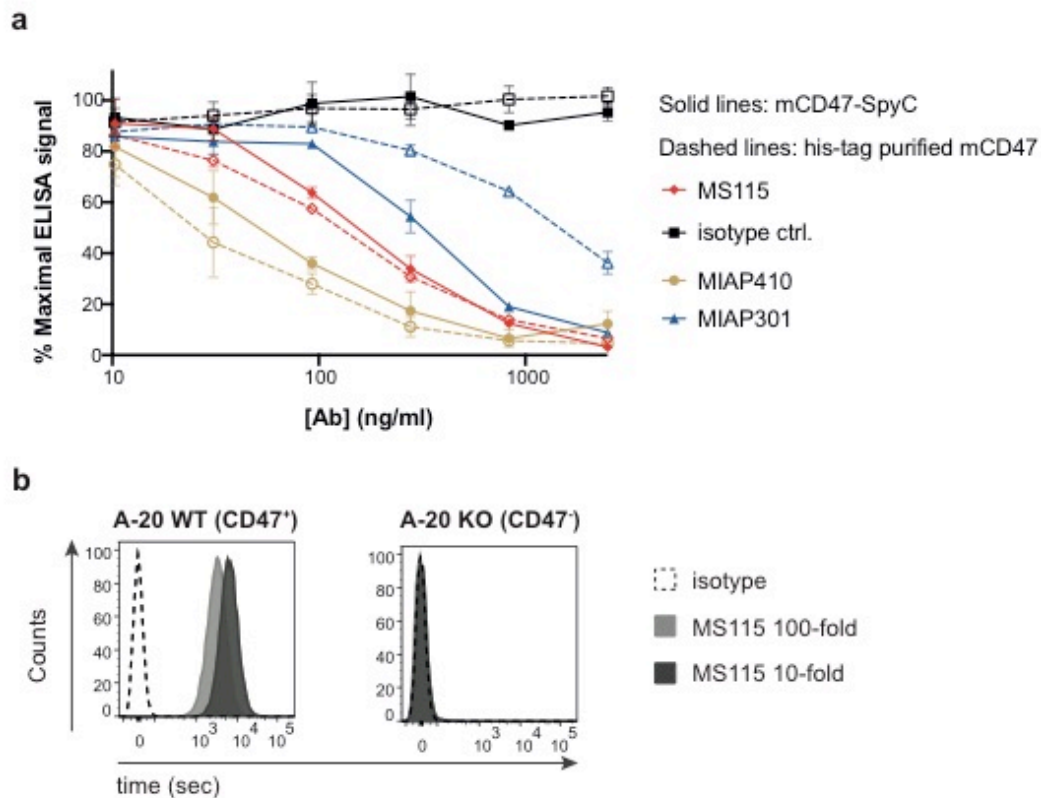
Supplementary Figure 2.5. Characterization of a mCD47-targeted neutralizing antibody Isolated by SpyC-fusion dCI phage display selection and screening.

(**a**) Competitive blocking of the interaction between soluble mSIRPα-Fc and immobilized mCD47. Dashed lines: Commercial his-tag purified mCD47 coated by passive adsorption. Solid lines: mCD47-SpyC captured and immobilized directly from expression media on Neutravidin/bSpyT pre-coated wells. Reference/control antibodies: Black, 9E10 mIgG1 (isotype control); blue, MIAP301 rIgG2a (commercial neutralizing mAb); red, dCI mCD47-SpyC selected clone MS115 mIgG2a; gold, MIAP410 mIgG1 (commercial neutralizing mAb). (**b**) Specific recognition of endogenous mCD47 on murine B cell lymphoma cell line A-20 by clone MS115. Cell binding was assessed by flow cytometry in the scFv-Fc (hIgG1) format at 10- and 100-fold dilution of transient HEK expression supernatant.

Screening Plate	Target Antigen	Library	Round	# Target binders	% Hit Rate[‡]	# SpyC binders	% SpyC binders[*]
MP01	hTEM1-SpyC	CHV101_DMλ	R2	49	55.7	1	4.5
MP02	hTEM1-SpyC	CHV101_DMκ	R2	37	42.0	1	4.8
MP03	mTEM1-SpyC	CHV101_DMλ	R2	60	68.2	1	2.3
MP04	mTEM1-SpyC	CHV101_DMκ	R2	39	44.3	0	0.0
MP07	hMeso-SpyC	CHV101_DMλ/κ	R2	52	59.1	0	0.0
MP37-40	hMeso-SpyC	CHV101_DMκ	R2	175	11.9	0	0.0
MP1914	spyC-hCD19	CHV101_DMλ/κ	R2	23	6.3	4	1.1
MP1915	spyC-hCD19	CHV101_DMλ/κ	R3	40	10.9	11	3.0
MP4701	mCD47-spyC	CHV101_DMλ	R2	10	11.9	4	4.8
MP4702	mCD47-spyC	CHV101_DMκ	R2	1	1.2	1	1.2
MP4703	mCD47-spyC	CHV101_DMλ/κ	R2	8	9.5	3	3.6

Supplementary Figure 2.6. Hit rates and frequency of SpyC-binders in selected dCI discovery projects.

Primary screening metrics illustrating respective primary ELISA hit-rates and frequencies of SpyC-reactive clones for selected scFv discovery projects using SpyC-antigens. Hit rates represent the frequency of clones binding to the respective SpyC-antigen in a primary screening. These hits were subsequently re-arrayed and screened for SpyC-reactive clones, the frequency of which is shown. Rd, selection round; [‡] signal threshold > 5x background. [*] signal threshold > 3x background.

Chapter 3 *De novo* discovery of a diverse panel of fully human scFvs targeting extracellular regions of native TEM1

This chapter describes the *de novo* discovery of novel scFv binders to different extracellular regions of human TEM1. The resulting fully human antibodies represent ideal candidates for the development of various therapeutic and diagnostic applications focusing on TEM1 as a biomarker and/or drug target.

3.1   Introduction

Tumor cell maintenance and growth requires support from surrounding cells which constitute the tumor stroma[353,354]. The stromal compartment represents a heterogeneous mixture of cells which interact and evolve with the tumor cells to form a favorable microenvironment. As part of this microenvironment, fibroblasts build and remodel the extracellular matrix (ECM) and contribute to tumor invasion[355]. Once solid tumors reach a diameter of 1-2 mm, the formation of supporting blood vessels is essential for ensuring the supply of oxygen and nutrients[253]. The sprouting of new vessels from existing vasculature is termed angiogenesis, a process that is not only critical for tumor development, but also for physiological and embryonic tissue growth, as well as for wound healing[356,357]. Multiple molecular and cellular adaptations are required for angiogenesis to take place. Fibroblasts secrete ECM proteins that constitute a structural scaffold for proliferating endothelial cells as well as tumor cells[355]. Surrounding the endothelial cells, pericytes additionally support and stabilize the sprouting vessels[358]. Tumor angiogenesis is however an erroneous process, resulting in a disorganized network of often unstable vessels with incomplete pericyte coverage that is clearly distinct from physiological vasculature[254,256]. In light of the critical role of the tumor microenvironment in supporting tumor progression, extensive efforts have been undertaken to identify specific markers of the tumor stromal and neoangiogenic cell compartments.

Tumor Endothelial Marker 1 (TEM1), also called endosialin or CD248, was first discovered as a surface antigen present on tumor stromal cells as well as malignant cells of mesenchymal origin[264]. An independent study then identified the same protein as a marker of primary tumor endothelium[265]. Since then, extensive gene expression studies have confirmed TEM1/endosialin as a surface antigen upregulated within the tumor neo-vasculature and stroma of various human carcinomas including, but not limited to, colorectal cancer[272], breast cancer[274], and invasive glioblastoma[275]. Moreover, malignant cells of mesenchymal origin, such as sarcoma[271,276] and melanoma[359,360], have been found to express TEM1 directly. More detailed characterization of the tumor stromal compartment has revealed TEM1 expression mainly on tumor-associated pericytes and fibroblasts, with very low levels detected in healthy adult (micro)vasculature[266].

In contrast to the expression pattern of TEM1 under physiological and pathological conditions, the molecular function of the protein remains elusive. The observation that TEM1 knockout mice appear to develop

normally and display functional wound healing suggests that TEM1 is dispensable for angiogenesis during fetal development and wound healing. However, the lack of TEM1 within the tumor microenvironment greatly reduced tumor growth, invasion and metastasis in an orthotopic colorectal cancer model[290], indicating that stromal TEM1 expression promotes tumor growth. Structural homology of the extracellular domain (ECD) with two receptor proteins, thrombomodulin and C1qRp (CD93), suggest that TEM1 might be a cell surface receptor and indeed, TEM1 was shown to bind to fibronectin and collagen types I and IV[292]. Responsible for this interaction is the N-terminal c-type lectin-like domain (CTLD), which is followed by a sushi-like domain and three EGF repeats. These three extracellular domains are separated from the membrane by a heavily O-glycosylated sialomucin stalk[288]. In light of the complexity of the TEM1 ECD and given the absence of structural information, it remains to be determined which region(s) are critical for any tumor-promoting role of the molecule.

Given the high incidence of TEM1 expression within the tumor vasculature of many different tumor types as well as the majority of human sarcomas, TEM1 represents an attractive new target for the development of anti-cancer therapies[271]. Antibodies remain indispensable tools for targeted cancer therapies, and so a handful of antibodies targeting TEM1 have been developed. Among those, a humanized version of the monoclonal antibody used to originally identify TEM1, called ontuxizumab (MORAb-004), has been shown to decrease TEM1-levels on pericytes through antibody-mediated internalization, resulting in dysfunctional tumor microvasculature and impaired tumor growth[298]. Underlining a potential role for TEM1 in supporting neo-angiogenesis and promoting tumor growth, these findings have prompted the clinical investigation of MORAb-004 for the treatment of relapsed or refractory solid tumors[300-302]. The first fully human antibody against TEM1, termed scFv78[306], has been investigated as a tool for solid tumor imaging and as an antibody-drug-conjugate (ADC)[308,309,335].

Given the dual expression profile and cryptical biological function of TEM1, it is likely that multiple therapeutic approaches will be needed to explore the full potential of TEM1-targeting in cancer. Moreover, targeting strategies directed at disrupting stroma-modulating functions versus T cell mediated elimination of TEM1-positive cells, may require distinct and different molecular properties in the targeting antibody entity.

Here we describe the generation of a panel of novel fully human scFv clones using phage display and our previously developed dCI methodology. The isolated clones are characterized as having different biophysical properties and as recognizing different epitopes of the TEM1 protein. These newly available scFv clones will critically contribute to the development of TEM1-directed anti-cancer therapies, particularly engineered immunotherapy approaches.

3.2   Results

3.2.1 *De novo* discovery of a panel of fully human scFv clones recognizing TEM1 using phage display

As part of the validation of our newly developed dCI methodology (chapter 2), we first expressed the extracellular domain of human or murine TEM1 (N-terminal mature 353 and 460 amino acids, respectively) as SpyCatcher fusions using a mammalian HEK293-6E transient expression system. Capturing these fragments directly onto SpyT-coated streptavidin beads, they served as antigens for two rounds of phage display selection using large, fully human and essentially germline naïve scFv libraries (pCHV101_DMκ and pCHV101_DMλ)[361]. In this case both libraries, encompassing the respective lambda and kappa light chain repertoires were kept separate during phage display selection (Fig. 3.1a). All four selection branches showed strong enrichment for binders at round two (see Table 2.2) and ELISA screening of the selection outputs revealed high hit frequencies for both antigens and for both lambda and kappa libraries (Fig. 3.1b and Table 2.2). After confirming that all hits also recognized the corresponding purified full length ECDs of h/mTEM1 (mature 668 and 680 residues, respectively), unique hits were screened for human/murine cross-reactivity (Fig. 3.1c and d) and the strongest ELISA hits were sequenced. Sequence analysis revealed considerable clonal diversity (Fig. 3.1e and f) with ~83 % of clones representing a unique sequence (Table 3.1). Finally, the 15 unique cross-reactive clones with the strongest binding signals were selected for downstream characterization.

clone	VH			VL			%
	CDR1	CDR2	CDR3	CDR1	CDR2	CDR3	
1C1	GGTFSSYA	IIPIFGTA	ASLTSYYGDPTGFDY	SSNIGSNT	SNN	AAWDDSLNALV	2.94
1C10	GGTFSSYA	IIPILGIA	ARGYYYDSSGYYYNYYYGMDV	SSNIGAGYD	GNS	QSFWV	2.94
1F7	GYIFSGYY	IDPNSGAT	AREERFFAAPAFDY	SSNIGDNY	RNN	AVWDDSLNGWV	2.94
1H1	GYTFTRYG	ISASNDNT	ARDKCSSSDCFARAGHYYNGMDV	KLGDKY	QDS	QAWDSGTDVV	2.94
2B11	GFTFNTYT	ISSSSTYI	AKSIVGATHDAFDI	QSISRW	DAS	QQYKNYSPT	2.94
2B6	GYTFTSYY	INPSGGST	ARANDWLLGGALDY	QSVSSSY	GAS	QQYGSSPRA	2.94
2C6	GFTFDDYA	ISWNSGSI	AKDWNYGSGSYYNPYFDY	QGISSW	AAS	QQANSFPLT	2.94
2D11	GYTLTELS	FDPEDGET	ATAQRGWYGGGYYFDY	QGISSW	AAS	QQANSFPPFT	2.94
2G3	GFTFSSYG	ISYDGSNK	AKDQGYYDFWSGYLDY	QSISSW	KAS	QQSYSTPQT	5.88
2H11	GGTFSSYA	IIPIFGTA	ARVSGDGHPLNWFDP	QSFTS	EAS	QQYNNYPIS	2.94
3B6	GYTFTGYY	INPNSGGT	ARVRGSHPWFDP	SSNIGINT	STY	ATWDDSLNGVV	8.82
3C7	GFTFSYFA	ISSGGGST	ATVYYGSGEADY	SSDIGGYNY	EVT	FSYAGSNNFI	2.94
3D1	GYTFASYG	INTYNDNT	AREGYRGNDNYYYKYGMDV	SSNIGAGYD	GNS	QSYDSSLSGSRVV	8.82
3E5	GYTFTSYG	IIPIFGTA	ARDSSGYGGWFDP	NIGSKS	YDS	QVWDSSSDHVV	2.94
3E6	GYTFTSYY	INPSGGST	AREWFGGAHFDY	SDINVGSYN	YYSDSDK	MIWPSNASGV	2.94
3F11	GGTFSSYA	IIPIFGTA	AREDYGGNSRPLAFDI	SSNIGSNT	SNN	FSYAGSNNFI	2.94
3F2	GGTFSSYA	IIPIFGTA	ARDPIIYYYGMDV	SSDVGGYNY	DVS	SSYTHTGALV	2.94
3F4	GGTFxNYA	INTNTGNP	ARNPSYCSST				2.94
4A1	GGSISSSNW	IYHSGST	ARGNWYFDL	QSVSSSY	DAS	QHYGDSVYT	2.94
4D4	GYTFSSYG	VSPNTGNI	ARDAERNGGFAEAWLDP	QSIRSW	EAS	QQYNVYFRT	2.94
4D8	GFTFSSYG	ISSSGSTI	ARGGGYSYGFDY	QSISSY	AAS	QQSYSTPLT	2.94
4E11	GYTFKNYG	ISAYNGNI	AR	SGESNA	DAS	KxxYRNFLS	2.94

Table 3.1. CDR amino acid sequences and frequencies of TEM1-ECD binders.
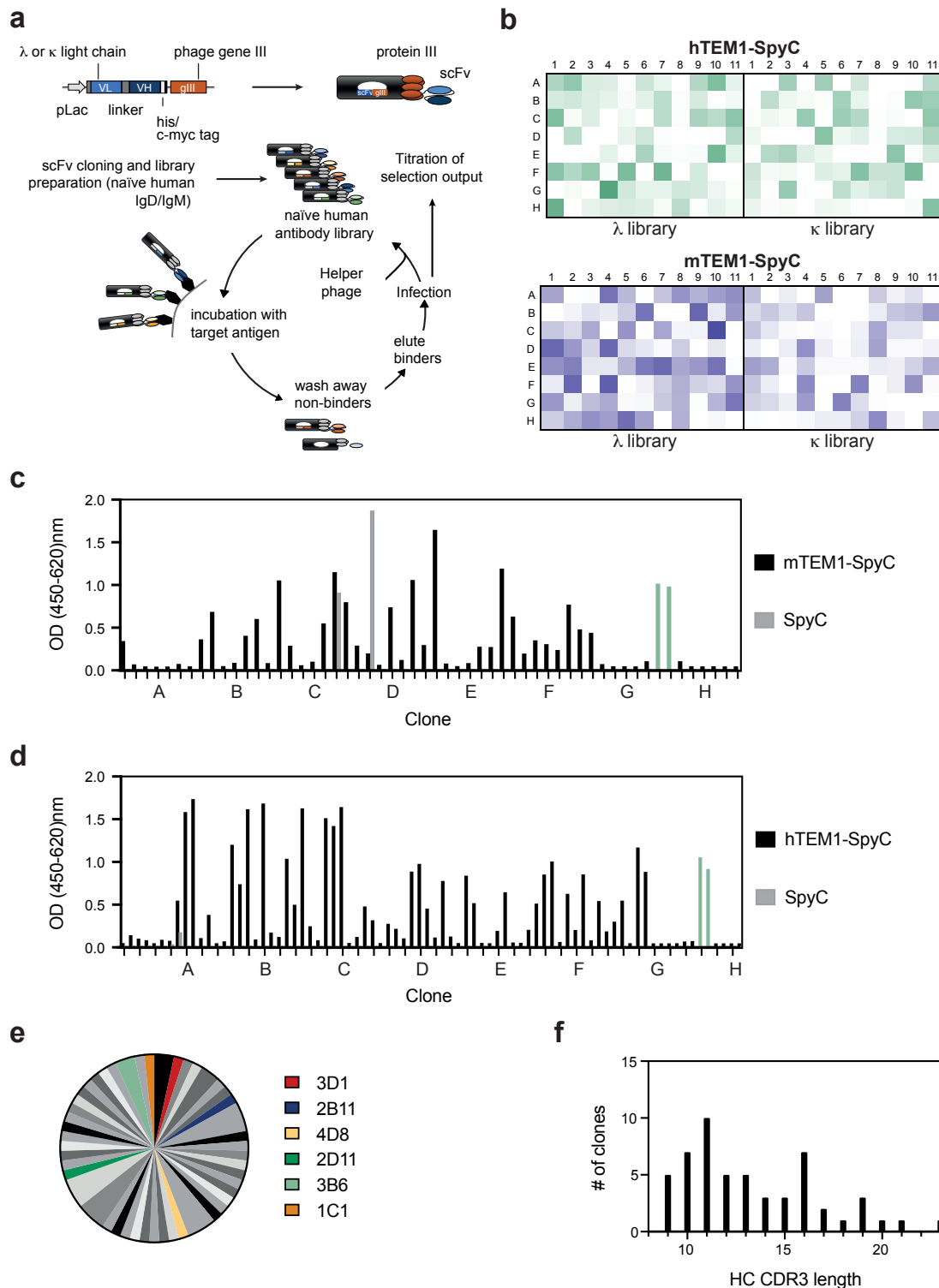
Figure 3.1. *De novo* **discovery of a panel of fully human scFv clones using phage display.**

(**a**) Schematic representation of the phage display selection process for the discovery of scFv binders. (**b**) Heatmap representation of primary ELISA screenings of soluble scFv clones against plate-bound h/mTEM1-SpyC antigens. Phage display outputs of lambda (λ) and kappa (κ) light chain libraries were screened separately. (**c, d**) SpyC-ELISA screening of re-arrayed hits illustrating the high frequency of human/murine cross-reactive binders. Soluble scFvs selected against hTEM1 were screened for binding of mTEM1-SpyC (**c**) and vice versa (**d**). Green bars represent positive controls sc78 (**c**) or MORAb-004 (**d**). (**e**) Clonal diversity of cross-reactive TEM1-binders. Each segment of the pie chart represents a unique clone sequence. Highlighted clones will be discussed below. (**f**) Heavy chain CDR3 length distribution among selected cross-reactive clones.

3.2.2   Functional screening of anti-TEM1 scFv-Fc candidates

To facilitate functional testing and detection, these 15 clones were reformatted in scFv-Fc format by fusing the scFv to the constant domain of human IgG1 (Fig. 3.2a), and transiently expressed in HEK293-6E cells. With one exception, all clones expressed robustly in this system and showed concentration-dependent binding to biotinylated hTEM1 in an ELISA titration experiment (Fig. 3.2b).
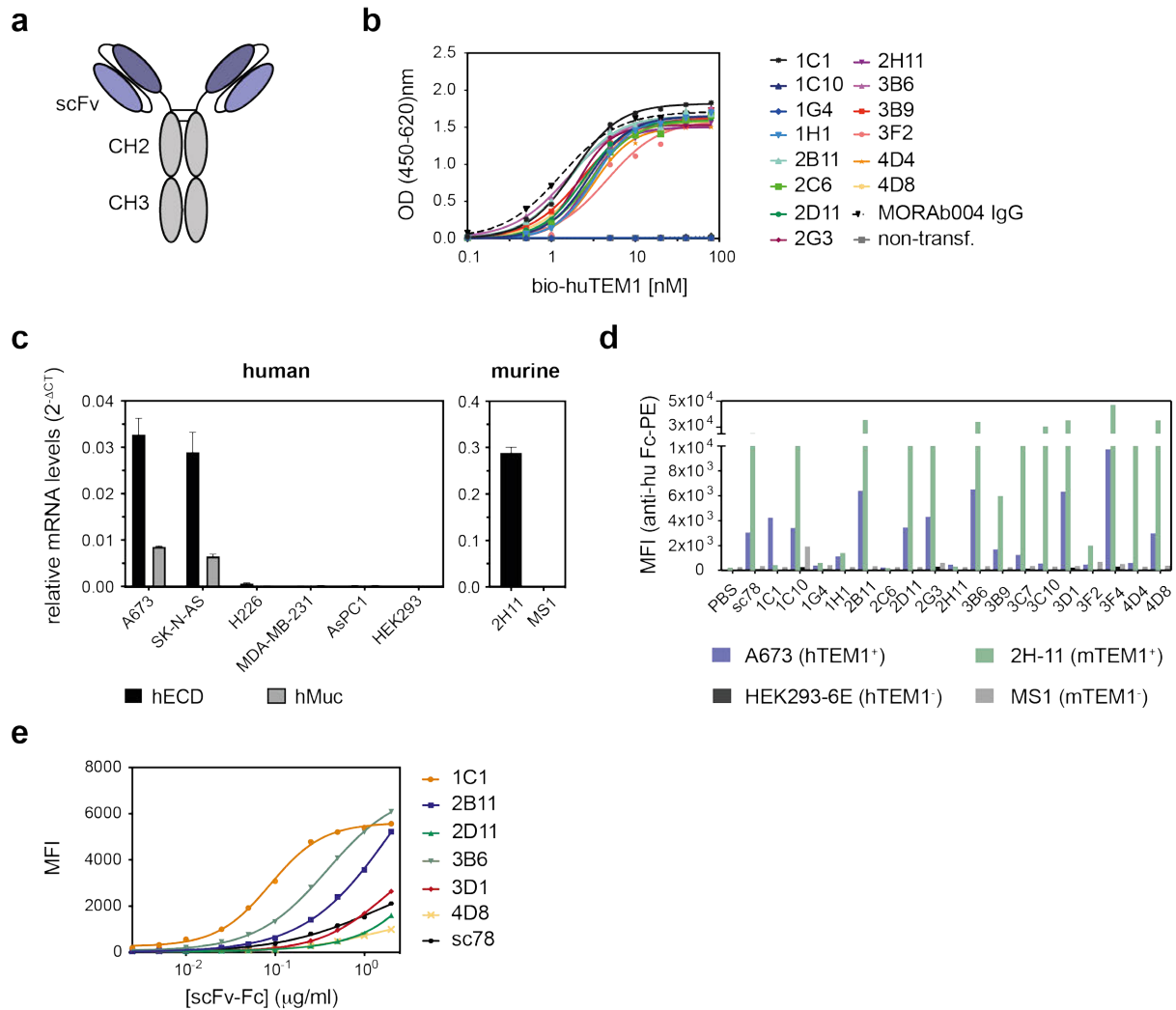
Figure 3.2. Functional screening of anti-TEM1 scFv-Fc candidates.

(**a**) Schematic representation of an scFv-Fc fusion protein. (**b**) ELISA titration of anti-TEM1 scFv-Fc candidates (mammalian expression supernatants diluted 1:10) against plate-bound hTEM1 ECD. TEM1 coating density ranging from 0.1 to 100 nM. (**c**) The comparative mRNA expression of TEM1 was quantified by RT-qPCR. TEM1 mRNA levels were quantified based on the comparative threshold method and are presented relative to glyceraldehyde-3-phosphate-dehydrogenase (GAPDH). A673, Ewing's sarcoma; SK-N-AS, neuroblastoma; H2-226, mesothelioma; MDA-MB-231, mammary carcinoma; AsPC-1, pancreatic adenocarcinoma; HEK293, embryonic kidney epithelium; 2H11, murine tumor vascular endothelium; MS1, murine pancreatic islet endothelium; hECD, extracellular domains of human TEM1; hMuc, sialomucin stalk region of human TEM1.(**d**) Exemplary flow cytometry ranking experiment illustrating the differential binding of a panel of scFv-Fc clones to endogenous TEM1-expressing cell lines A673 and SK-N-AS and to TEM1-negative HEK293-6E and MS1 cells. (**e**) Clones with higher or equivalent MFI binding signals compared to sc78-Fc were serially diluted and titrated against A673 cells. scFv-Fc concentrations ranging from 0.25 ng/ml to 2 μg/ml. CH2/3: hIgG1 heavy chain constant domain 2 or 3. MFI: median fluorescence intensity. PE: phycoerythrin.

Next, we aimed to identify scFv clones that would be able to specifically recognize native TEM1 on the cell surface. To this end, we incubated our candidate scFv-Fc clones with A673 Ewing's sarcoma cells or endothelial 2H-11 cells, expressing endogenous human or murine TEM1, respectively. Similarly, we incubated the scFv-Fc panel with HEK293-6E and MS1 cells, which were confirmed to be negative for TEM1 (Fig. 3.2c). These flow cytometry-based functional screening experiments allowed us to eliminate certain false-positive clones that did not show any binding to native (human) TEM1 in the scFv-Fc format, and confirmed human-murine cross-reactivity for the majority of the hTEM1 binders. Several iterations of such ranking experiments identified six top candidates, selected primarily by equal or higher binding signals compared to the current benchmark clone sc78 (Fig. 3.2d). Those lead candidates were then serially diluted and titrated against hTEM1-expressing A673 cells. In this way, we intended to gain insights into the relative functional binding affinities/avidities of these new scFv-Fc clones. Although all clones recognized A673 cells in a concentration-dependent manner, three candidates, 1C1, 2B11 and 3B6, displayed higher apparent binding affinities and so were chosen for subsequent biophysical characterization alongside the published benchmark clone sc78 (Fig. 3.2e).

3.2.3 Novel anti-TEM1 candidates display favorable biophysical properties and span a wide range of affinities towards hTEM1.

One important metric for the characterization of antibodies is their monovalent affinity towards their cognate targets. We therefore determined the affinities of 1C1, 2B11 and 3B6 to the ECD of human TEM1 by surface plasmon resonance (SPR). Multiple-cycle kinetics data obtained for the purified binders in a simple monovalent bispecific T cell engager (BiTE) format revealed the following affinities: 22 nM for 1C1, 390 nM for 2B11 and 115 nM for 3B6 (Fig. 3.3a). These modest affinities are in line with our expectations for antibodies isolated from naïve natural germline repertoire libraries. Although higher than previously recorded, the monovalent affinity for 1C1 obtained in this experiment is comparable with the values obtained for the same clone using a different experimental set-up (68 nM and 80 nM, respectively; see chapter 2). The higher K_D obtained with 1C1 BiTE may be caused by possible aggregates of this experimental format.

Another parameter that is considered to impact on the developability and performance of scFv-based therapeutics is the stability of the scFv. Differential scanning fluorimetry (DSF) measurements revealed first thermal unfolding transitions occurring at 70.2 °C for 1C1, 75.0 °C for 2B11 and 64.9 °C for 3B6 (Fig. 3.3b). Encouragingly, the stability of our panel of novel TEM1-binders appeared comparable or superior to the current benchmark clone, sc78 (63.3 °C).

Furthermore, in order to map the relative epitope locations targeted by our anti-TEM1 clones, we subjected them to a competition ELISA experiment, where each scFv competed with each scFv-Fc molecule for binding of immobilized hTEM1 ECD. Figure 3.3c shows that 1C1 competes with 2B11 for the binding of hTEM1, while 2B11 only incompletely displaces 1C1, presumable due to the far lower affinity of the molecule. Thus, 1C1 and 2B11 seem to be targeting an overlapping, but clearly distinct epitope, since in contrast to 1C1, 2B11 binds mouse TEM1 very efficiently (compare Fig. 3.2d and Fig. 2.3a). 3B6 however binds to a distinct site on the TEM1 ECD. It is worth noting also that the benchmark clone sc78 binds to a different epitope close to the mucin stalk, which is absent in the ECD fragment used for our phage display selections[306].
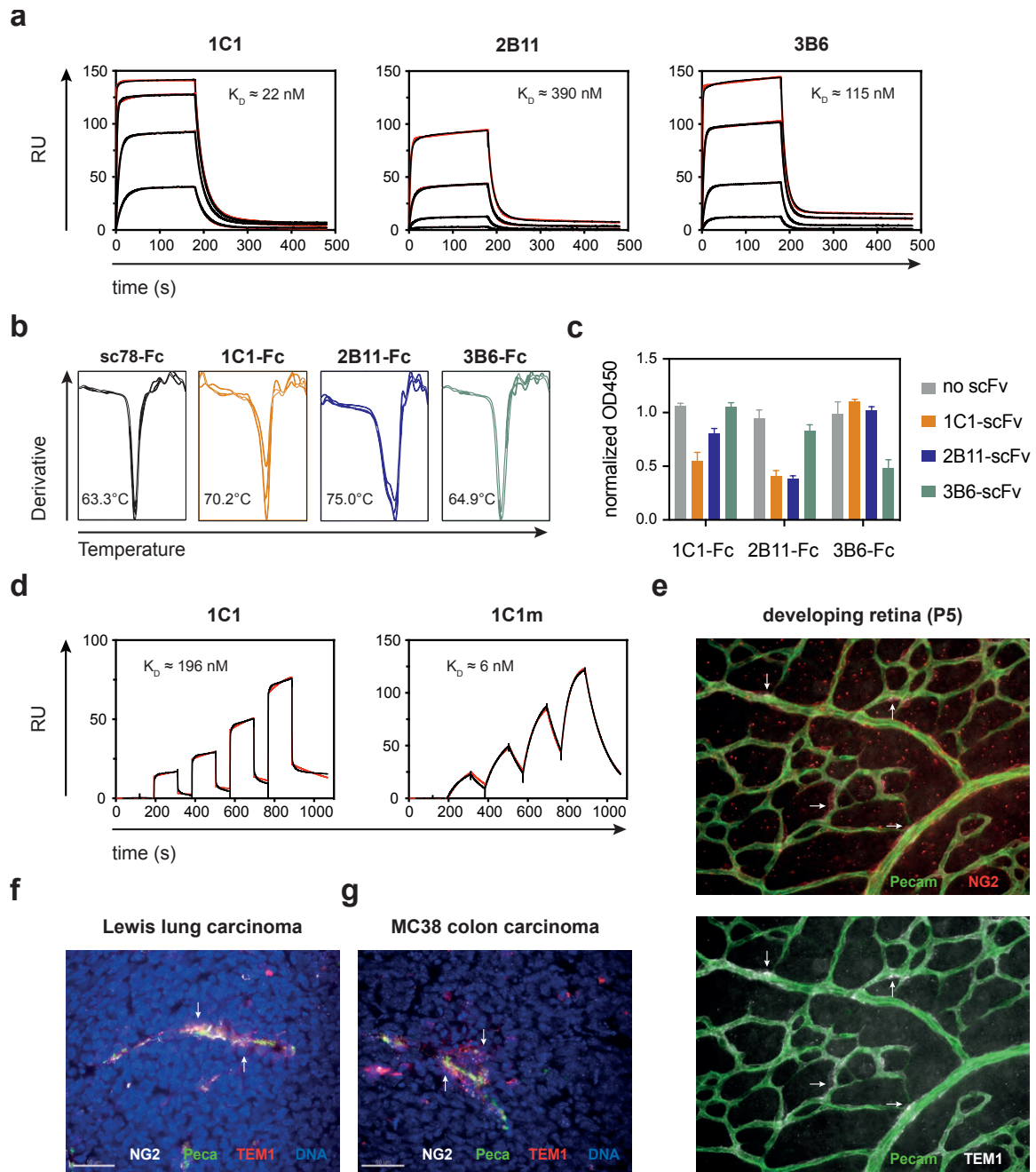
Figure 3.3. Biophysical and functional characterization of anti-TEM1 scFv clones.

(**a**) SPR monovalent affinity determination of anti-TEM1 clones 1C1, 2B11 and 3B6. Biotinylated hTEM1 has been used as the immobilized ligand and monovalent anti-TEM1 bispecific T cell engagers (BiTE) as the soluble analyte, with concentration ranges of 0 nM, 8 nM, 40 nM, 200 nM and 1 µM. (**b**) DSF measurement of the thermostability of anti-TEM1 scFv-Fc clones. Protein unfolding in response to temperature allows interaction and fluorescence of a hydrophobic reporter dye. ScFv melting temperatures are calculated using the derivative of the fluorescence signal. (**c**) ELISA competition of bacterial expressed scFv and purified scFv-Fc clones for binding of immobilized hTEM1 (0.5 µg/ml). A decrease in signal (anti-human Fc-HRP detection) indicates competition of the scFv. (**d**) SPR monovalent affinity determination of 1C1 and the affinity-matured variant 1C1m. mTEM1-SpyC has been immobilized on a streptavidin-chip and monovalent BiTEs have served as the soluble analyte. Analyte concentration ranges were 0 nM, 62.5 nM, 125 nM, 250 nM and 500 nM for 1C1 and 0 nM, 1.25 nM, 2.5 nM, 5 nM and 10 nM for 1C1m. (**e**) IHC of the developing murine retina (P5) using 1C1m-Fc as a primary antibody. 1C1m staining (white) co-localizes with a subset of pericytes (stained against NG2; red). Cryo-sections of Lewis lung carcinoma (**f**) and (**g**) MC38 colon carcinoma xenografts were stained with 1C1m-Fc (red) or anti-NG2 (white). Endothelial cells are stained in green (pecam) and nuclei are visualized with DAPI. 1C1m-Fc staining signal overlaps with TEM1 expression on a subset of pericytes and fibroblasts within the tumor stromal compartment (**f, g**). IHC experiments were performed by Laureline Wetterwald, Tatiana Petrova lab, UNIL.

As described in chapter 2, all of the clones were able to stain several endogenous TEM1 expressing cell lines as well as HEK293T cells transfected with full-length TEM1, but not confirmed negative cell lines (Fig. 2.3a). These functional binding assays also revealed the significantly reduced binding of 1C1 to murine TEM1$^+$ cells, which was further confirmed by SPR affinity measurements (K_D = 196 nM; Fig. 3.3d).

3.2.4 Affinity maturation of selected candidates

Given the relatively modest affinities of our panel of anti-TEM1 clones, we performed affinity maturation of the scFv by directed evolution. To this end, the whole scFv coding sequence was subjected to random mutagenesis using error-prone PCR. The resulting three mutant libraries were then either panned separately against hTEM1, or combined and panned consecutively against human and murine TEM1. In both cases, stringent washing conditions and intra-experimental competition were applied to select for high-affinity binders. Limited sequencing of the selection outcomes after two rounds of selection revealed a striking enrichment of a threonine to isoleucine mutation in the CDR3 loop of the heavy chain of 1C1 in the cross-reactivity selection branch. While the single-clone libraries did not show any detectable enrichment at this rather limited depth of sequence analysis, this mutation was found in 40 % of the sequences in this condition and was therefore characterized in more depth.

Strikingly, SPR affinity measurements revealed that this mutation significantly increased the affinity of 1C1 to both human and murine TEM1, yielding a monovalent affinity of 1 nM towards hTEM1 (see Fig. 2.3b and Supplementary Fig. 2.4) and 6 nM towards mTEM1 (Fig. 3.2d). Together, this single point mutation greatly improved the binding affinity (≈ 70 to 80-fold improvement) and restored cross-reactivity of 1C1, making this clone a promising candidate for further investigation.

3.2.5 Tissue specificity and application in immunohistochemistry (IHC)

In order to further assess the specificity of 1C1m, we next sought to evaluate the specificity of this clone in staining TEM1-expressing cells within tissue sections. As a marker for neo-vasculature, TEM1 has been described to be expressed by a subset of pericytes in developing tissues[266,268]. Taking advantage of the restored human/murine cross-reactivity of 1C1m, we stained tissue sections of the developing murine retina. Encouragingly, staining signal originating from 1C1m-Fc co-localized with a proportion of neonatal pericytes, which were cross-stained for the pericyte marker NG2 (Fig. 3.3e).

In the tumor setting, multiple cell types have been shown to express TEM1, such as pericytes and fibroblasts[266,267,269,275,281]. In line with this more diffuse expression pattern, 1C1m-Fc predominantly stained perivascular cells, but also stromal cells in sections of Lewis lung carcinoma (Fig. 3.3f) and MC38 colon carcinoma tissue (Fig. 3.3g). As was the case in the developing retina, 1C1m staining signal co-localized with pericyte marker NG2. Together, 1C1m clearly stained the expected TEM1-expressing cell types in developing and tumor tissue samples.

3.2.6 Targeting a membrane-proximal epitope of hTEM1

The extracellular domain of TEM1 is separated from the membrane by a large and heavily O-glycosylated mucin stalk domain[288]. To-date, most published antibodies targeting TEM1, including our panel of novel scFv binders, recognize the ECD or the junction of ECD and mucin stalk[305,306,362]. However, several studies have shown that targeting a more membrane-proximal epitope and thus decreasing the bridging distance between the membrane of the T cell and the target cell can improve T cell activation both by CARs[200,201] and soluble

engager molecules[247,248,363]. With this in mind, we aimed to increase the diversity of our panel of TEM1 antibodies by isolating scFv binders to the mucin stalk region of human TEM1.

Using our previously developed dCI method[361], we performed two rounds of phage display selection against a recombinant N-terminally truncated fragment of the hTEM1 ECD (TEM1(nΔ)), comprising only the sialomucin stalk domain (amino acids 547-683). To enrich for binders of native TEM1, this was followed by a third round of phage display against either endogenous TEM1 expressing A673 cells, or HEK293-6E cells transduced with full-length TEM1. In both cases, a negative selection step was performed using untransfected HEK293-6E cells, in order to subtract any irrelevant binders to the general cell surface. Selection outputs were collected after R2 (recombinant antigen) and R3 (cell panning), scFvs were expressed and screened for binding of recombinant TEM1(nΔ) protein using a multiplexed flow-cytometry based screening protocol (see Supplementary Fig. 2.3). Sequencing of primary hits revealed moderate diversity at R2 and a high degree of enrichment at R3, with one clone (7A6) representing 89.3% of all sequences (Fig. 3.4a and b and Table 3.2). Unique binding clones were selected and screened for specific binding of native TEM1-expressing cell lines in scFv-Fc format (Fig. 3.4c and Supplementary Fig. 3.1). Clones that recognized both A673 and SK-N-AS cells, but that did not bind to cells described as negative for TEM1, were selected for in-depth characterization.

3.2.7 Functional characterization and affinity maturation of TEM1 mucin stalk binders

In the first instance, selected scFv-Fc clones were titrated against TEM1^{+} (Fig. 3.4d and Supplementary Fig. 3.1) cells to rank them according to their apparent functional binding affinity. In this ranking experiment, four clones stood out that were able to recognize endogenous TEM1 expressing cells at a higher dilution. These binders were purified by protein A affinity chromatography (see Supplementary Fig. 3.1) and re-assessed for concentration-dependent binding of TEM1^{+} cells. With the exception of clone 1G9, all of the mucin stalk binders recognized A673 cells with higher (1-2 log) apparent EC_{50} than the ECD binders 1C1 and sc78 (Fig. 3.4e).

Given the presumably very modest binding affinities of the TEM1(nΔ)-specific clones, we aimed to enrich for clone variants with improved affinity by random mutagenesis. To this end, the full panel of ten specific cell binders (clones 1G9, 2E1, 3A9, 3L7, 7I2, 7C10, 7G12, 7O22, 7A6 and 9G12) was mutagenized by error-prone PCR, as described previously. The resulting mutant clone libraries were pooled, phages were produced and the mutant library was incubated with bead-captured SpyC-TEM1(nΔ) for two consecutive rounds of phage display selection, applying stringent washing conditions. Subsequently, bacterial scFv clone supernatants were screened for binding of TEM1(nΔ) in a multiplexed flow cytometry-based screening assay. The median fluorescence intensity (MFI) of each binder was plotted and compared to binding signals obtained with parental scFv clones (see Supplementary Fig. 2.3). Two mutations were enriched among the strongest binders, both representing variants of the same parental clone, 7A6. These affinity-matured clone variants were thus selected and reformatted as scFv-Fc fusion molecules. Since one of these variants harbored the mutation in the heavy chain (CDR2 loop) and the second variant contained the mutation in the light chain FR3, these modified heavy and light chains were additionally combined to generate a 'hybrid' variant.

All three variants expressed robustly in HEK293-6E cells and displayed uniform monomeric properties when analyzed by size-exclusion chromatography (Fig. 3.4f). As an indication for functional binding affinity, 7A6

and its three matured variants were titrated for binding of hTEM1+ A673 cells, alongside the ECD-specific clone 1C1m.
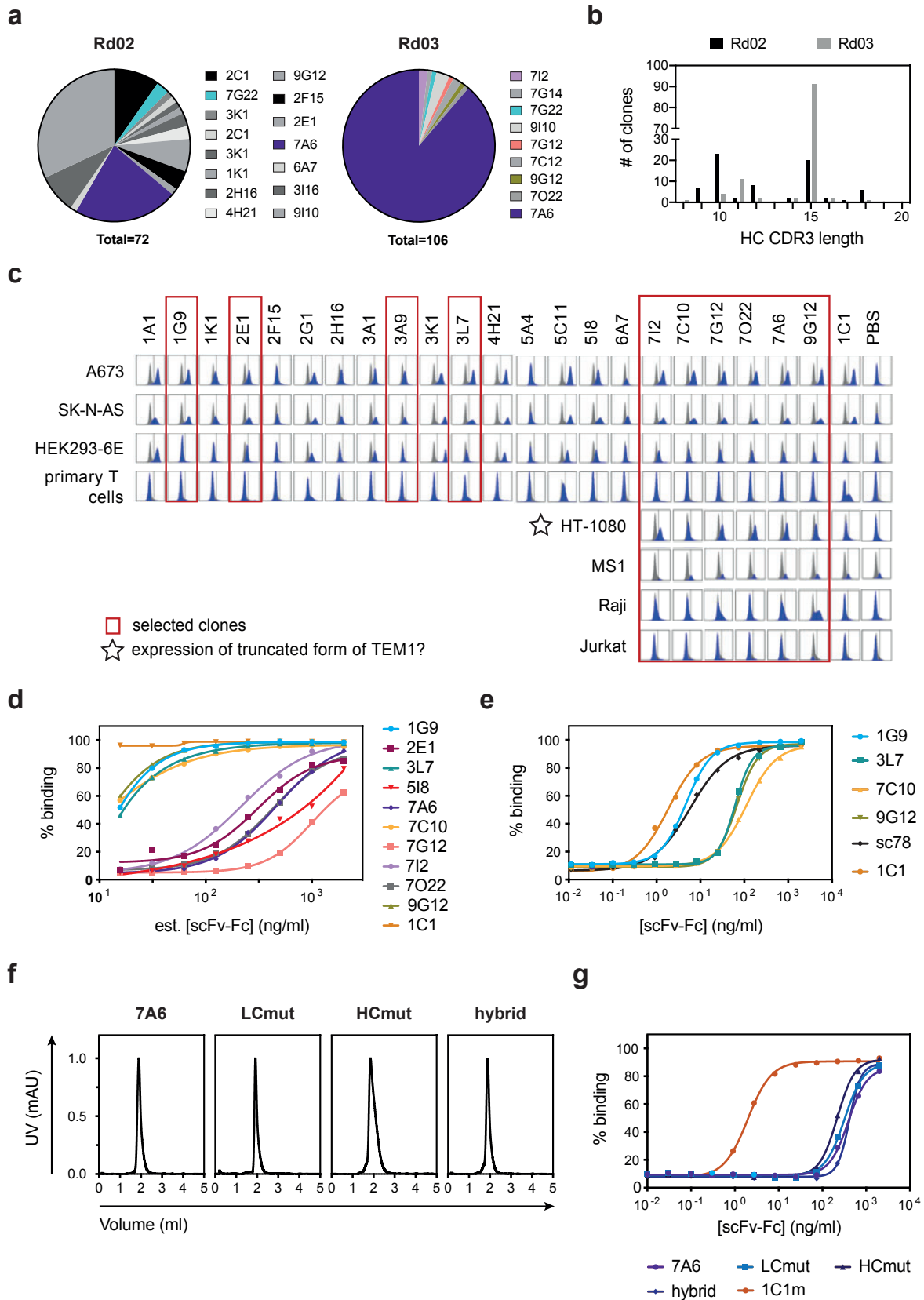
Figure 3.4. Targeting the sialomucin stalk domain of hTEM1.

(**a**) Clonal diversity of anti-hTEM1(Δn) ELISA hits after two rounds of phage display selection against recombinant hTEM1(Δn) and after a third round of selection against TEM1⁺ A673 cells or HEK293-6E cells transfected with full-length hTEM1. Colored clones will be discussed further below. (**b**) Heavy chain CDR3 length distribution of hTEM1(Δn)-binders sequenced after R2 or R3. (**c**) Flow cytometry screening of unique scFv-Fc clones for binding of a panel of TEM1-positive and -negative cell lines. Mammalian scFv-Fc clone supernatants were incubated with the different cells at a 1/100 dilution and binding was revealed with anti-human Fc detection (Alexa647). HT-1080 cells might express a truncated isoform of TEM1. HT-1080: human fibrosarcoma, Raji: human B cell lymphoma. (**d, e**) Flow cytometry titration of serially diluted mammalian expression supernatants containing anti-hTEM1(Δn) scFv-Fc clones (estimated concentrations ranging from 20 ng/ml to 2 µg/ml) (**d**) or purified scFv-Fc protein (0.01 ng/ml – 2 µg/ml) (**e**) against A673 cells. Binding has been revealed with Alexa647 and is displayed relative to background binding (secondary only). 1C1-Fc and sc78-Fc have been used as reference and positive control. (**f**) Analysis of protein homogeneity of purified affinity-matured 7A6 clone variants by size-exclusion chromatography. All variants show homogenous monomeric fractions. (**g**) Flow cytometry titration of purified 7A6-Fc and affinity-matured variants (0.01 ng/ml – 2 µg/ml) against A673 cells. Binding has been revealed with anti-human Fc (Alexa647) detection and is expressed relative to background binding (secondary only).

R2	VH			VL			%
clone	CDR1	CDR2	CDR3	CDR1	CDR2	CDR3	
1A1	GFTFSSYA	ISGSGGST	AKAPGFDY	SSNIGSNT	SNN	AAWDDSLNGPV	2.78
3K1	GFTFSSYA	ISGSGGST	AKGGNSVFPTRY	QSVTRKY	GAS	QQYGSSPRT	1.39
6A7	GFTFDDYA	ISWNSGSI	AKGSYSDY	QDISNY	DAS	QQYDNLPYT	1.39
2C1	GFTFSSYA	ISYDGSNK	ARDPSMIVGFDL	SSDIGSNT	SNN	AAWDDSLNGHYV	8.33
5M15	GFTFSSYG	IWYDGSNK	ARGDYMDV	SSDVGGYNY	EVS	SSYTSSSTVV	4.17
1K1	GGTFSSYA	IIPIFGTA	ARGRYSSSWGYFDY	NLGNKY	QDN	QAWDGSTPYV	1.39
2H16	GYSFTNYW	IYPGDSDT	ARHGPRVEVFDAFHI	QSLVYSDGNTY	KVS	MQGTHWPYT	2.78
4H21	GYTFTSYG	ISAYNGNT	ARNVVVPALYYYGMDV	QSLLHSNGYNY	LGS	MQSLQTPWT	2.78
1A6	GYSFTNYW	IYPGDSDT	ARRYYDSSGYYSLSAFDI	SSNIGNNY	ENN	GTWDSSLSAGV	6.94
5C11	GFTFSSYG	IWYDGSNK	ARSNWFDP	RSDIGSYNY	EVN	SSYTSSSTVV	26.39
2F15	GFPFSGYP	IDESGGRT	ARVEVSGGYYRGFHP	QSLLHSNGYNY	LGS	MQALQTPTT	4.17
2E1	GYSFTSYW	IYPGDSDT	ARWGAQGAVAGSRDAFDI	QSISSW	KAS	QQYNSYWT	1.39
3B5	GYTFTSYY	INPSGGST	ASSGGATRASDAFDI	SSNIGANYD	GNN	QSYDTDLRASV	23.61
3I16	GYSFTSYW	IYPGDSDT	ATWGVGSSGYPIDP	QSVLYSSNNKNY	WAS	QQYYSTPLT	8.33
R3							
7G22	GFTFSSYA	ISGSGGST	AKAPGFDY	SSNIGSNT	SNN	AAWDDSLNGPV	0.89
7I2	GFTFDDYA	ISWNSGSI	AKVAAAGAFDY	SSNIGSNY	RNN	AAWDDTLTGPV	1.79
9I10	GFTFSSYW	IKQDGSEK	ARDQNWNYDY	SSDVGGYDF	EVS	SSYSSSSTYV	2.68
7G12	GYTFTGYY	INPDNGGT	ARGDLDH	TGTVTTGHY	DTS	LLYDDGGRF	0.89
7C12	GFTFSSYA	ISYDGSNK	ARGRSRAGYYYMDV	ESVSDF	RTS	QQYDRYSWG	1.79
7G14	GFTFSSYA	ISYDGSNK	ARGVGDSSGSYYFDY	SSNIGSNT	SNN	AGWDDSLNGWV	0.89
9G12	GYSFTNYW	IYPGDSDT	ARRYYDSSGYYSLSAFDI	SSNIGNNY	ENN	GTWDSSLSAGV	0.89
7O22	GYSFTSYW	IYPGDSDT	ARSDTGATAFDY	QSLVHSNGNTY	KVS	MQGTHWPPYT	0.89
7A6	GYTFTSYY	INPSGGST	ASSGGATRASDAFDI	SSNIGANYD	GNN	QSYDTDLRASV	89.29

Table 3.2. CDR amino acid sequences and frequencies of TEM1(Δn) binders.

However, although all variants stained A673 cells in a concentration-dependent manner, 7A6 and its mutants still only bound the cells at approximately 100-fold higher concentrations, compared to 1C1m (Fig. 3.4g).

Collectively, these results show the *de novo* discovery of a diverse panel of TEM1-specific scFv clones, displaying different biophysical and functional properties and targeting different epitopes on both the ECDs and the sialomucin stalk region of TEM1.

3.3   Discussion

In the present study, we have developed a diverse set of fully human and essentially germline TEM1-specific antibodies using our recently published dCI methodology[361]. Given the greatly reduced immunogenicity risk using fully human targeting scFvs[364], these clones represent ideal candidates for the pre-clinical and clinical development of antibody-based therapeutic agents. Additionally, the murine cross-reactivity offers the potential for readily translatable pre-clinical testing in endogenous murine models.

Given its exclusive expression within the tumor stroma and neo-vasculature, TEM1 represents an ideal biomarker for the detection and monitoring of cancerous lesions. In this context, the previously developed sc78 has been proposed as a tool for near-infrared (NIR) optical imaging. Pre-clinical evaluation of this 78Fc-NIR tracer showed robust discrimination of TEM1-expressing tumor tissue from healthy organs and thus confirmed the suitability of TEM1 as a tumor biomarker[308,335,365]. With its high affinity towards human (1 nM) and murine (6 nM) TEM1, 1C1m compares well with clone sc78 (affinity towards hTEM1 reported as 5.6 nM)[306] and thus represents an additional promising candidate for both pre-clinical and clinical testing. To this end, we have established collaborations that aim to employ our lead candidate 1C1m as the targeting entity for radioimaging and radiotherapy of solid tumors. Encouragingly, Lu177-labeled 1C1m-Fc has been shown to selectively localize to TEM1$^+$ tumor tissue in xenograft mouse models (Judith Delage and David Viertl, CHUV, unpublished).

Besides tumor stromal cells, cancer cells of mesenchymal origin, notably sarcoma, have been found to express TEM1 directly[276,309,366]. Although a heterogeneous group of tumors, sarcomas often share an aggressive pathological behavior and resistance to chemotherapy, leaving surgery with or without radiation as the only therapeutic option. In light of the high prevalence of TEM1 expression across the different sarcoma subtypes, several studies have explored TEM1-targeted therapies as a new treatment strategy for human sarcoma. To our knowledge, all of these efforts have focused on the development of antibody-drug conjugates (ADC) directed against TEM1[304,305,307,309]. Conceptually, ADCs employ the exquisite target specificity of an antibody or antibody-derived targeting moiety for the local delivery of toxins to the tumor, thereby allowing higher local exposure of the tumor to the drug compared to systemic delivery. In this context, sc78 has been explored as an immunotoxin for the treatment of human sarcoma[309,335]. Similarly, other TEM1-specific antibodies have been conjugated with potent toxins to generate ADCs that have shown efficacy in pre-clinical osteosarcoma models[271,304,305]. In a preliminary line of investigation, one of our new clones, 1C1-Fc, has been conjugated to monomethyl auristatin-E, an antimitotic agent blocking the polymerization of tubulin, alongside sc78-Fc. Given its superior thermal stability and functional binding profile, 1C1 and its affinity-matured variant represent equally attractive candidates for ADC-type molecules.

As a prerequisite for investigating therapeutic efficacy, we have shown that both 1C1-Fc and sc78-Fc are internalized by hTEM-expressing cells and, further, that they exert specific cytotoxicity towards human TEM1+ cell lines (preliminary data not shown).

Besides these more traditional antibody applications, scFvs can be utilized as targeting 'warheads' in engineered immunotherapy approaches, typically exemplified by CARs and T cell engaging bispecifics. Such therapies have been employed successfully for the treatment of hematological malignancies, mainly via CD19 targeting[160,168-171,180,214,215,367-369]. However, the development of targeted immunotherapies directed against solid tumors have revealed a number of obstacles that have thus far hindered the clinical impact of these therapies. Key among these are the limited availability of adequately selective tumor-specific antigens, which together with physical and immunosuppressive barriers mediated by the solid tumor microenvironment, present significant challenges with regard to both tissue penetration and therapeutic efficacy[160]. The targeting of TEM1 aims to address both of these aspects. Firstly, TEM1, which as discussed above has a restricted/negligible expression profile in normal somatic tissues, has been shown to be strongly expressed with high incidence on the surface of sarcoma and osteosarcoma tumor cells, thus providing a sound therapeutic targeting rationale[271,276,281,309]. Secondly, the widespread association of TEM1 expression with neo-vasculature provides a conceptual mechanism for physically disrupting tumor integrity in the relative absence of stroma-mediated immunosuppression[266-269,274,275,281,360]. This latter consideration offers the opportunity of general tumor targeting irrespective of the tissue of origin. Encouragingly, T cell responses directed against TEM1 have been shown to reduce tumor vascularity and control tumor progression in a DNA vaccination approach, underlining the potential of TEM1 as a target for cancer immunotherapy. Moreover, TEM1 vaccination did not affect physiological angiogenesis-dependent processes, such as wound healing[310].

Given their encouraging functional and biophysical properties and the low risk of immunogenicity, we anticipate that the isolated TEM1 scFv warhead domains may have significant potential for the development of tumor therapeutic targeting agents. While classical antibody applications, such as ADCs, generally require high affinity to achieve optimal selective efficacy, lower targeting affinities may be favorable for certain adoptive or engager-mediated T cell-based strategies, since a rapid dissociation would allow serial recognition of target antigen, and better recapitulate the weaker receptor/ligand interactions that drive T cell functional activation and killing[370]. Besides scFv affinity, epitope location plays a critical role for the efficacy of T cell engagement. Depending on the structure of the target antigen, recognition of more membrane-proximal epitopes has been found to facilitate T cell retargeting through bispecific engager molecules and CARs[247,248,363]. O'Shannessy and colleagues have previously identified an extensive panel of TEM1 domain-specific monoclonal antibodies with different molecular properties and human-murine cross-reactivity patterns[61]. However, although these tools may help provide insights into the molecular function of the multi-domain protein TEM1, the fact that they were generated in rats may present a roadblock for any clinical development efforts, due to potential immunogenicity issues.

Ultimately, the diverse panel of TEM1-specific scFvs presented here offers the opportunity to fine-tune antigen recognition and biophysical properties for different therapeutic applications. Therefore, in the next chapter, we describe the application of the isolated scFv clones as targeting 'warheads' for T cell engaging bi-specifics and CARs.

3.4 Materials and Methods

3.4.1 Protein expression, phage display and primary screening

Recombinant eukaryotic and prokaryotic protein expression

ECD fragments of human or murine TEM1 were synthesized (GeneArt, Thermo Fisher Scientific) and fused N-terminally to SpyC in a pTT-based mammalian episomal expression vector (pSTEVe20). For phage display selections or bead capture analysis, SpyC-antigens were directly captured from the expression supernatant and immobilized on magnetic streptavidin beads (M-280 Dynabeads; Life Technologies #11206D) pre-coated with 1 µM biotinylated SpyT peptide. For prokaryotic expression of phage display selection outputs, individual *E.coli* TG1 colonies were picked into 2TY medium supplemented with 2% glucose and 100 µg/ml ampicillin (2TYAG) in round-bottom 96-well plates and grown overnight at 30 °C. The following day, the cultures were diluted into Terrific Broth (TB) containing 0.1% glucose and 100 µg/ml ampicillin and grown until reaching an OD600 of 0.6. Protein expression was induced by adding Isopropyl-b-D-thiogalactopyranoside (IPTG; Merck #420322) to a final concentration of 100 µM and proteins were expressed overnight at 30 °C with shaking at 750 rpm. Selected scFv candidates were reformatted into a pTT expression vector containing the constant region of human IgG1 to produce scFv-Fc fusion proteins. Recombinant protein was produced using the HEK293-6E/pTT expression system and FectoPRO transfection protocol (Polyplus, #116-010), as described previously. ScFv-Fc fusions were purified from clarified expression media using a HiTrap™ MabSelect column (GE Healthcare, #11003494), followed by extensive dialysis against phosphate-buffered saline (PBS; Slide-A-Lyzer G2 dialysis cassettes; Life Technologies, #87731).

Selection of naïve human scFvs using phage display

Experimental details of phage display selections are described in chapter 2. Briefly, two fully human scFv libraries (pCHV101_DMk and pCHV101_DMl) were constructed from the IgD/IgM VH and Vk/Vl domain repertoires of 120 healthy donors. Variable regions were amplified, pooled, purified and cloned into the gIII display cassette of a proprietary phagemid vector (pCHV101) in VL – VH orientation. The resulting phage library was rescued using M13KO7 helper phage (Life Technologies, #18311019), pre-blocked with phosphate buffered saline (PBS) containing 0.1% Tween-20, 2% skimmed milk and 1% BSA and incubated with SpyC-coated streptavidin beads to subtract non-specific or SpyC-specific binders. De-selected phage particles were subsequently transferred to tubes containing immobilized SpyC-antigens and incubated at RT for 1 h. Deviating from the protocol detailed in chapter 2, the stringency of washing was not increased at the second round of selection during the panning against h/mTEM1 ECD-fragments. Bound phage were eluted with trypsin, collected and allowed to infect *E.coli* TG1 cells, which were subsequently plated on 2TYAG agar for antibiotic selection of infected cells. Generally, two rounds of phage display were performed for each target selection. For the selection against the sialomucin stalk domain of hTEM1, a third round of phage display selection was performed using cellular targets. To this end, HEK293-6E cells were transfected with a pTAG-CMV expression vector harboring the full-length hTEM1 cDNA ORF (extracted from Genbank RefSeq NM_020404.3), 48 h before the third round of phage selection. Transfections were performed using FectoPRO (Polyplus, #116-010), according to the supplier's recommendations (see chapter 2 for details regarding the transfection and maintenance of HEK293-6E cells). On the day of the experiment, pre/selected phage populations were pre-blocked as described above and then incubated with 10^7 TEM1-negative HEK293-6E cells for 1 h at 4°C to eliminate any non-specific cell binders. Subsequently, the de-selected phage

libraries were transferred to tubes containing either TEM1+ A673 cells, or HEK293-6E cells transfected with full-length hTEM1 and incubated for 1 h at 4°C with gentle rotation. Non-specific phage were removed by 6 x 1ml washes in PBST, followed by 1 x wash in PBS; each time gently collecting the cells by centrifugation (4min at 250 x g). Finally, bound phage were eluted with trypsin allowed to infect TG1 cells and finally stored frozen in 2TYG containing 15% glycerol, analogous to the standard phage display protocol.

For primary screening, individual colonies were picked into 2TYAG liquid medium, grown until turbid and then diluted into TB medium supplemented with ampicillin for recombinant protein expression.

Enzyme-linked immunosorbent assay (ELISA)

Primary selection outputs were screened by dCl SpyC-antigen ELISA, as described previously. For ELISA titration experiments, Nunc Maxisorp 96-well plates (Thermo Fisher Scientific, #442404) were coated with 10 μg/ml Neutravidin (Life Technologies, #31000) in PBS over-night at 4 °C, washed 3x in PBST and blocked with 300 μl 5% skimmed milk in PBST for 45 min at RT. After washing 3x with PBST, 100 μl biotinylated hTEM ECD (produced in-house, see chapter 2) was added to each well, in a 2-fold dilution series ranging from 100 nM to 0.1 nM, diluted in PBS/1% BSA and incubated for 1 h at RT, followed by 3x PBST washes. Selected scFv-Fc fusion molecules were diluted 1:10 in 1% BSA/ PBS and added to the plate at 100 μl per well. Incubation was at RT for 1 h and the well were washed 4x in PBST, before detection with goat anti-human IgG Fc polyclonal HRP conjugate (Sino Biologicals, #SSA001; 1:5000 dilution), using TMB as a substrate. All wash steps were performed by dispensing 300 μl PBST from a BioTek405 automatic plate washer.

For assessing competition of scFv clones for binding of hTEM1, ELISA plates were first coated with Neutravidin overnight, then blocked as described above and subsequently incubated with 0.5 μg/ml biotinylated hTEM1 ECD, diluted in 1% BSA/PBST for 1 h at RT. To set up the competition, scFv-Fc clones were diluted to 0.1 μg/ml and mixed 1:1 with cleared scFv containing TG1 expression supernatants pre-blocked with 5% skimmed milk/PBST. After 10 min of pre-incubation, the competition mixture was added to the washed (3x PBST) ELISA plate and allowed to interact with hTEM1 for 1.5 h at RT. The plate was washed 4x with PBST and bound scFv-Fc were revealed as described above.

Affinity maturation and multiplexed bead-based screening assays

Selected scFv clones were subjected to random mutagenesis across the whole scFv, using error-prone PCR with the Diversify PCR random mutagenesis kit (Takara, #630703). The complete affinity maturation method for both TEM1 ECD-binders and scFvs specific for the sialomucin stalk of TEM1 (SpyC-hTEM1(Δn) is described in chapter 2. Similarly, the multiplexed bead-based no wash screening assay used to screen scFv clone outputs from the SpyC-hTEM1(Δn) primary selection and affinity maturation for specific binding of cognate SpyC-antigen has been described previously.

3.4.2   Biophysical protein characterization

Surface Plasmone Resonance (SPR)

SPR analysis was performed on a Biacore T200 instrument (GE Healthcare) and in 1x filtered Biacore running buffer (HBS-EP+; 0.01 M HEPES, 0.15 M NaCl, 0.05% Surfactant P20, 3 mM EDTA, pH 7.4; GE Healthcare, #BR-1006-69). Experiments probing the monovalent affinities of anti-TEM1 scFv candidates used a Series S SA sensor chip (GE Healthcare, #BR-1005-31). To immobilize hTEM1, 1 μg/ml biotinylated hTEM1 were injected at 30 μl/min until reaching a target density of 150 RU, following the manufacturer's instructions. For kinetic

analysis, monovalent scFv candidates fused in tandem to an anti-CD3 scFv were injected at 30 µl/min and data was acquired in Multiple Cycle Kinetics mode. Analytes were diluted to 8 nM, 40 nM, 200 nM and 1 µM in running buffer. The chip surface was regenerated between cycles by injecting 10 mM glycine-HCl, pH 1.5 for 30 s. For kinetics analysis, the signal of a reference cell devoid of ligand was subtracted from the active cell to correct for bulk shift and refractive index changes.

SPR experiments involving mTEM1-SpyC ligand were performed as described in chapter 2. Analyte concentration ranges were 0 nM, 62.5 nM, 125 nM, 250 nM and 500 nM for 1C1 and 0 nM, 1.25 nM, 2.5 nM, 5 nM and 10 nM for 1C1m.

Differential Scanning Fluorimetry (DSF) stability assay

In order to compare the relative thermal stability of different scFv clones, a thermal shift assay was performed following the Protein Thermal Shift Assay protocol from Applied Biosystems (#4461146). Therefore, purified scFv-Fc fusion proteins were diluted to 5 µM with PBS and mixed with 5 µl Protein Thermal Shift Buffer and 2.5 µl 8x Protein Thermal Shift Dye. Each reaction was prepared in triplicate in a MicroAmp Fast Optical Reaction Plate (Lifetechnologies, #4346907) and sealed with MicroAmp Optical Adhesive Film (Lifetechnologies, #4360954). Melting curves were generated with a 7500 Fast RT-PCR machine (Applied Biosystems), starting at 25 °C and gradually increasing the temperature by 0.05 °C/s until reaching 99 °C. To obtain relative melting temperatures based on the transition point of the melting curve, the derivative of the fluorescence signal was calculated as a function of temperature. Data analysis was carried out using Applied Biosystems 7500 Fast RT-PCR software.

Analytical size-exclusion chromatography (SEC)

The integrity and homogeneity of protein candidates was assessed by SEC using an ÄKTApure chromatography system (GE Healthcare). To this end, 100 µl concentrated (≈1 mg/ml) protein sample was injected and separated over a Superdex 200 Increase 5/150 GL analytical grade column (GE Healthcare, #28990945) at a flow rate of 0.45 ml/min. PBS (0.01 M phosphate, 0.14 M NaCl, pH 7.4) was used as sample diluent and eluent.

Analysis of proteins by SDS-PAGE

For analyzing purified proteins by gel electrophoresis, typically 2 µg protein sample were mixed with 1x LDS buffer (NuPAGE; Life Technologies, #NP0007) with or without 10% reducing agent (NuPAGE; Life Technologies #NP0009) and heated at 70 °C for 10 min. To confirm protein expression, mammalian expression supernatants were mixed with LDS buffer and reducing agent and processed in the same way. Samples were collected by centrifugation and separated on a Novex 4-12% Bis-Tris gel (Life Technologies, #NP0321) for 38 min at 200 V. Separated protein bands were visualized by Coomassie Blue staining (InstantBlue; Expedeon, #ISB1L).

3.4.3   Cell assays and functional characterization

Cell culture and flow cytometry

All cell lines were obtained from the ATCC via LGC Standards. References and culture conditions, as well as a general protocol for flow cytometry are detailed in chapter 2. For flow cytometry based functional screening, mammalian expression supernatants containing scFv-Fc fusion proteins were diluted 1/10 in FACS buffer (5%

FBS in PBS) and added to 0.5x10^6 cells per sample. After washing three times in FACS buffer, PE-conjugated anti-human Fc secondary antibody (Biolegend, #409303) was added and incubated for 30 min on ice. For flow cytometry titration experiments, scFv-Fc molecules were serially diluted in FACS buffer, typically in a concentration range spanning 0.2 or 2 ng/ml to 2 µg/ml, before adding to the cells. In titration experiments, Alexa Fluor 647 AffiniPure Goat Anti-Human IgG was used as a secondary antibody (Jackson Immunoresearch, #109-605-098, 1:200 dilution). Data was acquired using an LSR-II flow cytometer equipped with FACSDIVA software (BD Biosciences). Data analysis and plotting were carried out using FlowJo v10 (FlowJo LLC).

For high-throughput screenings of hTEM1(Δn)-binding clones, mammalian expression supernatants containing scFv-Fc protein were diluted 1/100 in FACS buffer and incubated with the blocked cells as described above. Any cell binding was revealed using an Alexa Fluor 647 AffiniPure Goat Anti-Human IgG secondary antibody (Jackson Immunoresearch, #109-605-098, 1:200 dilution). Wash steps after both primary and secondary antibody incubation were 3x 100 µl FACS buffer. Data for these experiments was acquired using an Intellicyt iQue TM Screener PLUS instrument (10 s sampling; 1 µl/s) and data analysis was performed using Forecyt software (Intellicyt).

Quantifying mRNA expression by reverse transcription quantitative polymerase chain reaction (RT-qPCR)

For mRNA isolation, 10^7 cells were seeded into a T75 tissue culture flask and harvested with trypsin-EDTA after 24 h. Detached cells were collected by centrifugation (5 min at 250x g) and washed once in ice-cold PBS. The cell pellets were either snap-frozen on dry ice and stored at -80 °C or immediately processed for mRNA isolation. Cells were lysed by adding 600 µl buffer RLT and samples were homogenized by passing the lysate through an RNAse-free syringe with 20-gauge needle (Braun). Subsequently, mRNA was isolated by absorption of RNA longer than 200 bases to the silica-based membrane of microspin columns using the Qiagen RNeasy Mini kit (Qiagen, #74106), following the manufacturer's instructions. Then, mRNA was reverse transcribed into cDNA using the Takara Primescript First Strand cDNA synthesis kit (Takara, #6110B). Briefly, 5 µM oligo dT primer were annealed with 1 µg total mRNA in a total volume of 10 µl containing dNTP (1 mM each), by incubating at 65 °C for 5 min. 20 units RNase inhibitor and 200 units PrimeScript reverse transcriptase were added to the annealed RNA/primer mixture and the reaction was allowed to take place for 1 h at 42 °C. The reaction was stopped by heating to 70 °C for 15 min and the samples were immediately cooled on ice before snap-freezing on dry ice for storage (at -80 °C) or analysis by qPCR. For TaqMan qPCR, approximately 50 ng cDNA were mixed with 10 µl TaqMan Fast Universal Master Mix (Applied Biosystems, #4352042) and 1 µl TaqMan probe in a total reaction volume of 20 µl. The following FAM-MGB-TaqMan probes were used to detect target and reference genes: hCD248 (#4331182_Hs00535586_s1), mCD248 (#4331182_Mm00547485_s1), hGAPDH (#4331182_Hs02786624_g1) and mGAPDH ((#4331182_Mm99999915_g1), all from ThermoFisher Scientific. Real-time PCR amplification of target and housekeeping genes was performed in a 7500 Fast RT-PCR machine (Applied Biosystems) and relative gene expression levels in different cell lines were analyzed by comparative threshold cycle (Ct) quantification. Expression levels are presented relative to GAPDH.

Immunohistochemistry

Retinas were collected from newborn pups at day 5, fixed in 4% paraformaldehyde (PFA) for 4 h at 4 °C and, after washing with PBS, blocked overnight at 4 °C with 5% donkey serum, 0.5% BSA, 0.3% Triton X-100, 0.1% sodium azide, in PBS. For tumor staining experiments, 5x 10^5 Lewis lung carcinoma (ATCC, #CRL-1642) or MC38 colon carcinoma (Kerafast, # ENH204-FP) cells were resuspended in PBS and injected subcutaneously

into the right flank of adult C57BL/6 mice. Once the tumors reached a volume of 1 cm^3, the animals were perfused with 4% PFA, sacrificed and the tumors were collected and further fixed overnight in 4% PFA. Washed tumors were then incubated in 30% sucrose for 12 h before embedding in optimal cutting temperature (OCT) compound (Tissue-Tek, #4583) for frozen sectioning. 8 µm cryosections were prepared at the histology facility of UNIL and blocked as described above. For the staining, both retinas and tumor sections were incubated overnight at 4 °C with 5 µg/ml 1C1m-Fc, diluted in blocking buffer. The following day, the retinas were washed 5x 10 min and the tumor sections 3x 10 min with blocking buffer and then incubated with an Alexa Fluor 555-conjugated goat anti-human antibody (diluted 1:500 in blocking buffer; Invitrogen, #A21433) overnight at 4 °C. Wash steps were repeated and imaged were acquired using an upright Zeiss Axio Imager Z1 microscope.

3.5   Supplementary Information
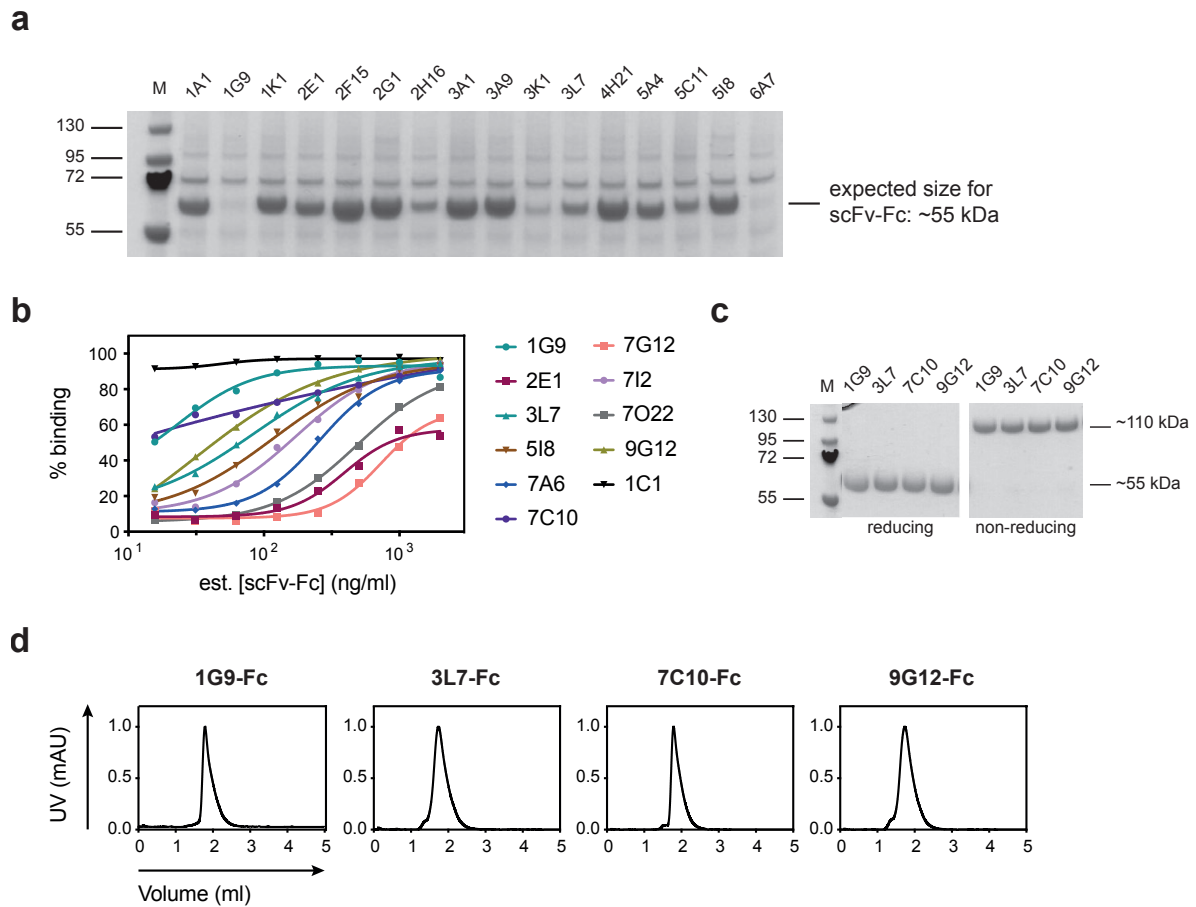
Supplementary Figure 3.1. Expression and characterization of TEM1(Δn) binders.

(**a**) Reducing SDS-PAGE of anti-TEM1(Δn) primary hits in scFv-Fc format. 6.5 μl crude expression supernatants were loaded and separated in a 4-12 % Bis-Tris gradient gel. Expected size for an intact scFv-Fc molecule is ~55 kDa. (**b**) Flow cytometry titration of serially diluted mammalian expression supernatants containing anti-hTEM1(Δn) scFv-Fc clones (estimated concentrations ranging from 20 ng/ml to 2 μg/ml) against hTEM1+ SK-N-AS cells. (**c**) Reducing and non-reducing SDS-PAGE of 2μg purified anti-TEM1(Δn) clones in scFv-Fc format. Expected molecular weight is ~55 kDa for reduced samples and ~110 kDa for intact dimers. (**d**) Analysis of protein homogeneity of purified hTEM1(Δn) scFv-Fc clones by size-exclusion chromatography. All variants show homogenous monomeric fractions.

Chapter 4   Novel trivalent T cell engagers and Chimeric Antigen Receptors targeting TEM1 for cancer immunotherapy

The following chapter describes the design and validation of a versatile new bispecific T cell engager format, that we have termed TriloBiTE (**Tri**-lobed **Bi**-directional **T** cell **E**ngager). Further, this study focuses on the application of our diverse panel of anti-TEM1 single-chain antibodies as targeting 'warheads' for soluble T cell engagers (TriloBiTEs) and chimeric antigen receptors (CARs). This chapter is based on an article that is currently under preparation.

Authors and affiliations:

Julie K. **Fierle**[1], Mariastella deTiani[1], Johan Abram[1], Vasileios Atsaves[1], Matteo Brioschi[1], Laureline Wetterwald[1], Tatiana Petrova[1], George Coukos[1,2,3] and Steven M. Dunn[1,2]

[1] Ludwig Center for Cancer Research of the University of Lausanne, Lausanne, Switzerland.
[2] Department of Oncology, Hospital of the University of Lausanne (CHUV), Lausanne, Switzerland.
[3] Ovarian Cancer Research Center, Perelman School of Medicine, University of Pennsylvania, Philadelphia, USA.

Author contributions:

JKF and SMD conceived and designed the experiments. JKF performed the experiments and analyzed the data. MdT helped with cloning and molecular biology experiments. JAS isolated and characterized the anti-mesothelin scFv clones. VA helped with T cell isolation. MB helped with protein purification and SPR experiments. LW performed IHC experiments and provided the images. JKF, SMD, and GC wrote/reviewed the manuscript.

4.1 Introduction

It is a well-established concept that T cells are able to recognize malignant cells and participate in the control of tumor growth[371]. This observation has paved the road to cancer immunotherapy, aiming to harness the potential of the immune system to eliminate cancer cells. Under physiological conditions, T cells recognize unique, mutated (neo-) and aberrantly expressed peptides presented on major histocompatibility class (MHC) molecules through the T cell receptor (TCR). However, cancer cells often develop mechanisms to escape immune surveillance, for instance by downregulating the expression of MHC molecules[112]. Therefore, besides strategies to boost natural anti-tumor defense mechanisms[141,143,372-375], several engineering approaches have been developed, equipping T cells with tumor-targeting capabilities that can bypass individual T cell receptor (TCR) specificities[160,212,368,376]. Thus, these approaches aim at recruiting and redirecting the cytotoxic potential of bulk T cell populations towards malignant cells, with the objective of overcoming (or overwhelming) immune tolerance and tumor-mediated suppression.

In order to redirect the cytotoxic effector function of T cells, bispecific antibody-derived mediators have been developed comprising a tumor-targeting moiety fused to an anti-CD3 recognition domain for the engagement and activation of T cells[203,204]. The most advanced molecules of this class are the so-called bispecific T cell engagers (BiTEs)[214]. These soluble molecules are based on two distinct single-chain antibodies (scFvs) separated by an appropriate flexible linker. This approach allows the recruitment and activation of a broad polyclonal population of unstimulated T cells to the tumor cell surface irrespective of individual TCR specificities[206,207]. To date, a vast array of molecular formats have been developed for T cell engaging bispecifics, all of them conferring different binding geometries and molecular properties[212,213]. The choice of targeting geometry and affinity, as well as the binding epitope are of paramount importance for the efficacy of these bispecific mediators, and have to be optimized for each tumor-associated antigen[212,213,248].

Instead of using soluble mediators to recruit T cells to the tumor site, T cells can also be engineered to express synthetic tumor targeting receptors, termed chimeric antigen receptors (CARs). To redirect antigen specificity, a ligand-binding domain, typically a scFv, is linked to an intracellular signaling module that includes an assemblage of immunoreceptor tyrosine-based activation motifs (ITAMs), such as is found in the cytoplasmic tail of CD3ζ, which mediate T cell activation upon antigen recognition. In order to mimic co-stimulation as it is provided by antigen presenting cells during T cell activation, the signaling endodomains of CD28, 4-1BB and/or OX40 are typically fused to CD3ζ, thereby attempting to achieve full physiological T cell activation[163,164]. CAR structural design has a major impact on the efficacy of adoptive T cell therapy *in vivo*, which in turn depends not only on efficient antigen recognition, but also on T cell expansion and persistence[162,377]. Antigen recognition is mainly driven by the affinity and specificity of the target-binding. Depending on the antigen density, CAR potency has been shown to improve with increasing scFv affinity or to be subjected to an avidity threshold, above which T cell function reaches a plateau or may even decrease[193,194,196]. Also, the spatial distance between the CAR T cell and the target cell plays a crucial role in T cell activation. Here, the factors determining optimal distance are epitope location and length/flexibility of the linker between CAR targeting domain and transmembrane domain[199-202]. Generally, however, few studies exist that have sought to comprehensively address the interplay between target epitope, scFv affinity and cellular bridging distance. Moreover, the proliferation and persistence of CAR T cells *in vivo* can be profoundly influenced by constitutive antigen-independent signaling. This phenomenon, termed tonic signaling, has been shown to drive early T cell exhaustion and limit T cell efficacy, and its extent is determined by the choice of co-stimulatory endodomain and by the specificity and biophysical properties of the targeting scFv[378].

Altogether, the design of both T cell engaging bispecifics and CARs requires significant engineering efforts with a multitude of parameters to be optimized for each new target antigen. However, once in place, both T cell retargeting strategies have proven efficacious in numerous clinical trials[167-171,180,214,215,367-369]. Thus, both an anti-CD19xCD3 BiTE (blinatumomab/ Blincyto) and a CD19-targeting CAR (tisagenlecleucel/ Kymriah) have been recently approved for the treatment of severe relapsed B-cell malignancies. Following these pioneering approvals, there has emerged strong interest in the development of T cell retargeting therapies that have novel antigen specificities and that may prove efficacious in solid tumors. To this end, and in order to achieve maximum efficacy while limiting toxicity, it is of paramount importance to identify novel tumor-associated or tumor-specific antigens that facilitate the selective targeting of tumor tissue.

The cell-surface antigen Tumor Endothelial Marker 1 (TEM1, Endosialin, CD248) is largely undetectable in normal tissues, but is selectively expressed in the stroma and neo-vasculature of many solid tumors[264,266,267,270,271,275,288]. More specifically, TEM1 expression has been detected on pericytes, endothelial precursor cells, fibroblasts and smooth muscle cells throughout the tumor vasculature[266,269,379]. Furthermore, TEM1 is expressed on tumor cells in a number of high-grade sarcomas[276]. Although its molecular function remains elusive, TEM1 is implicated in vascular cell adhesion and migration, angiogenesis and tumor progression[292]. Importantly, TEM1$^{-/-}$ mice show impaired tumor growth, invasiveness and metastasis, while exhibiting normal wound healing[290]. As a specific marker of tumor vasculature, TEM1 has emerged as an attractive target for cancer therapy[266,271,275,304]. Substantial therapeutic results can be achieved by targeting the supporting cells of the tumor vasculature, in part because these cells otherwise present a barrier that shields tumor cells from the immune system[254,380]. Moreover, as a vascular antigen, TEM1 should be relatively accessible to peripherally circulating drugs and T cells and may be expected to display lower mutational escape rates than more traditional antigens located directly on tumor cells[381]. Finally, since TEM1 is not restricted to a specific tissue of origin, any emerging therapies could be applied to a wide range of tumor types[310].

Therefore, the aim of this study is to explore the potential of TEM1 as a target for engineered cancer immunotherapy approaches using *de novo* discovered scFv antibodies.

4.2   Results

4.2.1   TriloBiTEs: A novel trivalent T cell engager format.

We initially sought to develop an intermediate-sized T cell engager molecule that would allow flexible mono- or bivalent antigen binding, yet have sufficient mass to resist direct renal elimination whilst still permitting efficient tissue penetration. Inspired by the use of the disulfide-stabilized interaction of LC and VH-CH1 as an heterodimerization scaffold proposed by Schoonjans, R. et al.[382] , we C-terminally fused a scFv domain to both heavy (VH-CH1(IgG1)) and light chain (VL-Cκ) of a humanized and chimeric anti-CD3 Fab (derived from the murine mAb clone UCHT1). In contrast to the previously published 'tribody' format[382], which employs murine CH1 and Cκ domains for dimerization, we utilized fully human Fab constant domain sequences. However, since the interaction between the isolated human CH1 and Cκ domains alone is generally quite weak, and would require significant co-operative stabilization via the interface generated by the appended

UCHT1 VH and Vκ domains to maintain structural integrity[57], we aimed to further stabilize the human CH1-Cκ Fab interface. Previously, structural exploration of the CH1-CK interface has revealed a relative absence of buried hydrophobic packing interactions at the N-terminal region of the interface. To address this, stabilizing mutations have been introduced in this region using phage display[383]. Guided by this study, we have inserted the S64E and S66V mutations into the human CH1 (IgG1) domain and the S69L and T71S mutations into the human Cκ domain of the chimeric UCHT1 Fab (Fig. 4.1a). The resulting T cell engager molecule, which we term "TriloBiTE" (tB), now allows the modular combination of a stabilized anti-CD3 Fab with one or two antigen-targeting scFvs, separated from each chain of the Fab by carefully considered flexible (Gly/Ser-rich) linkers (Fig. 4.1a).

4.2.2 TriloBiTEs specifically redirect human T cells to target relevant cancer cells.

As a proof-of-concept, we first engineered a bivalent CD19-specific TriloBiTE by fusing the clinically validated murine anti-CD19 scFv clone FMC63 to both chains of the anti-CD3 arm[384]. Transient expression from recombinant HEK293-6E cells yielded robust protein quantities (≈ 20 mg/l; Fig. 4.1b) with the purified material comprising predominantly homogeneous heterodimeric monomer (Fig. 4.1c). TCR signaling via CD3ζ activates a number of molecular pathways, such as the induction of the calcium-calmodulin-dependent phosphatase calcineurin, which dephosphorylates members of the nuclear factor of activated T cells (NFAT) family. The NFAT transcription factors then migrate to the nucleus and induce a number of genes involved in cytokine production, T cell proliferation and survival[32]. Since NFAT signaling depends on the strength and duration of T cell activation[385], reporter systems have been developed that couple NFAT signaling with the expression of a reporter gene in order to probe and compare T cell engagement via the TCR/CD3 complex[386,387]. We thus employed a Jurkat reporter cell line expressing luciferase under the control of an NFAT-driven promoter to assess T cell activation by the αCD19-tB. Encouragingly, our proof-of-concept αCD19-tB molecule induced NFAT-signaling in a concentration-dependent manner and specifically in the presence of CD19+ Raji cells, while no luciferase signal was detected in the presence of irrelevant cells (Fig. 4.1d). We next sought to assess the potential of the TriloBiTE engagers to redirect the effector function of primary T cells. In a co-culture set-up, the αCD19-tB was able to specifically activate a polyclonal population of primary human CD8+ T cells, which in turn lysed CD19+ Raji cells, but spared CD19-negative HEK293 cells (Fig. 4.1e). Moreover, T cells activated with the TriloBiTE secreted relevant effector cytokines with the magnitude of the cytokine response being dependent on the TriloBiTE concentration (Fig. 4.1f).

4.2.3 TriloBiTEs induce potent cytotoxicity of human T cells towards mesothelin-expressing human cancer cells.

Having validated our TriloBiTE T cell engager format with the well-characterized anti-CD19 'warhead' FMC63, we next aimed to test the TriloBiTE format with more experimental scFv clones isolated in-house from *de novo* phage display using our dCI-technology (see chapter 2). We therefore reformatted two novel scFv clones specific for human mesothelin (meso) in the bivalent TriloBiTE format, alongside a published benchmark clone, hP4[340]. After confirming that the resulting αMeso-tBs were able to engage T cells via CD3 (see Fig. 2.4b, c), we assessed the potential of these molecules in redirecting primary human T cells. All three molecules induced target-specific cytotoxicity (see Fig. 4.1g and Fig. 2.4c, d) and effector cytokine production (Fig. 4.1h), directed exclusively against mesothelin-expressing tumor cells, indicating that our αMeso-tBs efficiently activated a polyclonal pool of primary human T cells in an antigen-dependent manner.
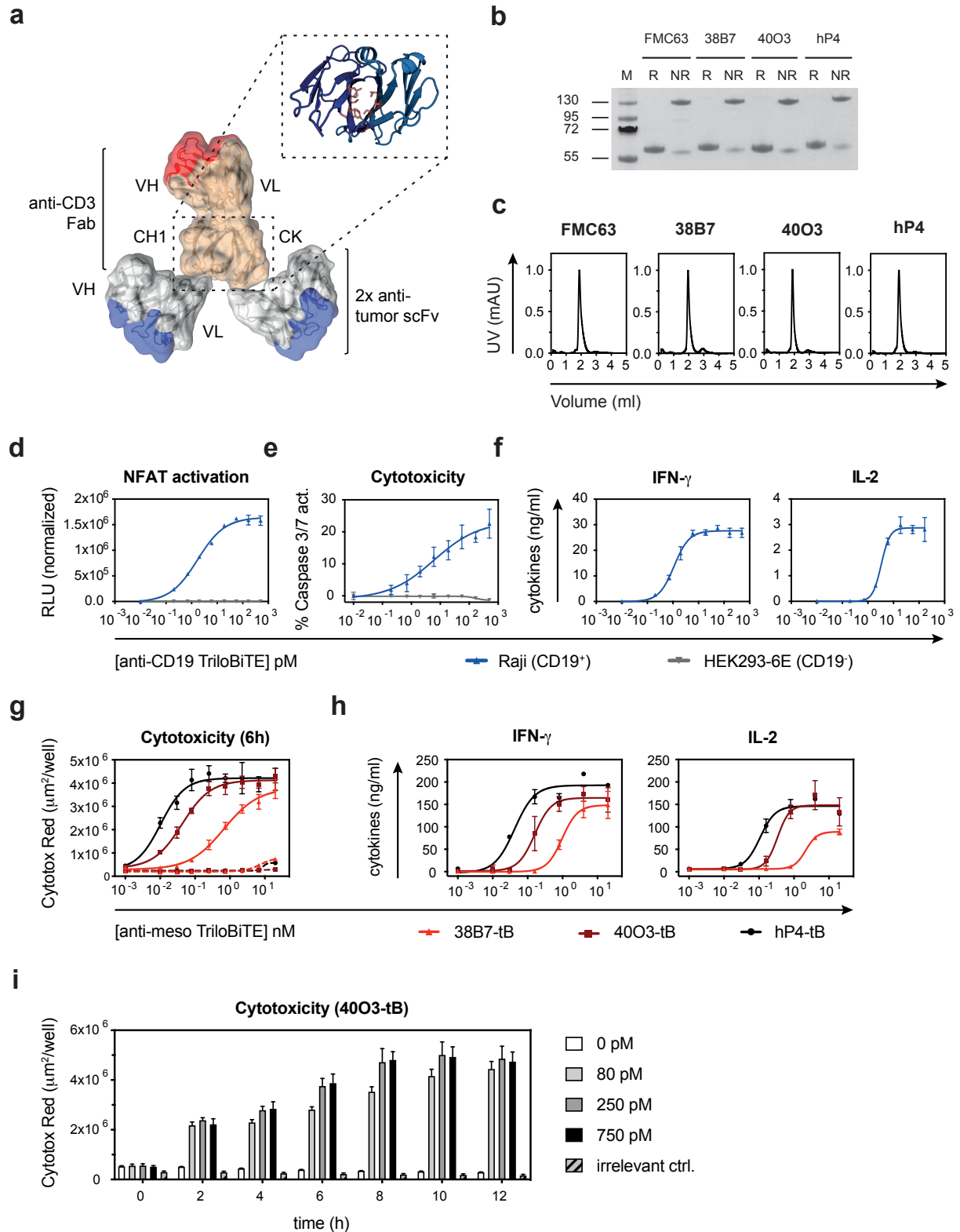
Figure 4.1. TriloBiTEs specifically redirect human T cells to target relevant cancer cells.

(**a**) Schematic representation of the TriloBiTE format. A tumor-antigen specific scFv is fused to both heavy and light chain of a chimeric humanized anti-CD3 Fab UCHT1. The human CH1 – Cκ interface serves as the heterodimerization scaffold and has been reinforced by stabilizing mutations, shown in bold stick representation. The structural representation has been generated with PyMOL molecular graphics software (Schrödinger) based on PDB entry 1HZH. (**b**) Reducing and non-reducing SDS-PAGE of various TriloBiTEs (1 µg loaded). Expected molecular weight is ~55 kDa for reduced tB and ~110 kDa for non-reduced protein. (**c**) Analytical size-exclusion

chromatography of purified TriloBiTE variants in PBS (pH 7.4) following a single freeze-thaw cycle. (**d**) Jurkat-NFAT reporter assay showing target- and concentration-dependent induction of luciferase activity by the αCD19-tB (0.01 pM – 0.5 nM) at an E:T ratio of 5:1. (**e**) Specific killing of CD19+ target cells by purified human CD8+ T cells in response to stimulation with αCD19-tB (0.01 pM – 0.5 nM). Cell death was assessed using a caspase 3/7-cleavable fluorescent dye after 4 h of co-culture at an E:T ratio of 5:1. (**f**) Quantification of effector cytokines secreted by human CD8+ T cells activated with αCD19-tB (0.01 pM – 0.5 nM) in the presence of CD19+ Raji cells (E:T 5:1). (**g**) Specific cytotoxicity of human CD8+ T cells redirected against meso-expressing H-226 mesothelioma cells (solid lines) by different αMeso-tB variants (1 pM – 20 nM). Cell death was observed by time-lapse fluorescence microscopy and analyzed after 6 h of co-culture. Meso⁻ A673 cells (dashed lines) were not killed in response to tB treatment. E:T ratio 5:1. (**h**) Quantification of effector cytokines secreted by TriloBiTE-activated primary CD8+ T cells. T cells have been co-cultured with meso+ H-226 cells (5:1) and different αMeso-tB (1 pM – 20 nM) for 24 h. (**i**) Anti-meso clone 40O3 redirects primary human CD8+ T cells to kill meso+ H-226 target cells in TriloBiTE format. Image-based acquisition of Cytotox Red fluorescence reports the real-time kinetics of killing. Baseline killing was determined against irrelevant meso-negative A673 cells using 750 pM tB. The anti-meso clones utilized here were isolated by Johan Abram, L-AbCore. They correspond to the following clones presented in chapter 2: 38B7, HS201; 40O3, HS202; hP4, P4.

4.2.4 Design and functional characterization of TEM1-specific TriloBiTEs.

We first generated TEM1-specific TriloBiTEs by fusing each clone in our panel of anti-TEM1 scFvs to both chains of the TriloBiTE cassette, generating bivalent engager molecules. Recombinant expression in HEK293-6E cells followed by affinity chromatography again yielded good protein quantities (≈ 20 mg/l) of the expected size (≈ 110 kDa; Fig. 4.2a). Analyses of protein homogeneity of the purified material by analytical SEC revealed >95 % monomeric species for the clones 1C1, 1C1m, 3B6 and 7G22, but both sc78-tB and 2B11-tB showed a significant proportion of higher molecular mass oligomers and/or aggregated species in the basic non-optimized PBS buffer (Fig. 4.2b). Since these clones represent early-stage experimental molecules, it is probable that optimization of expression and purification methodology, together with extended buffer/excipient screening would result in significant improvements in monomeric yield and quality. In order to assess the thermostability of this anti-TEM1 TriloBiTE (αTEM1-tB) panel, we subjected the purified molecules to a Differential Scanning Fluorimetry (DSF) stability assay. Encouragingly, the DSF measurements revealed melting transitional temperatures comparable to those obtained in the scFv-Fc fusion format: 62.6 °C for sc78-tB, 71.4 °C for 1C1-tB, 64.9 °C for 1C1m-tB, 75.2 °C for 2B11-tB, 57.9 °C for 3B6-tB and 70.1 °C for 7G22-tB (compare Fig. 4.2c with the scFv-Fc data shown in Fig. 3.3b).

Extending our investigations to a more functional characterization of the αTEM1-tB panel, we next probed whether all clones were able to recognize cognate target cells. Importantly, all αTEM1-tB variants specifically bound to endogenous TEM1-expressing A673 cells, as well as to Jurkat cells, which express human CD3 (Fig. 4.2d). Since all TriloBiTEs use the same anti-CD3 clone (UCHT1), binding to Jurkat cells was very consistent between the clones, while binding signals on A673 cells varied slightly, in line with the different affinities towards TEM1. Most TriloBiTEs displayed negligible binding to irrelevant HEK293-6E cells, with the exception of sc78-tB and 7G22-tB (Fig. 4.2d).
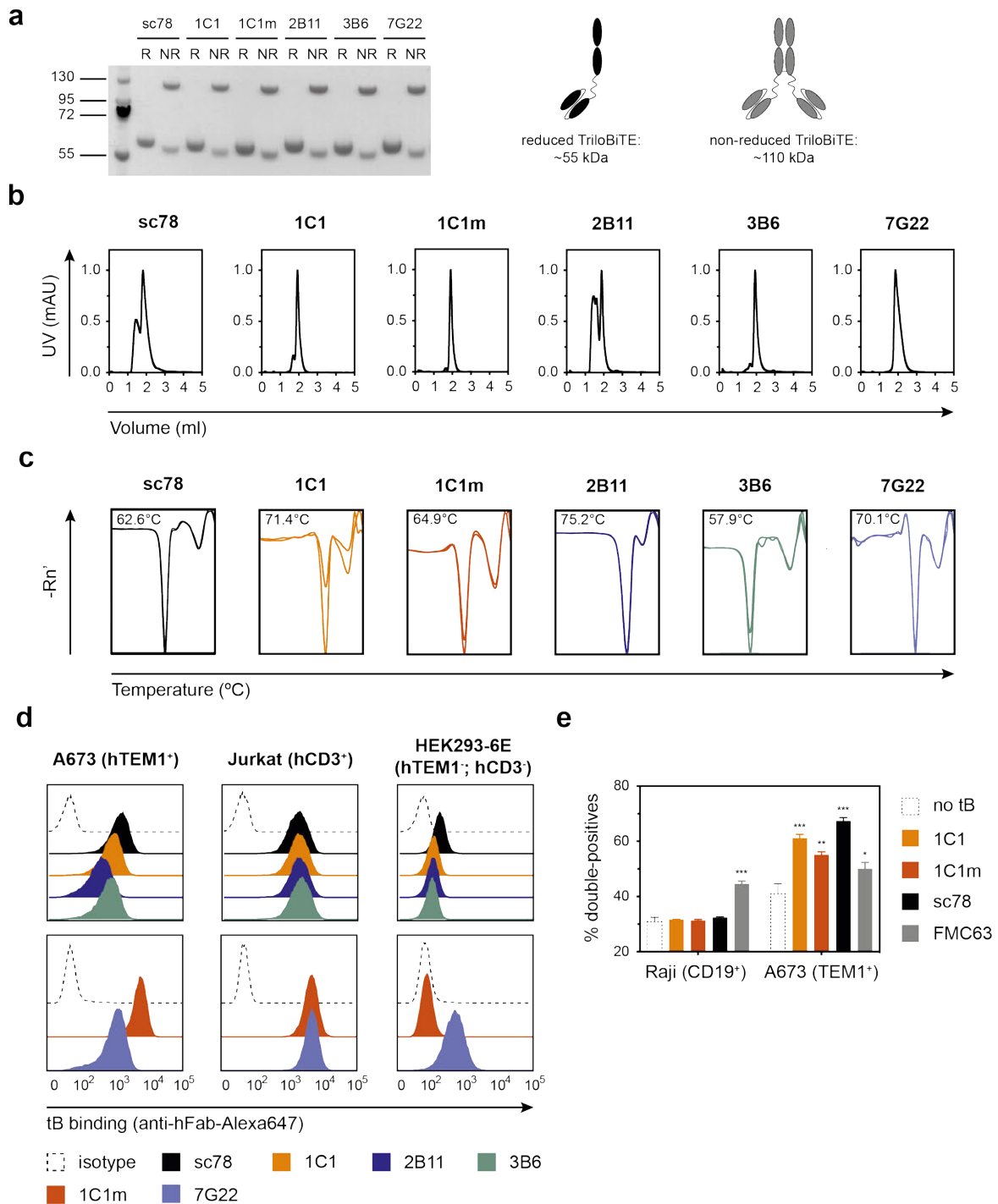
Figure 4.2. Biophysical and functional characterization of anti-TEM1 TriloBiTEs.

(**a**) SDS-PAGE of anti-TEM1 scFv clones reformatted as TriloBiTEs (1 μg loaded). The expected protein structure and molecular weight for reduced and non-reduced engager molecules is shown in the schematic on the right. (**b**) Analytical size-exclusion chromatography of αTEM1-tB variants in PBS (pH 7.4), following a single freeze-thaw cycle. (**c**) ScFv thermostability of purified αTEM1-tBs was determined by differential scanning fluorimetry. Melting temperatures were calculated based on the minima of the derivative of fluorescence as a function of temperature for the first unfolding transition. (**d**) Binding of purified αTEM1-tB variants (1 μg/ml) to hTEM1^{+} A673 Ewing's sarcoma cells, hCD3^{+} Jurkat cells and hTEM1^{-}/hCD3^{-} HEK293-6E cells. Cell binding was detected using an Alexa Fluor 647-conjugated anti-hFab antibody. (**e**) Cross-linking of primary human T cells and relevant target cells by TriloBiTEs. TEM1^{+} A673 cells and CD19^{+} Raji cells were stained with DiD and incubated with CellTrace Violet-stained human T cells in the presence of different TriloBiTEs (5 nM). Double-positive events were quantified by flow cytometry. FMC63 targets human CD19. Statistical significance was assessed using student's t test.

This residual binding signal might be due to insufficient blocking of the inherently "sticky" cell surface for this suspension-adapted cell line, or it may be caused by a transient or culture-context expression of a truncated isoform of TEM1 on HEK cells, consistent with published observations from other investigators[306].

Interestingly, unlike the other clones in our study which recognize epitopes within the TEM1 multi-domain region situated distal from the membrane, both sc78 and 7G22 clones recognize epitopes that either overlap with, or reside within the upstream membrane-proximal mucin stalk region, consistent with binding to one or more truncated or splice variants. Confirming the dual functionality of the αTEM1-tB panel, these results led us to investigate whether TriloBiTE molecules could sterically engage both targets simultaneously, thereby bridging T cells and tumor cells. We therefore labeled target cells (A673 or Raji) and Jurkat cells with different fluorochromes and then incubated this cell mixture with 1 µg/ml TriloBiTE. Quantifying double-positive events by FACS, we found that αTEM1-tBs significantly increased the frequency of A673 – Jurkat hetero-doublets, but did not induce doublets between Raji and Jurkat cells. The opposite was observed with the CD19-tB, suggesting that TriloBiTEs can specifically cross-link T cells and relevant target cells (Fig. 4.2e).

Taken together, the αTEM1-tBs appear to possess not only promising expression and biophysical properties, but also the desired functionality, recognizing and cross-linking TEM1$^+$ tumor cells and human T cells.

4.2.5 TEM1 TriloBiTEs mediate specific cytotoxicity of primary human T cells against TEM1$^+$ target cells.

Following the initial validation of TriloBiTEs as a new molecular engager format, we next aimed to test the potential of our original panel of TEM1 ECD binders to engage and activate primary human T cells in the TriloBiTE format. As an early marker of T cell activation, we first measured expression of CD69 and CD25 in primary human T cells that were co-cultured overnight with TEM1$^+$/CD19$^-$ A673 cells or TEM1$^-$/CD19$^+$ Raji cells in the presence of 5 nM TriloBiTE. All TriloBiTE clones clearly activated both CD8$^+$ and CD4$^+$ T cells, upregulating the early expression markers CD69 and CD25, although activation with 2B11-tB was quite weak (Fig. 4.3a). In contrast to the other TriloBiTEs, the previously published anti-TEM1 clone sc78[306], which led to the strongest upregulation of activation markers of any of the αTEM1-tBs, also up-regulated these markers in the presence of TEM1-negative Raji cells. A possible explanation for this apparent nonspecific activation of T cells is the presence of oligomeric/aggregated species in the sc78-tB preparation (see Fig. 4.2b) and the high tB concentrations (5 nM) used in this experiment. Similarly, the CD19-tB stimulated strong activation marker up-regulation in the presence of cognate Raji target cells, and also to a significant extent in the presence of A673 cells (Fig. 4.3a).

A crucial effector function of activated T cells is the production of pro-inflammatory cytokines. Encouragingly, with the exception of 2B11-tB, all αTEM1-tB molecules induced the secretion of IFN-γ by primary human T cells, when co-cultured with relevant endogenous TEM1-expressing cells. 1C1m-tB induced the highest levels of effector cytokines, alongside sc78-tB, a trend that is consistent with the higher molecular affinity of these clones (Fig. 4.3b). In line with these findings, the same αTEM1-tBs also redirected human T cells to kill relevant target cells. Interestingly, 1C1 and the affinity-matured variant 1C1m were able to mobilize T cell killing at a significantly lower concentration than the other clones, including sc78 (Fig. 4.3c). Given the superior apparent killing activation potential of 1C1m-tB, we subjected this clone to a head-to-head kinetic comparison with the benchmark clone sc78. In a time-lapse microscopy-based killing assay, both clones

specifically and rapidly redirected primary human T cells to lyse relevant target cells, with complete lysis reached after 12 h for both lines (Fig. 4.3d, e).
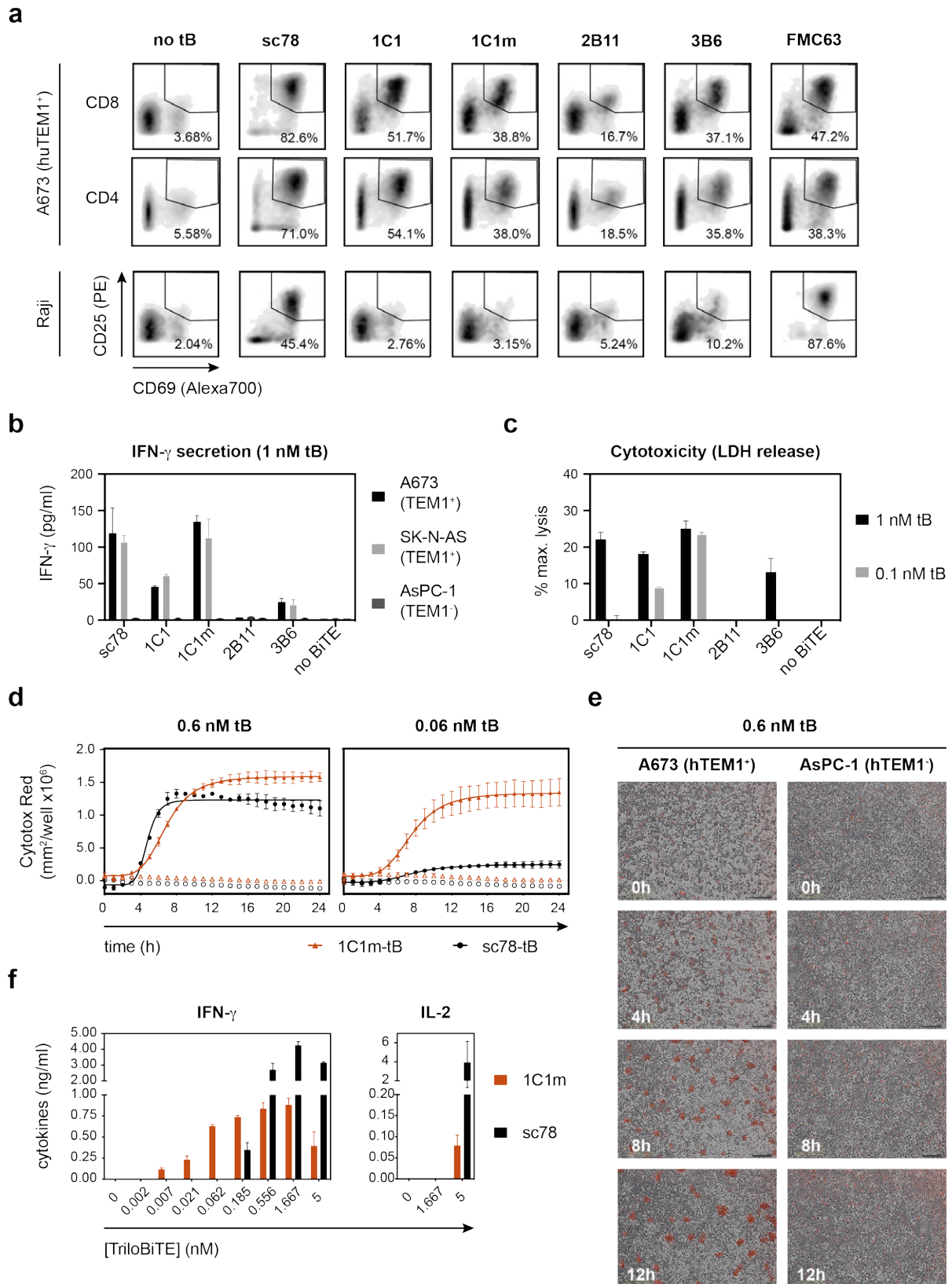
Figure 4.3. TEM1 TriloBiTEs mediate specific cytotoxicity of primary human T cells against TEM1+ target cells.

(**a**) αTEM1-tBs specifically activate both CD8$^+$ and CD4$^+$ T cells in the presence of TEM1-expressing A673 cells. Upregulation of early activation markers CD69 and CD25 was measured by flow cytometry after 16 h of co-culture (E:T ratio 1:1). Expression of CD69/CD25 by CD8$^+$ T cells co-cultured with Raji cells is shown as a control. (**b**) IFN-γ secretion by primary human T cells activated with αTEM1-tB variants (1 nM) in the presence of different target cell lines: A673 (hTEM1$^+$), SK-N-AS (hTEM1$^+$), AsPC-1 (hTEM1$^-$). Cytokine concentration in the supernatant was measured after 24 h of co-culture. (**c**) Anti-TEM1 clones redirect primary human T cells to kill TEM1-expressing A673 cells in TriloBiTE format. TriloBiTEs were added at 1 nM or 0.1 nM and LDH activity was measured after 24 h as a reporter of lysed cells. Specific cell killing was calculated as a percentage of complete lysis achieved with 1 % Triton-X 100. (**d**) Real-time kinetics of cell killing by primary T cells activated with 0.6 nM or 60 pM TriloBiTE. Image-based acquisition of Cytotox Red signal indicates lysis of TEM1$^+$ A673 cells (closed symbols and connected lines), while TEM1-negative AsPC-1 cells (open symbols) are spared. (**e**) Time-dependent killing of TEM1-positive A673 cells by primary human T cells in the presence of 0.6 nM 1C1m-tB. Clusters of dead cells emit red fluorescence. (**f**) Induction of effector cytokine production in human pan-T cells with increasing concentrations of anti-TEM1 tB. Cytokine levels in the supernatant were measured after 24 h of co-culture with TEM1$^+$ A673 cells. T cells used in **a-c** were derived from a different donor than in **d-f**. E:T ratio was 5:1 unless indicated differently.

Although the data suggests that sc78-tB induces a steeper kill curve and is more potent at the higher dose, 1C1m-tB was able to efficiently mediate complete lysis of TEM1-expressing target cells at a ten-times lower molecular concentration than sc78-tB. Furthermore, neither of these molecules activated T cells in the presence of irrelevant cells, thereby sparing them from T cell mediated cytotoxicity (Fig. 4.3d, e). Finally, T cells activated with both sc78-tB and 1C1m-tB secreted effector cytokines in response to TriloBiTE dose (Fig. 4.3f). Interestingly, stimulation with sc78-tB achieved higher levels of cytokine production overall, but 1C1m-tB induced measurable dose-dependent IFN-γ secretion at far lower concentrations (Fig. 4.3f). Therefore, at least for *in vitro* functional assays that directly score cell killing, cytokine production levels alone can only be considered indicative of T cell activation, and not as a predictor for end-point tB-mediated killing outcome. Follow-on studies that examine post-killing T cell exhaustion/proliferation may be more informative in understanding the relationship between tB-induced cytokine levels, immunotherapeutic safety, and optimal post-killing T cell fate. Nevertheless, these results clearly suggest that our novel *de novo* isolated panel of anti-TEM1 scFvs can serve as 'warheads' for T cell engager molecules, specifically redirecting T cells to kill TEM1$^+$ target cells. To our knowledge, this is the first demonstration that a T cell engager paradigm may have application for the targeting of TEM1$^+$ tumor cells. Clone 1C1m especially, with its improved affinity over the parental 1C1 and tight coupling of functional T cell activation to the presence of TEM1 target, represents an exciting candidate for the development of a TriloBiTE-based T cell engager.

4.2.6 The TriloBiTE format allows fine-tuning of avidity and affinity in order to achieve optimal selectivity and functionality.

A key design feature of our TriloBiTE format is its modular design. By C-terminally fusing an antigen-specific scFv domain to the CH1 or Cκ domain of the anti-CD3 Fab, bi- or trivalent engager molecules can be created (Fig. 4.4a). In this way, target binding can be modulated in order to achieve optimal selectivity and T cell engagement. Depending on the density of the target antigen on the cell surface, monovalent binding may be sufficient, or bivalent antigen recognition may be required for optimal T cell retargeting. Another critical parameter impacting on target cell recognition is the affinity of the targeting scFv. Several studies have established the concept that increasing the targeting affinity improves the potency of bispecific T cell engagers in most cases[388]. In order to achieve strong and specific antigen binding, bivalent targeting using two low-affinity targeting moieties represents an intriguing alternative to high-affinity monovalent targeting. This approach thus relies on avidity stabilization (and/or rapid rebinding) rather than raw affinity, a strategy that has recently been applied successfully to achieve tumor-selectivity with targets that are expressed at

low levels in normal tissues[245]. With the modest-affinity 1C1 parent and its high-affinity 1C1m variant, differing by a sole VH CDR3 residue, at hand, we decided to illustrate the interplay of affinity and avidity in the context of soluble T cell engagers. To do so, we expressed mono- and bivalent TriloBiTE variants of both 1C1 and 1C1m (Fig. 4.4a) and employed them as cytotoxic mediators in a co-culture assay. Unsurprisingly, the bivalent 1C1m-engager induced specific cytotoxicity at the lowest concentrations and mediated the highest potency of cell killing, while the low-affinity monovalent variant barely achieved T cell activation (Fig. 4.4b). The bivalent low-affinity TriloBiTE (1C1-tB) performed equivalently to the high-affinity monovalent variant, thus illustrating the requirement for avid binding to drive killing. As avidity-based binding is sensitive to target density, 1C1-tB may demonstrate improved discrimination between target-rich tumor and residual levels of TEM1 that may be present in healthy tissues and some reported cell subsets[265,283,287].

In summary, the combination of the modular TriloBiTE format and our diverse panel of TEM1-specific scFvs provides a unique opportunity to fine-tune affinity and avidity in order to achieve an optimal balance between antigen target selectivity, functional T cell activation and killing, and minimization of potential (on-target) off-tumor autoimmunity.

4.2.7 Specific targeting of the sialomucin stalk domain of TEM1 may facilitate optimal T cell engagement.

As discussed in the previous chapter, targeting more membrane-proximal epitopes may improve T cell engagement by soluble mediators[247,248,363]. We therefore aimed to develop novel scFv clones targeting the membrane-proximal sialomucin domain of TEM1. In chapter 5, I describe an alternative phage library output screening approach for the direct selection and identification of phenotypically functional CAR-active scFv warheads. Using this method, we have identified a promising TEM1(Δn)-specific scFv clone, 7G22, which we subsequently tested for functional activity in CAR and TriloBiTE format. Strikingly, the 7G22-tB induced a more pronounced cytotoxic T cell response than both 1C1m- and sc78-tB, while sparing irrelevant TEM1-negative cells (Fig. 4.4c, e). Similarly, T cells stimulated with 7G22-tB secreted higher levels of effector cytokines in the presence of TEM1^{+} A673 or SK-N-AS cells, when compared to 1C1m-tB (Fig. 4.4d). In contrast, other clones isolated against the TEM1(Δn) domain (see chapter 3, especially Fig. 3.4) failed to redirect T cell effector functions towards TEM1-expressing target cells (Supplementary Fig. 4.1).

Albeit still preliminary, these results suggest that epitope location may indeed be a relevant parameter for the engineering of immunotherapies directed against TEM1. This is especially true in light of the presumably modest affinity of the non-affinity matured clone 7G22. However, a deeper investigation of the activation kinetics and, importantly, the *in vivo* efficacy of 1C1m-tB and 7G22-tB will be required to dissect the impact of affinity, avidity and epitope location on the potency of a TEM1-directed TriloBiTE.
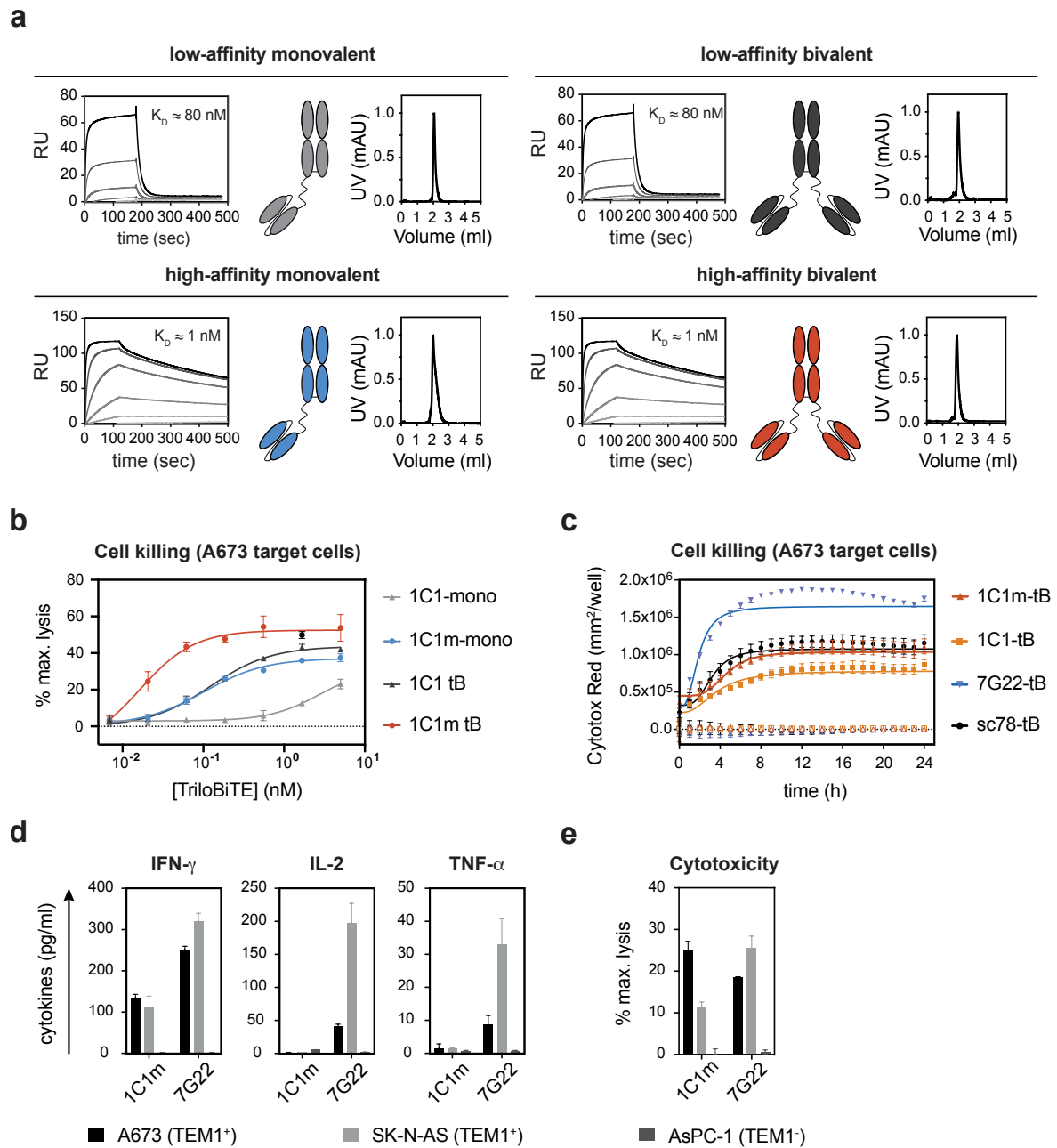
Figure 4.4. Target affinity and epitope location play a key role for the potency of anti-TEM1 TriloBiTEs.

(**a**) The modular design of the TriloBiTE allows the production of mono- or bivalent variants. Mono- and bivalent TriloBiTEs have been generated using 1C1 or the high-affinity variant 1C1m as the tumor-targeting moiety. Surface plasmon resonance (SPR) curves and SEC profiles are shown for illustrative purpose. (**b**) Comparison of high- and low-affinity mono- and bivalent 1C1-tB variants (7 pM – 5 nM) as mediators of cytotoxic T cell activity. Lysis of target cells (A673) by polyclonal human T cells was quantified based on LDH released from dead cells. Cell killing is expressed as a fraction of maximal lysis achieved with 1 % Triton-X 100. (**c**) Real-time kinetics of cell killing by pan-T cells redirected by different αTEM1-tBs (5 nM) over the course of 24 h (E:T ratio 5:1). Increased detection of Cytotox Red fluorescence indicates lysis of TEM1⁺ A673 cells (filled symbols), while TEM1⁻ AsPC-1 cells (open symbols) are spared. (**d**) Quantification of effector cytokines secreted by polyclonal human T cells stimulated with 1C1m- or 7G22-tB in the presence of TEM-expressing A673 or SK-N-AS cells, or in the presence of irrelevant AsPC-1 cells. Cytokines were quantified after 24 h of co-culture (E:T ratio 5:1). IFN-γ and TNF-α secretion was quantified after stimulation with 1 nM tB and IL-2 was measured after activation with 10 nM tB. (**e**) LDH-release assay comparing the tB-mediated lytic activity of human T cells towards the TEM1⁺ cell lines A673 and SK-N-AS and the TEM1⁻ cell line AsPC-1. T cells and target cells were co-cultured with 1 nM TriloBiTE for 24 h (E:T ratio 5:1) before measuring LDH activity in the supernatant.

4.2.8   1C1m-tB prevents the outgrowth of A673 tumors *in vivo*

In light of the promising *in vitro* results achieved with 1C1m- and 7G22-tB in particular, we next sought to investigate the potential of TEM1-specific TriloBiTEs to redirect T cell activity *in vivo*. Initially, we aimed to establish the experimental conditions and feasibility of T cell retargeting using αTEM1-tBs *in vivo.* In order to gain insights into the appropriate dosing schedule, we first assessed the serum clearance of TriloBiTE molecules. To this end, female NOD/SCID/IL-2Rγ KO (NSG) mice were injected i.v. with 1 mg/kg 1C1-tB. Blood samples were taken at baseline as well as after 10 min, 30 min, 1 h, 2 h, 4 h, 6 h, 8 h, 24 h, 48 h and 1 week (Fig. 4.5b). Subsequently, TriloBiTE serum levels were analyzed by ELISA and concentrations were calculated using a standard curve (Fig. 4.5a, b). Peak serum concentration of 4.604 µg/ml was reached after 60 min and baseline was reached after 48 h (Fig. 4.5b). However, over 90 % of the material was cleared after 24 h, and so we reasoned that a daily dosing regimen may be appropriate to maintain TriloBiTE levels in an initial proof-of-concept study.

As a pilot study, we next aimed to assess the potential of our lead candidate 1C1m-tB to redirect primary human T cells in an A673 xenograft model. Therefore, 10^6 A673 cells were implanted s.c. into the right flank of female NSG mice, either alone or mixed with 10^7 purified and expanded primary human pan-T cells. One hour after tumor implantation, the mice received 1 mg/kg 1C1m-tB or PBS vehicle control, administered i.v. into the tail vein. The TriloBiTE dose was repeated 24 h and 48 h after tumor implantation. Subsequently, the outgrowth of s.c. tumors was followed for 45 days, or until animals had to be sacrificed for ethical reasons. Encouragingly, neither the injection of human T cells, nor the administration of 1C1m-tB had an impact on body weight and no apparent toxicities were observed over the course of the experiment (Fig. 4.5c). As expected, the A673 cells rapidly formed tumors in the untreated animals (Fig. 4.5d). The administration of human T cells together with the tumor cells substantially delayed tumor outgrowth, but all animals eventually developed tumors (Fig. 4.5e). In contrast, the treatment with 1C1m-tB prevented tumor establishment, or significantly suppressed tumor formation, compared to the T cells only group (Fig. 4.5f-h). In fact, five out of ten animals never developed any tumor, indicating that all tumor cells were eradicated initially (Fig. 4.5g, h). Other animals only developed flat, scar-like lesions, which never grew to a three-dimensional tumor mass.

Albeit preliminary, the results from this pilot study suggest that 1C1m-tB is active *in vivo*, redirecting human T cells to kill TEM1-expressing target cells. However, several parameters will need to be assessed in subsequent studies before drawing any definite conclusions. First, the requirement of TEM1 engagement for T cell activation will have to be confirmed either using a TEM1-negative tumor model or an inert knock-down TriloBiTE. The latter approach would also exclude any tonic impact of the anti-CD3 arm alone. In addition, it should be tested whether the observed anti-tumor effect of the 1C1m-tB is T cell dependent. Finally, the full potential of T cell redirecting therapy using αTEM1-tBs will require validation in tumor regression models, administrating both T cells and TriloBiTE systemically after tumor establishment. Ultimately, these studies will reveal the therapeutic potential of TEM1-targeting via soluble T cell engagers.
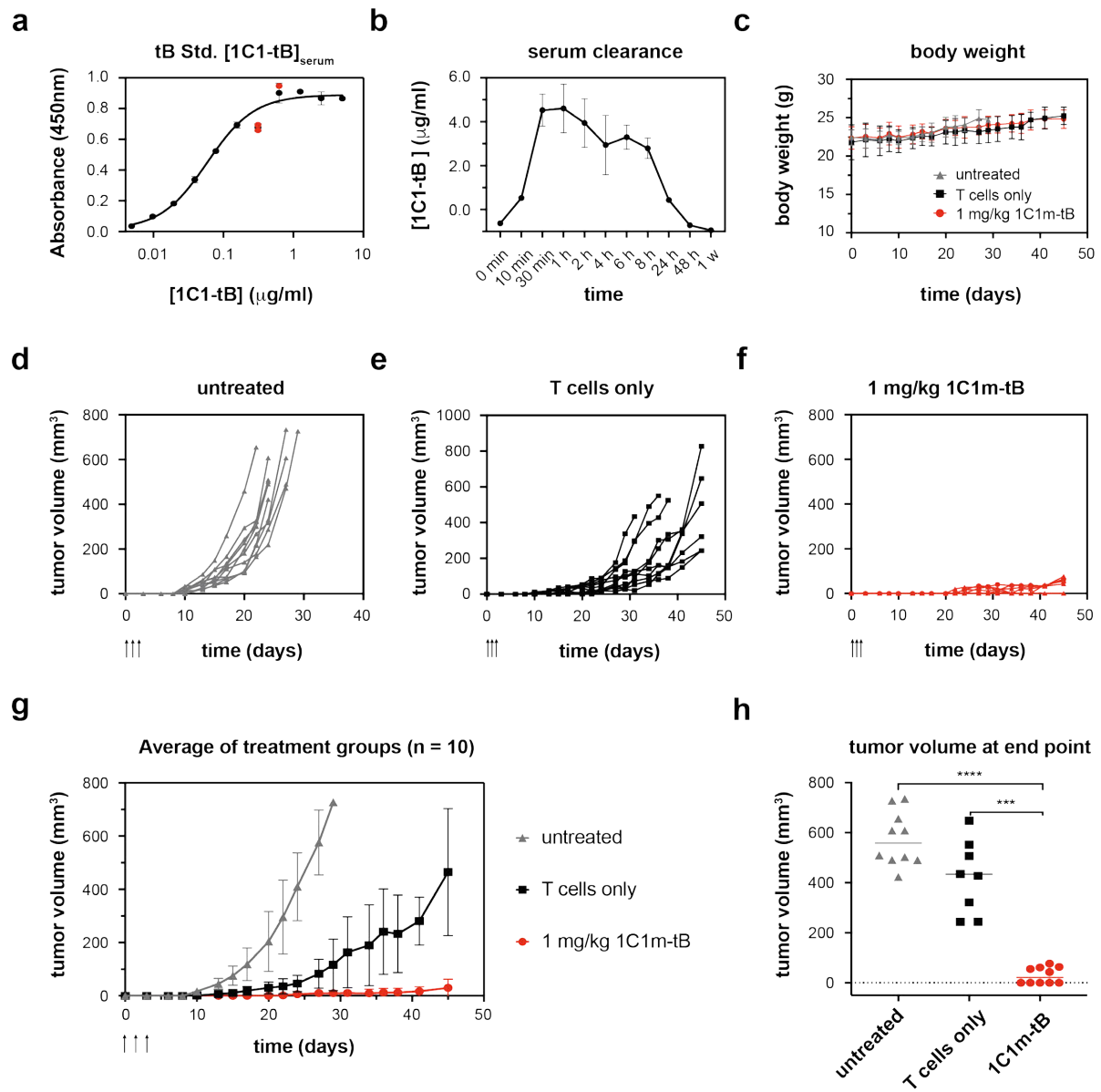
Figure 4.5. 1C1m-tB prevents A673 tumor formation in an A673 xenograft pilot study.

(**a, b**) Serum clearance of 1C1-tB was analyzed in a pilot PK study. After administration of 1 mg/kg 1C1-tB, serum was collected at different time points and TriloBiTE concentrations in the serum were measured by ELISA (**b**). Serum concentrations were calculated using a standard curve (**a**). Serum from two animals was pooled for each time point. The following parameters were calculated: c_{max} = 4.604 µg/ml at t_{max} = 1 h; AUC = 8859. (**c-h**) The potential of 1C1m-tB to induce the lysis of A673 cells by primary human T cells was assessed in a s.c. xenograft model. 10^6 A673 Ewing's sarcoma cells were implanted s.c. into the right flank of 10 week-old female NSG mice, either alone or admixed with 10^7 purified human pan-T cells. 1 h, 24 h, and 48 h after tumor implantation, mice received 1 mg/kg 1C1m-tB in 100 µl PBS, or PBS only, administered i.v. (**c**) No apparent toxicities were observed upon TriloBiTE administration, and body weight remained comparable between the groups throughout the study. (**d-f**) Tumor volume was measured three times a week until the end of the study (day 45) or until tumors reached ~1000 mm³. Each line represents an individual animal. Arrows indicate the time of tB administration. (**g**) Mean tumor growth in the three experimental groups. The mean and SD of each treatment group are plotted. Statistical significance (multiple paired *t*-test) between the "T cells only" and "1C1m-tB" treatment groups was reached at day 15 (P value = 0.016916) and maintained until the end of the study (P value = 0.000045 on day 45). (**h**) Tumor volume was compared at end point: day 45 for "T cells only" and "1C1m-tB" treatment groups and day 22-29 for the untreated group. Statistical significance was assessed with a paired two-tailed *t*-test. P value (untreated vs. 1C1m-tB) <0.0001; P value (T cells only vs. 1C1m-tB) = 0.0002. n = 10 animals per group.

4.2.9 Selected anti-TEM1 scFvs show potential as targeting 'warheads' for CAR-T cells.

The therapeutic potential of classical paradigm soluble T cell engager molecules (e.g. blinatumumab) can be limited by their rapid clearance from the circulation and by the need for continuous infusion administration in order to maintain steady state systemic drug levels within, typically, narrow therapeutic safety windows[367]. An alternative strategy of redirecting autologous T cells to the tumor tissue focuses on the genetic modification of T cells to combine the antigen-binding domain of an antibody or other targeting moiety with intracellular co-stimulatory and T-cell activation domains. These chimeric antigen receptor (CAR)-modified T cells have shown great promise in various clinical trials, particularly those targeting B-cell malignancies via lineage specific antigens such as CD19, which to-date comprise the only approved CAR-T cell therapeutic treatments[167-171,180,369].

We therefore sought to evaluate the utility of our new panel of TEM1-specific scFvs as targeting moieties for CARs. Our anti-TEM1 scFv clones were thus embedded in a modular second-generation CAR construct comprising a CD28 spacer, transmembrane (TM) domain and cytosolic domain fused to CD3ζ immunoreceptor tyrosine-based activation motif (ITAM) signaling elements and an in frame monomeric GFP reporter. As a first indication of the activating potential of these novel CARs, Jurkat NFAT-reporter cells engineered to express the fluorescent protein mCherry under the control of an NFAT-driven promoter were virally transduced with the resulting CAR panel. Again, the clinically validated anti-CD19 FMC63 scFv and the published anti-TEM1 clone sc78 were included as controls. Among all anti-TEM1 clones, only 1C1m and 7G22 triggered a differential induction of CD3ζ-driven NFAT signaling in response to TEM1-expressing target cells, compared to irrelevant control cells (Fig. 4.6a). None of the other αTEM1-CARs, including sc78, induced TEM1-specific mCherry responses. The apparent inactivity of sc78 in this human CAR scaffold is surprising and cannot easily be attributed to, for example, the use of an inappropriate fixed scFv-TM CD28 extracellular spacer length, as 1C1m and 7G22 recognize TEM1 epitopes both more distal from, and more proximal to, the TM domain than sc78.

Following on from these initial results, we next transduced primary human T cells with lentiviral constructs containing the 1C1m- and 7G22-CARs. In contrast to the Jurkat reporter cells, where high transduction efficiencies were achieved for most clones (84.6 % for 1C1m-CAR), far fewer primary T cells expressed the CAR-constructs after lentiviral delivery. Reduced transduction efficiencies are commonly observed in primary T cells, but 7G22-CAR expressed especially poorly, with only 10.2 % of T cells displaying measurable GFP signals, as compared to the ~35-40 % transduction efficiency observed with the other clones (Fig. 4.6b). 1C1m and 7G22 CAR-T cells were able to recognize their cognate target antigen fragments, with the high affinity 1C1m-CAR cells showing a strong GFP-correlated diagonal shift in response to biotinylated TEM1 ECD. In the case of 7G22, a weak diagonal shift is evident in the minor GFP-positive population in response to expression supernatants containing the mucin stalk TEM1(Δn)-SpyC fragment, consistent with weak GFP expression levels and the expected weaker affinity of this primary naïve clone. As expected, the sc78-CAR did not recognize the biotinylated TEM1 fragment bound by 1C1m as its epitope resides in a region of TEM1 not present in either of the ECD fragments used in our *de novo* discovery campaigns. Extending to functional investigation of theses CAR clones, we next sought to measure and compare the expression of early T cell activation markers in response to cognate target cells. Both 1C1m and 7G22-CAR-T cells upregulated CD69 and CD25 expression markers upon stimulation with TEM1^{+} A673 cells, with the magnitude of expression by 1C1m-CAR-T cells reaching levels comparable with FMC63-CAR-T cells co-cultured with CD19^{+} Raji cells (Fig. 4.6c).
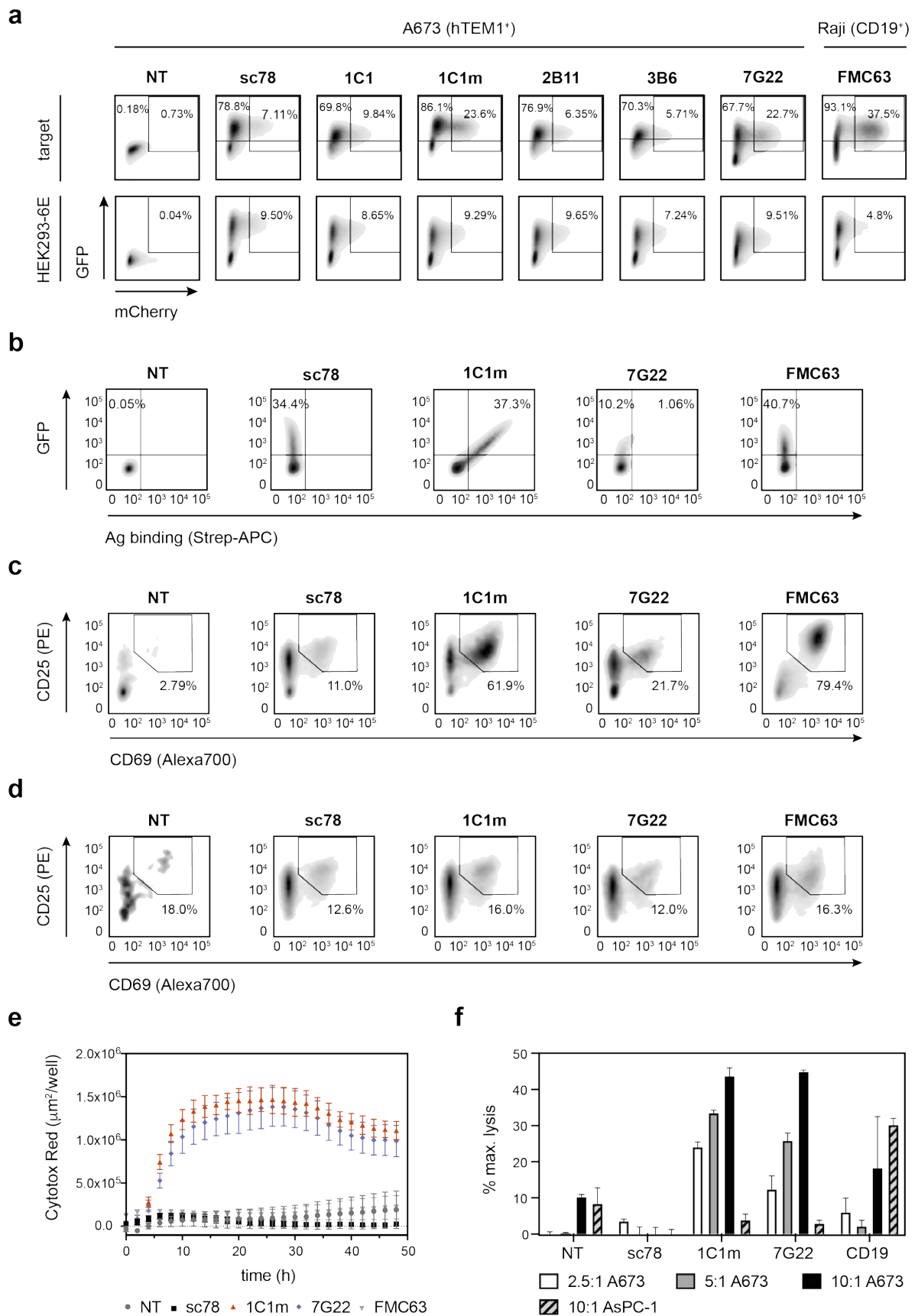
Figure 4.6. Functionality of anti-TEM1 scFvs as targeting moieties for CAR-T cells.

(**a**) Jurkat NFAT-reporter cells transduced with 2nd generation αTEM1-CARs express mCherry in response to stimulation with cognate target cells: A673 (TEM1+) for anti-TEM1 CARs and Raji (CD19+) for the anti-CD19 CAR FMC63. CAR-transduced Jurkat reporters were equally co-cultured with irrelevant HEK293-6E cells as a negative control. CAR expression was tracked via GFP. 2nd generation CAR constructs comprise a targeting scFv, followed by hCD28-derived hinge and transmembrane region, intracellular CD3ζ and an in-frame eGFP. (**b**) CAR-expression and antigen binding by primary human T cells transduced with selected CAR constructs. Binding of cognate biotinylated recombinant antigen (sc78: mTEM1(ECD); 1C1m: hTEM1(ECD); 7G22: TEM1(Δn)-SpyC-bioSpyT was visualized with APC-conjugated streptavidin. The anti-CD19 CAR FMC63 was treated as a negative control for non-specific binding of bio-hTEM1(ECD). (**c, d**) Expression of early activation markers CD69 and CD25 by TEM1-CAR-T cells in the presence of endogenous TEM1-expressing A673 cells (**c**) or TEM1-negative AsPC-1 cells (**d**). CD69/CD25 expression was quantified by flow cytometry after 16 h of co-culture. (**e**) Real-time kinetics of target cell killing (TEM1+ A673 cells) by αTEM1-CAR-T cells over the course of 48 h. Cell killing was quantified based on the image-based acquisition of Cytotox Red signal. (**f**) Lysis of TEM1+ A673 target cells by T cells equipped with αTEM1-CARs and added at different effector-to-target (E:T) cell ratios. Cell killing was quantified by measuring LDH activity after 24 h of co-culture and normalized to complete lysis with detergent. TEM1-independent killing of TEM1- AsPC-1 cells at the highest E:T ratio (10:1) and cytotoxicity of anti-CD19 CAR-T cells (clone FMC63) towards CD19- A673 cells were assessed as negative controls. CAR-T cells and target cells were co-cultured in an E:T ratio of 5:1, unless indicated differently.

Importantly, CD69/CD25 expression observed in the presence of irrelevant target cells remained low (Fig. 4.6d). Of note, sc78 again did not seem to induce significant activation of CD3ζ-ITAM signaling (Fig. 4.6c, d). Consistent with the observed 1C1m and 7G22-CAR-T cell marker activation, both CAR-T cells specifically lysed TEM1-expressing tumor cells, while sparing TEM1-negative cells (Fig. 4.6e, f). Maximum lysis was completed after 24 h of co-culture (Fig. 4.6e) and increasing the effector-to-target (E:T) cell ratio improved TEM1-mediated cytotoxicity for both clones, although 1C1m-CAR-T cells killed a significant proportion of target cells at E:T ratios as low as 2.5:1 (Fig. 4.6f). Neither of the two clones mediated unspecific killing at higher E:T ratios, in contrast to the clinically employed FMC63.

Taken together, our collated data show that TEM1 may be an amenable target for both soluble T cell engager and CAR-engineered immunotherapeutic strategies. Further, our studies suggest that not all anti-TEM1 scFvs perform equally in this regard, with a scFv constructed from the previously reported sc78 molecule having significant shortcomings in both formats. In contrast, our novel early lead candidates 1C1m and 7G22, which recognize distinctly different epitopes of TEM1, both demonstrate convincing and interesting levels of functional and selective target activity. Although both of these scFvs in the CAR format show similar potency and specificity in *in vitro* killing assays, roughly three-times fewer primary T cells seemed to express the 7G22-CAR compared to 1C1m-CAR-T cells. Hence follow-on studies aimed at balancing expression levels would be desirable in order to balance CAR expression levels for a true comparative assessment of efficacy. Additional explorations may also take into consideration the influence of membrane spacer length and biophysical properties, parameters that have been shown to impact on CAR potency[189,199,200,202]. In summary therefore, these fully human scFv clones clearly merit further investigation in the context of T cell targeting of TEM1 expressing tumors.

4.3   Discussion

In the current study, our objective was to engineer a novel T cell engaging bispecific targeting TEM1. With this in mind, we designed and constructed a heterodimeric T cell engager format, termed TriloBiTE (tB), combining the flexible mono- or bivalent binding of target cells with simultaneous T cell engagement via the activating CD3 complex. For proof-of-concept we first confirmed that soluble TriloBiTEs could be produced and purified, and could kill target cells expressing the established engager and CAR targets CD19 and mesothelin. For the former, we utilized an existing, clinically approved scFv derived from the reverse engineering of a murine mAb, and for the latter, we exploited a published benchmark human scFv clinical development candidate alongside a panel of novel molecules obtained via *de novo* discovery activities within our lab.

To our knowledge, this study represents the first attempt to explore the potential of TEM1 as a target for bi-specific engager-based anti-tumor therapy. Our diverse panel of anti-TEM1 single-chain antibodies provides the unique opportunity of comparing clones with different affinities, epitopes and presumably different binding geometries in order to identify those 'warheads' that are most suitable for effective binding and cell bridging/T cell activation.

Our results clearly show that soluble T cell engagers can redirect human T cells to target tumor cells via TEM1. Although a more in depth and systematic comparative study would be required to better illuminate the impact of different biophysical properties on the efficacy of T cell engagement, our data indicates that two key determinants for effective TEM1-targeting are binding affinity and epitope location.

In direct comparison, the two clones with the highest monovalent affinity towards TEM1, our affinity-matured clone 1C1m and the previously described clone sc78[306] clearly outperform the remaining clones in terms of T cell activation and cytotoxic potential (Fig. 4.3). In line with this observation, others have reported previously that the potency of bispecific molecules increases with increasing targeting affinity, especially for targets with low cell-surface abundance[388]. As an example of bispecific mediators directed against very low-density antigens, ImmTACs, which recognize peptide-MHC, require TCR affinities in the pM range[389]. Furthermore, we have shown that bivalent antigen binding can to some extent compensate for lower monovalent affinities (Fig. 4.4), underlining the importance of tight antigen binding especially for soluble T cell engagers which cannot benefit from the extreme 'synaptic' avidities conferred by multiple cell-mediated stabilizing and re-binding interactions.

As a class, bi-specific engagers acting via CD3 are extraordinarily potent, typically with narrow therapeutic windows. Hence, safety and the avoidance/minimization of background toxicity are of key concern when advancing these molecules towards the clinic. Here, the nature of the target antigen can play a crucial role. While engager molecules directed against proteins with very specific/restricted expression patterns may benefit from increased functional affinity, generally, many solid tumor-associated antigen targets require molecules able to adequately discriminate between antigen expression in tumor and normal tissue. In this case, lower-affinity scFvs can be employed in a bivalent engager format in order to increase tumor-selectivity and mitigate on-target off-tumor adverse effects[245]. Since TEM1 is relatively poorly explored as a therapeutic target, thorough pre-clinical investigations will be required of any potential T cell engager candidate in order to demonstrate desired levels of *in vivo* anti-tumor efficacy, and also to assess the scope and severity of any off-tumor toxicity.

Besides the high-affinity clone 1C1m, another clone, 7G22, has also shown strong potential to redirect T cells to TEM1-expressing targets, both as a soluble TriloBiTE and as a CAR. As a clone isolated directly from an IgM/D-derived naïve library, the affinity of 7G22 is expected to be rather modest. This clone has been selected against a truncated version of human TEM1, comprising only the heavily glycosylated membrane-proximal sialomucin stalk domain (TEM1(Δn)). Targeting a more membrane-proximal epitope has been shown to improve the potency of both soluble T cell engagers[247,248,363] and CARs[200,201] directed against protein antigens of considerable size. This phenomenon can be explained by considering the "kinetic segregation" model of T cell activation. The close apposition of the two membranes excludes the bulky ECD of the phosphatase CD45 from the immune synapse, thereby allowing the stable phosphorylation of the TCR complex[370]. Given the relatively large size of the multidomain TEM1 ECD, this may explain the fact that 7G22 induced stronger T cell activation than the other TriloBiTE variants (Fig. 4.4) Future studies will aim to explore the potential of clone 7G22 in more depth.

Although our αTEM1-tBs clearly redirect the cytotoxic potential of primary human T cells, other T cell functions are stimulated less efficiently. It has been established that different cellular responses are triggered at different thresholds of T cell activation, with the onset of cytolytic activity requiring less TCR signaling than the release of cytokines[390,391]. Moreover, IFN-γ secretion occurs at a lower threshold than IL-2 release, which is consistent with our data[392]. The fact that our lead TriloBiTE candidates require relatively high concentrations to induce the release of IL-2 may reflect a general characteristic of the tB format which, unlike classical 'back-to-back' scFv BiTEs contains a structural 'spacer' moiety (the CH1/Cκ domains) with additional flexible GS linker sequences connecting the scFvs. However, as this format is structurally analogous to the highly potent ImmTAC engager paradigm (which employs the Cα/Cβ TCR constant domains as a 'spacer')[389], a clear explanation for the observed weaker cytokine induction is not immediately apparent, particularly for the αTEM1-tBs.

Besides tumor targeting affinity and epitope distance from the membrane, three other aspects have been shown to impact strongly on the potency and performance of bispecific T cell engagers (recently reviewed by Ellerman, D.)[393]. Firstly, the accessible copy number of the tumor-associated cell-surface antigen; secondly, the affinity and specific epitope recognized by the anti-CD3 binder; and finally, the molecular format and targeting geometry of the engager molecule. Low target copy number of tumor-specific antigens can be addressed with increased targeting affinity (e.g. ImmTacs)[389]. However, many tumor-associated targets are characterized by elevated expression levels, and so copy number may be less of an issue. Different activating anti-CD3 clones, notably OKT3, are available and could be tested in the TriloBiTE format in place of UCHT1. Similarly, the length and composition of intra-molecular linkers and, in the case of CARs, transmembrane domains, can be modified to enhance T cell functional effector functions. Conversely, in light of the extreme potency of T cell-based therapies and the risk of severe adverse effects, induction of clear target-specific cytotoxicity whilst avoiding excessive cytokine release may even prove therapeutically advantageous.

Since the use of fully human targeting scFvs greatly reduces the risk of immunogenicity in the clinical setting[364], our novel single-chain antibodies, which have been isolated from a fully human antibody library with minimal somatic V-gene mutations, represent ideal candidates for clinical development. Although a certain interest has emerged in exploiting TEM1 as a cancer target, it remains to be determined how to best target TEM1 for therapeutic effect. Several pre-clinical studies have highlighted the therapeutic potential of

antibody-drug-conjugates (ADCs) directed against TEM1[304,305,307,309], but to date, no study has been published attempting the immunotherapeutic targeting of TEM1. As our studies suggests, αTEM1-tBs and CARs both show promise *in vitro* and preliminary results suggest promising *in vivo* activity of 1C1m-tB, but any therapeutic advantage of one strategy over the other remains to be elucidated. Generally, CAR-T cells are thought to be more potent than bispecific engagers at redirecting T cells[394]. Currently, approved clinical CAR therapies and most late stage clinical trials come with large associated manufacturing and treatment costs due to the generation of personalized engineered cell products. Soluble, "off-the shelf" T cell engager biologics may have cost and operational advantages in this regard. To overcome this economic hurdle, several strategies to generate generic allogeneic engineered CAR-T cells are currently being explored in the clinic[395-397]. Furthermore, the therapeutic efficacy of both CAR-T cells and soluble T cell engagers can be limited by toxicological side effects and by the persistence of tumor-directed T cells[171]. For soluble mediators, the dosing regimen has to be adapted according to the pharmacokinetic properties of each engager format in order to achieve sustained T cell activation. While formats with molecular weights below the glomerular filtration rate, such as the classical BiTE format, are rapidly cleared from the circulation and thus require administration by continuous infusion[398], medium-sized formats, such as the TriloBiTE, seek to balance the potential advantages of increased half-life (reduced frequency dosing) with clearance properties that are still favorable in the event of unexpected severe adverse events.

It is widely acknowledged that the potency and safety of any antibody-based therapeutic agent relies heavily on the performance and properties of the targeting fragment moiety. Although traditional selection and hybridoma campaigns have generated a plethora of powerful antibodies, the development of functional therapeutics based on these antibodies is often laborious and requires many engineering and screening iterations. Frequently, simple antigen binding criteria do not correlate with the desired functionality in the therapeutic format of choice and many clones have to be tested before finding a promising candidate. Therefore, in the next chapter we describe and develop an approach for the *de novo* discovery of novel CARs using phenotypic reporter-based screening.

4.4   Materials and Methods

4.4.1   Recombinant protein expression, purification and characterization

Recombinant protein expression and purification

To generate the TriloBiTE construct, heavy and light chain of the humanized and chimeric anti-CD3 clone UCHT1 were synthesized in Fab format (GeneArt, Thermo Fisher Scientific). Stabilizing mutations have been introduced into the human CH1-CK interface[383]. Both heavy and light chain of the resulting chimeric molecule were separately cloned into a pTT-based mammalian episomal expression vector. Both constructs contained modular cloning sites (NcoI/SalI) to accommodate scFv clones, which were C-terminally fused to the CH1 or CK domain of UCHT1 via a flexible (GS)-linker: GGGGSGGGSGGGS for CK and DKTHTGGGGSGGGGS for CH1. The sequence of the anti-CD19 scFv (FMC63) was extracted from Sequence 2, patent US7446179. Recombinant protein was produced using the HEK293-6E/pTT expression system and FectoPRO transfection protocol (Polyplus, #116-010), as described previously. TriloBiTEs were purified from clarified expression

media by immobilized metal ion affinity chromatography (IMAC) using a HisTrap excel column (GE Healthcase, #17371205) at a flow-rate of 1 ml/min. The column was equilibrated with 50 mM Tris, 0.5 M NaCl, 10 mM imidazole, pH 7.5 and protein was eluted with 50 mM Tris, 0.5 M NaCl, 300 mM imidazole, pH 7.4 in 1 ml fractions. Monomeric peak fractions were immediately separated by preparative size-exclusion chromatography using a Superdex 200 Increase 10/300 GL column (GE Healthcare, #28990944) at a flow-rate of 0.75 ml/min. PBS (0.01 M phosphate, 0.14 M NaCl, pH 7.4) was used as sample diluent and eluent. All chromatography experiments were run on an ÄKTApure chromatography system (GE Healthcare).

Biophysical protein characterization

Purified protein samples were typically quality controlled by SDS-PAGE, loading 2 µg per sample on a Novex 4-12% Bis-Tris gel (Life Technologies, #NP0321) under reducing/non-reducing conditions. Additionally, the homogeneity of purified TriloBiTEs was assessed and controlled by analytical size-exclusion chromatography using a Superdex 200 Increase 5/150 GL analytical grade column (GE Healthcare, #28990945). ScFv stability in the TriloBiTE format was confirmed by differential scanning fluorimetry following the Protein Thermal Shift Assay protocol from Applied Biosystems (#4461146). All three methods are described in detail in chapter 3.

4.4.2   T cell assays

Cell culture

All cell lines were purchased from the ATCC via LGC Standards. References and general culture conditions can be found in chapter 2.

Purification of primary human T cells

For the isolation of primary T cells, peripheral blood mono-nucleated cells (PBMCs) were isolated from fresh buffy coats obtained from healthy volunteer donors (Service de transfusion, Epalinges, Switzerland). PBMCs were seperated by density centrifugation using Lymphoprep (Axonlab, #1114545). Pan-T cells were subsequently extracted by magnetic separation using a human pan-T cell isolation kit (Miltenyi Biotec, #130-096-535) and stimulated with human T cell activator CD3/CD28 beads (Life Technologies, #11161D) and 50 RU IL-2 (Peprotech, #200-02-50UG) for 5 days. After the removal of the beads, primary T cells were further expanded with IL-7 and IL-15 (Miltenyi Biotec, #130-095-367 and #130-095-765) for a further 5 – 10 days.

Manufacturing of CAR-T cells

For the manufacturing of CAR-T cells, sequences encoding human anti-mesothelin or anti-TEM1 scFv (developed in-house) or anti-CD19 (FMC63; sequence extracted from patent US7446179) were fused to a spacer/hinge transmembrane region and intracellular costimulatory domain derived from hCD28, followed by an intracellular hCD3ζ signaling domain. The resulting 2nd generation CAR cassettes were cloned in-frame to a monomeric green fluorescent protein ORF (TagGFP2, Evrogen) into a modified pRRL lentiviral vector (originally developed by Didier Trono, EPFL). Lentivirus was produced by transient transfection of HEK293T cells using pCMVR8.74 and pMD2.G plasmids for packaging (origin: Didier Trono lab, EPFL) and Turbofect transfection reagent (Life Technologies, #R0532). Virus-containing supernatant was harvested after 48 h, concentrated by ultracentrifugation and 100 µl were added directly to 5 x 10^6 Jurkat-NFAT reporter cells or primary human T cells pre-plated in 48-well plates on the previous day. Primary T cells were transduced the day after isolation. All transduced cells were expanded for 10 – 14 days before performing functional assays.

Jurkat NFAT activation reporter cell assays

In order to measure anti-CD19 TriloBiTE-mediated NFAT activation responses, 10^5 Raji target cells were seeded in 96-well U-bottom plates. Subsequently, 10^5 Jurkat NFAT-Lucia reporter cells (Invivogen), were added to each well. Purified TriloBiTEs (diluted in PBS) were added in 3-fold serial dilution, starting from 1 nM. Phorbol myristate acetate (PMA)/ionomycin was included as a positive response control. After 24 h of co-culture, the supernatants were collected and mixed with an equal volume of QUANTI-Luc luciferase substrate (Invivogen, #rep-qlc-1). Luminescence was measured immediately using a BioTec H1MFG Synergy plate reader.

For the assessment of CAR-induced ITAM-signaling, Jurkat-NFAT-mCherry reporter cells (kindly provided by Melita Irving, Lausanne) were transduced with CAR-GFP constructs as described above. 10-14 days after transduction, 10^6 transduced Jurkat reporters were seeded in 24-well plates together with 10^6 target cells. After 24 h of co-culture, Jurkat-NFAT-mCherry cells were harvested by pipetting, washed in FACS buffer (5% FBS, PBS) and analyzed for GFP and mCherry expression by flow cytometry.

Primary T cell cytotoxicity assays

Target cell killing mediated by the CD19-tB was assessed using a Caspase 3/7 flow cytometry assay (Lifetechnologies, # C10427). Specifically, 10^5 target cells and 0.5×10^6 primary human CD8+ T cells (isolated using a human CD8 T cell isolation kit; Miltenyi Biotec, #130-096-495) were mixed in 96-well assay plates. CD19-TriloBiTEs were added in 3-fold serial dilution starting at 5 nM. Additionally, cells in control wells were lysed with 20% ethanol. After 4 h of incubation, the supernatant was removed and the cells were resuspended in 20 µl Caspase 3/7 solution (previously diluted 1:1000 in FACS buffer, as recommended by the manufacturer). Cells were incubated with the caspase dye for 30 min at 37 °C and the sample plate was read directly on an Intellicyt iQue TM Screener PLUS instrument (10 s sampling; 1 µl/s).

For the assessment of specific target cell killing using real-time kinetic cell imaging, 2×10^4 adherent target cells were seeded in 96-well flat-bottom plates and allowed to attach for ~20 h. When approximately 30 % confluency was observed, soluble TriloBiTEs were added as 3-fold serial dilutions, typically starting from 5 nM. Positive control wells were lysed using 1 % Triton X-100. 1.25×10^6 purified and expanded primary human T cells were added to the plate to reach an E:T ratio of around 5:1. Transduced and expanded CAR-T cells (prepared as described above) were equally added at 1.25×10^6 cells/well, in this case omitting the soluble engager molecules. Cytotox Red reagent (Essen Bioscience, #4632) was added to a final dilution of 1:4000, and resultant cell death was monitored as an increase in fluorescence over time.

Alternatively, specific target cell killing was assessed by measuring LDH release with the CytoTox 96 kit from Promega (#G1780), following the manufacturer's instructions. Target cells, (CAR-)T cells and TriloBiTEs were prepared as described above and the assay was incubated for 24 h at 37 °C. Control wells were lysed using 10 % Triton X-100. Subsequently, 50 µl clarified culture supernatant was mixed with 50 µl CytoTox 96 Reagent and incubated at RT for 30 min (protected from light). The reaction was stopped by adding 50 µl stop solution and LDH activity was quantified colorimetrically, measuring absorbance at 490 nm on a BioTec H1MFG Synergy plate reader. Background signal was subtracted from all samples and corrected cell killing (spontaneous release by targets and effectors subtracted) were calculated as a percentage of maximum lysis.

Quantification of effector cytokines

Supernatants of co-cultures set up as described above were tested for the presence of T cell-secreted effector cytokines. Cytokines were either quantified by sandwich ELISA (human IFN-γ or IL-2 ELISA MAX Standard kits, Biolegend #430102 and #431801) or by cytokine bead array (MultiCyt QBeads customized Human 3-Plex (IFN-γ, IL-2, TNF-α), Bucher Biotec #90603). Both assays were performed according to the manufacturer's instructions. In both cases, standard curves were prepared to quantify secreted cytokines. ELISA-based assays were read out on a BioTec H1MFG Synergy plate reader using TMB as a substrate for the HRP-conjugated secondary antibody. Plates for the MultiCyt bead array were analyzed on an Intellicyt iQue TM Screener PLUS instrument (10 s sampling; 1 µl/s).

Flow cytometry assays

To test TriloBiTEs for binding of TEM1$^+$ or CD3$^+$ target cells, adherent cells were detached using 10 mM EDTA and 0.5x10^6 pre-blocked cells were resuspended in 100 µl purified TriloBiTE (diluted to 1 µg/ml in 5% FBS, PBS). After 45 min of incubation on ice, the wells were washed 3x with FACS buffer. 50 µl Alexa Fluor 647-conjugated goat anti-human Fab antibody (Jackson ImmunoResearch, #109-605-097) was added for 30 min on ice to detect binding TriloBiTEs. Then, the samples were washed again 3x with FACS buffer.

In order to assess simultaneous antigen binding by TriloBiTEs, A673 and Raji cells were stained with Vibrant DiD lipophilic cell dye (Lifetechnologies, #V22887; final dilution 1:1000) for 5 min at 37 °C. Unbound dye was removed by washing 3x with serum-free RPMI. Primary T cells (prepared and expanded as described above) were stained with CellTrace Violet (Lifetechnologies, #C34557; final dilution 5 µM), incubating the cells for 20 min at 37 °C and quenching excess dye with complete RPMI. 10^5 stained tumor cells were subsequently mixed with 10^5 stained T cells in a V-bottom 96-well plate. TriloBiTEs were added at a final concentration of 1 µg/ml and the assay was incubated for 1 h at RT. Following incubation, the cells were washed carefully with 150 µl FACS buffer per well and then fixed in 2 % PFA for 20 min on ice. The fixed cells were carefully washed 3x with FACS buffer before data acquisition.

For measuring early T cell activation, 0.5x10^6 A673 or Raji target cells were seeded into 24-well plates. Subsequently, 0.5x10^6 purified and expanded (CAR-)T cells were added the wells. When measuring TriloBiTE-mediated T cell activation, purified tB protein was added to a final concentration of 5 nM. After 16-18 h of co-culture, the stimulated T cells were recovered and washed once in FACS buffer. Cells were blocked with FACS buffer for 20 min on ice and incubated with the following staining mix: APC anti-hCD8 (Biolegend #344722), BV785 anti-hCD4 (Biolegend #317441), Alexa Fluor 700 anti-hCD69 (Biolegend #310922), PE anti-hCD25 (Biolegend #302606). After 30 min of incubation on ice, the cells were washed again three times.

Antigen binding by CAR-T cells was assessed by incubating 0.5x10^6 CAR-T cells with 1 µg/ml bio-hTEM1 (produced in-house, see chapter 2) and APC-conjugated streptavidin (1:2000; Biolegend #405207), both diluted and mixed in FACS buffer. Mammalian expression supernatant containing TEM1(Δn)-SpyC fusion protein was mixed with 1 µM of bio-SpyT at RT for 2 h with gentle rotation. The resulting covalent TEM1-SpyC:bSpyT complex was separated from free bSpyT by buffer-exchange into PBS using a spin column with a 10 KDa cut-off (Vivaspin 6; GE Healthcare, # 28932296).The resulting biotinylayed SpyT-SpyC-antigen complex was used as the staining antigen for 7G22-CAR-T cells. The cells were incubated with the staining mix for 30 min on ice and subsequently washed three times with FACS buffer. Immediately before data acquisition, dead cells were stained with 4',6-Diamidino-2-phenylindole (DAPI, 1:2000 dilution). Data was

acquired using an LSR-II flow cytometer equipped with FACSDIVA software (BD Biosciences). Data analysis and plotting were carried out using FlowJo v10 (FlowJo LLC).

4.4.3 *In vivo* experiments

To gain insights into the pharmacokinetics of TriloBiTE molecules, 1 mg/kg 1C1-tB was injected into the tail vein of 10 8-week-old female NSG mice. The TriloBiTE was purified and prepared as described above and injected in a total volume of 100 µl, in PBS. Blood was collected by tail vein puncture at two time points per animal, resulting in 10 different duplicate time points (10 min, 30 min, 1 h, 2 h, 4 h, 6 h, 8 h, 24 h, 48 h and 1 week after TriloBiTE injection). In addition, prior to TriloBiTE administration, a sample was taken from the facial vein of each animal. Serum was obtained by centrifugation and stored at -80 °C.

For the PK ELISA, Nunc maxisorb plates were pre-coated with neutravidin, blocked, and coated with 0.5 µg/ml biotinylated hTEM1-ECD protein, according to the standard ELISA protocol described in chapter 2. A TriloBiTE standard curve was prepared by 2-fold dilution of purified 1C1-tB in 2 % pooled murine serum (baseline)/ PBST/ 1 % BSA, starting at 10 µg/ml. Serum samples from duplicate animals were pooled and diluted 1/50 in 1 % BSA/ PBST. Both samples and standard curve were added to the coated ELISA plate and incubated for 1 h at RT. TriloBiTEs were detected using an HRP-conjugated anti-human Fab antibody (Jackson ImmunoResearch, #209-035-097; 1:10000). ELISA plates were read on a BioTec H1MFG Synergy plate reader using TMB as a substrate. 1C1-tB serum concentrations were calculated based on the obtained standard curve.

For the A673 xenograft pilot, 30 female NSG mice (10-weeks old) were implanted with 10^6 A673 cells s.c. on the right flank. 10 out of the 30 animals received only A673 cells and 20 mice received the tumor cells mixed with 10^7 primary human T cells. Human pan-T cells were isolated from a fresh buffy coat and expanded using CD3/CD28 beads as described previously. One hour after tumor implantation, 10 of the T cell-implanted mice received 1 mg/kg 1C1m-tB in 100 µl PBS into the tail vein. Control groups (n=10) received 100 µl PBS. The i.v. dosing of 1C1m-tB or PBS vehicle control was repeated 24 h and 48 h after tumor implantation. Subsequently, mice were monitored three times a week and tumors were measured using calipers for a total of 45 days, or until the tumor volume approached ~1000 mm^3. NSG mice were bred and housed in a specific and opportunistic pathogen-free environment. All animal experimentation was performed in accordance to the guidelines of the Swiss Federal Veterinary Office and approved by the Cantonal Veterinary Office under the license number 2797.1.

4.5 Supplementary information
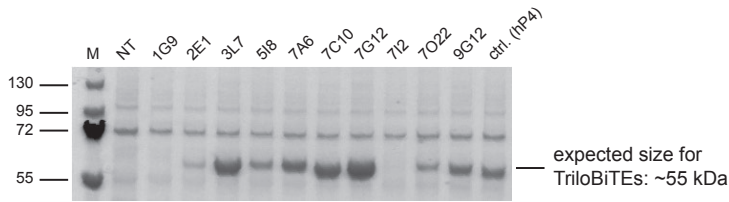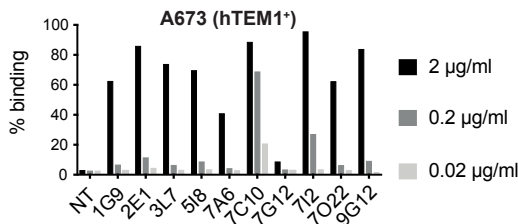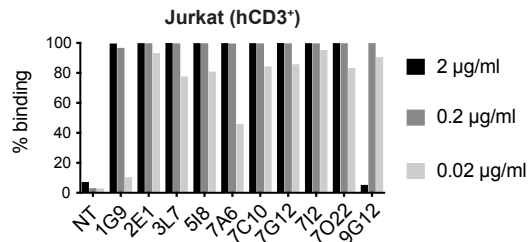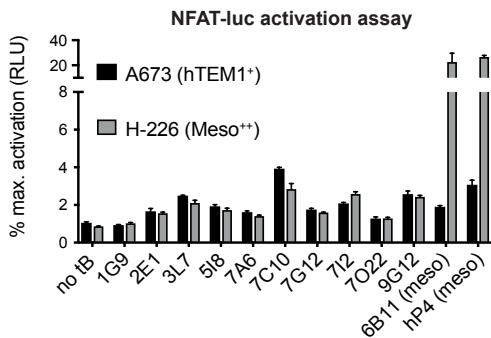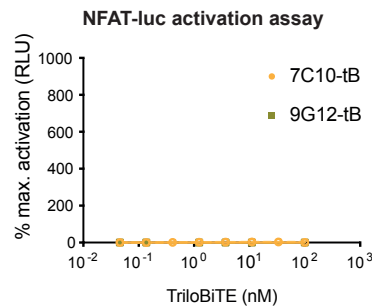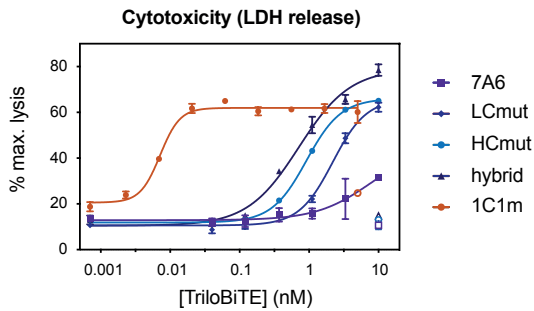
Supplementary Figure 4.1. Functional testing of anti-TEM1(Δn) clones in TriloBiTE format.

(**a**) SDS-PAGE of crude HEK293-6E expression supernatants containing αTEM1(Δn)-tBs (6.5 µl loaded). (**b, c**) Binding of αTEM1(Δn)-tBs to hTEM1-expressing A673 cells (**b**) or hCD3⁺ Jurkat cells (**c**). TriloBiTE protein concentrations were estimated based on relative expression levels (**a**). The percentage of stained cells was calculated based on gating on supernatants from non-transduced (NT) controls. (**d**) Jurkat NFAT-Lucia reporter cell assay revealing the activation potential of unpurified αTEM1(Δn)-tBs (estimated concentration ~25 nM) in the presence of TEM1⁺/meso⁻ A673 cells or TEM1⁻/meso⁺ H-226 cells (E:T ratio 5:1). Expression supernatants containing αMeso-tB (~25 nM; 6B11 and hP4) served as positive controls. (**e**) Jurkat NFAT-Lucia activation assay using purified αTEM1(Δn)-tBs (0.01 – 100 nM) and TEM1⁺ A673 cells (E:T ratio 5:1). (**f**) Cytotoxicity assay assessing the potential of purified 7A6-tB and its affinity-matured variants (0.001 – 10 nM) to redirect primary human pan-T cells towards TEM1⁺ A673 cells (E:T ratio 5:1). Lysis of target cells was quantified based on LDH in the supernatant after 24 h of co-culture and is represented relative to maximum cell lysis achieved with 1 % Triton-X100. Open symbols represent LDH release by TEM1⁻ AsPC-1 cells in the presence of 10 nM tB.

Chapter 5 Development of a phenotypic reporter-based screening platform for the rapid *de novo* discovery of Chimeric Antigen Receptors ('CAR-Factory').

The following chapter describes investigations into the feasibility of developing a practical phenotypic screening method for the direct *de novo* discovery of functional Chimeric Antigen Receptors (CARs) from large scFv clone populations. The CAR Factory platform employs Jurkat NFAT-fluorescent protein reporter cells displaying pre-enriched scFv libraries in a modular and flexible CAR format, which can be selected and enriched for functional activity upon stimulation with cognate target cells. Here, I present a proof-of-concept for this phenotypic screening approach, which led to the discovery of functional CARs directed against human TEM1 and mesothelin.

5.1 Introduction

Chimeric antigen receptors (CARs) are synthetic tumor targeting receptors, elegantly combining an extracellular recognition domain, typically a scFv, and an activating intracellular signaling domain including the CD3ζ chain of the T cell receptor (TCR) complex[159,162]. In this way, antigen specificity can be redirected in order to target tumor cells expressing a specific cell surface antigen. While first-generation CARs only contained the intracellular CD3ζ signaling domain (signal 1), second- and third-generation CARs additionally include one or more co-stimulatory endodomains derived from CD28, 4-1BB and/or OX40 (signal 2), thereby mimicking co-stimulation as provided by antigen-presenting cells (APCs)[163,164]. Finally, fourth-generation CARs, or TRUCKs, are further engineered to secrete activating mediators, such as pro-inflammatory cytokines[165].

CARs directed against the lineage marker CD19 have shown great promise for the treatment of refractory B cell malignancies, achieving complete remission in a substantial proportion of patients[167-171,180,369]. However, this powerful therapeutic approach can be accompanied by serious cytokine release syndromes and other severe side effects related to the massive activation of T cell effector functions[170,171,369]. Much current research and development activity — including that aimed at advancing the technology and utility of CAR T cell therapy to solid tumor indications — therefore seeks to balance potency and safety, for instance through the introduction of engineered safety switches[399,400], or related innovations designed to improve target-specific T cell activation[183-188]. In principle, the CAR technology allows retargeting of effector cells towards any extracellular antigen, provided that a suitable and specific targeting moiety — usually an antibody fragment — is available.

Commonly, methods for the generation of specific targeting antibodies rely on the use of recombinant antigen. This can be used as an immunogen to elicit polyclonal antibody responses *in vivo*, and/or as the

target antigen for *in vitro* library technologies such as phage or yeast display. However, the need for recombinant protein production and purification may present a challenge for some 'difficult' classes of cell surface molecules, such as G-protein coupled receptors or molecules with extensive post-translational modifications. In some cases, recombinant protein expression and immobilization may also lead to (partial) unfolding or altered protein conformation. Therefore, it is not uncommon for antibodies elicited against such molecules to show significantly altered, or even no recognition of the target protein in its native context. Furthermore, it cannot be assumed that any given antibody or derivative fragment isolated purely on the basis of raw antigen targeting criteria will be effective, or function as expected, in the context of a CAR. For example, scFvs with insufficient stability and/or solubility that have a greater propensity to aggregate or oligomerize may trigger undesirable non-specific or constitutive CAR T cell 'tonic' activation leading to impaired function and/or toxicity[378,401]. Additionally, immune synapse formation between effector and target cells is, for any given extracellular spacer/hinge, dependent on the ability of scFvs to engage those specific epitopes that result in optimal bridging geometry and facilitate appropriate levels of CAR clustering to drive effective signal transduction[199-202]. Thus, the identification of a functional CAR retargeting domain with the desired behavioral properties often requires extensive empirical testing of many scFv binders.

As an alternative to traditional screening campaigns, some efforts have been undertaken to develop phenotypic screening approaches for the direct selection of "functional" scFv targeting moieties. In a proof-of-concept study, Alonso-Camino et al. have described a mammalian cell-based antibody display platform, using the expression of the early T cell activation marker CD69 as a read-out for successful antibody-antigen interaction[402]. They later employ the same technology to isolate activating binders to tumor-associated antigens (TAA) from a human scFv library, which they displayed on the surface of Jurkat cells as a first-generation CAR construct[403]. Similarly, Rydzek and colleagues designed a CAR-screening platform by equipping Jurkat cells with a dual nuclear factor κB (NF-κB)/ nuclear factor of activated T cells (NFAT) reporter, which enabled them to select functional CAR constructs in a reproducible and time-efficient manner[404]. During T cell activation, the transcription factors NF-κB and NFAT translocate into the nucleus upon phosphorylation of CD3ζ and subsequently mediate effector functions, such as the expression of cytokines[32,405]. Both NF-κB and NFAT responses are indicators of the magnitude of the TCR signal[385] and therefore represent ideal reporters for the selection of functional CAR 'warheads'.

Hence, we decided to investigate the feasibility of establishing a phenotypic screening platform (CAR Factory) for the selection of functional CARs using human Jurkat T cells engineered to express a fluorescent reporter protein under the control of a NFAT-responsive promoter. Following on from previously published studies[402-404], which essentially describe variations of spiking experiments that did not result in the isolation of any novel scFvs, we have sought to further develop this strategy for practical accelerated CAR discovery, starting from large and minimally pre-selected naïve scFv libraries. In this way, we aim to demonstrate that functional scFv-context specific phenotypic screening can successfully bypass classical laborious discovery campaign approaches that primarily enrich for and emphasize those clones that perform best in affinity-driven assays. In the following chapter, a proof-of-concept for the successful isolation of functional CARs from human scFv libraries that were pre-enriched for binding of recombinant antigen by phage display is presented. Importantly, we demonstrate differential outcomes of traditional recombinant screening versus phenotypic screening using the CAR Factory approach and identify novel functional CAR candidates against three target moieties.

5.2 Results

5.2.1 Experimental design for CAR Factory phenotypic screening.

Since the NFAT signaling pathways of human T cells are generally conserved in the human T cell lymphoma line Jurkat[406], we considered that Jurkat cells containing an NFAT-responsive mCherry reporter gene would be a useful starting point for the development of a functional screening platform. These engineered cells were then further modified via lentiviral transfection to express a 2nd generation CAR construct comprising an N-terminal scFv targeting moiety fused to a fixed CAR scaffold comprising the spacer, transmembrane (TM) and cytosolic domains of CD28 fused to a CD3ζ immunoreceptor tyrosine-based activation motif (ITAM).
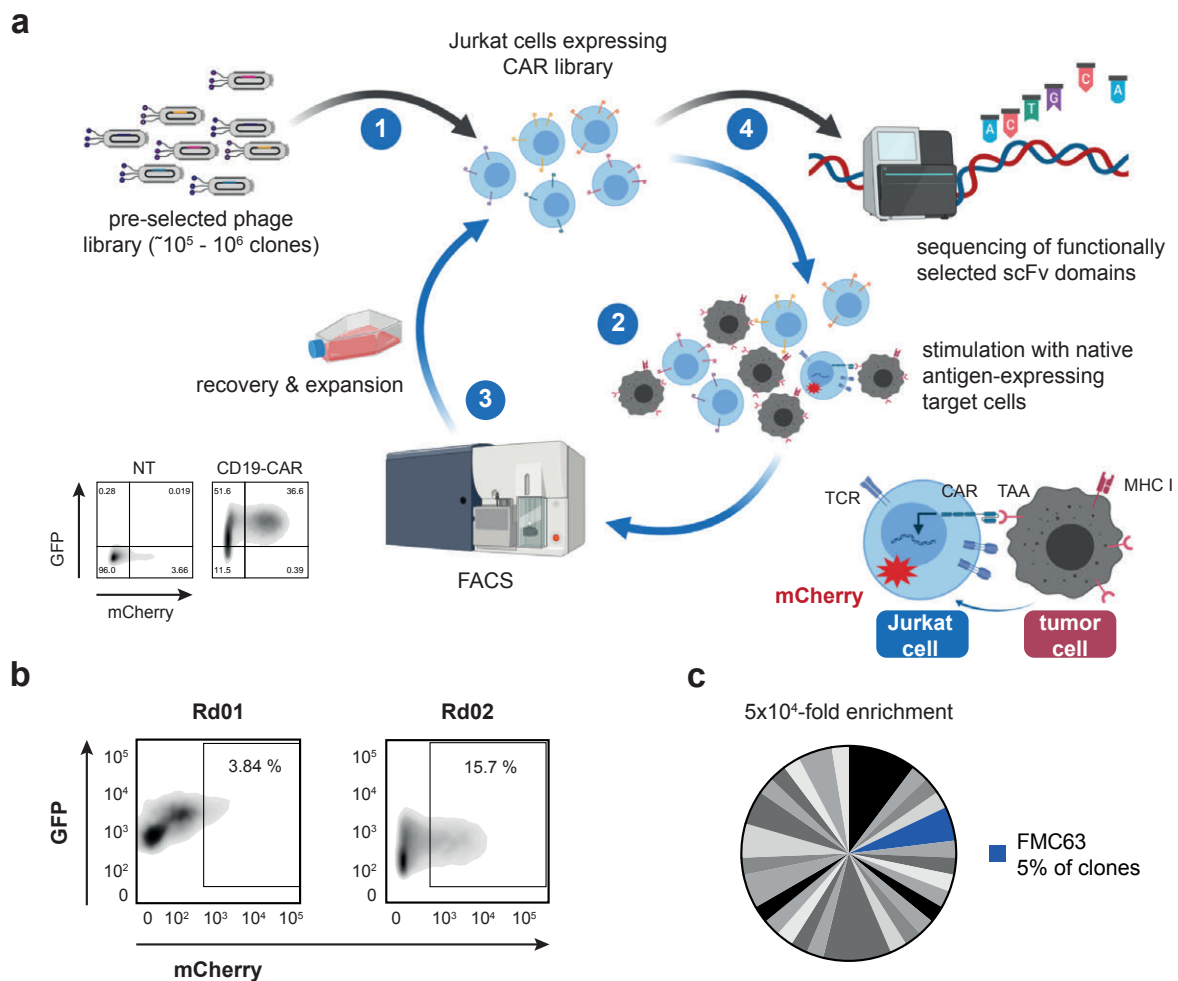
Figure 5.1. The CAR Factory phenotypic screening platform.

(**a**) Schematic representation of the CAR Factory phenotypic screening platform. A library of potential targeting scFvs is initially pre-selected by phage display and cloned into a 2nd-generation CAR cassette containing an in-frame monomeric eGFP. The resulting CAR population is introduced into Jurkat NFAT-mCherry reporter cells via lentiviral delivery (1). Reporter cells displaying the CAR library are stimulated with tumor cells expressing a native tumor antigen (2). Jurkat cells harboring a CAR with a functional activating targeting scFv express mCherry and can be collected by cell sorting (3). Selected reporter cells are expanded and subjected to a subsequent round of phenotypic screening. Alternatively, mRNA is isolated and the scFv region is sequenced to identify enriched clones (4). (**b**) As a proof-of-concept, a single CD19-specific CAR (FMC63) was spiked into 10^6 irrelevant clones, comprising the combined R2 phage display output resulting from selections against mesothelin, TEM1(ECD) and TEM1(Δn). By incubating the resulting population of CAR-expressing Jurkat cells with CD19+ Raji cells, activating (mCherry+) clones are enriched during two rounds of phenotypic screening. (**c**) Sequencing of the selected population revealed a 5x10^4-fold enrichment of the CD19-specific clone FMC63. Pie segments represent discrete clone sequences.

In order to track CAR expression, an enhanced monomeric GFP domain was fused in-frame and downstream of the CAR signaling domains. The Jurkat NFAT-mCherry reporter system has been functionally validated using various discrete scFvs housed in our second-generation CAR, which upon stimulation with cognate target cells, induce potent and robust expression of mCherry (for example, Fig. 4.6a). A process schematic is shown figure 5.1a. We therefore hypothesized that, by extension, the Jurkat reporter cell system could potentially be used to enrich directly for functional activating scFv 'warheads' from a library of scFv-CAR clones displayed on the cell surface.

5.2.2 Enrichment of a single functional scFv-CAR from a pool of irrelevant clones.

The *de novo* isolation of functional CARs from large, minimally pre-selected Jurkat libraries will require the reliable and robust enrichment of a presumed small population of activating clones from a large pool of non-functional and/or non-specific CARs. We therefore first set out to test the feasibility of retrieving a single functional CAR from a large population of 'irrelevant' clones. To do so, we spiked one Jurkat-mCherry cell expressing a CAR containing the clinically validated anti-CD19 scFv FMC63 into 10^6 Jurkat reporter cells displaying other, irrelevant scFv-CAR clones. Those comprised the combined R2 output of phage display selections against recombinant mesothelin and two different TEM1 antigen fragments, all with a typical size of ~10^5 different clones. Due to the pre-selection by phage display, some dominating clones were enriched in these binder pools (see Fig. 5.a, d). The resulting population of Jurkat cells was then cultured with CD19$^+$ B cell lymphoma cells (Raji) at an effector-to-target (E:T) ratio of 1:1 in order to induce NFAT signaling through the CD19-specific CAR. After 24 h of co-incubation, the cells were recovered and activated GFP$^+$/mCherry$^+$ double-positive cells were isolated by FACS sorting. The resulting cell population was expanded and submitted for another round of phenotypic selection (as depicted in Fig. 5.1a). As expected, only a minor fraction of Jurkat cells expressed mCherry during the first round of stimulation, but the percentage of mCherry-positive cells was clearly enriched at the second round of screening (Fig. 5.1b). Subsequent recovery of scFv sequences after two rounds of selection revealed that ~5 % of the clones corresponded to FMC63, the CD19-specific CAR (Fig. 5.1c and Supplementary table 5.1). This represents an impressive 50,000-fold enrichment over the initial starting spiked Jurkat library and provides encouraging validation for our phenotypic CAR experimental design. In addition to FMC63, a couple of other clones from the irrelevant background starting pool also appeared enriched. Some of these already dominated the pre-selected starting libraries and were likely carried over due to their frequency. Other clones may be cross-reactive or to some extent non-specific, suggesting that further experiments aimed at *de novo* discovery would likely benefit from the inclusion of appropriate cell deselection steps.

5.2.3 Phenotypic screening of phage display outputs against cognate antigen leads to demonstrable enrichment of CAR-activating clones.

Following our initial proof-of-concept spiking experiment with FMC63, we sought to evolve this method for the true *de novo* isolation of CAR-activating scFvs present in early outputs from phage display selections. Traditionally, following phage display selections, hundreds to many thousands of binder clones would be randomly and individually arrayed and entered into a primary plate-based screening cascade, initially as soluble scFv or scFv-phage, in order to evaluate antigen binding. In this process, some signal amplitude acceptance criteria are usually applied to filter hit numbers. Collated hits are typically only then reformatted to better reflect the functional context of interest before conducting activity testing.
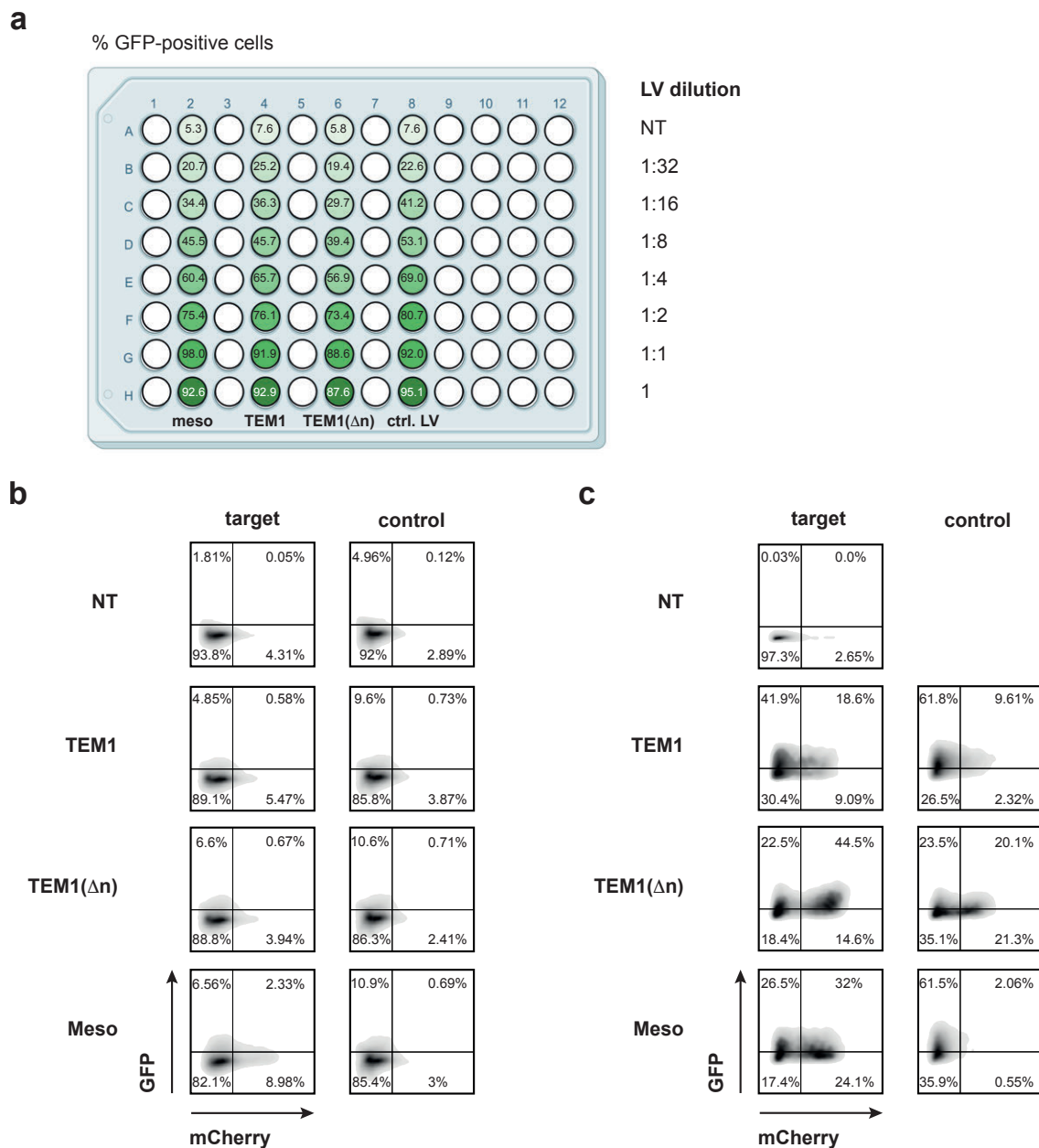
Figure 5.2. Phenotypic screening of pre-selected scFv libraries for the *de novo* isolation of functional CARs.

(**a**) Jurkat NFAT-reporter cells were transduced with diluted lentiviral supernatants, aiming to achieve 10-20 % transduction in order to avoid reporter cells transduced with more than one CAR. Three libraries, each pre-selected for binding of recombinant cognate antigen, were sampled. Meso, human mesothelin; TEM1, human tumor endothelial marker 1; TEM1(Δn), N-terminally truncated fragment of TEM1, comprising only the sialomucin stalk; LV, lentivirus; NT, non-transduced. (**b, c**) The transduced Jurkat CAR libraries were stimulated with cognate target cells, or irrelevant cells at an effector-to-target (E:T) ratio of 1:1. After 24 h of co-culture, Jurkat cells were collected and assessed for CAR expression (GFP) and NFAT activation (mCherry). (**b**) Proportion of GFP+/mCherry+ cells prior to cell screening and sorting. (**c**) Proportion of GFP+/mCherry+ cells after three rounds of cell screening and sorting. Utilized target cell lines are AsPC-1 pancreatic adenocarcinoma (NT and mesothelin), A673 Ewing's sarcoma (TEM1 and TEM1(Δn)) and HEK293-6E (control).

Thus, screening emphasis is principally driven by clone affinity and soluble expression/'fitness' characteristics of an arbitrary sampling of a phage selection output. We reasoned that this screening paradigm may not be

optimal for the isolation of scFv CAR 'warhead' clones whose productive functional activity is determined by a more complex and subtle interplay of several co-dependent variables that govern cell-cell receptor interactions.

To investigate this hypothesis, we used existing phage display selection outputs that were generated in the course of performing classical selection and screening campaigns against three recombinant antigen targets: hTEM1 (ECD, upstream of the stalk region), the truncated membrane-proximal sialomucin stalk domain of hTEM1 (TEM1(Δn)), and human mesothelin. These diverse scFv populations were cloned into 2nd generation CAR constructs and packaged into lentiviral particles for delivery into Jurkat-NFAT-mCherry reporter cells to generate the corresponding phenotypic CAR libraries. Importantly, to avoid transduction with multiple constructs, which could confound downstream sequence deconvolution, we titered the experiment to obtain a transduction efficiency of 10-20 %, as determined by flow cytometry on the basis of GFP-CAR expression (Fig. 5.2a), whilst using sufficient cells to ensure representation of all scFv clones. Ten days after lentiviral transfection of the CAR libraries, the resulting Jurkat cell populations were enriched for GFP expression by fluorescent cell sorting. In order to deplete for scFv clones that non-specifically activate NFAT signaling in the absence of cognate cell antigen, we stimulated the libraries with irrelevant HEK293-6E cells, a line reported as being negative for mesothelin and having negligible TEM1 expression based on our own RT-PCR analysis (see Fig. 3.2b). Jurkat populations stimulated in this way were subsequently sorted for mCherry negatives. Finally, the transduced Jurkat reporter cells were incubated with relevant tumor cell lines expressing the native TAA. After 24 h of co-culture, the cells were collected and analyzed for CAR expression (GFP) and bulk activation (mCherry) (Fig. 5.2b; see Fig. 5.1a for a schematic of the CAR Factory phenotypic screening platform). While only a small proportion of Jurkat^{TEM1} and Jurkat$^{TEM1(\Delta n)}$ were positive for mCherry at baseline, the mesothelin library apparently already contained a substantial number of activating clones. This observation suggests clear differences between the two antigens as prospective CAR targets. Moreover, even though we had aimed for 10-20 % transduction efficiency, the GFP expression in this experiment indicated a lower (5-10 %) proportion of successfully transduced cells (Fig. 5.2b).

All target-specific GFP/mCherry double-positive cells from this first round were collected by FACS sorting and expanded for 14 days to ensure recovery and to allow mCherry levels to return to basal, unstimulated, levels. Subsequently, the enriched Jurkat-CAR libraries were subjected to two additional rounds of phenotypic screening, again using native antigen presented on tumor cells to stimulate the CAR-induced expression of mCherry, as described above. After three rounds of cell screening (CS03), we observed a substantial enrichment of GFP$^+$ CAR-expressing cells for all three libraries, as well as a strong enrichment of mCherry$^+$ activated CAR-T cells (Fig. 5.2c). Although clearly enriched, the fraction of target-specific double-positive Jurkats differed markedly for the different antigens, as did the proportion of cells expressing mCherry upon stimulation with irrelevant cells, with the two TEM1 fragment libraries showing significant residual HEK293-6E binding (Fig. 5.2c).

The latter could be accounted for by a possible cryptic context-specific expression of TEM1 (a possibility alluded to briefly in chapter 4), or by the inadequate depletion of cross-reactive off-target scFv-CARs. The molecular characteristics of the target antigen itself may contribute significantly in this regard.
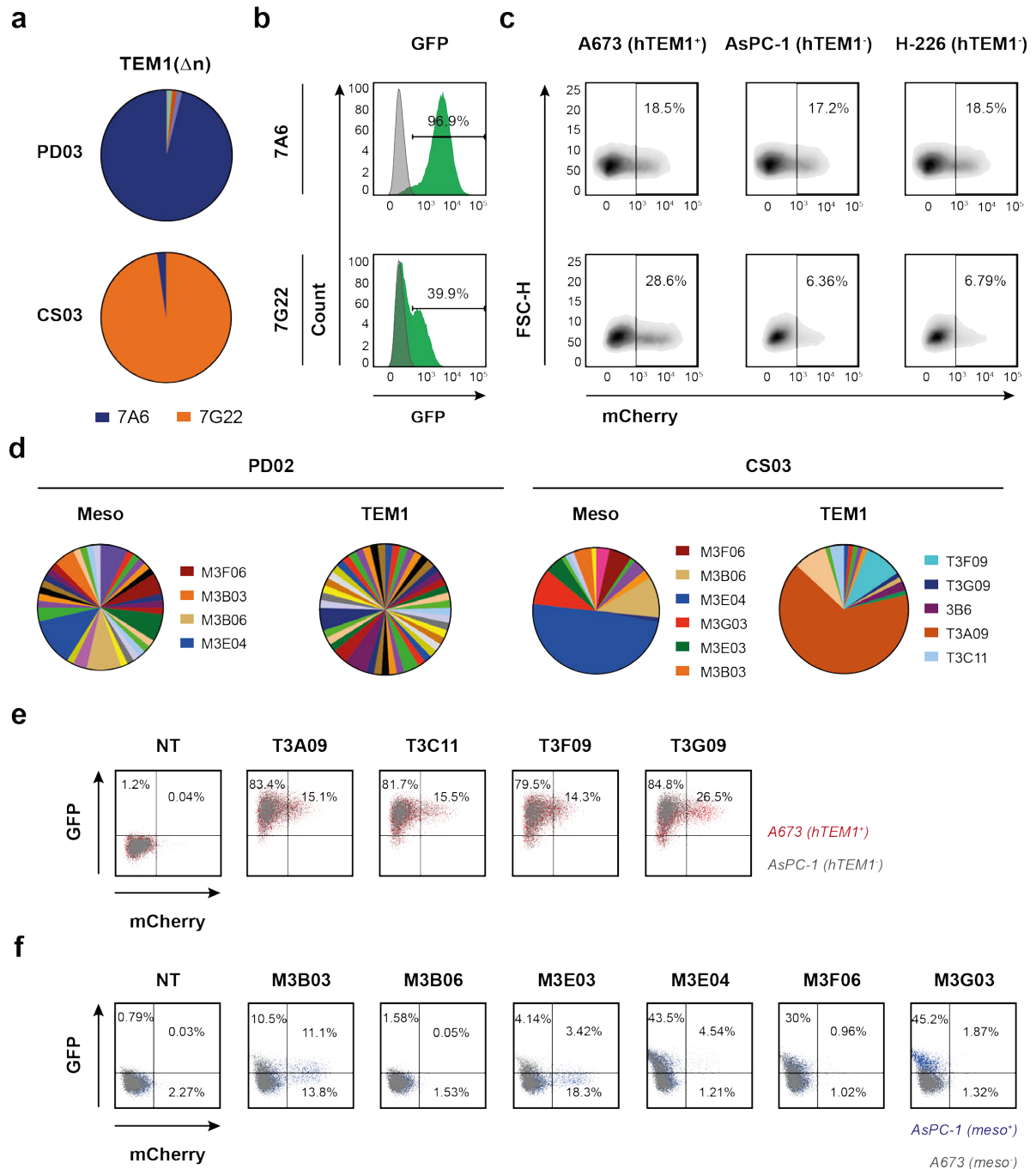
Figure 5.3. Identification of novel CARs targeting relevant tumor antigens.

(**a**) Sequencing of the Jurkat$^{TEM1(\Delta n)}$ library after three rounds of phage display (PD03) or cell screening (CS03) revealed strong enrichment of different clones. (**b**) Efficiency of Jurkat reporter cell transduction with individual CAR constructs, as measured by GFP expression. (**c**) Induction of T cell/NFAT signaling in CAR-expressing Jurkat cells stimulated with different target cells for 24 h (E:T, 1:1), as measured by mCherry expression. Single live cells were gated on GFP. Utilized target cell lines are A673 Ewing's sarcoma (hTEM1$^+$), AsPC-1 pancreatic adenocarcinoma (hTEM1$^-$), and H-226 mesothelioma (hTEM1$^-$). (**d**) Sequence diversity of Jurkat^{meso} and Jurkat^{TEM1} libraries before (PD02) and after (CS03) phenotypic screening. Enriched clones highlighted in the right panel were selected for further characterization. Clone 3B6 had been identified previously by traditional ELISA screening using recombinant TEM1. (**e, f**) Jurkat reporter cells transduced with individual CARs were stimulated with cognate target cells, or irrelevant cells at an effector-to-target (E:T) ratio of 1:1. After 24 h of co-culture, Jurkat cells were collected and assessed for CAR expression (GFP) and NFAT activation (mCherry). (**e**) Activation of mCherry reporter signals by individual CAR constructs selected against hTEM1. Grey dots represent cells stimulated with TEM1-negative AsPC-1 cells. Red dots represent cells stimulated with TEM1-expressing A673 cells. (**f**) Activation of mCherry reporter signals by individual CAR constructs selected against mesothelin. Grey dots represent cells stimulated with meso$^-$ A673 cells. Blue dots represent cells stimulated with meso$^+$ AsPC-1 cells.

In the case of the highly *O*-glycosylated TEM1(Δn) stalk fragment, common glycan motifs may contribute significantly to epitope features recognized by the library scFvs. As the starting point for this experiment was a phage display output generated against TEM1(Δn), produced (and glycosylated) in HEK293-6E cells, it is not surprising that resultant clones may recognize, to varying extents, such recognition elements in the context of other cell surface glycoproteins, thus accounting for higher control activation signals against this cell line.

5.2.4 Phenotypic cell screening efficiently enriches clones independently of their frequency in the starting phage display pools.

To identify selected scFv clones, mRNA was isolated from the CS03 sorted Jurkat cell population as well as the naïve libraries and the scFv domain was amplified and subcloned. For each target library, 96 clones were randomly selected and sequenced. Sequence analysis revealed that the majority of clones comprised full-length in-frame VH and VL chains without internal stop codons or indels (see Supplementary tables 5.2-5.7). In the pre-selected Jurkat$^{TEM1(Δn)}$ library, one clone, 7A6, was highly abundant, and comprised 96 % of all sequenced clones. Thus, this clone had been strongly enriched in the preceding phage display selection steps against the recombinant TEM1(Δn) protein (Fig. 5.3a). In contrast, phenotypic screening using the CAR Factory approach effectively and strikingly reversed this enrichment in favor of a different clone, 7G22, which was massively amplified from the residual diverse background of low frequency clones present in the starting pool (Fig. 5.3a). To explore this observation further, we generated discrete CAR constructs for both 7A6 and 7G22 in Jurkat NFAT-mCherry cells. Both CARs were expressed as indicated by the presence of a GFP-positive population, albeit to different extents (Fig. 5.3b). When co-cultured with TEM1$^+$ target cells, 7G22 induced NFAT-dependent expression of mCherry. However, the dominant phage display output clone 7A6 appeared to activate TCR/NFAT signaling non-specifically, both in the presence of TEM1$^+$ cells and when co-cultured with irrelevant, TEM1-negative cell lines (Fig. 5.3c) with no obvious discrimination. Alternatively, the observed mCherry levels may reflect background 'tonic' signaling. Collectively, these observations highlight an extreme example of divergence between scFv clones isolated according to classical soluble expression screening and affinity criteria, and clones whose isolation is dependent on functional context.

5.2.5 Identification and characterization of novel CARs targeting the TEM1 ECD or the mesothelin tumor antigen.

In contrast to the Jurkat$^{TEM1(Δn)}$ library, the original clone libraries directed against mesothelin and TEM1 were more diverse, although the Jurkat^{meso} library displayed some clear clone enrichment preference (Fig. 5.3d). Although the majority of clones analyzed represented unique sequences, ~20 % of the sequences in the Jurkat^{meso} starting library encoded two distinct enriched clones (M3B06 and M3E04). The function-based enrichment of activating CARs over the three rounds of phenotypic selection constrained the composition and diversity of both libraries substantially, with clone M3E04 now constituting 49 % of all sequences (Fig. 5.3d). For TEM1 ECD, the initially very broad library diversity was similarly constrained after the cell-based selection rounds and 65 % of all clones now shared the same sequence (T3A09). Additionally, a variant of this clone was found using a slightly different light chain (T3G09; Fig. 5.3d). Interestingly, only one clone (3B6) was found to overlap with the ELISA screening campaign performed following the initial phage display selection (see Table 3.1 and Fig. 3.1e).

Jurkat NFAT-mCherry reporter cells were subsequently transfected with individual CAR constructs comprising scFv 'warheads' corresponding to the functionally enriched clones. With the exception of clone T3G09,

functional testing of the individual clones revealed only very modest TEM1-specific mCherry activation potential for the TEM1-selected clones, despite strong CAR-GFP expression (Fig. 5.3e). In comparison, Jurkat cells expressing CARs selected against mesothelin displayed significantly reduced GFP expression and two of the selected clones barely showed detectable GFP signals (Fig. 5.3f).
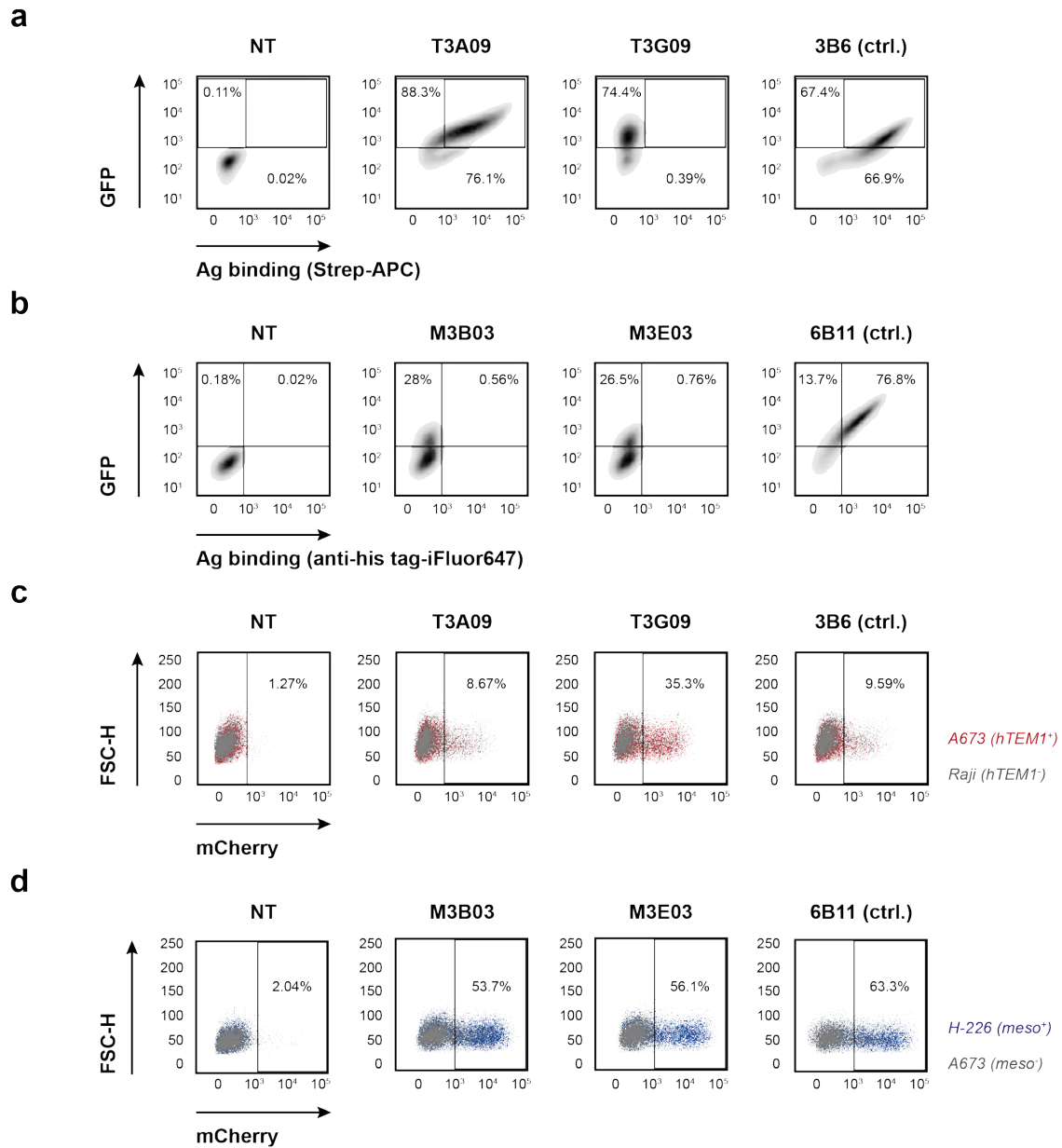
Figure 5.4. CARs identified by phenotypic screening specifically activate NFAT signaling in the presence of cognate target cells.

(**a**) Novel CARs enriched for functional binding of TEM1-expressing cells were individually introduced into Jurkat NFAT-mCherry reporter cells. One clone, 3B6, previously identified by recombinant screening, served as positive control. 7 days after lentiviral transduction, CAR expression and binding of biotinylated recombinant hTEM1 (ECD) was assessed by flow cytometry, detecting APC-conjugated streptavidin. (**b**) Jurkat NFAT-mCherry cells expressing newly identified anti-mesothelin CARs or the previously identified clone 6B11 were assessed for binding of recombinant human mesothelin protein. Binding was revealed with an iFluor647-conjugated anti-his tag antibody. (**c**) Anti-TEM1 CAR expressing Jurkat cells were co-cultured with TEM1+ A673 cells (red dots) or TEM1- Raji cells (grey dots) at a 1:1 ratio. After 24 h, CAR-bearing Jurkat cells were tested for activation induced mCherry expression. Cell populations are shown gated on single live GFP+ cells. (**d**) NFAT-induced mCherry expression by CAR-transduced Jurkat reporter cells was measured after 24 h of co-culture with meso+ H-226 cells (blue dots) or meso- A673 cells (1:1 cell ratio). Cell populations are shown gated on single live GFP+ cells.

Nevertheless, two of these CARs, when stimulated with native mesothelin presented on tumor cells, induced measurable mCherry expression. Surprisingly, the strongly enriched clone M3E04 did not seem to activate robust NFAT signaling, but it expressed at higher levels (~44 % GFP$^+$ cells) compared to most of the other clones, raising the possibility that additional 'fitness' criteria and/or sorting carryover could account for its robust representation in the final pool.

Subsequently, several prospective activating clones were chosen for further characterization. Those CAR constructs were reintroduced into Jurkat NFAT-mCherry reporter cells by lentiviral transduction. After 10 days of expansion, the transduced reporter cells were assessed for CAR expression and soluble cognate antigen binding. (Fig. 5.4a, b). For both TEM1 ECD and mesothelin antigens, binders that had been identified following classical phage display screening campaigns were included as positive controls. For the selected anti-TEM1 CARs, the transduction efficiency was high (86.3 % for T3A09 and 74.4 % for T3G09), but only the T3A09 CAR seemed to bind appreciably to recombinant hTEM1 protein (Fig. 5.4a). In contrast, neither of the CAR Factory selected anti-mesothelin CARs were stained with monomeric recombinant mesothelin protein (Fig. 5.4b). In addition, although higher than in previous experiments, the proportion of GFP expressing cells was rather low (28.6 % for M3B03 and 26.6 % for M3E03), especially compared to the previously identified anti-mesothelin clone 6B11 (90.5 %; Fig. 5.4b).

Nevertheless, we proceeded to test all CARs for specific T cell activation in a co-culture experiment. Surprisingly, T3G09, which did not show any binding to recombinant monomeric TEM1, induced NFAT-driven mCherry expression specifically in the presence of TEM1$^+$ cells. As observed previously (see Fig. 4.6a), the previously identified clone 3B6, which recognized TEM1 protein, failed to mediate any differential mCherry response. Clone T3A09 showed a similar binding/activation pattern (Fig. 5.4c). Similarly, both novel anti-mesothelin CARs specifically induced T cell signaling in the presence of mesothelin expression cancer cells, leading to mCherry expression in a substantial proportion of Jurkat reporters (Fig. 5.4d). Together, despite the apparent lack of recombinant antigen binding (discussed below), a subset of CAR targeting moieties identified using the CAR Factory phenotypic screening platform appear functional and merit further investigation in primary T cell Selective killing assays.

5.3   Discussion

In the present study, we have explored phenotypic cell-based screening as an alternative approach for the rapid identification of functional CAR scFv 'warheads' from complex starting libraries. Employing an NFAT-driven mCherry reporter system, we have shown that this 'CAR Factory' platform is capable of retrieving rare scFvs from a pool of irrelevant clones, which are capable of driving CAR activation. In this preliminary study, we have identified and partially characterized novel CAR-active scFv clones specific for three distinct antigen fragments.

In our experimental framework, scFvs that drive CAR activation are expected to represent a subset within larger pools of general 'binders' that have undergone some preliminary capture/enrichment on immobilized recombinant antigen protein. As these CAR-compatible clones would appear to have no defined competitive advantage in terms of either soluble expression fitness or raw binding affinity, they may enrich only slowly — if at all — during conventional phage display selections, and be disregarded (or just not sampled) during typical primary ELISA or protein-interaction assay cascades.

The TEM1(Δn) recombinant domain study described above illustrates such a scenario. Here, the immunodominant phage display-selected scFv (7A6) was unable to compete in a phenotypic functional context. Despite the extreme over-representation of 7A6 in the phage output, phenotypic selection using native antigen-expressing cells enabled the retrieval and enrichment of the low frequency, but apparently superior, 7G22 clone, which displayed significant TEM1 selective activation potency at low apparent CAR expression levels (GFP basis; Fig. 5.3a-c). Interestingly, 7G22 not only activated NFAT signaling in Jurkat CAR reporter cells, but was able to potently and specifically redirect primary T cell effector functions as both a CAR and a soluble T cell engager (see chapter 4). Similarly, the fact that functional molecules appear to be rare in the Jurkat[TEM1] library, despite the high ELISA hit rates in the phage display primary screening (see Table 2.2 and Fig. 3.1b), supports the hypothesis that binding does not necessarily predict functionality. Overall, this clearly demonstrates how the specific discovery/screening method can impact on the enrichment of desirable scFv candidates.

As observed in our lab, and in line with many published and anecdotal accounts, antibodies raised against isolated antigens in solution often do not perform as expected against the respective proteins in their native membrane-bound forms[407,408]. Such discrepancies may be attributable to several non-mutually exclusive possibilities, such as the masking of epitopes on the cell due to complexation with other membrane components, differences in key post-translational modifications that impact on epitope structure, or more simply, incorrectly folded recombinant protein used in the selection campaign. Moreover, certain antigen epitopes or protein regions can assume different main- or side-chain conformations or dynamic conformation equilibria that may be distinct between recombinant antigen in solution and membrane-bound forms[409]. This may be particularly relevant for large or complex multidomain proteins such as TEM1. Thus, an intriguing possibility is that a sub-population of selected library phage may recognize such flexible regions of a recombinant antigen with particularly weak affinity constants, but nevertheless will propagate through selection rounds. Such scFv 'passenger' clones, if subsequently challenged against the corresponding native membrane antigen, may encounter stabilized structures or dominant conformations that facilitate better paratope interactions and the apparent restoration of binding.

Conversely, and equally compelling is the possibility that an apparent affinity gain could be achieved by subtle conformational shifts in the folded scFv molecule, brought about by a switch from prokaryotic (phage display) to eukaryotic (CAR format) expression. Such a hypothesis merits further investigation, but could account for situations, such as we describe above, whereby phage outputs selected on recombinant antigens contain scFv clones that have apparent target-specific functional activity against their cognate native antigens, but do not appear to recognize soluble recombinant antigen.

Indeed, the existence of variant conformational epitopes leading to differential antibody binding to soluble versus membrane-bound protein has been suggested for mesothelin and other glycosylphosphatidylinositol (GPI)-anchored proteins[409-411]. Asgarov and colleagues describe the identification of a novel anti-mesothelin antibody, which preferentially recognizes mesothelin-expressing cells, but does not bind to cleaved nor recombinant full-length mesothelin[409]. Since high concentrations of shed mesothelin in the serum of cancer patients can, in principle, act as an antigen sink and hinder the therapeutic effect of targeted therapies, antibodies specific for membrane-bound mesothelin may prove advantageous in the clinic[412]. However, validation of CAR Factory clones that appear to differentially recognize cognate native cell membrane antigens, but not the corresponding recombinant soluble reagents, would ideally require the availability of specific KO lines. In addition, such tools could prove useful as true null subtraction cell lines for use during the enrichment/sorting procedure.

Our current phenotypic screening workflow exploited relatively pre-enriched scFv libraries, which had undergone two rounds of phage display on recombinant antigen. As discussed above, this may introduce an undesired bias towards certain epitopes. Therefore, and in order to explore the full potential of the CAR Factory phenotypic screening approach, we next plan to sample minimally preselected scFv libraries that have undergone just a single round of phage display against recombinant antigen. This should ensure capture of all clones in the library that recognize the antigen across the widest range of epitopes and with the widest range of binding affinities, whilst reducing the scFv clone population to a number compatible with our CAR Factory library process (10^5-10^6 as a typical R1 clone output). In addition, the absence of a second phage amplification round should ensure that the rarest binder clones are retained in the experiment. In this way, we hope to further develop and adapt the potential of our CAR Factory platform approach to enable the optimal, unbiased, *de novo* discovery of rich panels of CAR-active scFv clones.

Finally, the modular CAR scaffold used in our studies has been designed to be fully compatible with CAR constituent element cloning, allowing full portability of linker/spacer regions, TM domains, ITAMs and costimulatory domains — all of which can have a major impact on T cell engagement and activation[189,196,199,202,378,401,413]. As previously discussed, optimal bridging distance is influenced not only by the scFv and its target epitope, but also by the length and structure of the linker/spacer region connecting the scFv to the CAR TM domain[193,199-202]. Hence, one can envisage future CAR Factory experiments where *de novo* isolated CAR-active scFv pools are further permutated against defined panels of linkers, TM domains and ITAM repertoires before being fed back into the phenotypic NFAT reporter screen to search for optimized and/or novel modular CAR assemblages.

In summary, we have shown that phenotypic CAR screening has the potential to accelerate (and rescue) the discovery of functional CAR warheads via context-appropriate mining of scFv libraries. Further development and refinement of the technology and its scope is ongoing, as is the validation of the identified CARs in primary T cells.

5.4   Materials and Methods

Cell culture

All target cell lines were sourced from the ATCC via LGC Standards and cultured as described in chapter 2. Jurkat NFAT-mCherry reporter cells were a kind gift from Melita Irving's lab, UNIL. They were maintained in RPMI-1640 Glutamax (Life Technologies, #61870010) containing 10% fetal bovine serum (FBS; Biowest # S1810-500, lot #S1614151810) and 100 U/ml penicillin/streptomycin (Gibco, Life Technologies, #15140122). All cells were cultured at 37 °C, 5 % CO2 in a humidified incubator and regularly tested for mycoplasma (GATC service).

Construction of CAR libraries

Phage display selection outputs stored as bacterial glycerol stocks were thawed and plasmid DNA was isolated using the ZymoPURE II Midiprep kit (Zymo Research, # D4201). The scFv gene was extracted by digestion with NheI-HF/SalI-HF (NEB, # R3131S and # R3138S) for 3 h at 37 °C. The corresponding DNA band (~800 bp) was extracted from a 1 % agarose gel using the ZymoCLEAN gel DNA recovery kit (Zymo Research, # D4002) and ligated into the cloning site of a modified pRRL vector harboring a spacer/hinge, TM region, hCD28-derived intracellular costimulatory domain and hCD3z signaling domain, followed by an in-frame monomeric GFP (TagGFP2, Evrogen) in the format of a 2nd generation CAR. Ligation was performed using T4 DNA ligase (1000 U, NEB # M0202S) and incubating at RT for 2 h followed by o/n at 16 °C. The ligations were purified using the Zymo DNA Clean & Concentrator kit (NEB, # D4006) before heat shock transformation (45 s at 42 °C) into *E.cloni* 10G chemically competent cells (Lucigen # 60107-2). pRRL plasmid DNA of successfully transformed clones was isolated with the ZymoPURE Maxiprep kit (Zymo Research, # D4202) and concentrated to 1 μg/μl.

Lentiviral transduction of Jurkat NFAT-mCherry cells

Lentivirus was produced in HEK293T cells transiently transfected with the resulting pRRL libraries and pCMVR8.74 and pMD2.G packaging plasmids (origin of lentiviral plasmids: Didier Trono lab, EPFL) using Turbofect transfection reagent (Life Technologies, #R0532) and protocol. Viral particles were harvested after 48 h and concentrated by ultracentrifugation. Concentrated lentiviral supernatants were diluted in a 2-fold dilution series (up to 1:32) and added immediately to 1 x 10^6 Jurkat NFAT-mCherry cells. Transduced cells were expanded and assessed for GFP expression by flow cytometry after 7 days. Cell populations containing 10-20 % transduced cells were selected and expanded for another 3-7 days before cell sorting.

CAR activation and phenotypic screening assays

The Jurkat libraries were first enriched for scFv.CAR.GFP expressing cells by sorting unstimulated GFP$^+$/mCherry$^-$ cells. The resulting enriched scFv.CAR.GFP expressing population was expanded for 7 days and subsequently stimulated with irrelevant, antigen negative HEK293-6E cells. Therefore, 3 x 10^6 HEK293-6E cells were co-cultured with 3 x 10^6 scFv.CAR.GFP library expressing Jurkat cells in sterile 6-well plates in a total volume of 2 ml. Additionally, non-transduced Jurkat NFAT-mCherry cells were stimulated with phorbol myristate acetate (PMA)/iomomycin cell stimulation cocktail (Thermo Fisher Scientific # 00-4970-03) as a positive control. After 24 h incubation at 37 °C, 5 % CO₂, the cells were resuspended and washed once with 2 ml 5 % FBS, PBS (FACS buffer) before proceeding to FAC sorting of GFP$^+$/mCherry$^-$ cells into single tubes. The resulting cleaned Jurkat libraries were expanded again for 7 days and then stimulated with target cells expressing the antigen of interest for a phenotypic cell sorting. To this end, adherent target cells (A673 cells

for Jurkat^{TEM1} and Jurkat$^{TEM1(\Delta n)}$ libraries and AsPC-1 for the Jurkat^{meso} library were harvested with trypsin-EDTA, counted and adjusted to 4 x 10^6 cells in a 6-well plate. Library-expressing Jurkat populations were added at 4 x 10^6 cells to obtain an effector-to-target (E:T) ratio of 1:1. Jurkat cells were stimulated for 24 h at 37 °C, 5 % CO$_2$ and subsequently harvested and washed as described above. Again, non-transduced Jurkat NFAT-mCherry cells stimulated with PMA/ionomycin served as a positive control. GFP$^+$/mCherry$^+$ cells from each library were sorted and expanded for 14 days prior to a subsequent round of cell stimulation and sorting. For all sorting experiments, dead cells were stained with 4',6-Diamidino-2-phenylindole (DAPI, 1:2000 dilution). Cells were sorted using a FACSAria III cell sorter equipped with FACSDIVA software (BD Biosciences).

Isolation, cloning and sequencing of selected scFvs

Before and after three rounds of phenotypic screening and cell sorting, mRNA was isolated from 10^7 sorted Jurkat pools using the Dynabeads mRNA DIRECT purification kit (Thermo Fisher Scientific, # 61011), following the manufacturer's instructions. Subsequently, 1 µg of the resulting mRNA served as the template for cDNA synthesis using the PrimeScript 1st strand cDNA kit (Takara, # 6110B) and oligo-dT primers. The scFv sequence was amplified from the cDNA template using Phusion High-Fidelity PCR Master Mix with GC Buffer (NEB # M0532S) and the following primer set: HT-CAR_amplif.FW1: CCT GCT AGT ACT CTT CTG GGC and HT-CAR_amplif.REV1: AGG TGG AGG ATA CAT AAC TTC GT. Successfully amplified scFv pools were purified from 1 % agarose gels using the ZymoCLEAN gel DNA recovery kit (Zymo Research, # D4002) and cloned into the in-house developed pCHV101 phagemid vector (see chapter 2) using NheI-HF/SalI-HF, as described above for the construction of CAR libraries. Single colonies of successfully transformed cells were picked and sequenced using the high-throughput plate sequencing service of Microsynth.

Flow cytometry assays

For co-culture NFAT activation assays, adherent cells were detached using 10 mM EDTA, counted and resuspended in fresh, complete culture medium. 0.5 x 10^6 target cells were seeded into 24-well assay plates and 10^6 CAR-transduced Jurkat NFAT-mCherry cells were added in a total volume of 1 ml complete RPMI. After 24 h of co-culture, the cells were harvested and washed once with 2 ml FACS buffer (5 % FBS, PBS). Antigen binding by anti-TEM1 CAR expressing Jurkat cells was assessed by incubating 0.5 x 10^6 Jurkat cells with 1 µg/ml bio-hTEM1 (produced in-house, see chapter 2) and APC-conjugated streptavidin (1:2000; Biolegend #405207), diluted in FACS buffer. Anti-meso CAR expressing Jurkat cells (0.5 x 10^6) were incubated with 1 µg/ml his-tagged human mesothelin protein (amino acids 296-580; R&D Systems #3265-MS-050) instead. Incubation with the antigen or staining mix was performed for 30 min on ice followed by three wash steps with 100 µl FACS buffer. Binding of recombinant mesothelin was revealed using an iFluor647-conjugated anti-His tag antibody (GenScript #A01802-100), diluted 1:1000 in FACS buffer. After another 30 min incubation on ice, stained cells were washed again three times. Immediately before data acquisition, dead cells were stained with 4',6-Diamidino-2-phenylindole (DAPI, 1:2000 dilution). Data was acquired using an LSR-II flow cytometer equipped with FACSDIVA software (BD Biosciences). Data analysis and plotting were carried out using FlowJo v10 (FlowJo LLC).

5.5 Supplementary Information

clone	HC			LC			%
	CDR1	CDR2	CDR3	CDR1	CDR2	CDR3	
C10				SSNIGAKYG	ETT	GA	0
C11				QTILYSSNNKNY	WAS	HQYYSIPHT	0
B02				QSVNSWH	STS		0
C05	GFTFSSYG	ISYDGSNK	AKAALLGGYSYGFNWFDP	KLGDKY	QDV	QAWDSSHVV	2.5
M3F06	GFTFDDYA	ISWNSGSI	AKDLAPYYYYMDV	QSISSR	RAS	QQFNTYPLT	2.5
A01	GFTFSSYA	ISGSGGST	AKGGGLFGY	SSNIGSNT	SNN	AAWDDSLNGLV	2.5
FMC63	GVSLPDYG	IWGSETT	AKHYYYGGSYAMDY	QDISKY	HTS	QQGNTLPYT	5.0
A12	GYTFTGYY	INPNSGGT	ARAGRLGWFDP	NIGRKN	RDS	QVWDSSGDPVV	2.5
D04	GFTFSSYS	ISSSSSYI	ARAPNSVGYAFDI	QSLLYTNGYNY	TLS	MQRIEFPFT	2.5
C08	GYSFIDHY	INPKGGDT	ARDKYYYLIDY	QDISNY	DAS	QQYDNLPPT	2.5
B01	GGSISSSNW	IYHSGST	ARDNPWGYGMDV	QSISSY	AAS	QQSYSTSIT	2.5
B06	GFTFSSYA	ISYDGSNK	ARDPSMIVGFDL	SSDIGSNT	SNN	AAWDDSLNGHYV	2.5
A06	GYTFTSYG	ISAYNGNT	ARDQSGDFWSGYFYYYGMDV	QGISSY	AAS	QQLNSYPPV	2.5
C02	GYTFTSYG	ISAYNGNT	ARDSGRRWLQSYFDY	QSISSY	AAS	QQSYSTPWT	2.5
D10	GFTFSSYA	ISYDGSNK	AREEGSGWYSVRSYWYFDL	NIGSKS	DDS	QVWDSSSDHPV	2.5
M3E04	GGSISSGDYY	IYYSGST	ARESVVAGAFDI	QSISSY	AAS	QQSYSTPYT	10
D03	GYTFTSYD	MNPNSGNT	ARGEDSGSYYRAGY	QSVSTY	DAS	QQRSKWPPV	2.5
A11	GGTFSSYA	IIPIFGTA	ARGLNTRGGGY	QSLVYSDGNTY	KVS	MQGTHWPPT	2.5
B07	GYTFTGxY	INPNSGGT	ARGVSSSPLISSxTFDP	xSNIGSNA	SNN	AAWDDSLSGWV	2.5
D08	GYSFTNYW	IYPGDSDT	ARRYYDSSGYYSLSAFDI	SSNIGNNY	ENN	GTWDSSLSAGV	2.5
B04	GYTFTGYY	INPNSGGT	ARSGYYYDSSGYYSDYFDY	SSNIGSDY	NND	AAWDDSLSGPNYV	2.5
A07	GYTFTSYG	ISAYNGNT	ARTFWGRTPFDY	QSVLYRSNNRNY	WAS	QQYYSIPLT	5
A02	GGSFSGYY	INHSGST	ARVPLIAVAGTGYYYYGMDV	QSIANY	AAS	QQSYSIPPT	2.5
B12	GYTFSSHA	INVFNGNT	ARVSLRRGGDYFYDY	QSISSY	AAS	QQSYSTPLT	5
B09	GGTFSSYA	IIPILGIA	ARVVLPLYGMDV	QTVSSAF	ATS	QHYSGSPPVYT	5
D11	GGTFSNYG	IIPIFGTA	ARVYSGAGDNRGYYFVY				2.5
B10	GYTFSSNA	INAGNGNT	ASFDYDY	QSVSSY	DAS	QQRSNWPGT	2.5
B05	GYTFTSYY	INPSGGST	ASSAWISDFDY	GSDFNY	DVT	HSHAARGTLSYI	2.5
C01	GYTLTELS	FDPEDGET	ATEWELLHDRNDAFDI	TSNIVHNS	DDS	ATWDTTLSAVV	5
C09	GFTFSSSD	IGLADDT	VREGLSGNWDNWYFDL	QSIRSH	GAS	QQSYSDPPT	2.5

Supplementary Figure 5.1. CDR sequences and diversity after phenotypic selection against CD19+ Raji cells.

CDR amino acid sequences and frequencies of a subsets of clones selected randomly after 2 rounds of cell selection on CD19+ Raji cells (CD19 spike; see Fig. 5.1b, c).

clone	HC			LC			%
	CDR1	CDR2	CDR3	CDR1	CDR2	CDR3	
B09	GYTFTSYD	MNPNSGNT		QSLLHSNGYNY	LGS	MQALQTPLT	1.04
H12				ESLLHTNGYNY	LAS	MQSLE	1.04
G08				QSVSSSY	GET	LNGHH	1.04
H04				VRVLAA	DAS	QQRGTGLSLSxGxWKSN	1.04
E08	GYTFTGYY	INPNSGGT	AGDYDFWSGFDP	SSDVGGYNY	DVS	SSYTSSSTWV	1.04
D04	SISSNSGAWN	YRSKWYN	AGGTHYNGMDV	QSISRY	TTS	QQGYSRPAT	1.04
A04	GFSLTTTAVG	IYWDGAQ	AHRQNLPASTWHHFDT	QSVGSY	AAS	QQTYSPPNT	1.04
G10	GFTFDDYA	ISWNSGSI	AKASDSSGWPSSYFDY	QNIRSW	KAS	QQYNSYPVT	1.04
C01	GFTFDDYA	ISWNSGSI	AKDIEYSYGAFDY	QNIRSW	KAS	QQYNSYPVT	1.04
M3F06	GFTFDDYA	ISWNSGSI	AKDLAPYYYYMDV	QSISSR	RAS	QQFNTYPLT	3.13
A03	GFTFDDYA	ISWNSGSI	AKDLEVVPAAIDY	QSISTW	KAS	QQYDSYPLTLGGGSKVDIK	1.04
E04	GFTFDDYA	ISWNSGSI	AKDLSSGWYLTGAFDI	SSNIGARDD	GDT	QSYDSVSGFV	2.08
B11	GFTFDDYA	ISWNSGSI	AKDNGSSGYYTGFDY	QSISSY	AAS	QQSYSTPRS	4.17
F07	GFTFSTYA	IxPNSERT	AKGGGSGTHQRSPDY	QSVGNW	RAS	QQYNSYPWT	1.04
E11	GFTFGDYA	ISWNSGSI	AKGLDRGYDPSDY	QSISGW	KAS	QQYDGYPLT	1.04
A02	GYTFTSYY	INPSGGST	ARAARVDILTGGLDY	QSISSW	KAS	QQYSSYPLT	1.04
H10	GFTFSSYA	STYDGSIK	ARDGHSSGWYDHGGFDF	QSVSSY	GAS	QQYGSYT	1.04
C06	GYTFTSYY	INPSGGST	ARDGLTVAGLNWFDP	QSVSSN	GAS	QQYNNWPS	1.04
B07	GYTFTSYG	ISAYNGNT	ARDHDFWSGYSPFDY	QSISSY	AAS	QQSYSTPYT	1.04
M3B06	GYTFTSYG	ISAYNGNT	ARDSGRRWLQSYFDY	QSISSY	AAS	QQSYSTPWT	5.21
D10	GYIFSSYG	INSYAGNT	ARDVYGGVFDK	QSISSY	AAS	QQSYSTPLT	1.04
F10	GYTFTGYY	INPNSGGT	ARDVYGGVFDK	QGIRND	AAS	LQDYDSPYT	1.04
C09	GFTFSSYS	ISSSSSTI	ARDYYDSSGYFKFDY	SSDVGGYNY	EVS	SSYTTSSTWV	1.04
M3E04	GGSISSGDYY	IYYSGST	ARESVVAGAFDI	QSISSY	AAS	QQSYSTPYT	7.29
A12	VSSNSAAWN	YRSKWYN	ARGDSEWGSGNWFDP	QSISSY	AAS	QQSYSTPGT	2.08
H02	GGTFSSYA	IIPIFGTA	ARGRYDLVG	QSVSSS	DAS	QQYNNWPLT	1.04
E12	GYTFTSYG	ISAYNGNT	ARGSASGPLI	SSNIGAGYD	GNS	QSYDSSLSGWV	1.04
E07	GYTFTGYY	INPNSGGT	ARKNSGWYDYYFDY	QSISSY	AVS	QQSYSTPYT	1.04
H03	GYTFTNYY	INPGGGTT	ARKSLGGHSFGAFDD	QSIGRN	NAS	HQSANLPWTFGQWTKVDIK	1.04
E01	GGSISDSY	VYYSGST	ARSPVSSGWTPYFDL	QSVSSSY	GAS	QHYGSSPRWT	1.04
H11	GYTFTDYY	INPNSGGT	ARVGIDRKATRDYYYVMDV	QGISNS	AAS	QQYYSTPQT	1.04
G02	GYTFTSYG	ISAYNGNT	ARVGRGSSRD	SSNIGAGYD	GNN	QSSDNNMSGLV	1.04
M3B03	GYTFSSHA	INVFNGNT	ARVSLRRGGDYFYDY	QGIRND	AAS	LQDYDSPYT	3.13
G07	GGTFSSYA	IIPIFGTA	ASQRGPRSGVDY	SSNIGAGYD	GNN	QSSDNNMSGLV	1.04
H07	GFTFSSYS	ISSGSSTI	LVSARGFDYWxPGEPWSPSLQ	SSDVGSYNL	EVI	SSYTSSSTLERV	1.04
A08	GFTFSSYA	ISSNGGST	V*AMGGGFSSA	QSISGSY	WAS	QQYYTTPLT	1.04
G01	GGTFSSYA	IILPLVQ	VRECWTPTxTTVWTSGAKGPRSPSPQ	SSNIGNNY	DNN	GTWDSSLSAGV	1.04

Supplementary Figure 5.2. CDR sequences and diversity of the Jurkat^meso library prior to phenotypic selection.

CDR amino acid sequences and frequencies of a subsets of clones selected randomly prior to phenotypic selection.

clone	HC			LC			%
	CDR1	CDR2	CDR3	CDR1	CDR2	CDR3	
B01	GFTFSSYG	ISYGGSNK	AKGAMGYYYYYVMDV	QSVGSSH	GTS	QQYETSPTT	1.04
H05	GFTFSIYG	IRYDGGNK	AKRDASGTGSGYYYMDV	SSNIGNHY	NNR	GTWDSSLSAGI	1.04
D06	GDSISSGYY	IYHDGNT	ARAASTVTTRWFDP	QSISSY	AAS	QQTYSTWWT	1.04
E08	GFTFSSYS	ISSSSSYI	ARDGAVAGYFTLDY	SSNIGSKA	TNN	AAWDDSLNGWV	1.04
C11	GGTFSSYA	IIPIFGTA	ARDGGGYSYGPHYYYYGMDV	QSVLYSSDNKNY	WAS	QQYYSIPYT	1.04
G11	GYTFTSYA	INAGNGNT	ARDGLGSSSWYGAFDI	SNNVGNQG	RNN	SAWDSSLSAVV	1.04
G02	GGTFSSYA	IIPIFGTA	ARDGYSWDY	SSDVGGYNY	DVS	AAWDDSLNGLYV	1.04
E10	GFTFSSYA	ISYDGSNK	ARDHISASSGWYRYDAFDI	QSVGSF	DAS	QQRSNWPPYT	1.04
E02	GFTFSSYA	ISYDGSNK	ARDQVAVAGNYYYYYGMDV	QSVSSN	GAS	QQYGSSQFT	1.04
E05	GFTFSTYS	ITSDSSTI	ARDRGDNYYFDY	SSNIGSNT	SNK	AAWDDSLNGVV	1.04
B04	GDSFSSYA	IIPMFGST	ARDRNMMAEFFYHGMDV	QGISSY	AAS	LQDYNYPLT	1.04
A10	GGTFSSYA	IIPIFGTA	ARDSLYYFDY	RSNIGAGYP	ANT	QSYDSSLSAVV	1.04
C06	GFTFSSYS	ISSSSSYI	ARDTAMALDY	NAKIGNTY	RNN	AAWDDGLRGWV	1.04
B10	GYSFTSYG	ISAYNGNT	ARDTGWYGSDY	SSNIGSNT	SNN	AAWDDSLNGLYV	1.04
D09	GFTFSSYA	ISYDGSNK	ARDVSFSGDWTYPGVDY	QSISSW	KAS	QQYGSSPFT	1.04
G01	SSNSAAWN	YRSKWYN	AREEGSGWGPDFDY				1.04
A05	GGTFSSYA	IIPIFGTA	AREGDITGTNYNFDY	NIGSKS	DDS	QVWDSSSDHVV	1.04
D02	GYTFTSYY	INPSGGST	AREGEETGTAFGY	QSVLYRSNNRNY	WAS	QQYYSIPLT	1.04
H03	GYTFTSYG	ISAYNGNT	AREPGYSYGYSFDI	QSISSY	AAS	QQSYSTRT	1.04
F12	GFTFSSYA	ISYDGSNK	ARGGDMDI	SSNIGAGYD	GYS	QSYDSSLSGYV	1.04
C02	GGSFSGYY	INHSGST	ARGGIVVVPAASALSRRW	RSVLYSSDNSNF	WAS	QQYFDTPYT	1.04
D03	GYTFTNYG	ISPYNGNT	ARGGRGSGWAYDYFDP	QSISTW	KAS	QQYKSYPT	1.04
E12	GGTFSSYA	IIPIFGTA	ARGGSYYVFDY	NIGSKS	QDS	QAWDSSSVV	1.04
H12	GYTFTSYG	ISAYNGNT	ARGPEYYDFWSGYYGSGYGMDV				1.04
F05	GYTFTGYY	INPNSGGT	ARGPRLVQVGNWFDP	QSVSSSH	GAS	QQFGGSPRGA	1.04
B09	GGSISSYY	IHYSGST	ARGSSWNYYYGMDV	QSLLYSDGNTY	KAS	MQLAHWPPT	1.04
D12	GYTFTNYA	INAGNGNT	ARGTAVAGPVRVLQH	SSNIGAGYD	GNS	QSYDSSLSGYV	1.04
A09	GGTFSSYA	IIPIFGTA	ARGYSSSSPFDY	SSNIGSYT	SNI	AAWDDSLNGVV	1.04
F01	xHCL	C*RSLHPS	ARNFDSNGYGIDF				3.13
B08	GGSISSSSYY	IYYSGST	ARRAIFNKRFDP	QSISTY	GAS	QQSYSTQYT	2.08
D04	GFTFSSYW	INSDGSST	ARRGYGMDV	SLRSFY	GKN	HSQDTSANHLRVFAGGTKLTVL	1.04
G12	GGSISSSSYY	IYYSGST	ARRPLTSPDFDY	QSISSY	AAS	QKYNSAPFT	1.04
H11	GYTFTSYY	INPSGGST	ARRRSSGPYGMDV	SSNIGSNL	SNN	AVWDNSLNGRV	1.04
D11	GYTFTGYY	INPNSGGT	ARSGYYYDSSGYYSDYFDY	QSLLYSNGYNY	LGS	MQALQTPLT	1.04
D05	GGTFSSYA	IIPIFGTA	ARVGGSGRPFDY	GSRIGVAS	NDN	AAWDDSLNTYV	1.04
H06	GFTVSSNY	ISSSSSYI	ARVGSKWLRFNHYYGMDV	QSISSY	AAS	QQSYSTPRT	1.04
E11	GYTFKNYG	ISAYNGNI	ARVPPGYCSGGRCSFDH	QGISSA	DAS	QQFNSYLPT	1.04
G05	GYTLTELS	FDPEDGET	ASLYSSGWYPSGDAFDI	NIGSDS	YDT	QMWESDTDHRGV	1.04
C12	GFTFSSYA	ISYDGSNK	ASPVGSGYYYSSLAFDI	SSNIGAGYD	GNS	QSYDSSLSGYV	1.04
E06	GFTFSNYA	ISSDGSSK	ATEGFDI	QDISNY	DAS	QQYDNLPIT	1.04
G08	GFTVxNNY	IYxGGGT	ATHPSLGV	HVVHxSY	xLNS	QTWGTxIWV	1.04
B07	GFTFSSYE	ISSSGSTI	ATYGDSSPFDY	SSNIGARYD	GSK	QSYDRSLSGWV	1.04
D08	GFSLSSSGMC	IEGDDEK	SRIFSSGCPPQFDY	QGIRND	AAS	QQYYSTPLT	1.04
E03	GFTFSDAW	IKSKTDGGTA	TSPRGLLH	QSVSSN	GAS	QQYNNWPPMYT	1.04
B05	GFTFSSYG	ISYDGSNK	TTAPNYGDYGVGRQSYMDV	QSISSY	AAS	QQSYSTPWT	1.04
E07	GGTFSSYA	IVPIFGTA	VLDGYSPFDY	RSNIGSNY	DNN	ETWDSSLSAAV	1.04
A04	GFTFNKYA	VRSKGGST	VRGASLGSPPLDY	SSNIGSRT	TDT	AVWDDSLSGWI	1.04

Supplementary Figure 5.3. CDR sequences and diversity of the Jurkat[TEM1] library prior to phenotypic selection.

CDR amino acid sequences and frequencies of a subsets of clones selected randomly prior to phenotypic selection.

clone	HC			LC			%
	CDR1	CDR2	CDR3	CDR1	CDR2	CDR3	
A01	GYTFTSYY	INPSGGST		SSNIGANYD	GNN	QSYDTDLRASV	1.22
A06	GYTFTSYA	ISYDGSNK	ARDPDYSKSFDY	SSNIGSNY	RNN	AAWDDSLSGLYV	1.22
D12	GYTFTSYY	ISYDGSNK	ARDPSMIVGFDL	SSNIGANYD	GNN	QSYDTDLRASV	1.22
D09	GYTFTSYY	IYPGDSDT	ARYGEAVAGFDY	QSVSSSY	GAS	QQYGSSQWT	1.22
7A6	GYTFTSYY	INPSGGST	ASSGGATRASDAFDI	SSNIGANYD	GNN	QSYDTDLRASV	94.94

Supplementary Figure 5.4. CDR sequences and diversity of the Jurkat$^{TEM1(\Delta n)}$ library prior to phenotypic selection.

CDR amino acid sequences and frequencies of a subsets of clones selected randomly prior to phenotypic selection.

clone	HC			LC			%
	CDR1	CDR2	CDR3	CDR1	CDR2	CDR3	
M3F06	GFTFDDYA	ISWNSGSI	AKDLAPYYYYMDV	QSISSR	RAS	QQFNTYPLT	5.95
A01	GYTFTNYY	INPSGGST	ARDLLGATSPDY	TSNVGTNF	DNT	GTWDRSLGIFV	3.57
H05	GYTFTSYD	MNPNSGNT	ARDRGVIPDFDY	TSNVGTNF	DNT	GTWDRSLGIFV	2.38
M3B06	GYTFTSYG	ISAYNGNT	ARDSGRRWLQSYFDY	QSISSY	AAS	QQSYSTPWT	11.90
M3E04	GGSISSGDYY	IYYSGST	ARESVVAGAFDI	QSISSY	AAS	QQSYSTPYT	26.19
M3G03	SVSSNSAAWN	YRSKWYD	AREVRGAFDI	QDISNY	DAS	QQYGSSPLT	9.52
M3E03	GYTFTSYG	ISAYNGNT	ARGMATATHYYYYGMDV	QSVNKY	AAS	QQSYSKPLT	4.76
B05	GYTFTSYG	ISAYNGNT	ARGSASGPLI	SSNIGAGYD	GNS	QSYDSSLSGWV	1.19
G06	GYTFTDFY	IHPNSGDT	ARRGPTRGLDY	QSISSY	AAS	QQSYSTPRT	1.19
C06	GYTFTSYA	INAGNGNT	ARSHTTNWNYVWFDT	QSISSY	AAS	QQSYSTPWT	1.19
M3B03	GYTFSSHA	INVFNGNT	ARVSLRRGGDYFYDY	QSISSY	AAS	QQSYSTPLT	4.76

Supplementary Figure 5.5. CDR sequences and diversity of the Jurkat^{meso} library after phenotypic selection.

CDR amino acid sequences and frequencies of a subsets of clones selected randomly after three rounds of cell sorting (CS03).

clone	HC			LC			%
	CDR1	CDR2	CDR3	CDR1	CDR2	CDR3	
D08	GFTFSSYA	ISGSGGST	AKDFWLTGALEY	QSVSSY	DAS	QQYYTTPFT	1.19
H10	VSSNSAAWN	YRSKWYN	AREEGSGWGPDFDY	QGISSY	WAS	QQYYSSPRT	1.19
H07	GYTFTGYY	INPNSGGT	AREGWGSYAFDI	SSNIGAGYD	GNS	QSYDSSLTRLTV	1.19
A07	GGSISSYY	ISYSGTI	ARRTPRGNFFDF	QDISGY	TTS	QQGFSLPIT	1.19
T3F09	GYTFTGYY	INPNSGGT	ARSGYYYDSSGYYSDYFDY	SSNIGSNT	NND	AAWDDSLSGPNYV	11.90
T3G09	GYTFTGYY	INPNSGGT	ARSGYYYDSSGYYSDYFDY	SSNIGSNT	SNN	AAWDDSLSGPNYV	2.38
3B6	GYTFTGYY	INPNSGGT	ARVRGSHPWFDP	SSNIGINT	STY	ATWDDSLNGVV	2.38
C08	GYSFTTYW	IYPYDSDT	ARYPGYCSGGSCYSWYFDV	QSVSSTY	GAS	QQYGSSPQT	1.19
T3A09	GGTFSSYA	IIPIFGTA	ASPGYSYGYLS	RSNIGSNT	SNN	AAWDDSLNGYV	64.29
B04	GGTFSSYA	IIPIFGTA	ASSSSGYYYYGMDV	SSNIGSDY	NND	AAWDDSLSGPNYV	1.19
A11	WRG*PCHGIS	VYDNGKT	TLATPDQHQLLSEVFAS	x	x	x	8.33
C10	GFTFSNAW	IKSKTDGGTT	TTSAVVVPAENDY	QGISSY	AAS	QQFSSYPLT	1.19
T3C11	GYTFTSYG	ISGYNGNT	VRDRSYYDFWSGYGSAFDI	SSNIGSNT	SNN	AAWDDSLSGPNYV	3.57

Supplementary Figure 5.6. CDR sequences and diversity of the Jurkat^{TEM1} library after phenotypic selection.

CDR amino acid sequences and frequencies of a subsets of clones selected randomly after three rounds of cell sorting (CS03).

clone	HC			LC			%
	CDR1	CDR2	CDR3	CDR1	CDR2	CDR3	
7G22	GFTFSSYA	ISGSGGST	AKAPGFDY	SSNIGSNT	SNN	AAWDDSLNGPV	89.58
7A6	GYTFTSYY	INPSGGST	ASSGGATRASDAFDI	SSNIGSNT	GNN	QSYDTDLRASV	2.08

Supplementary Figure 5.7. CDR sequences and diversity of the Jurkat^TEM1(Δn) library after phenotypic selection.

CDR amino acid sequences and frequencies of a subsets of clones selected randomly after three rounds of cell sorting (CS03).

Chapter 6   Conclusions & Discussion

Cancer immunotherapy was deemed "breakthrough of the year" in 2013 and continues to emerge as one of the most promising approaches to fight cancer. Generally, many immunotherapeutic approaches aim at harnessing the cytotoxic potential of T cells to target malignant cells. To this end, T cells can be equipped with a synthetic CAR or they can be redirected towards tumor cells via a soluble T cell engager molecule. Some of the key challenges of both approaches are the identification of suitable tumor-specific antigens, the rapid and reliable development of specific and tunable targeting moieties, balancing exceptional potency and safety and, importantly, increasing tissue penetration and infiltration into solid tumors.

Specifically, this thesis aimed to contribute to the development of novel potent and specific antibody-derived targeting moieties for cancer immunotherapy and beyond, with the following conclusions arising from the presented work:

<u>Conclusion 1:</u> The integration of SpyCatcher/SpyTag covalent fusion tag technology into phage display workflows led to the discovery of a novel panel of fully human scFv binders targeting TEM1, among which the affinity-matured clone 1C1m represents a promising candidate for (pre)-clinical development.

A prerequisite for the development of antibody-based cancer therapies is the availability of antibodies that meet the desired biochemical and biophysical properties, such as specificity, affinity, stability, solubility and low immunogenicity. Robust methods for the *de novo* discovery of antibodies are therefore indispensable. One of the process bottlenecks of display technologies for the rapid discovery of antibodies is the production and purification of sufficient quantities of native, correctly folded antigen that accurately recapitulates the endogenous (cell surface or tumor milieu) target.

To address this challenge, chapter 2 presents the practical utility of the covalent SpyC/SpyT interaction as a tagging/immobilization tool for *de novo* antibody hit discovery, selection, screening and characterization[331,361]. By expressing a number of mammalian cell-surface antigens as SpyC fusions, we demonstrated that therapeutically relevant antigens can be captured and immobilized *directly* onto streptavidin surfaces pre-coated with SpyT, circumventing the requirement for traditional antigen purification/processing. We showed that antigens immobilized in this way were fully compatible with antibody discovery by phage display as well as downstream applications such as hit screening and affinity maturation, and could survive the associated prolonged incubations and extensive washing steps[361]. Representing a minimal, cost-effective solution to mammalian cell-surface antigen production and bypassing the need for laborious purification and biotinylation steps, the dCI methodology using SpyC/SpyT could in principle be integrated into any other binder discovery platform involving solid-phase antigen capture, i.e. ribosome display or phage display selections using non-immunoglobulin or synthetic libraries.

Using the SpyC/SpyT dCI methodology, we isolated a number of functional antibody candidates recognizing different therapeutic targets, notably mesothelin and TEM1, with the latter being the focus of this work. Our diverse panel of fully human TEM1 binders specifically recognize recombinant TEM1 protein as well as endogenous TEM1 expressing cell lines, but not TEM1-negative cells. While all of our scFv clones display good thermostability in an scFv-Fc format and PBS buffer context, their target affinities vary from mid-nanomolar to low single-digit nanomolar in the case of an affinity-matured variant, 1C1m. Also, scFv binders were isolated in two separate and distinct campaigns using both a relatively membrane-distal fragment of TEM1 containing the five extracellular domains (ECD), and an N-terminally truncated fragment (TEM1Δ(n)) comprising only the membrane-proximal sialomucin stalk. Thus, our anti-TEM1 strategy was intentionally conceived to drive the isolation of scFv clones distinct from the published sc78 benchmark molecule, which binds an epitope thought to reside within the junctional region separating these two fragments[306]. Additionally, several of our clones, including the affinity-matured variant 1C1m, display cross-reactivity towards murine TEM1, opening the possibility of readily translatable pre-clinical testing in endogenous murine models. Together with the greatly reduced immunogenicity risk of using fully human targeting scFvs[364], these properties make our novel TEM1 antibody panel attractive starting candidates for the development of antibody-based therapeutics.

The reduced risk of immunogenicity using fully human scFv sequences confers an important advantage over antibodies isolated by traditional immunization approaches, such as MORAb004 (ontuxizumab). Despite humanization efforts, some residual murine sequence motifs may remain that can raise immune responses against the therapeutic antibody[364]. Also, the fact that our new clones arise from a naïve IgD/IgM, essentially germline, library with minimal donor-specified somatic mutations further reduces the risk of immunogenicity in the clinical setting.

In addition, the quality and source of antigen used for binder selection is of paramount importance for the specificity of the selected antibody panel. For instance, antigens produced in mammalian expression systems retain native folding and post-translational modifications typical for eukaryotic proteins[414]. In contrast, antigens produced in prokaryotic cells typically lack post-translational modifications, such as glycosylation. For heavily glycosylated proteins such as TEM1, the lack of these added glycans may strongly impact on protein folding and epitope accessibility. Therefore, antibodies that have been isolated using antigens derived from prokaryotic expression systems, such as sc78, which was isolated against a GST-fused TEM1-ECD fragment (residues 25-395) produced in *E.coli*[306], have to be assessed carefully for specific binding of the native target antigen expressed on the cell surface. Indeed in our hands sc78 occasionally showed signs of non-specific binding, in contrast to our panel of scFv clones which were isolated against TEM1 fragments that were expressed in human HEK293-6E cells and immobilized directly with minimal intermediary handling[361]. The rapid, small-scale capture of TEM1 protein from fresh expression supernatants may well have contributed to retaining the native protein conformation of this antigen, which had previously appeared unstable in traditionally produced and purified formats.

The development of a panel of TEM1-specific antibodies, among which 1C1m emerged as our lead candidate, opens the door to the evaluation of multiple diagnostic and therapeutic applications. Based on its highly preferential expression within the stroma and neo-vasculature of tissues undergoing active angiogenesis, TEM1 has been proposed as a biomarker for the detection, monitoring and therapeutic targeting of human cancer[304,307,308,365]. Classical strategies to exploit such biomarkers include the development of optical tracers for tumor imaging as well as the antibody-mediated delivery of radio-, chemical- or biological toxins to the

tumor site. In this context, the previously described clone sc78 has been investigated as an optical tracer for tumor imaging, including positron emission tomography (PET) and near-infrared (NIR) optical imaging of cancerous lesions[365,308]. In addition to neo-angiogenesis, TEM1 is commonly expressed by cancer cells of mesenchymal origin, notably sarcoma cells[276,309]. Thus, a number of studies focused on the development of ADC therapeutics directed against TEM1[304,305,309]. Among them, sc78 has been proposed as a targeting entity for ADC therapeutics[309,335]. Even more so than for optical imaging, efficient antigen binding and high specificity are critical for the development of clinically employable and safe ADCs. Therefore, high affinity binding is usually a prerequisite for a successful antibody candidate. In this regard, our affinity-matured clone 1C1m could represent a promising candidate, as it binds both human and murine TEM1 with a monovalent affinity constant of 1 nM and 6 nM, respectively. This clone thus compares favorably with the previously published clone sc78, the affinity of which was reported as 5.6 nM against human TEM1[306]. Moreover, the data presented in chapter 3 and 4 highlights the exquisite apparent specificity and encouraging biophysical properties of our lead candidate 1C1m. Building on these promising results, the potential of 1C1m is currently being explored by collaborators as a tumor targeting entity for both radio-imaging, (Prior, J., CHUV Lausanne; Rocha Paulo, A., Instituto Superior Técnico Lisbon), and for real-time image guided surgery using 1C1m IR-dye conjugates (Van Driel, LUMC; Goun, E., EPFL). Additional interest has led to a study using an antibody-drug conjugated form of 1C1m in the context of melanoma and TEM1-expressing cancer associated fibroblasts (Homicsko C., EPFL).

Finally, given the high incidence of TEM1 expression within the tumor vasculature[266,267,272,280], and the apparent restriction to the tumor tissue in adults[271,280], TEM1 could represent an attractive target for engineered cancer immunotherapy. In light of the outstanding potency of T cell-based therapies, the specificity of the targeting antibody is of paramount importance. Moreover, in contrast to more traditional antibody applications, affinity is not always the key determinant for effective CARs or bispecific T cell engagers[193,194]. Other parameters, such as epitope location and binding geometry can equally impact on the efficiency of T cell retargeting[199,200,248]. Thus, our panel of fully human anti-TEM1 scFv clones enabled us to explore the anti-tumor potential of redirecting T cells towards TEM1-expressing target cells.

Conclusion 2: TriloBiTEs derived from novel anti-TEM1 scFvs potently and specifically redirect the cytotoxic effector functions of primary human T cells towards TEM1-expressing target cells.

Both CARs and soluble T cell engagers directed against CD19 have generated impressive results in the treatment of B cell malignancies[169,171,214,215,368,369]. Many attempts have since been undertaken to apply these strategies for the therapy of solid tumors. However, the availability of suitable tumor-restricted antigens has proven a limiting factor for the broad application of both CARs and soluble engager molecules. In light of its expression profile and prevalence among human cancer samples, my thesis work aimed to investigate whether our newly developed anti-TEM1 antibodies would effectively redirect T cells when embedded in a bispecific format.

Despite the tremendous clinical impact of the minimalistic BiTE format (tandem scFv1-scFv2), it may not be generally applicable or effective against many target antigens. For example, very low abundance targets (10-

100 of copies per cell) require supra-physiological low picomolar monovalent affinity (e.g. ImmTacs)[389] against the target to achieve threshold levels of functional T cell activation. The need for such exceptional binding in the case of low-density antigens can be circumvented to some degree by exploiting avidity-driven stabilization/rebinding through the use of bi- or oligovalent targeting formats[242,245]. In our study, we initially attempted to explore T cell engagement with our anti-TEM1 scFvs using the classical monovalent BiTE paradigm. However, despite making several variant molecules on this theme, we observed only negligible T cell activation potency in cell assays. We thus asked whether a structurally distinct, heterodimeric engager format comprising a bivalent anti-TEM1 'warhead' could overcome these deficits. To this end, we designed the modular **TriloBiTE** format, drawing inspiration from the murine 'tribody' scaffold first reported by Schoonjans and colleagues[382]. However, unlike 'tribodies' our TriloBiTEs are constructed on a dimerizing CH1/Cκ human Fab core that we have further stabilized through the incorporation of interface mutations.

Strikingly, TriloBiTEs equipped with bivalent dual-arm anti-TEM1 targeting moieties effectively redirected primary human T cells to lyse TEM1$^+$ target cells *in vitro*, as described in chapter 4. Notably, the two higher-affinity clones sc78 and 1C1m consistently mediated stronger T cell responses in our initial comparative experiments and lower affinity clones consistently performed sub-optimally. Thus, affinity plays a crucial role for efficient TEM1 engagement, and it is possible that additional maturation of 1C1m could result in further improvement of T cell engagement and activation. Although the sc78-tB induced the secretion of higher levels of IFN-γ and IL-2, we occasionally observed non-specific sc78-tB mediated T cell activation in the presence of TEM1-negative cells (Fig. 4.3a), suggesting either some structural instability (aggregation/oligomerization) or some off-target specificity. In addition, 1C1m also showed potential as a targeting moiety for human CAR-T cells, while sc78, surprisingly, did not seem to be active in this format (Fig. 4.6), possibly reflecting misfolding of the scFv or geometric/flexibility constraints in engaging the human TEM1 epitope when in the membrane anchored context.

Although 1C1m clearly stimulates cytotoxic effector functions both as a TriloBiTE and as a CAR, cytokine production, especially IL-2 secretion, is triggered less efficiently, especially compared to TriloBiTEs directed against other targets such as mesothelin (compare Fig. 4.1h and Fig. 4.3f). However, this weak apparent cytokine response may well be sufficient to sustain initial proliferation and cytotoxic T cell effector functions[415-417]. Lower levels of cytokines may rather affect long-term expansion and memory formation[392,418,419], which may pose a problem for CARs, the efficacy of which depends on initial expansion and persistence. In contrast, a soluble T cell engager, which is administered repeatedly, will constantly (re-) trigger a polyclonal T cell response without the need for long-term persistence of individual T cell clones. In this case, the exact role and requirement of individual cytokines is less clear. Interestingly, a recent study reports that elevated cytokine responses elicited by T cell engaging bispecifics, particularly mediated by T cell derived TNF-α, are dispensable for cytotoxic activity[415]. In fact, the authors propose to block TNF-α signaling prior to biAb administration in order to prevent CRS[415]. Thus, a more subtle and more transient cytokine response, such as observed with 1C1m-tB, might prove advantageous, especially in light of the severe side effects (CRS) caused by excess cytokine production (CRS) in response to T cell therapy[215,367].

Besides 1C1m, another clone, 7G22, isolated for binding to the membrane-proximal sialomucin stalk region of TEM1, potently redirected primary human T cells towards TEM1$^+$ target cells, both as a TriloBiTE (Fig. 4.4c-e) and as a CAR (Fig. 4.6). Cell binding experiments, as well as the fact that it was isolated from a naïve human antibody library suggest that the monovalent binding affinity of 7G22 is relatively low. Although this will need to be confirmed experimentally, the *in vitro* activity of 7G22 highlights the importance of epitope location

for efficient TEM1 targeting. Several studies have established that the potency of both T cell engagers and CAR-T cells strongly depends on the location of the target epitope, with membrane-proximal epitopes usually mediating stronger T cell activation[200,202,247,248]. Underlying these observations is the architecture of the immune synapse, where the membranes of T cell and target cell/APC are brought into close proximity, excluding large phosphatases such as CD45[197]. The sialomucin stalk of TEM1 followed by five ECDs suggests a bulky structure protruding from the membrane, which could require membrane-proximal targeting in order to achieve the appropriate positioning of T cell and target cell. However, no crystal structure of the TEM1 ECD is available to date, and so any advantage of membrane-proximal epitopes will have to be determined empirically. In any case, the promising *in vitro* activity of 7G22 warrants further investigation *in vitro* and *in vivo*.

As a perspective, the TriloBiTE format offers the possibility to design a trivalent engager molecule, utilizing two distinct tumor-targeting scFvs as an alternative to bivalent tumor binding. These could be directed against different tumor targets, tuning the respective affinities according to the desired functionality. In this way, logic-gated T cell engagers could be designed which either redirect T cells to kill tumor cells based on binding to either antigen independently ('OR' logic), or preferentially induce killing of cells that express both targets ('AND' logic). In both cases, the efficacy of such a trispecific molecule would be driven by the engagement of targets in close proximity through avidity and/or rapid cell rebinding. Another trispecific option includes the integration of a co-stimulatory specificity, for instance by engaging both CD3 and CD28 on the T cell[251,420]. Similarly, two epitopes on the same TAA could be targeted with a biparatopic TriloBiTE, for instance using 1C1m and 7G22 combined in the same molecule. Such biparatopic targeting[421] has proven effective in the case of therapeutic antibodies and ADCs directed against Her2 and MET, both by increasing binding strength through avidity effects, and by cross-linking the antigen, leading to increased receptor-mediated internalization and degradation[422,423]. Moreover, a biparatopic T cell engager directed against Her2 has been reported, exhibiting strong antigen binding and superior cytotoxicity against breast cancer cells expressing low levels of Her2[424]. Thus, in order to further explore the concept of biparatopic T cell engagers, we are planning to investigate the anti-tumor potential of a TriloBiTE variant combining 1C1m and 7G22 tumor-targeting scFvs.

Importantly, we are also planning to expand our *in vivo* studies in order to determine the full potential of TEM1-targeting TriloBiTEs. In a preliminary murine xenograft study, the systemic administration of 1C1m-tB appeared to show significant T cell retargeting activity, preventing the outgrowth of A673 tumor cells co-inoculated with human T cells. This initial experiment presents a first *in vivo* indication that TEM1 can be targeted via an immunotherapeutic soluble engager molecule. Subsequent experiments will aim to robustly verify these findings, and to investigate whether 1C1m-tB can induce regression of pre-established tumors. In this context, it would also be desirable to characterize the *in vivo* activity of the membrane-proximal binder 7G22-tB. However, the described xenograft studies only model the targeting of tumor cells that directly express TEM1. Clinically, far more patients could benefit from therapies directed against TEM1 expressed by the tumor neo-vasculature. Thus, investigating the potential of anti-TEM1 TriloBiTEs to mediate tumor regression in syngeneic tumor models with endogenous TEM1 expression within the tumor stroma and vasculature would be key to fully explore the potential and risks of immunotherapeutic targeting of TEM1. Although the strong cross-reactivity of 1C1m towards murine TEM1 is directly compatible with translation to such syngeneic models, the anti-CD3 clones employed in the current TriloBiTE core binds only to human CD3. Hence, for syngeneic models, where endogenous T cells need to be recruited to the tumor site, a murine CD3

surrogate tB would need to be constructed and thoroughly validated *in vitro*. One further attraction of a surrogate molecule would be to better evaluate the safety implications of co-incidental targeting of endogenous levels of TEM1 present in non-tumor cell compartments.

As mentioned above, the molecular expression pattern of TEM1 suggests two different therapeutic applications. Firstly, since the majority of human sarcoma expresses TEM1[276,304,309], TEM1-targeted immunotherapies could be applied for the treatment of this rare but aggressive cancer type. Additionally, the expression of TEM1 within the neo-vasculature of many solid tumors offers the possibility of "universal" tumor-targeting independent of the tissue of origin. In this context, it remains to be investigated whether eliciting a targeted and durable T cell killing response against the supporting neo-vasculature can be achieved and, further, would translate into a significant therapeutic potential. Conceptually, disrupting the neo-vasculature/stromal compartment could lead to (limited) tumor cell death and to a subsequent spreading of tumor-associated antigens, as was observed with a cancer vaccine directed against TEM1[310]. This in turn could improve any existing anti-tumor immunity, possibly assisted by combinatorial immune-enhancing treatments, such as PD1-blockade[425]. These concepts would however require careful validation, since tumor vascular targeting, for instance via VEGFR blockade, have been found to favor therapy resistance and the outgrowth of more aggressive cancer cells[254].

Collectively, this work presents a proof-of-principle for the immunotherapeutic targeting of TEM1, both using soluble T cell engagers and human CARs. Our promising *in vitro* results with 1C1m and 7G22 in both formats thus lay the foundation for subsequent studies aiming to assess the potential of TEM1 targeting within the tumor vasculature. In addition, we present the TriloBiTE platform as a tractable and potent modular T cell engager format, allowing the fine-tuning of affinity and avidity for optimal T cell engagement.

Conclusion 3: Phenotypic reporter-based cell screening offers the potential to accelerate the *de novo* discovery of functional engager immunotherapeutics.

Both potency and safety of engineered T cell therapies largely depend on the availability of a suitable targeting antibody. As discussed above, a number of parameters can impact on the efficacy of T cell engagement, such as affinity, relative epitope location, linker/spacer length and targeting geometry[193,199-202]. Currently, warheads for both soluble engager molecules and CARs have to be validated empirically, especially for novel and poorly characterized targets, leading to labor-intensive iterative screening campaigns. In addition, clones that show promising functional and biophysical properties as soluble antibodies do not always function adequately in the context of a membrane-embedded CAR, as we have observed with sc78 (Fig. 4.6). To overcome this bottleneck, we aimed to develop a phenotypic screening platform for the *de novo* discovery of functional targeting moieties for CARs.

As described in chapter 5, we employed Jurkat reporter cells to display pre-selected scFv libraries and subsequently enriched cells harboring a functional CAR construct. As a proof-of-principle, we identified novel CARs against mesothelin and TEM1, among them the TEM1 mucin stalk binder 7G22, which proved to be functional both as a CAR and as a TriloBiTE. In principle, as an integrated phenotypic screening pipeline, the CAR Factory approach could allow the isolation of functional CAR targeting moieties directed against any given cell surface antigen.

Recombinant antigens, however well produced and quality controlled, may differ from native antigens expressed in the context of the cell surface. Glycosylation and other PTMs as well as neighboring or interacting molecules may impact on protein folding or mask certain epitopes. Therefore, binder selection against recombinant versus native antigens can yield very different outcomes, as observed in our study for TEM1(Δn). The fact that 7G22 did not flag as a strong binder of recombinant TEM1(Δn) protein, but later appeared to be functional both as a CAR (Fig. 4.6e, f) and as a TriloBiTE (Fig. 4.4c-e), highlights the shortcomings of traditional binder selection for "difficult" cell-surface antigens. Despite labor-intensive screening and reformatting efforts, the functional clone 7G22 would have been missed. In summary, this example demonstrates how phenotypic screening of clone repertoires pre-formatted as CARs, can, as compared to typical phage display screening, lead to apparently superior outcomes (in terms of desirable hit clone characteristics) against heterogeneous and complex targets such as TEM1(Δn).

In addition, the observation that 7G22 is functional both as a CAR and as a TriloBiTE raises the interesting possibility that our phenotypic CAR screen may enrich concomitantly for scFvs with characteristics that are also required by soluble engagers. Hence, this approach may have considerable general utility for immunotherapeutic discovery.

Preliminary activation experiments in Jurkat NFAT-mCherry reporter cells suggested specific CAR signaling with the novel CAR scFvs identified against TEM1(ECD) and mesothelin in the presence of relevant target cells (Fig. 5.4). Although clearly activating, some of these CARs, including 7G22, induce mCherry expression only in a proportion of CAR-expressing Jurkat cells. This could indicate suboptimal T cell engagement or activation, which will have to be assessed in primary T cells. Beyond the targeting moiety, the length and structure of the CAR linker/spacer domain has a major impact on T cell engagement and synapse formation[199,202]. Furthermore, the choice of intracellular co-stimulatory domain can strongly influence T cell activation, proliferation and persistence[378]. Thus, by leveraging the modular cloning nature of our CAR Factory vector scaffold, libraries of CAR components other than scFvs could be integrated into the phenotypic selection workflow. We envisage that cell-based screening of such combinatorial CAR libraries could then permit the direct selection of CAR clones comprising optimal or 'tuned' assemblages of scFv, linker, and TM domain. These latter library elements — which will be modest in number and well-defined — could be screened either by direct permutation against the initial scFv input library, or sequentially, after having identified suitable targeting scFvs (hierarchically). As a starting point, we have designed a panel of 12 different extracellular linkers/spacers derived from the membrane-proximal regions of natural human transmembrane proteins and comprising various lengths, molecular weights, cysteine- and glycan content as well as domain structures. Preliminary investigations suggest an impact of the length and nature of the CAR linker on the activation potential of the 1C1-CAR, paving the road for further studies using the same CAR linker/spacer panel.

Following initial discovery, early *in vitro* and *in vivo* efficacy and safety studies of CARs and T cell engagers provide only limited insights into the potential for successful clinical translation. A number of complex and cooperating factors are known to strongly impact on the efficacy of T cell therapies in the clinic. Key among these are the often hostile, immunosuppressive TME, possible unwanted side effects, and, in the case of CARs, the proliferation and persistence of the infused T cells[160]. Moreover, it will have to be confirmed that any T cell activation observed *in vitro* leads to a lasting anti-tumor response *in vivo*. Thus, the true potential of any novel CAR or T cell engager will only be revealed in early clinical studies.

Over the last decade, immunotherapy has revolutionized cancer therapy, yielding a plethora of potential new treatment concepts. Besides checkpoint blockade and personalized therapies aiming to mount an immune response against individual neo-antigens, antibody-based retargeting of T cells has emerged as a powerful strategy to combat cancer. The work presented in this thesis contributes to the field in three ways. First, the described and published novel methods for the direct capture and immobilization of antigens, when combined with a phenotypic screening platform for CARs, greatly accelerates the *de novo* discovery of functional targeting moieties. With both workflows in place, we are now in the position to rapidly generate tailored antibody warheads with the required biophysical and functional properties. Secondly, several of my anti-TEM1 scFv candidates are the subject of a patent application, with one molecule currently undergoing investigation by 3rd party collaborators for radio/IR-conjugate clinical imaging applications. Finally, this work presents a proof-of-concept for redirecting T cells towards human TEM1 and lays the foundation for further investigations and the development of TEM1-targeted therapies.

References

1   Murphy, K. & Weaver, C. Janeway's Immunobiology, 9th Edition. *Janeway's Immunobiology, 9th Edition*, 1-904 (2017).

2   Hajishengallis, G., Reis, E. S., Mastellos, D. C., Ricklin, D. & Lambris, J. D. Novel mechanisms and functions of complement. *Nat Immunol* **18**, 1288-1298, doi:10.1038/ni.3858 (2017).

3   Krogsgaard, M. & Davis, M. M. How T cells 'see' antigen. *Nat Immunol* **6**, 239-245, doi:10.1038/ni1173 (2005).

4   Raff, M. C. T and B lymphocytes and immune responses. *Nature* **242**, 19-23, doi:10.1038/242019a0 (1973).

5   Suan, D., Sundling, C. & Brink, R. Plasma cell and memory B cell differentiation from the germinal center. *Curr Opin Immunol* **45**, 97-102, doi:10.1016/j.coi.2017.03.006 (2017).

6   Chang, J. T., Wherry, E. J. & Goldrath, A. W. Molecular regulation of effector and memory T cell differentiation. *Nat Immunol* **15**, 1104-1115, doi:10.1038/ni.3031 (2014).

7   Morris, G. P. & Allen, P. M. How the TCR balances sensitivity and specificity for the recognition of self and pathogens. *Nat Immunol* **13**, 121-128, doi:10.1038/ni.2190 (2012).

8   Neefjes, J., Jongsma, M. L., Paul, P. & Bakke, O. Towards a systems understanding of MHC class I and MHC class II antigen presentation. *Nat Rev Immunol* **11**, 823-836, doi:10.1038/nri3084 (2011).

9   Parham, P. & Ohta, T. Population biology of antigen presentation by MHC class I molecules. *Science* **272**, 67-74, doi:10.1126/science.272.5258.67 (1996).

10   Kurts, C., Robinson, B. W. & Knolle, P. A. Cross-priming in health and disease. *Nat Rev Immunol* **10**, 403-414, doi:10.1038/nri2780 (2010).

11   Vyas, J. M., Van der Veen, A. G. & Ploegh, H. L. The known unknowns of antigen processing and presentation. *Nat Rev Immunol* **8**, 607-618, doi:10.1038/nri2368 (2008).

12   Robinson, J. H. & Delvig, A. A. Diversity in MHC class II antigen presentation. *Immunology* **105**, 252-262, doi:10.1046/j.0019-2805.2001.01358.x (2002).

13   Trowsdale, J. HLA genomics in the third millennium. *Curr Opin Immunol* **17**, 498-504, doi:10.1016/j.coi.2005.07.015 (2005).

14   Zinkernagel, R. M. & Doherty, P. C. MHC-restricted cytotoxic T cells: studies on the biological role of polymorphic major transplantation antigens determining T-cell restriction-specificity, function, and responsiveness. *Adv Immunol* **27**, 51-177, doi:10.1016/s0065-2776(08)60262-x (1979).

15   Huppa, J. B. & Davis, M. M. T-cell-antigen recognition and the immunological synapse. *Nat Rev Immunol* **3**, 973-983, doi:10.1038/nri1245 (2003).

16   Norcross, M. A. A synaptic basis for T-lymphocyte activation. *Ann Immunol (Paris)* **135D**, 113-134, doi:10.1016/s0769-2625(84)81105-8 (1984).

17   Grakoui, A. *et al.* The immunological synapse: a molecular machine controlling T cell activation. *Science* **285**, 221-227, doi:10.1126/science.285.5425.221 (1999).

18   Monks, C. R., Freiberg, B. A., Kupfer, H., Sciaky, N. & Kupfer, A. Three-dimensional segregation of supramolecular activation clusters in T cells. *Nature* **395**, 82-86, doi:10.1038/25764 (1998).

19   Chen, L. & Flies, D. B. Molecular mechanisms of T cell co-stimulation and co-inhibition. *Nat Rev Immunol* **13**, 227-242, doi:10.1038/nri3405 (2013).

20   Bretscher, P. & Cohn, M. A theory of self-nonself discrimination. *Science* **169**, 1042-1049, doi:10.1126/science.169.3950.1042 (1970).

21   June, C. H., Ledbetter, J. A., Gillespie, M. M., Lindsten, T. & Thompson, C. B. T-cell proliferation involving the CD28 pathway is associated with cyclosporine-resistant interleukin 2 gene expression. *Mol Cell Biol* **7**, 4472-4481, doi:10.1128/mcb.7.12.4472 (1987).

22   Mueller, D. L., Jenkins, M. K. & Schwartz, R. H. Clonal expansion versus functional clonal inactivation: a costimulatory signalling pathway determines the outcome of T cell antigen receptor occupancy. *Annu Rev Immunol* **7**, 445-480, doi:10.1146/annurev.iy.07.040189.002305 (1989).

23   Vantourout, P. & Hayday, A. Six-of-the-best: unique contributions of gammadelta T cells to immunology. *Nat Rev Immunol* **13**, 88-100, doi:10.1038/nri3384 (2013).

24   Call, M. E., Pyrdol, J., Wiedmann, M. & Wucherpfennig, K. W. The organizing principle in the formation of the T cell receptor-CD3 complex. *Cell* **111**, 967-979, doi:10.1016/s0092-8674(02)01194-7 (2002).

25   Geisler, C., Kuhlmann, J. & Rubin, B. Assembly, intracellular processing, and expression at the cell surface of the human alpha beta T cell receptor/CD3 complex. Function of the CD3-zeta chain. *J Immunol* **143**, 4069-4077 (1989).

26   Blumberg, R. S. *et al.* Assembly and function of the T cell antigen receptor. Requirement of either the lysine or arginine residues in the transmembrane region of the alpha chain. *J Biol Chem* **265**, 14036-14043 (1990).

27   Kuhns, M. S. & Davis, M. M. TCR Signaling Emerges from the Sum of Many Parts. *Front Immunol* **3**, 159, doi:10.3389/fimmu.2012.00159 (2012).

28   Navarro, M. N. & Cantrell, D. A. Serine-threonine kinases in TCR signaling. *Nat Immunol* **15**, 808-814, doi:10.1038/ni.2941 (2014).

29   Chan, A. C., Iwashima, M., Turck, C. W. & Weiss, A. ZAP-70: a 70 kd protein-tyrosine kinase that associates with the TCR zeta chain. *Cell* **71**, 649-662, doi:10.1016/0092-8674(92)90598-7 (1992).

30   Zhang, W., Sloan-Lancaster, J., Kitchen, J., Trible, R. P. & Samelson, L. E. LAT: the ZAP-70 tyrosine kinase substrate that links T cell receptor to cellular activation. *Cell* **92**, 83-92, doi:10.1016/s0092-8674(00)80901-0 (1998).

31   Okkenhaug, K. & Vanhaesebroeck, B. PI3K in lymphocyte development, differentiation and activation. *Nat Rev Immunol* **3**, 317-330, doi:10.1038/nri1056 (2003).

32   Macian, F. NFAT proteins: key regulators of T-cell development and function. *Nat Rev Immunol* **5**, 472-484, doi:10.1038/nri1632 (2005).

33   Boyman, O. & Sprent, J. The role of interleukin-2 during homeostasis and activation of the immune system. *Nat Rev Immunol* **12**, 180-190, doi:10.1038/nri3156 (2012).

34   Taniguchi, T. & Minami, Y. The IL-2/IL-2 receptor system: a current overview. *Cell* **73**, 5-8, doi:10.1016/0092-8674(93)90152-g (1993).

35   Masson, D. & Tschopp, J. A family of serine esterases in lytic granules of cytolytic T lymphocytes. *Cell* **49**, 679-685, doi:10.1016/0092-8674(87)90544-7 (1987).

36   Masson, D., Nabholz, M., Estrade, C. & Tschopp, J. Granules of cytolytic T-lymphocytes contain two serine esterases. *EMBO J* **5**, 1595-1600 (1986).

37   Peters, P. J. *et al.* Cytotoxic T lymphocyte granules are secretory lysosomes, containing both perforin and granzymes. *J Exp Med* **173**, 1099-1109, doi:10.1084/jem.173.5.1099 (1991).

38   Tschopp, J., Schafer, S., Masson, D., Peitsch, M. C. & Heusser, C. Phosphorylcholine acts as a Ca2+-dependent receptor molecule for lymphocyte perforin. *Nature* **337**, 272-274, doi:10.1038/337272a0 (1989).

39   Voskoboinik, I., Whisstock, J. C. & Trapani, J. A. Perforin and granzymes: function, dysfunction and human pathology. *Nat Rev Immunol* **15**, 388-400, doi:10.1038/nri3839 (2015).

40   Nagata, S. Apoptosis by death factor. *Cell* **88**, 355-365, doi:10.1016/s0092-8674(00)81874-7 (1997).

41   Krammer, P. H. CD95's deadly mission in the immune system. *Nature* **407**, 789-795, doi:10.1038/35037728 (2000).

42   Kuwano, K., Kawashima, T. & Arai, S. Antiviral effect of TNF-alpha and IFN-gamma secreted from a CD8+ influenza virus-specific CTL clone. *Viral Immunol* **6**, 1-11, doi:10.1089/vim.1993.6.1 (1993).

43   Zhu, J. & Paul, W. E. Peripheral CD4+ T-cell differentiation regulated by networks of cytokines and transcription factors. *Immunol Rev* **238**, 247-262, doi:10.1111/j.1600-065X.2010.00951.x (2010).

44   Schroder, K., Hertzog, P. J., Ravasi, T. & Hume, D. A. Interferon-gamma: an overview of signals, mechanisms and functions. *J Leukoc Biol* **75**, 163-189, doi:10.1189/jlb.0603252 (2004).

45   Martorelli, D. *et al.* Role of CD4+ cytotoxic T lymphocytes in the control of viral diseases and cancer. *Int Rev Immunol* **29**, 371-402, doi:10.3109/08830185.2010.489658 (2010).

46   Hombach, J., Tsubata, T., Leclercq, L., Stappert, H. & Reth, M. Molecular components of the B-cell antigen receptor complex of the IgM class. *Nature* **343**, 760-762, doi:10.1038/343760a0 (1990).

47   Kurosaki, T. Molecular dissection of B cell antigen receptor signaling (review). *Int J Mol Med* **1**, 515-527, doi:10.3892/ijmm.1.3.515 (1998).

48   Batista, F. D., Iber, D. & Neuberger, M. S. B cells acquire antigen from target cells after synapse formation. *Nature* **411**, 489-494, doi:10.1038/35078099 (2001).

49   Oracki, S. A., Walker, J. A., Hibbs, M. L., Corcoran, L. M. & Tarlinton, D. M. Plasma cell development and survival. *Immunol Rev* **237**, 140-159, doi:10.1111/j.1600-065X.2010.00940.x (2010).

50   Edelman, G. M. Antibody structure and molecular immunology. *Science* **180**, 830-840, doi:10.1126/science.180.4088.830 (1973).

51   Porter, R. R. Structural studies of immunoglobulins. *Science* **180**, 713-716, doi:10.1126/science.180.4087.713 (1973).

52   Harris, L. J. *et al.* The three-dimensional structure of an intact monoclonal antibody for canine lymphoma. *Nature* **360**, 369-372, doi:10.1038/360369a0 (1992).

53   Edelman, G. M. Dissociation of Gamma-Globulin. *J Am Chem Soc* **81**, 3155-3156, doi:DOI 10.1021/ja01521a071 (1959).

54   Porter, R. R. The hydrolysis of rabbit y-globulin and antibodies with crystalline papain. *Biochem J* **73**, 119-126, doi:10.1042/bj0730119 (1959).

55   Schroeder, H. W., Jr. & Cavacini, L. Structure and function of immunoglobulins. *J Allergy Clin Immunol* **125**, S41-52, doi:10.1016/j.jaci.2009.09.046 (2010).

56   Huber, R., Deisenhofer, J., Colman, P. M., Matsushima, M. & Palm, W. Crystallographic structure studies of an IgG molecule and an Fc fragment. *Nature* **264**, 415-420, doi:10.1038/264415a0 (1976).

57   Rothlisberger, D., Honegger, A. & Pluckthun, A. Domain interactions in the Fab fragment: a comparative evaluation of the single-chain Fv and Fab format engineered with variable domains of different stability. *J Mol Biol* **347**, 773-789, doi:10.1016/j.jmb.2005.01.053 (2005).

58   Chitarra, V. *et al.* Three-dimensional structure of a heteroclitic antigen-antibody cross-reaction complex. *Proc Natl Acad Sci U S A* **90**, 7711-7715, doi:10.1073/pnas.90.16.7711 (1993).

59   Rajewsky, K. Clonal selection and learning in the antibody system. *Nature* **381**, 751-758, doi:10.1038/381751a0 (1996).

60   Schatz, D. G. & Ji, Y. Recombination centres and the orchestration of V(D)J recombination. *Nat Rev Immunol* **11**, 251-263, doi:10.1038/nri2941 (2011).

61   Lewis, S. M. The mechanism of V(D)J joining: lessons from molecular, immunological, and comparative analyses. *Adv Immunol* **56**, 27-150, doi:10.1016/s0065-2776(08)60450-2 (1994).

62   Swanson, P. C. The bounty of RAGs: recombination signal complexes and reaction outcomes. *Immunol Rev* **200**, 90-114, doi:10.1111/j.0105-2896.2004.00159.x (2004).

63   Ji, Y. *et al.* The in vivo pattern of binding of RAG1 and RAG2 to antigen receptor loci. *Cell* **141**, 419-431, doi:10.1016/j.cell.2010.03.010 (2010).

64   Komori, T., Okada, A., Stewart, V. & Alt, F. W. Lack of N regions in antigen receptor variable region genes of TdT-deficient lymphocytes. *Science* **261**, 1171-1175, doi:10.1126/science.8356451 (1993).

65   Griffiths, G. M., Berek, C., Kaartinen, M. & Milstein, C. Somatic mutation and the maturation of immune response to 2-phenyl oxazolone. *Nature* **312**, 271-275, doi:10.1038/312271a0 (1984).

66   Weigert, M. G., Cesari, I. M., Yonkovich, S. J. & Cohn, M. Variability in the lambda light chain sequences of mouse antibody. *Nature* **228**, 1045-1047, doi:10.1038/2281045a0 (1970).

67   Arakawa, H., Hauschild, J. & Buerstedde, J. M. Requirement of the activation-induced deaminase (AID) gene for immunoglobulin gene conversion. *Science* **295**, 1301-1306, doi:10.1126/science.1067308 (2002).

68   Harris, R. S., Sale, J. E., Petersen-Mahrt, S. K. & Neuberger, M. S. AID is essential for immunoglobulin V gene conversion in a cultured B cell line. *Curr Biol* **12**, 435-438, doi:10.1016/s0960-9822(02)00717-0 (2002).

69   Muramatsu, M. *et al.* Class switch recombination and hypermutation require activation-induced cytidine deaminase (AID), a potential RNA editing enzyme. *Cell* **102**, 553-563, doi:10.1016/s0092-8674(00)00078-7 (2000).

70   Bachl, J., Carlson, C., Gray-Schopfer, V., Dessing, M. & Olsson, C. Increased transcription levels induce higher mutation rates in a hypermutating cell line. *J Immunol* **166**, 5051-5057, doi:10.4049/jimmunol.166.8.5051 (2001).

71   Gearhart, P. J. & Wood, R. D. Emerging links between hypermutation of antibody genes and DNA polymerases. *Nat Rev Immunol* **1**, 187-192, doi:10.1038/35105009 (2001).

72   Honjo, T., Kinoshita, K. & Muramatsu, M. Molecular mechanism of class switch recombination: linkage with somatic hypermutation. *Annu Rev Immunol* **20**, 165-196, doi:10.1146/annurev.immunol.20.090501.112049 (2002).

73   Okazaki, I. M., Kinoshita, K., Muramatsu, M., Yoshikawa, K. & Honjo, T. The AID enzyme induces class switch recombination in fibroblasts. *Nature* **416**, 340-345, doi:10.1038/nature727 (2002).

74   Avery, D. T., Bryant, V. L., Ma, C. S., de Waal Malefyt, R. & Tangye, S. G. IL-21-induced isotype switching to IgG and IgA by human naive B cells is differentially regulated by IL-4. *J Immunol* **181**, 1767-1779, doi:10.4049/jimmunol.181.3.1767 (2008).

75   Stavnezer, J. Immunoglobulin class switching. *Curr Opin Immunol* **8**, 199-205, doi:10.1016/s0952-7915(96)80058-6 (1996).

76   Bashford-Rogers, R. J. *et al.* Network properties derived from deep sequencing of human B-cell receptor repertoires delineate B-cell populations. *Genome Res* **23**, 1874-1884, doi:10.1101/gr.154815.113 (2013).

77   Georgiou, G. *et al.* The promise and challenge of high-throughput sequencing of the antibody repertoire. *Nat Biotechnol* **32**, 158-168, doi:10.1038/nbt.2782 (2014).

78   Briney, B., Inderbitzin, A., Joyce, C. & Burton, D. R. Commonality despite exceptional diversity in the baseline human antibody repertoire. *Nature* **566**, 393-397, doi:10.1038/s41586-019-0879-y (2019).

79   Huse, W. D. *et al.* Generation of a large combinatorial library of the immunoglobulin repertoire in phage lambda. *Science* **246**, 1275-1281, doi:10.1126/science.2531466 (1989).

80   Lerner, R. A., Kang, A. S., Bain, J. D., Burton, D. R. & Barbas, C. F., 3rd. Antibodies without immunization. *Science* **258**, 1313-1314, doi:10.1126/science.1455226 (1992).

81   Marks, J. D. *et al.* By-passing immunization. Human antibodies from V-gene libraries displayed on phage. *J Mol Biol* **222**, 581-597, doi:10.1016/0022-2836(91)90498-u (1991).

82   Vaughan, T. J. *et al.* Human antibodies with sub-nanomolar affinities isolated from a large non-immunized phage display library. *Nat Biotechnol* **14**, 309-314, doi:10.1038/nbt0396-309 (1996).

83   Persson, M. A. Twenty years of combinatorial antibody libraries, but how well do they mimic the immunoglobulin repertoire? *Proc Natl Acad Sci U S A* **106**, 20137-20138, doi:10.1073/pnas.0912118106 (2009).

84   Orlandi, R., Gussow, D. H., Jones, P. T. & Winter, G. Cloning immunoglobulin variable domains for expression by the polymerase chain reaction. *Proc Natl Acad Sci U S A* **86**, 3833-3837, doi:10.1073/pnas.86.10.3833 (1989).

85   Wardemann, H. *et al.* Predominant autoantibody production by early human B cell precursors. *Science* **301**, 1374-1377, doi:10.1126/science.1086907 (2003).

86   Lerner, R. A. Combinatorial antibody libraries: new advances, new immunological insights. *Nat Rev Immunol* **16**, 498-508, doi:10.1038/nri.2016.67 (2016).

87   McCafferty, J., Griffiths, A. D., Winter, G. & Chiswell, D. J. Phage antibodies: filamentous phage displaying antibody variable domains. *Nature* **348**, 552-554, doi:10.1038/348552a0 (1990).

88   Smith, G. P. Filamentous fusion phage: novel expression vectors that display cloned antigens on the virion surface. *Science* **228**, 1315-1317, doi:10.1126/science.4001944 (1985).

89   Barbas, C. F., 3rd, Kang, A. S., Lerner, R. A. & Benkovic, S. J. Assembly of combinatorial antibody libraries on phage surfaces: the gene III site. *Proc Natl Acad Sci U S A* **88**, 7978-7982, doi:10.1073/pnas.88.18.7978 (1991).

90   Kang, A. S., Barbas, C. F., Janda, K. D., Benkovic, S. J. & Lerner, R. A. Linkage of recognition and replication functions by assembling combinatorial antibody Fab libraries along phage surfaces. *Proc Natl Acad Sci U S A* **88**, 4363-4366, doi:10.1073/pnas.88.10.4363 (1991).

91   Endemann, H. & Model, P. Location of filamentous phage minor coat proteins in phage and in infected cells. *J Mol Biol* **250**, 496-506, doi:10.1006/jmbi.1995.0393 (1995).

92   Welsh, L. C., Symmons, M. F., Sturtevant, J. M., Marvin, D. A. & Perham, R. N. Structure of the capsid of Pf3 filamentous phage determined from X-ray fibre diffraction data at 3.1 A resolution. *J Mol Biol* **283**, 155-177, doi:10.1006/jmbi.1998.2081 (1998).

93   Chang, C. N., Model, P. & Blobel, G. Membrane biogenesis: cotranslational integration of the bacteriophage f1 coat protein into an Escherichia coli membrane fraction. *Proc Natl Acad Sci U S A* **76**, 1251-1255, doi:10.1073/pnas.76.3.1251 (1979).

94   Crissman, J. W. & Smith, G. P. Gene-III protein of filamentous phages: evidence for a carboxyl-terminal domain with a role in morphogenesis. *Virology* **132**, 445-455, doi:10.1016/0042-6822(84)90049-7 (1984).

95   Nilsson, N., Malmborg, A. C. & Borrebaeck, C. A. The phage infection process: a functional role for the distal linker region of bacteriophage protein 3. *J Virol* **74**, 4229-4235, doi:10.1128/jvi.74.9.4229-4235.2000 (2000).

96   Boder, E. T. & Wittrup, K. D. Yeast surface display for directed evolution of protein expression, affinity, and stability. *Methods Enzymol* **328**, 430-444, doi:10.1016/s0076-6879(00)28410-3 (2000).

97   Schaffitzel, C., Hanes, J., Jermutus, L. & Pluckthun, A. Ribosome display: an in vitro method for selection and evolution of antibodies from libraries. *J Immunol Methods* **231**, 119-135, doi:10.1016/s0022-1759(99)00149-0 (1999).

98   Zhou, C., Jacobsen, F. W., Cai, L., Chen, Q. & Shen, W. D. Development of a novel mammalian cell surface antibody display platform. *MAbs* **2**, 508-518, doi:10.4161/mabs.2.5.12970 (2010).

99   Philippides, A. The top 25 best-selling drugs of 2014. (2015).

100   Elia, G., Fugmann, T. & Neri, D. From target discovery to clinical trials with armed antibody products. *J Proteomics* **107**, 50-55, doi:10.1016/j.jprot.2014.02.034 (2014).

101   Ferlay, J. *et al.* Cancer incidence and mortality patterns in Europe: Estimates for 40 countries and 25 major cancers in 2018. *Eur J Cancer* **103**, 356-387, doi:10.1016/j.ejca.2018.07.005 (2018).

102   Hanahan, D. & Weinberg, R. A. The hallmarks of cancer. *Cell* **100**, 57-70, doi:10.1016/s0092-8674(00)81683-9 (2000).

103   Hanahan, D. & Weinberg, R. A. Hallmarks of cancer: the next generation. *Cell* **144**, 646-674, doi:10.1016/j.cell.2011.02.013 (2011).

104   Kim, R., Emi, M. & Tanabe, K. Cancer immunoediting from immune surveillance to immune escape. *Immunology* **121**, 1-14, doi:10.1111/j.1365-2567.2007.02587.x (2007).

105   Boon, T., Cerottini, J. C., Van den Eynde, B., van der Bruggen, P. & Van Pel, A. Tumor antigens recognized by T lymphocytes. *Annu Rev Immunol* **12**, 337-365, doi:10.1146/annurev.iy.12.040194.002005 (1994).

106   Feizi, T. Demonstration by monoclonal antibodies that carbohydrate structures of glycoproteins and glycolipids are onco-developmental antigens. *Nature* **314**, 53-57, doi:10.1038/314053a0 (1985).

107 Rodrlguez, E., Schetters, S. T. T. & van Kooyk, Y. The tumour glyco-code as a novel immune checkpoint for immunotherapy. *Nat Rev Immunol* **18**, 204-211, doi:10.1038/nri.2018.3 (2018).

108 Rossig, C., Kailayangiri, S., Jamitzky, S. & Altvater, B. Carbohydrate Targets for CAR T Cells in Solid Childhood Cancers. *Front Oncol* **8**, 513, doi:10.3389/fonc.2018.00513 (2018).

109 Mellman, I., Coukos, G. & Dranoff, G. Cancer immunotherapy comes of age. *Nature* **480**, 480-489, doi:10.1038/nature10673 (2011).

110 Chen, D. S. & Mellman, I. Oncology meets immunology: the cancer-immunity cycle. *Immunity* **39**, 1-10, doi:10.1016/j.immuni.2013.07.012 (2013).

111 Moser, M. & Murphy, K. M. Dendritic cell regulation of TH1-TH2 development. *Nat Immunol* **1**, 199-205, doi:10.1038/79734 (2000).

112 Reeves, E. & James, E. Antigen processing and immune regulation in the response to tumours. *Immunology* **150**, 16-24, doi:10.1111/imm.12675 (2017).

113 Joshi, N. S. *et al.* Regulatory T Cells in Tumor-Associated Tertiary Lymphoid Structures Suppress Anti-tumor T Cell Responses. *Immunity* **43**, 579-590, doi:10.1016/j.immuni.2015.08.006 (2015).

114 Dunn, G. P., Bruce, A. T., Ikeda, H., Old, L. J. & Schreiber, R. D. Cancer immunoediting: from immunosurveillance to tumor escape. *Nat Immunol* **3**, 991-998, doi:10.1038/ni1102-991 (2002).

115 Kooi, S. *et al.* HLA class I expression on human ovarian carcinoma cells correlates with T-cell infiltration in vivo and T-cell expansion in vitro in low concentrations of recombinant interleukin-2. *Cell Immunol* **174**, 116-128, doi:10.1006/cimm.1996.0301 (1996).

116 Sharpe, A. H. & Pauken, K. E. The diverse functions of the PD1 inhibitory pathway. *Nat Rev Immunol* **18**, 153-167, doi:10.1038/nri.2017.108 (2018).

117 Munn, D. H. & Mellor, A. L. IDO in the Tumor Microenvironment: Inflammation, Counter-Regulation, and Tolerance. *Trends Immunol* **37**, 193-207, doi:10.1016/j.it.2016.01.002 (2016).

118 Bak, S. P., Alonso, A., Turk, M. J. & Berwin, B. Murine ovarian cancer vascular leukocytes require arginase-1 activity for T cell suppression. *Mol Immunol* **46**, 258-268, doi:10.1016/j.molimm.2008.08.266 (2008).

119 Curiel, T. J. *et al.* Specific recruitment of regulatory T cells in ovarian carcinoma fosters immune privilege and predicts reduced survival. *Nature medicine* **10**, 942-949, doi:10.1038/nm1093 (2004).

120 Gabrilovich, D. I. & Nagaraj, S. Myeloid-derived suppressor cells as regulators of the immune system. *Nat Rev Immunol* **9**, 162-174, doi:10.1038/nri2506 (2009).

121 Bouzin, C., Brouet, A., De Vriese, J., Dewever, J. & Feron, O. Effects of vascular endothelial growth factor on the lymphocyte-endothelium interactions: identification of caveolin-1 and nitric oxide as control points of endothelial cell anergy. *J Immunol* **178**, 1505-1511, doi:10.4049/jimmunol.178.3.1505 (2007).

122 Schwartzentruber, D. J. *et al.* gp100 peptide vaccine and interleukin-2 in patients with advanced melanoma. *N Engl J Med* **364**, 2119-2127, doi:10.1056/NEJMoa1012863 (2011).

123 Vansteenkiste, J. *et al.* Final results of a multi-center, double-blind, randomized, placebo-controlled phase II study to assess the efficacy of MAGE-A3 immunotherapeutic as adjuvant therapy in stage IB/II non-small cell lung cancer (NSCLC). *Journal of Clinical Oncology* **25**, doi:Doi 10.1200/Jco.2006.09.7097 (2007).

124 Kreiter, S. *et al.* Mutant MHC class II epitopes drive therapeutic immune responses to cancer. *Nature* **520**, 692-696, doi:10.1038/nature14426 (2015).

125 Matsushita, H. *et al.* Cancer exome analysis reveals a T-cell-dependent mechanism of cancer immunoediting. *Nature* **482**, 400-404, doi:10.1038/nature10755 (2012).

126 Ott, P. A. *et al.* An immunogenic personal neoantigen vaccine for patients with melanoma. *Nature* **547**, 217-221, doi:10.1038/nature22991 (2017).

127 Sahin, U. *et al.* Personalized RNA mutanome vaccines mobilize poly-specific therapeutic immunity against cancer. *Nature* **547**, 222-226, doi:10.1038/nature23003 (2017).

128 Dong, H. *et al.* Tumor-associated B7-H1 promotes T-cell apoptosis: a potential mechanism of immune evasion. *Nature medicine* **8**, 793-800, doi:10.1038/nm730 (2002).

129 Taube, J. M. *et al.* Colocalization of inflammatory response with B7-h1 expression in human melanocytic lesions supports an adaptive resistance mechanism of immune escape. *Sci Transl Med* **4**, 127ra137, doi:10.1126/scitranslmed.3003689 (2012).

130 Hathcock, K. S. *et al.* Identification of an alternative CTLA-4 ligand costimulatory for T cell activation. *Science* **262**, 905-907, doi:10.1126/science.7694361 (1993).

131 Linsley, P. S. *et al.* CTLA-4 is a second receptor for the B cell activation antigen B7. *J Exp Med* **174**, 561-569, doi:10.1084/jem.174.3.561 (1991).

132 Waterhouse, P. *et al.* Lymphoproliferative disorders with early lethality in mice deficient in Ctla-4. *Science* **270**, 985-988, doi:10.1126/science.270.5238.985 (1995).

133   Leach, D. R., Krummel, M. F. & Allison, J. P. Enhancement of antitumor immunity by CTLA-4 blockade. *Science* **271**, 1734-1736, doi:10.1126/science.271.5256.1734 (1996).

134   Hodi, F. S. *et al.* Improved survival with ipilimumab in patients with metastatic melanoma. *N Engl J Med* **363**, 711-723, doi:10.1056/NEJMoa1003466 (2010).

135   Phan, G. Q. *et al.* Cancer regression and autoimmunity induced by cytotoxic T lymphocyte-associated antigen 4 blockade in patients with metastatic melanoma. *Proc Natl Acad Sci U S A* **100**, 8372-8377, doi:10.1073/pnas.1533209100 (2003).

136   Freeman, G. J. *et al.* Engagement of the PD-1 immunoinhibitory receptor by a novel B7 family member leads to negative regulation of lymphocyte activation. *J Exp Med* **192**, 1027-1034, doi:10.1084/jem.192.7.1027 (2000).

137   Keir, M. E. *et al.* Tissue expression of PD-L1 mediates peripheral T cell tolerance. *J Exp Med* **203**, 883-895, doi:10.1084/jem.20051776 (2006).

138   Nishimura, H., Nose, M., Hiai, H., Minato, N. & Honjo, T. Development of lupus-like autoimmune diseases by disruption of the PD-1 gene encoding an ITIM motif-carrying immunoreceptor. *Immunity* **11**, 141-151, doi:10.1016/s1074-7613(00)80089-8 (1999).

139   Francisco, L. M. *et al.* PD-L1 regulates the development, maintenance, and function of induced regulatory T cells. *J Exp Med* **206**, 3015-3029, doi:10.1084/jem.20090847 (2009).

140   Barber, D. L. *et al.* Restoring function in exhausted CD8 T cells during chronic viral infection. *Nature* **439**, 682-687, doi:10.1038/nature04444 (2006).

141   Rosenberg, S. A. & Restifo, N. P. Adoptive cell transfer as personalized immunotherapy for human cancer. *Science* **348**, 62-68, doi:10.1126/science.aaa4967 (2015).

142   Rosenberg, S. A. *et al.* Use of tumor-infiltrating lymphocytes and interleukin-2 in the immunotherapy of patients with metastatic melanoma. A preliminary report. *N Engl J Med* **319**, 1676-1680, doi:10.1056/NEJM198812223192527 (1988).

143   Dudley, M. E. *et al.* Cancer regression and autoimmunity in patients after clonal repopulation with antitumor lymphocytes. *Science* **298**, 850-854, doi:10.1126/science.1076514 (2002).

144   Besser, M. J. *et al.* Adoptive transfer of tumor-infiltrating lymphocytes in patients with metastatic melanoma: intent-to-treat analysis and efficacy after failure to prior immunotherapies. *Clin Cancer Res* **19**, 4792-4800, doi:10.1158/1078-0432.CCR-13-0380 (2013).

145   Rosenberg, S. A. *et al.* Durable complete responses in heavily pretreated patients with metastatic melanoma using T-cell transfer immunotherapy. *Clin Cancer Res* **17**, 4550-4557, doi:10.1158/1078-0432.CCR-11-0116 (2011).

146   Lawrence, M. S. *et al.* Mutational heterogeneity in cancer and the search for new cancer-associated genes. *Nature* **499**, 214-218, doi:10.1038/nature12213 (2013).

147   Lu, Y. C. *et al.* Efficient identification of mutated cancer antigens recognized by T cells associated with durable tumor regressions. *Clin Cancer Res* **20**, 3401-3410, doi:10.1158/1078-0432.CCR-14-0433 (2014).

148   Robbins, P. F. *et al.* Mining exomic sequencing data to identify mutated antigens recognized by adoptively transferred tumor-reactive T cells. *Nature medicine* **19**, 747-752, doi:10.1038/nm.3161 (2013).

149   Morgan, R. A. *et al.* Cancer regression in patients after transfer of genetically engineered lymphocytes. *Science* **314**, 126-129, doi:10.1126/science.1129003 (2006).

150   Aleksic, M. *et al.* Different affinity windows for virus and cancer-specific T-cell receptors: implications for therapeutic strategies. *Eur J Immunol* **42**, 3174-3179, doi:10.1002/eji.201242606 (2012).

151   Johnson, L. A. *et al.* Gene therapy with human and mouse T-cell receptors mediates cancer regression and targets normal tissues expressing cognate antigen. *Blood* **114**, 535-546, doi:10.1182/blood-2009-03-211714 (2009).

152   Cameron, B. J. *et al.* Identification of a Titin-derived HLA-A1-presented peptide as a cross-reactive target for engineered MAGE A3-directed T cells. *Sci Transl Med* **5**, 197ra103, doi:10.1126/scitranslmed.3006034 (2013).

153   Morgan, R. A. *et al.* Cancer regression and neurological toxicity following anti-MAGE-A3 TCR gene therapy. *J Immunother* **36**, 133-151, doi:10.1097/CJI.0b013e3182829903 (2013).

154   Sewell, A. K. Why must T cells be cross-reactive? *Nat Rev Immunol* **12**, 669-677, doi:10.1038/nri3279 (2012).

155   Linette, G. P. *et al.* Cardiovascular toxicity and titin cross-reactivity of affinity-enhanced T cells in myeloma and melanoma. *Blood* **122**, 863-871, doi:10.1182/blood-2013-03-490565 (2013).

156   Rapoport, A. P. *et al.* NY-ESO-1-specific TCR-engineered T cells mediate sustained antigen-specific antitumor effects in myeloma. *Nature medicine* **21**, 914-921, doi:10.1038/nm.3910 (2015).

157   Kato, T. *et al.* Effective screening of T cells recognizing neoantigens and construction of T-cell receptor-engineered T cells. *Oncotarget* **9**, 11009-11019, doi:10.18632/oncotarget.24232 (2018).

158 Matsuda, T. *et al.* Induction of Neoantigen-Specific Cytotoxic T Cells and Construction of T-cell Receptor-Engineered T Cells for Ovarian Cancer. *Clin Cancer Res* **24**, 5357-5367, doi:10.1158/1078-0432.CCR-18-0142 (2018).

159 Gross, G., Waks, T. & Eshhar, Z. Expression of immunoglobulin-T-cell receptor chimeric molecules as functional receptors with antibody-type specificity. *Proc Natl Acad Sci U S A* **86**, 10024-10028, doi:10.1073/pnas.86.24.10024 (1989).

160 June, C. H., O'Connor, R. S., Kawalekar, O. U., Ghassemi, S. & Milone, M. C. CAR T cell immunotherapy for human cancer. *Science* **359**, 1361-1365, doi:10.1126/science.aar6711 (2018).

161 Kershaw, M. H. *et al.* A phase I study on adoptive immunotherapy using gene-modified T cells for ovarian cancer. *Clin Cancer Res* **12**, 6106-6115, doi:10.1158/1078-0432.CCR-06-1183 (2006).

162 Kowolik, C. M. *et al.* CD28 costimulation provided through a CD19-specific chimeric antigen receptor enhances in vivo persistence and antitumor efficacy of adoptively transferred T cells. *Cancer Res* **66**, 10995-11004, doi:10.1158/0008-5472.CAN-06-0160 (2006).

163 Imai, C. *et al.* Chimeric receptors with 4-1BB signaling capacity provoke potent cytotoxicity against acute lymphoblastic leukemia. *Leukemia* **18**, 676-684, doi:10.1038/sj.leu.2403302 (2004).

164 Maher, J., Brentjens, R. J., Gunset, G., Riviere, I. & Sadelain, M. Human T-lymphocyte cytotoxicity and proliferation directed by a single chimeric TCRzeta /CD28 receptor. *Nat Biotechnol* **20**, 70-75, doi:10.1038/nbt0102-70 (2002).

165 Chmielewski, M. & Abken, H. TRUCKs: the fourth generation of CARs. *Expert Opin Biol Ther* **15**, 1145-1154, doi:10.1517/14712598.2015.1046430 (2015).

166 Pieper, K., Grimbacher, B. & Eibel, H. B-cell biology and development. *J Allergy Clin Immunol* **131**, 959-971, doi:10.1016/j.jaci.2013.01.046 (2013).

167 Brentjens, R. J. *et al.* CD19-targeted T cells rapidly induce molecular remissions in adults with chemotherapy-refractory acute lymphoblastic leukemia. *Sci Transl Med* **5**, 177ra138, doi:10.1126/scitranslmed.3005930 (2013).

168 Grupp, S. A. *et al.* Chimeric antigen receptor-modified T cells for acute lymphoid leukemia. *N Engl J Med* **368**, 1509-1518, doi:10.1056/NEJMoa1215134 (2013).

169 Kochenderfer, J. N. *et al.* Eradication of B-lineage cells and regression of lymphoma in a patient treated with autologous T cells genetically engineered to recognize CD19. *Blood* **116**, 4099-4102, doi:10.1182/blood-2010-04-281931 (2010).

170 Porter, D. L., Levine, B. L., Kalos, M., Bagg, A. & June, C. H. Chimeric antigen receptor-modified T cells in chronic lymphoid leukemia. *N Engl J Med* **365**, 725-733, doi:10.1056/NEJMoa1103849 (2011).

171 Maude, S. L. *et al.* Chimeric antigen receptor T cells for sustained remissions in leukemia. *N Engl J Med* **371**, 1507-1517, doi:10.1056/NEJMoa1407222 (2014).

172 Gust, J. *et al.* Endothelial Activation and Blood-Brain Barrier Disruption in Neurotoxicity after Adoptive Immunotherapy with CD19 CAR-T Cells. *Cancer Discov* **7**, 1404-1419, doi:10.1158/2159-8290.CD-17-0698 (2017).

173 Ali, S. A. *et al.* T cells expressing an anti-B-cell maturation antigen chimeric antigen receptor cause remissions of multiple myeloma. *Blood* **128**, 1688-1700, doi:10.1182/blood-2016-04-711903 (2016).

174 Fry, T. J. *et al.* CD22-targeted CAR T cells induce remission in B-ALL that is naive or resistant to CD19-targeted CAR immunotherapy. *Nature medicine* **24**, 20-28, doi:10.1038/nm.4441 (2018).

175 Joyce, J. A. & Fearon, D. T. T cell exclusion, immune privilege, and the tumor microenvironment. *Science* **348**, 74-80, doi:10.1126/science.aaa6204 (2015).

176 Richman, S. A. *et al.* High-Affinity GD2-Specific CAR T Cells Induce Fatal Encephalitis in a Preclinical Neuroblastoma Model. *Cancer Immunol Res* **6**, 36-46, doi:10.1158/2326-6066.CIR-17-0211 (2018).

177 Morgan, R. A. *et al.* Case report of a serious adverse event following the administration of T cells transduced with a chimeric antigen receptor recognizing ERBB2. *Mol Ther* **18**, 843-851, doi:10.1038/mt.2010.24 (2010).

178 Thistlethwaite, F. C. *et al.* The clinical efficacy of first-generation carcinoembryonic antigen (CEACAM5)-specific CAR T cells is limited by poor persistence and transient pre-conditioning-dependent respiratory toxicity. *Cancer Immunol Immunother* **66**, 1425-1436, doi:10.1007/s00262-017-2034-7 (2017).

179 Sotillo, E. *et al.* Convergence of Acquired Mutations and Alternative Splicing of CD19 Enables Resistance to CART-19 Immunotherapy. *Cancer Discov* **5**, 1282-1295, doi:10.1158/2159-8290.CD-15-1020 (2015).

180 Porter, D. L. *et al.* Chimeric antigen receptor T cells persist and induce sustained remissions in relapsed refractory chronic lymphocytic leukemia. *Sci Transl Med* **7**, 303ra139, doi:10.1126/scitranslmed.aac5415 (2015).

181 Hudecek, M. *et al.* The B-cell tumor-associated antigen ROR1 can be targeted with T cells modified to express a ROR1-specific chimeric antigen receptor. *Blood* **116**, 4532-4541, doi:10.1182/blood-2010-05-283309 (2010).

182   Yu, A. L. *et al.* Anti-GD2 antibody with GM-CSF, interleukin-2, and isotretinoin for neuroblastoma. *N Engl J Med* **363**, 1324-1334, doi:10.1056/NEJMoa0911123 (2010).

183   Grada, Z. *et al.* TanCAR: A Novel Bispecific Chimeric Antigen Receptor for Cancer Immunotherapy. *Mol Ther Nucleic Acids* **2**, e105, doi:10.1038/mtna.2013.32 (2013).

184   Kloss, C. C., Condomines, M., Cartellieri, M., Bachmann, M. & Sadelain, M. Combinatorial antigen recognition with balanced signaling promotes selective tumor eradication by engineered T cells. *Nat Biotechnol* **31**, 71-75, doi:10.1038/nbt.2459 (2013).

185   Wilkie, S. *et al.* Dual targeting of ErbB2 and MUC1 in breast cancer using chimeric antigen receptors engineered to provide complementary signaling. *J Clin Immunol* **32**, 1059-1070, doi:10.1007/s10875-012-9689-9 (2012).

186   Roybal, K. T. *et al.* Precision Tumor Recognition by T Cells With Combinatorial Antigen-Sensing Circuits. *Cell* **164**, 770-779, doi:10.1016/j.cell.2016.01.011 (2016).

187   Cho, J. H., Collins, J. J. & Wong, W. W. Universal Chimeric Antigen Receptors for Multiplexed and Logical Control of T Cell Responses. *Cell* **173**, 1426-1438 e1411, doi:10.1016/j.cell.2018.03.038 (2018).

188   Fedorov, V. D., Themeli, M. & Sadelain, M. PD-1- and CTLA-4-based inhibitory chimeric antigen receptors (iCARs) divert off-target immunotherapy responses. *Sci Transl Med* **5**, 215ra172, doi:10.1126/scitranslmed.3006597 (2013).

189   Srivastava, S. & Riddell, S. R. Engineering CAR-T cells: Design concepts. *Trends Immunol* **36**, 494-502, doi:10.1016/j.it.2015.06.004 (2015).

190   Watanabe, K. *et al.* Target antigen density governs the efficacy of anti-CD20-CD28-CD3 zeta chimeric antigen receptor-modified effector CD8+ T cells. *J Immunol* **194**, 911-920, doi:10.4049/jimmunol.1402346 (2015).

191   Hoerter, J. A. *et al.* Coreceptor affinity for MHC defines peptide specificity requirements for TCR interaction with coagonist peptide-MHC. *J Exp Med* **210**, 1807-1821, doi:10.1084/jem.20122528 (2013).

192   Krogsgaard, M. *et al.* Agonist/endogenous peptide-MHC heterodimers drive T cell activation and sensitivity. *Nature* **434**, 238-243, doi:10.1038/nature03391 (2005).

193   Hudecek, M. *et al.* Receptor affinity and extracellular domain modifications affect tumor recognition by ROR1-specific chimeric antigen receptor T cells. *Clin Cancer Res* **19**, 3153-3164, doi:10.1158/1078-0432.CCR-13-0330 (2013).

194   Chmielewski, M., Hombach, A., Heuser, C., Adams, G. P. & Abken, H. T cell activation by antibody-like immunoreceptors: increase in affinity of the single-chain fragment domain above threshold does not increase T cell activation against antigen-positive target cells but decreases selectivity. *J Immunol* **173**, 7647-7653 (2004).

195   Oren, R. *et al.* Functional comparison of engineered T cells carrying a native TCR versus TCR-like antibody-based chimeric antigen receptors indicates affinity/avidity thresholds. *J Immunol* **193**, 5733-5743, doi:10.4049/jimmunol.1301769 (2014).

196   Stone, J. D., Chervin, A. S. & Kranz, D. M. T-cell receptor binding affinities and kinetics: impact on T-cell activity and specificity. *Immunology* **126**, 165-176, doi:10.1111/j.1365-2567.2008.03015.x (2009).

197   Cordoba, S. P. *et al.* The large ectodomains of CD45 and CD148 regulate their segregation from and inhibition of ligated T-cell receptor. *Blood* **121**, 4295-4302, doi:10.1182/blood-2012-07-442251 (2013).

198   Irles, C. *et al.* CD45 ectodomain controls interaction with GEMs and Lck activity for optimal TCR signaling. *Nat Immunol* **4**, 189-197, doi:10.1038/ni877 (2003).

199   Guest, R. D. *et al.* The role of extracellular spacer regions in the optimal design of chimeric immune receptors: evaluation of four different scFvs and antigens. *J Immunother* **28**, 203-211, doi:10.1097/01.cji.0000161397.96582.59 (2005).

200   Hombach, A. A. *et al.* T cell activation by antibody-like immunoreceptors: the position of the binding epitope within the target molecule determines the efficiency of activation of redirected T cells. *J Immunol* **178**, 4650-4657 (2007).

201   James, S. E. *et al.* Antigen sensitivity of CD22-specific chimeric TCR is modulated by target epitope distance from the cell membrane. *J Immunol* **180**, 7028-7038, doi:10.4049/jimmunol.180.10.7028 (2008).

202   Hudecek, M. *et al.* The nonsignaling extracellular spacer domain of chimeric antigen receptors is decisive for in vivo antitumor activity. *Cancer Immunol Res* **3**, 125-135, doi:10.1158/2326-6066.CIR-14-0127 (2015).

203   Loffler, A. *et al.* A recombinant bispecific single-chain antibody, CD19 x CD3, induces rapid and high lymphoma-directed cytotoxicity by unstimulated T lymphocytes. *Blood* **95**, 2098-2103 (2000).

204   Mack, M., Riethmuller, G. & Kufer, P. A small bispecific antibody construct expressed as a functional single-chain molecule with high tumor cell cytotoxicity. *Proc Natl Acad Sci U S A* **92**, 7021-7025 (1995).

205   Offner, S., Hofmeister, R., Romaniuk, A., Kufer, P. & Baeuerle, P. A. Induction of regular cytolytic T cell synapses by bispecific single-chain antibody constructs on MHC class I-negative tumor cells. *Mol Immunol* **43**, 763-771, doi:10.1016/j.molimm.2005.03.007 (2006).

206   Dreier, T. *et al.* T cell costimulus-independent and very efficacious inhibition of tumor growth in mice bearing subcutaneous or leukemic human B cell lymphoma xenografts by a CD19-/CD3- bispecific single-chain antibody construct. *J Immunol* **170**, 4397-4402, doi:10.4049/jimmunol.170.8.4397 (2003).

207   Dreier, T. *et al.* Extremely potent, rapid and costimulation-independent cytotoxic T-cell response against lymphoma cells catalyzed by a single-chain bispecific antibody. *Int J Cancer* **100**, 690-697, doi:10.1002/ijc.10557 (2002).

208   Kufer, P. *et al.* Minimal costimulatory requirements for T cell priming and TH1 differentiation: activation of naive human T lymphocytes by tumor cells armed with bifunctional antibody constructs. *Cancer Immun* **1**, 10 (2001).

209   Brischwein, K. *et al.* Strictly target cell-dependent activation of T cells by bispecific single-chain antibody constructs of the BiTE class. *J Immunother* **30**, 798-807, doi:10.1097/CJI.0b013e318156750c (2007).

210   Hoffmann, P. *et al.* Serial killing of tumor cells by cytotoxic T cells redirected with a CD19-/CD3-bispecific single-chain antibody construct. *Int J Cancer* **115**, 98-104, doi:10.1002/ijc.20908 (2005).

211   Godar, M., de Haard, H., Blanchetot, C. & Rasser, J. Therapeutic bispecific antibody formats: a patent applications review (1994-2017). *Expert Opin Ther Pat* **28**, 251-276, doi:10.1080/13543776.2018.1428307 (2018).

212   Labrijn, A. F., Janmaat, M. L., Reichert, J. M. & Parren, P. Bispecific antibodies: a mechanistic review of the pipeline. *Nat Rev Drug Discov* **18**, 585-608, doi:10.1038/s41573-019-0028-1 (2019).

213   Spiess, C., Zhai, Q. & Carter, P. J. Alternative molecular formats and therapeutic applications for bispecific antibodies. *Mol Immunol* **67**, 95-106, doi:10.1016/j.molimm.2015.01.003 (2015).

214   Bargou, R. *et al.* Tumor regression in cancer patients by very low doses of a T cell-engaging antibody. *Science* **321**, 974-977, doi:10.1126/science.1158545 (2008).

215   Topp, M. S. *et al.* Safety and activity of blinatumomab for adult patients with relapsed or refractory B-precursor acute lymphoblastic leukaemia: a multicentre, single-arm, phase 2 study. *Lancet Oncol* **16**, 57-66, doi:10.1016/S1470-2045(14)71170-2 (2015).

216   Klinger, M. *et al.* Immunopharmacologic response of patients with B-lineage acute lymphoblastic leukemia to continuous infusion of T cell-engaging CD19/CD3-bispecific BiTE antibody blinatumomab. *Blood* **119**, 6226-6233, doi:10.1182/blood-2012-01-400515 (2012).

217   Lowe, D. *et al.* Aggregation, stability, and formulation of human antibody therapeutics. *Adv Protein Chem Struct Biol* **84**, 41-61, doi:10.1016/B978-0-12-386483-3.00004-5 (2011).

218   Harwood, S. L. *et al.* ATTACK, a novel bispecific T cell-recruiting antibody with trivalent EGFR binding and monovalent CD3 binding for cancer immunotherapy. *Oncoimmunology* **7**, e1377874, doi:10.1080/2162402X.2017.1377874 (2017).

219   Milstein, C. & Cuello, A. C. Hybrid hybridomas and their use in immunohistochemistry. *Nature* **305**, 537-540, doi:10.1038/305537a0 (1983).

220   Davis, J. H. *et al.* SEEDbodies: fusion proteins based on strand-exchange engineered domain (SEED) CH3 heterodimers in an Fc analogue platform for asymmetric binders or immunofusions and bispecific antibodies. *Protein Eng Des Sel* **23**, 195-202, doi:10.1093/protein/gzp094 (2010).

221   Gunasekaran, K. *et al.* Enhancing antibody Fc heterodimer formation through electrostatic steering effects: applications to bispecific molecules and monovalent IgG. *J Biol Chem* **285**, 19637-19646, doi:10.1074/jbc.M110.117382 (2010).

222   Merchant, A. M. *et al.* An efficient route to human bispecific IgG. *Nat Biotechnol* **16**, 677-681, doi:10.1038/nbt0798-677 (1998).

223   Ridgway, J. B., Presta, L. G. & Carter, P. 'Knobs-into-holes' engineering of antibody CH3 domains for heavy chain heterodimerization. *Protein Eng* **9**, 617-621, doi:10.1093/protein/9.7.617 (1996).

224   Lewis, S. M. *et al.* Generation of bispecific IgG antibodies by structure-based design of an orthogonal Fab interface. *Nat Biotechnol* **32**, 191-198, doi:10.1038/nbt.2797 (2014).

225   Lindhofer, H., Mocikat, R., Steipe, B. & Thierfelder, S. Preferential species-restricted heavy/light chain pairing in rat/mouse quadromas. Implications for a single-step purification of bispecific antibodies. *J Immunol* **155**, 219-225 (1995).

226   Schaefer, W. *et al.* Immunoglobulin domain crossover as a generic approach for the production of bispecific IgG antibodies. *Proc Natl Acad Sci U S A* **108**, 11187-11192, doi:10.1073/pnas.1019002108 (2011).

227   Spiess, C. *et al.* Bispecific antibodies with natural architecture produced by co-culture of bacteria expressing two distinct half-antibodies. *Nat Biotechnol* **31**, 753-758, doi:10.1038/nbt.2621 (2013).

228   Labrijn, A. F. *et al.* Efficient generation of stable bispecific IgG1 by controlled Fab-arm exchange. *Proc Natl Acad Sci U S A* **110**, 5145-5150, doi:10.1073/pnas.1220145110 (2013).

229 Wu, C. *et al.* Molecular construction and optimization of anti-human IL-1alpha/beta dual variable domain immunoglobulin (DVD-Ig) molecules. *MAbs* **1**, 339-347, doi:10.4161/mabs.1.4.8755 (2009).

230 Ruf, P. & Lindhofer, H. Induction of a long-lasting antitumor immunity by a trifunctional bispecific antibody. *Blood* **98**, 2526-2534, doi:10.1182/blood.v98.8.2526 (2001).

231 Borlak, J., Langer, F., Spanel, R., Schondorfer, G. & Dittrich, C. Immune-mediated liver injury of the cancer therapeutic antibody catumaxomab targeting EpCAM, CD3 and Fcgamma receptors. *Oncotarget* **7**, 28059-28074, doi:10.18632/oncotarget.8574 (2016).

232 Labrijn, A. F. *et al.* Efficient Generation of Bispecific Murine Antibodies for Pre-Clinical Investigations in Syngeneic Rodent Models. *Sci Rep* **7**, 2476, doi:10.1038/s41598-017-02823-9 (2017).

233 Schlothauer, T. *et al.* Novel human IgG1 and IgG4 Fc-engineered antibodies with completely abolished immune effector functions. *Protein Eng Des Sel* **29**, 457-466, doi:10.1093/protein/gzw040 (2016).

234 Vafa, O. *et al.* An engineered Fc variant of an IgG eliminates all immune effector functions via structural perturbations. *Methods* **65**, 114-126, doi:10.1016/j.ymeth.2013.06.035 (2014).

235 Steinmetz, A. *et al.* CODV-Ig, a universal bispecific tetravalent and multifunctional immunoglobulin format for medical applications. *MAbs* **8**, 867-878, doi:10.1080/19420862.2016.1162932 (2016).

236 Pessano, S., Oettgen, H., Bhan, A. K. & Terhorst, C. The T3/T cell receptor complex: antigenic distinction between the two 20-kd T3 (T3-delta and T3-epsilon) subunits. *EMBO J* **4**, 337-344 (1985).

237 Bortoletto, N., Scotet, E., Myamoto, Y., D'Oro, U. & Lanzavecchia, A. Optimizing anti-CD3 affinity for effective T cell targeting against tumor cells. *Eur J Immunol* **32**, 3102-3107, doi:10.1002/1521-4141(200211)32:11<3102::AID-IMMU3102>3.0.CO;2-C (2002).

238 Mandikian, D. *et al.* Relative Target Affinities of T-Cell-Dependent Bispecific Antibodies Determine Biodistribution in a Solid Tumor Mouse Model. *Mol Cancer Ther* **17**, 776-785, doi:10.1158/1535-7163.MCT-17-0657 (2018).

239 Pahl, J. H. W. *et al.* CD16A Activation of NK Cells Promotes NK Cell Proliferation and Memory-Like Cytotoxicity against Cancer Cells. *Cancer Immunol Res* **6**, 517-527, doi:10.1158/2326-6066.CIR-17-0550 (2018).

240 Yun, H. D. *et al.* Trispecific killer engager CD16xIL15xCD33 potently induces NK cell activation and cytotoxicity against neoplastic mast cells. *Blood Adv* **2**, 1580-1584, doi:10.1182/bloodadvances.2018018176 (2018).

241 Laszlo, G. S. *et al.* Cellular determinants for preclinical activity of a novel CD33/CD3 bispecific T-cell engager (BiTE) antibody, AMG 330, against human AML. *Blood* **123**, 554-561, doi:10.1182/blood-2013-09-527044 (2014).

242 Lopez-Albaitero, A. *et al.* Overcoming resistance to HER2-targeted therapy with a novel HER2/CD3 bispecific antibody. *Oncoimmunology* **6**, e1267891, doi:10.1080/2162402X.2016.1267891 (2017).

243 Oberst, M. D. *et al.* CEA/CD3 bispecific antibody MEDI-565/AMG 211 activation of T cells and subsequent killing of human tumors is independent of mutations commonly found in colorectal adenocarcinomas. *MAbs* **6**, 1571-1584, doi:10.4161/19420862.2014.975660 (2014).

244 Friedrich, M. *et al.* Regression of human prostate cancer xenografts in mice by AMG 212/BAY2010112, a novel PSMA/CD3-Bispecific BiTE antibody cross-reactive with non-human primate antigens. *Mol Cancer Ther* **11**, 2664-2673, doi:10.1158/1535-7163.MCT-12-0042 (2012).

245 Slaga, D. *et al.* Avidity-based binding to HER2 results in selective killing of HER2-overexpressing cells by anti-HER2/CD3. *Sci Transl Med* **10**, doi:10.1126/scitranslmed.aat5775 (2018).

246 Pfosser, A., Brandl, M., Salih, H., Grosse-Hovest, L. & Jung, G. Role of target antigen in bispecific-antibody-mediated killing of human glioblastoma cells: a pre-clinical study. *Int J Cancer* **80**, 612-616, doi:10.1002/(sici)1097-0215(19990209)80:4<612::aid-ijc21>3.0.co;2-k (1999).

247 Li, J. *et al.* Membrane-Proximal Epitope Facilitates Efficient T Cell Synapse Formation by Anti-FcRH5/CD3 and Is a Requirement for Myeloma Cell Killing. *Cancer Cell* **31**, 383-395, doi:10.1016/j.ccell.2017.02.001 (2017).

248 Bluemel, C. *et al.* Epitope distance to the target cell membrane and antigen size determine the potency of T cell-mediated lysis by BiTE antibodies specific for a large melanoma surface antigen. *Cancer Immunol Immunother* **59**, 1197-1209, doi:10.1007/s00262-010-0844-y (2010).

249 Trabolsi, A., Arumov, A. & Schatz, J. H. T Cell-Activating Bispecific Antibodies in Cancer Therapy. *J Immunol* **203**, 585-592, doi:10.4049/jimmunol.1900496 (2019).

250 Schmohl, J. U. *et al.* Engineering of Anti-CD133 Trispecific Molecule Capable of Inducing NK Expansion and Driving Antibody-Dependent Cell-Mediated Cytotoxicity. *Cancer Res Treat* **49**, 1140-1152, doi:10.4143/crt.2016.491 (2017).

251 Wu, L., Seung, E., Xu, L. Ercole Rao, Dana M. Lord, Ronnie R. Wei, Virna Cortez-Retamozo, Beatriz Ospina, Valeriya Posternak, Gregory Ulinski, Peter Piepenhagen, Elisa Francesconi, Nizar El-Murr, Christian Beil, Patrick Kirby, Aiqun Li, Jennifer Fretland, Rita Vicente, Gejing Deng, Tarik Dabdoubi, Beatrice Cameron, Thomas Bertrand, Paul Ferrari, Stéphanie Pouzieux, Cendrine Lemoine, Catherine Prades, Anna Park, Huawei Qiu, Zhili

Song, Bailin Zhang, Fangxian Sun, Marielle Chiron, Srinivas Rao, Katarina Radošević, Zhi-yong Yang and Gary J. Nabel 1. Trispecific antibodies enhance the therapeutic efficacy of tumor-directed T cells through T cell receptor co-stimulation. *Nature Cancer* **doi:10.1038/s43018-019-0004-z** (2019).

252 Quail, D. F. & Joyce, J. A. Microenvironmental regulation of tumor progression and metastasis. *Nature medicine* **19**, 1423-1437, doi:10.1038/nm.3394 (2013).

253 Folkman, J. Tumor angiogenesis. *Adv Cancer Res* **43**, 175-203, doi:10.1016/s0065-230x(08)60946-x (1985).

254 Viallard, C. & Larrivee, B. Tumor angiogenesis and vascular normalization: alternative therapeutic targets. *Angiogenesis* **20**, 409-426, doi:10.1007/s10456-017-9562-9 (2017).

255 Abramsson, A., Lindblom, P. & Betsholtz, C. Endothelial and nonendothelial sources of PDGF-B regulate pericyte recruitment and influence vascular pattern formation in tumors. *J Clin Invest* **112**, 1142-1151, doi:10.1172/JCI18549 (2003).

256 Morikawa, S. *et al.* Abnormalities in pericytes on blood vessels and endothelial sprouts in tumors. *Am J Pathol* **160**, 985-1000, doi:10.1016/S0002-9440(10)64920-6 (2002).

257 Jain, R. K., Martin, J. D. & Stylianopoulos, T. The role of mechanical forces in tumor growth and therapy. *Annu Rev Biomed Eng* **16**, 321-346, doi:10.1146/annurev-bioeng-071813-105259 (2014).

258 Galon, J. & Bruni, D. Approaches to treat immune hot, altered and cold tumours with combination immunotherapies. *Nat Rev Drug Discov* **18**, 197-218, doi:10.1038/s41573-018-0007-y (2019).

259 Feig, C. *et al.* Targeting CXCL12 from FAP-expressing carcinoma-associated fibroblasts synergizes with anti-PD-L1 immunotherapy in pancreatic cancer. *Proc Natl Acad Sci U S A* **110**, 20212-20217, doi:10.1073/pnas.1320318110 (2013).

260 Lesokhin, A. M. *et al.* Monocytic CCR2(+) myeloid-derived suppressor cells promote immune escape by limiting activated CD8 T-cell infiltration into the tumor microenvironment. *Cancer Res* **72**, 876-886, doi:10.1158/0008-5472.CAN-11-1792 (2012).

261 Zhu, Y. *et al.* CSF1/CSF1R blockade reprograms tumor-infiltrating macrophages and improves response to T-cell checkpoint immunotherapy in pancreatic cancer models. *Cancer Res* **74**, 5057-5069, doi:10.1158/0008-5472.CAN-13-3723 (2014).

262 Molon, B. *et al.* Chemokine nitration prevents intratumoral infiltration of antigen-specific T cells. *J Exp Med* **208**, 1949-1962, doi:10.1084/jem.20101956 (2011).

263 Motz, G. T. *et al.* Tumor endothelium FasL establishes a selective immune barrier promoting tolerance in tumors. *Nature medicine* **20**, 607-615, doi:10.1038/nm.3541 (2014).

264 Rettig, W. J. *et al.* Identification of endosialin, a cell surface glycoprotein of vascular endothelial cells in human cancer. *Proc Natl Acad Sci U S A* **89**, 10832-10836 (1992).

265 St Croix, B. *et al.* Genes expressed in human tumor endothelium. *Science* **289**, 1197-1202 (2000).

266 Bagley, R. G. *et al.* Endosialin/TEM 1/CD248 is a pericyte marker of embryonic and tumor neovascularization. *Microvasc Res* **76**, 180-188, doi:10.1016/j.mvr.2008.07.008 (2008).

267 Christian, S. *et al.* Endosialin (Tem1) is a marker of tumor-associated myofibroblasts and tumor vessel-associated mural cells. *Am J Pathol* **172**, 486-494, doi:10.2353/ajpath.2008.070623 (2008).

268 MacFadyen, J., Savage, K., Wienke, D. & Isacke, C. M. Endosialin is expressed on stromal fibroblasts and CNS pericytes in mouse embryos and is downregulated during development. *Gene Expr Patterns* **7**, 363-369, doi:10.1016/j.modgep.2006.07.006 (2007).

269 MacFadyen, J. R. *et al.* Endosialin (TEM1, CD248) is a marker of stromal fibroblasts and is not selectively expressed on tumour endothelium. *FEBS Lett* **579**, 2569-2575, doi:10.1016/j.febslet.2005.03.071 (2005).

270 Simonavicius, N. *et al.* Endosialin (CD248) is a marker of tumor-associated pericytes in high-grade glioma. *Mod Pathol* **21**, 308-315, doi:10.1038/modpathol.3801006 (2008).

271 Rouleau, C. *et al.* Endosialin protein expression and therapeutic target potential in human solid tumors: sarcoma versus carcinoma. *Clin Cancer Res* **14**, 7223-7236, doi:10.1158/1078-0432.CCR-08-0499 (2008).

272 O'Shannessy, D. J. *et al.* Influence of tumor microenvironment on prognosis in colorectal cancer: Tissue architecture-dependent signature of endosialin (TEM-1) and associated proteins. *Oncotarget* **5**, 3983-3995, doi:10.18632/oncotarget.2108 (2014).

273 Brown, L. F. *et al.* Vascular stroma formation in carcinoma in situ, invasive carcinoma, and metastatic carcinoma of the breast. *Clin Cancer Res* **5**, 1041-1056 (1999).

274 Davies, G., Cunnick, G. H., Mansel, R. E., Mason, M. D. & Jiang, W. G. Levels of expression of endothelial markers specific to tumour-associated endothelial cells and their correlation with prognosis in patients with breast cancer. *Clin Exp Metastasis* **21**, 31-37, doi:10.1023/b:clin.0000017168.83616.d0 (2004).

275 Brady, J., Neal, J., Sadakar, N. & Gasque, P. Human endosialin (tumor endothelial marker 1) is abundantly expressed in highly malignant and invasive brain tumors. *J Neuropathol Exp Neurol* **63**, 1274-1283, doi:10.1093/jnen/63.12.1274 (2004).

276   Rouleau, C. *et al.* Endosialin is expressed in high grade and advanced sarcomas: evidence from clinical specimens and preclinical modeling. *Int J Oncol* **39**, 73-89, doi:10.3892/ijo.2011.1020 (2011).

277   Rupp, C. *et al.* Mouse endosialin, a C-type lectin-like cell surface receptor: expression during embryonic development and induction in experimental cancer neoangiogenesis. *Cancer Immun* **6**, 10 (2006).

278   Lax, S. *et al.* CD248/Endosialin is dynamically expressed on a subset of stromal cells during lymphoid tissue development, splenic remodeling and repair. *FEBS Lett* **581**, 3550-3556, doi:10.1016/j.febslet.2007.06.063 (2007).

279   Brett, E. *et al.* Isolation of CD248-expressing stromal vascular fraction for targeted improvement of wound healing. *Wound Repair Regen* **25**, 414-422, doi:10.1111/wrr.12542 (2017).

280   Carson-Walter, E. B. *et al.* Cell surface tumor endothelial markers are conserved in mice and humans. *Cancer Res* **61**, 6649-6655 (2001).

281   Dolznig, H. *et al.* Characterization of cancer stroma markers: in silico analysis of an mRNA expression database for fibroblast activation protein and endosialin. *Cancer Immun* **5**, 10 (2005).

282   Hardie, D. L. *et al.* The stromal cell antigen CD248 (endosialin) is expressed on naive CD8+ human T cells and regulates proliferation. *Immunology* **133**, 288-295, doi:10.1111/j.1365-2567.2011.03437.x (2011).

283   Bagley, R. G. *et al.* Human mesenchymal stem cells from bone marrow express tumor endothelial and stromal markers. *Int J Oncol* **34**, 619-627, doi:10.3892/ijo_00000187 (2009).

284   Maia, M. *et al.* CD248 and its cytoplasmic domain: a therapeutic target for arthritis. *Arthritis Rheum* **62**, 3595-3606, doi:10.1002/art.27701 (2010).

285   Smith, S. W. *et al.* Genetic Deletion of the Stromal Cell Marker CD248 (Endosialin) Protects against the Development of Renal Fibrosis. *Nephron* **131**, 265-277, doi:10.1159/000438754 (2015).

286   Mogler, C. *et al.* Hepatic stellate cell-expressed endosialin balances fibrogenesis and hepatocyte proliferation during liver damage. *EMBO Mol Med* **7**, 332-338, doi:10.15252/emmm.201404246 (2015).

287   Bartis, D. *et al.* Role of CD248 as a potential severity marker in idiopathic pulmonary fibrosis. *BMC Pulm Med* **16**, 51, doi:10.1186/s12890-016-0211-7 (2016).

288   Christian, S. *et al.* Molecular cloning and characterization of endosialin, a C-type lectin-like cell surface receptor of tumor endothelium. *J Biol Chem* **276**, 7408-7414, doi:10.1074/jbc.M009604200 (2001).

289   Gardiol, D. PDZ-containing proteins as targets in human pathologies. *FEBS J* **279**, 3529, doi:10.1111/j.1742-4658.2012.08685.x (2012).

290   Nanda, A. *et al.* Tumor endothelial marker 1 (Tem1) functions in the growth and progression of abdominal tumors. *Proc Natl Acad Sci U S A* **103**, 3351-3356, doi:10.1073/pnas.0511306103 (2006).

291   Ohradanova, A. *et al.* Hypoxia upregulates expression of human endosialin gene via hypoxia-inducible factor 2. *Br J Cancer* **99**, 1348-1356, doi:10.1038/sj.bjc.6604685 (2008).

292   Tomkowicz, B. *et al.* Interaction of endosialin/TEM1 with extracellular matrix proteins mediates cell adhesion and migration. *Proc Natl Acad Sci U S A* **104**, 17965-17970, doi:10.1073/pnas.0705647104 (2007).

293   Khan, K. A. *et al.* Multimerin-2 is a ligand for group 14 family C-type lectins CLEC14A, CD93 and CD248 spanning the endothelial pericyte interface. *Oncogene* **36**, 6097-6108, doi:10.1038/onc.2017.214 (2017).

294   Armulik, A., Genove, G. & Betsholtz, C. Pericytes: developmental, physiological, and pathological perspectives, problems, and promises. *Dev Cell* **21**, 193-215, doi:10.1016/j.devcel.2011.07.001 (2011).

295   Tomkowicz, B. *et al.* Endosialin/TEM-1/CD248 regulates pericyte proliferation through PDGF receptor signaling. *Cancer Biol Ther* **9**, 908-915, doi:10.4161/cbt.9.11.11731 (2010).

296   Vestweber, D. & Blanks, J. E. Mechanisms that regulate the function of the selectins and their ligands. *Physiol Rev* **79**, 181-213, doi:10.1152/physrev.1999.79.1.181 (1999).

297   Viski, C. *et al.* Endosialin-Expressing Pericytes Promote Metastatic Dissemination. *Cancer Res* **76**, 5313-5325, doi:10.1158/0008-5472.CAN-16-0932 (2016).

298   Rybinski, K. *et al.* Targeting endosialin/CD248 through antibody-mediated internalization results in impaired pericyte maturation and dysfunctional tumor microvasculature. *Oncotarget* **6**, 25429-25440, doi:10.18632/oncotarget.4559 (2015).

299   Diaz, L. A., Jr. *et al.* A first-in-human phase I study of MORAb-004, a monoclonal antibody to endosialin in patients with advanced solid tumors. *Clin Cancer Res* **21**, 1281-1288, doi:10.1158/1078-0432.CCR-14-1829 (2015).

300   Grothey, A. *et al.* A Randomized, Double-Blind, Placebo-Controlled Phase II Study of the Efficacy and Safety of Monotherapy Ontuxizumab (MORAb-004) Plus Best Supportive Care in Patients with Chemorefractory Metastatic Colorectal Cancer. *Clin Cancer Res* **24**, 316-325, doi:10.1158/1078-0432.CCR-17-1558 (2018).

301   D'Angelo, S. P. *et al.* A phase 2 study of ontuxizumab, a monoclonal antibody targeting endosialin, in metastatic melanoma. *Invest New Drugs* **36**, 103-113, doi:10.1007/s10637-017-0530-4 (2018).

302   Norris, R. E. *et al.* Phase 1 trial of ontuxizumab (MORAb-004) in children with relapsed or refractory solid tumors: A report from the Children's Oncology Group Phase 1 Pilot Consortium (ADVL1213). *Pediatr Blood Cancer* **65**, e26944, doi:10.1002/pbc.26944 (2018).

303   Jones, R. L. *et al.* A phase 1 and randomized controlled phase 2 trial of the safety and efficacy of the combination of gemcitabine and docetaxel with ontuxizumab (MORAb-004) in metastatic soft-tissue sarcomas. *Cancer* **125**, 2445-2454, doi:10.1002/cncr.32084 (2019).

304   Rouleau, C. *et al.* Anti-Endosialin Antibody-Drug Conjugate: Potential in Sarcoma and Other Malignancies. *Mol Cancer Ther* **14**, 2081-2089, doi:10.1158/1535-7163.MCT-15-0312 (2015).

305   Capone, E. *et al.* Generation of a novel Antibody-Drug Conjugate targeting endosialin: potent and durable antitumor response in sarcoma. *Oncotarget* **8**, 60368-60377, doi:10.18632/oncotarget.19499 (2017).

306   Zhao, A. *et al.* Rapid isolation of high-affinity human antibodies against the tumor vascular marker Endosialin/TEM1, using a paired yeast-display/secretory scFv library platform. *J Immunol Methods* **363**, 221-232, doi:10.1016/j.jim.2010.09.001 (2011).

307   Li, C. *et al.* Antibody-based tumor vascular theranostics targeting endosialin/TEM1 in a new mouse tumor vascular model. *Cancer Biol Ther* **15**, 443-451, doi:10.4161/cbt.27825 (2014).

308   Li, C. *et al.* Development, optimization, and validation of novel anti-TEM1/CD248 affinity agent for optical imaging in cancer. *Oncotarget* **5**, 6994-7012, doi:10.18632/oncotarget.2188 (2014).

309   Guo, Y. *et al.* Tumour endothelial marker 1/endosialin-mediated targeting of human sarcoma. *Eur J Cancer* **90**, 111-121, doi:10.1016/j.ejca.2017.10.035 (2018).

310   Facciponte, J. G. *et al.* Tumor endothelial marker 1-specific DNA vaccination targets tumor vasculature. *J Clin Invest* **124**, 1497-1511, doi:10.1172/JCI67382 (2014).

311   McCafferty, J. & Schofield, D. Identification of optimal protein binders through the use of large genetically encoded display libraries. *Curr Opin Chem Biol* **26**, 16-24, doi:10.1016/j.cbpa.2015.01.003 (2015).

312   Rothe, A., Hosse, R. J. & Power, B. E. In vitro display technologies reveal novel biopharmaceutics. *FASEB J* **20**, 1599-1610, doi:10.1096/fj.05-5650rev (2006).

313   Galan, A. *et al.* Library-based display technologies: where do we stand? *Mol Biosyst* **12**, 2342-2358, doi:10.1039/c6mb00219f (2016).

314   Fairhead, M. & Howarth, M. Site-specific biotinylation of purified proteins using BirA. *Methods Mol Biol* **1266**, 171-184, doi:10.1007/978-1-4939-2272-7_12 (2015).

315   Luna, E. J. Biotinylation of proteins in solution and on cell surfaces. *Curr Protoc Protein Sci* **Chapter 3**, Unit 3 6, doi:10.1002/0471140864.ps0306s06 (2001).

316   Scholle, M. D., Collart, F. R. & Kay, B. K. In vivo biotinylated proteins as targets for phage-display selection experiments. *Protein Expr Purif* **37**, 243-252, doi:10.1016/j.pep.2004.05.012 (2004).

317   Tayapiwatana, C., Chotpadiwetkul, R. & Kasinrerk, W. A novel approach using streptavidin magnetic bead-sorted in vivo biotinylated survivin for monoclonal antibody production. *J Immunol Methods* **317**, 1-11, doi:10.1016/j.jim.2006.07.024 (2006).

318   Barat, B. & Wu, A. M. Metabolic biotinylation of recombinant antibody by biotin ligase retained in the endoplasmic reticulum. *Biomol Eng* **24**, 283-291, doi:10.1016/j.bioeng.2007.02.003 (2007).

319   Duffy, S., Tsao, K. L. & Waugh, D. S. Site-specific, enzymatic biotinylation of recombinant proteins in Spodoptera frugiperda cells using biotin acceptor peptides. *Anal Biochem* **262**, 122-128, doi:10.1006/abio.1998.2770 (1998).

320   Kulman, J. D., Satake, M. & Harris, J. E. A versatile system for site-specific enzymatic biotinylation and regulated expression of proteins in cultured mammalian cells. *Protein Expr Purif* **52**, 320-328, doi:10.1016/j.pep.2006.09.011 (2007).

321   Scholler, N. *et al.* Use of yeast-secreted in vivo biotinylated recombinant antibodies (Biobodies) in bead-based ELISA. *Clin Cancer Res* **14**, 2647-2655, doi:10.1158/1078-0432.CCR-07-1442 (2008).

322   Frangioni, J. V. & Neel, B. G. Solubilization and purification of enzymatically active glutathione S-transferase (pGEX) fusion proteins. *Anal Biochem* **210**, 179-187, doi:10.1006/abio.1993.1170 (1993).

323   Boraston, A. B., McLean, B. W., Guarna, M. M., Amandaron-Akow, E. & Kilburn, D. G. A family 2a carbohydrate-binding module suitable as an affinity tag for proteins produced in Pichia pastoris. *Protein Expr Purif* **21**, 417-423, doi:10.1006/prep.2001.1393 (2001).

324   Reuten, R. *et al.* Maltose-Binding Protein (MBP), a Secretion-Enhancing Tag for Mammalian Protein Expression Systems. *PLoS One* **11**, e0152386, doi:10.1371/journal.pone.0152386 (2016).

325   Bernard, M. P., Cao, D., Myers, R. V. & Moyle, W. R. Tight attachment of chitin-binding-domain-tagged proteins to surfaces coated with acetylated chitosan. *Anal Biochem* **327**, 278-283, doi:10.1016/j.ab.2003.12.029 (2004).

326   Lin, H. H., Stacey, M., Chang, G. W., Davies, J. Q. & Gordon, S. Method for selecting and enriching cells expressing low affinity ligands for cell surface receptors. *Biotechniques* **38**, 696, 698 (2005).

327   Lo, K. M. *et al.* High level expression and secretion of Fc-X fusion proteins in mammalian cells. *Protein Eng* **11**, 495-500 (1998).

328   Maru, Y., Afar, D. E., Witte, O. N. & Shibuya, M. The dimerization property of glutathione S-transferase partially reactivates Bcr-Abl lacking the oligomerization domain. *J Biol Chem* **271**, 15353-15357 (1996).

329   Miersch, S. *et al.* Scalable high throughput selection from phage-displayed synthetic antibody libraries. *J Vis Exp*, 51492, doi:10.3791/51492 (2015).

330   Li, L., Fierer, J. O., Rapoport, T. A. & Howarth, M. Structural analysis and optimization of the covalent association between SpyCatcher and a peptide Tag. *J Mol Biol* **426**, 309-317, doi:10.1016/j.jmb.2013.10.021 (2014).

331   Zakeri, B. *et al.* Peptide tag forming a rapid covalent bond to a protein, through engineering a bacterial adhesin. *Proc Natl Acad Sci U S A* **109**, E690-697, doi:10.1073/pnas.1115485109 (2012).

332   Arnett, K. L., Harrison, S. C. & Wiley, D. C. Crystal structure of a human CD3-epsilon/delta dimer in complex with a UCHT1 single-chain antibody fragment. *Proc Natl Acad Sci U S A* **101**, 16268-16273, doi:10.1073/pnas.0407359101 (2004).

333   Kastrup, J. *et al.* In vitro production and characterization of partly assembled human CD3 complexes. *Scand J Immunol* **56**, 436-442 (2002).

334   Steentoft, C. *et al.* Precision mapping of the human O-GalNAc glycoproteome through SimpleCell technology. *EMBO J* **32**, 1478-1488, doi:10.1038/emboj.2013.79 (2013).

335   Yuan, X. *et al.* Characterization of the first fully human anti-TEM1 scFv in models of solid tumor imaging and immunotoxin-based therapy. *Cancer Immunol Immunother* **66**, 367-378, doi:10.1007/s00262-016-1937-z (2017).

336   Willingham, S. B. *et al.* The CD47-signal regulatory protein alpha (SIRPa) interaction is a therapeutic target for human solid tumors. *Proc Natl Acad Sci U S A* **109**, 6662-6667, doi:10.1073/pnas.1121623109 (2012).

337   Hassan, R. *et al.* Mesothelin Immunotherapy for Cancer: Ready for Prime Time? *J Clin Oncol* **34**, 4171-4179, doi:10.1200/JCO.2016.68.3672 (2016).

338   Tang, Z., Qian, M. & Ho, M. The role of mesothelin in tumor progression and targeted therapy. *Anticancer Agents Med Chem* **13**, 276-280 (2013).

339   Bergan, L., Gross, J. A., Nevin, B., Urban, N. & Scholler, N. Development and in vitro validation of anti-mesothelin biobodies that prevent CA125/Mesothelin-dependent cell attachment. *Cancer Lett* **255**, 263-274, doi:10.1016/j.canlet.2007.04.012 (2007).

340   Lanitis, E. *et al.* Redirected antitumor activity of primary human lymphocytes transduced with a fully human anti-mesothelin chimeric receptor. *Mol Ther* **20**, 633-643, doi:10.1038/mt.2011.256 (2012).

341   Alam, M. K. *et al.* Synthetic Modular Antibody Construction by Using the SpyTag/SpyCatcher Protein-Ligase System. *Chembiochem* **18**, 2217-2221, doi:10.1002/cbic.201700411 (2017).

342   Gao, X., Fang, J., Xue, B., Fu, L. & Li, H. Engineering Protein Hydrogels Using SpyCatcher-SpyTag Chemistry. *Biomacromolecules* **17**, 2812-2819, doi:10.1021/acs.biomac.6b00566 (2016).

343   Ke, X. *et al.* SpyCatcher-SpyTag mediated in situ labelling of progeny baculovirus with quantum dots for tracking viral infection in living cells. *Chem Commun (Camb)* **54**, 1189-1192, doi:10.1039/c7cc08880a (2018).

344   Moon, H., Bae, Y., Kim, H. & Kang, S. Plug-and-playable fluorescent cell imaging modular toolkits using the bacterial superglue, SpyTag/SpyCatcher. *Chem Commun (Camb)* **52**, 14051-14054, doi:10.1039/c6cc07363h (2016).

345   Brune, K. D. *et al.* Plug-and-Display: decoration of Virus-Like Particles via isopeptide bonds for modular immunization. *Sci Rep* **6**, 19234, doi:10.1038/srep19234 (2016).

346   Fierer, J. O., Veggiani, G. & Howarth, M. SpyLigase peptide-peptide ligation polymerizes affibodies to enhance magnetic cancer cell capture. *Proc Natl Acad Sci U S A* **111**, E1176-1181, doi:10.1073/pnas.1315776111 (2014).

347   Turunen, L., Takkinen, K., Soderlund, H. & Pulli, T. Automated panning and screening procedure on microplates for antibody generation from phage display libraries. *J Biomol Screen* **14**, 282-293, doi:10.1177/1087057108330113 (2009).

348   Pundir, S., Martin, M. J. & O'Donovan, C. UniProt Protein Knowledgebase. *Methods Mol Biol* **1558**, 41-55, doi:10.1007/978-1-4939-6783-4_2 (2017).

349   Alegre, M. L. *et al.* An anti-murine CD3 monoclonal antibody with a low affinity for Fc gamma receptors suppresses transplantation responses while minimizing acute toxicity and immunogenicity. *J Immunol* **155**, 1544-1555 (1995).

350   Durocher, Y., Perret, S. & Kamen, A. High-level and high-throughput recombinant protein production by transient transfection of suspension-growing human 293-EBNA1 cells. *Nucleic Acids Res* **30**, E9 (2002).

351   O'Callaghan C, A. *et al.* BirA enzyme: production and application in the study of membrane receptor-ligand interactions by site-specific biotinylation. *Anal Biochem* **266**, 9-15, doi:10.1006/abio.1998.2930 (1999).

352   Guillaume, P. *et al.* Soluble major histocompatibility complex-peptide octamers with impaired CD8 binding selectively induce Fas-dependent apoptosis. *J Biol Chem* **278**, 4500-4509, doi:10.1074/jbc.M208863200 (2003).

353   Folkman, J. Tumor angiogenesis: therapeutic implications. *N Engl J Med* **285**, 1182-1186, doi:10.1056/NEJM197111182852108 (1971).

354   Mueller, M. M. & Fusenig, N. E. Friends or foes - bipolar effects of the tumour stroma in cancer. *Nat Rev Cancer* **4**, 839-849, doi:10.1038/nrc1477 (2004).

355   von Ahrens, D., Bhagat, T. D., Nagrath, D., Maitra, A. & Verma, A. The role of stromal cancer-associated fibroblasts in pancreatic cancer. *J Hematol Oncol* **10**, 76, doi:10.1186/s13045-017-0448-5 (2017).

356   Carmeliet, P. & Jain, R. K. Angiogenesis in cancer and other diseases. *Nature* **407**, 249-257, doi:10.1038/35025220 (2000).

357   Yancopoulos, G. D. *et al.* Vascular-specific growth factors and blood vessel formation. *Nature* **407**, 242-248, doi:10.1038/35025215 (2000).

358   De Palma, M., Biziato, D. & Petrova, T. V. Microenvironmental regulation of tumour angiogenesis. *Nat Rev Cancer* **17**, 457-474, doi:10.1038/nrc.2017.51 (2017).

359   Huber, M. A. *et al.* Expression of stromal cell markers in distinct compartments of human skin cancers. *J Cutan Pathol* **33**, 145-155, doi:10.1111/j.0303-6987.2006.00446.x (2006).

360   Kiyohara, E. *et al.* Endosialin Expression in Metastatic Melanoma Tumor Microenvironment Vasculature: Potential Therapeutic Implications. *Cancer Microenviron* **8**, 111-118, doi:10.1007/s12307-015-0168-8 (2015).

361   Fierle, J. K. *et al.* Integrating SpyCatcher/SpyTag covalent fusion technology into phage display workflows for rapid antibody discovery. *Sci Rep* **9**, 12815, doi:10.1038/s41598-019-49233-7 (2019).

362   O'Shannessy, D. J. *et al.* Novel antibody probes for the characterization of endosialin/TEM-1. *Oncotarget* **7**, 69420-69435, doi:10.18632/oncotarget.11018 (2016).

363   Qi, J. *et al.* Potent and selective antitumor activity of a T cell-engaging bispecific antibody targeting a membrane-proximal epitope of ROR1. *Proc Natl Acad Sci U S A* **115**, E5467-E5476, doi:10.1073/pnas.1719905115 (2018).

364   Harding, F. A., Stickler, M. M., Razo, J. & DuBridge, R. B. The immunogenicity of humanized and fully human antibodies: residual immunogenicity resides in the CDR regions. *MAbs* **2**, 256-265, doi:10.4161/mabs.2.3.11641 (2010).

365   Chacko, A. M. *et al.* Development of 124I immuno-PET targeting tumor vascular TEM1/endosialin. *J Nucl Med* **55**, 500-507, doi:10.2967/jnumed.113.121905 (2014).

366   O'Shannessy, D. J. *et al.* Endosialin and Associated Protein Expression in Soft Tissue Sarcomas: A Potential Target for Anti-Endosialin Therapeutic Strategies. *Sarcoma* **2016**, 5213628, doi:10.1155/2016/5213628 (2016).

367   Przepiorka, D. *et al.* FDA Approval: Blinatumomab. *Clin Cancer Res* **21**, 4035-4039, doi:10.1158/1078-0432.CCR-15-0612 (2015).

368   Topp, M. S. *et al.* Targeted therapy with the T-cell-engaging antibody blinatumomab of chemotherapy-refractory minimal residual disease in B-lineage acute lymphoblastic leukemia patients results in high response rate and prolonged leukemia-free survival. *J Clin Oncol* **29**, 2493-2498, doi:10.1200/JCO.2010.32.7270 (2011).

369   Kochenderfer, J. N. *et al.* Chemotherapy-refractory diffuse large B-cell lymphoma and indolent B-cell malignancies can be effectively treated with autologous T cells expressing an anti-CD19 chimeric antigen receptor. *J Clin Oncol* **33**, 540-549, doi:10.1200/JCO.2014.56.2025 (2015).

370   Davis, S. J. & van der Merwe, P. A. The kinetic-segregation model: TCR triggering and beyond. *Nat Immunol* **7**, 803-809, doi:10.1038/ni1369 (2006).

371   Shankaran, V. *et al.* IFNgamma and lymphocytes prevent primary tumour development and shape tumour immunogenicity. *Nature* **410**, 1107-1111, doi:10.1038/35074122 (2001).

372   Galon, J. *et al.* Type, density, and location of immune cells within human colorectal tumors predict clinical outcome. *Science* **313**, 1960-1964, doi:10.1126/science.1129139 (2006).

373   Palucka, K., Banchereau, J. & Mellman, I. Designing vaccines based on biology of human dendritic cell subsets. *Immunity* **33**, 464-478, doi:10.1016/j.immuni.2010.10.007 (2010).

374   Sharma, P. & Allison, J. P. The future of immune checkpoint therapy. *Science* **348**, 56-61, doi:10.1126/science.aaa8172 (2015).

375   Ribas, A. & Wolchok, J. D. Cancer immunotherapy using checkpoint blockade. *Science* **359**, 1350-1355, doi:10.1126/science.aar4060 (2018).

376   Kalos, M. *et al.* T cells with chimeric antigen receptors have potent antitumor effects and can establish memory in patients with advanced leukemia. *Sci Transl Med* **3**, 95ra73, doi:10.1126/scitranslmed.3002842 (2011).

377   Robbins, P. F. *et al.* Cutting edge: persistence of transferred lymphocyte clonotypes correlates with cancer regression in patients receiving cell transfer therapy. *J Immunol* **173**, 7125-7130 (2004).

378 Long, A. H. *et al.* 4-1BB costimulation ameliorates T cell exhaustion induced by tonic signaling of chimeric antigen receptors. *Nature medicine* **21**, 581-590, doi:10.1038/nm.3838 (2015).

379 Bagley, R. G. *et al.* Human endothelial precursor cells express tumor endothelial marker 1/endosialin/CD248. *Mol Cancer Ther* **7**, 2536-2546, doi:10.1158/1535-7163.MCT-08-0050 (2008).

380 Motz, G. T. & Coukos, G. The parallel lives of angiogenesis and immunosuppression: cancer and other tales. *Nat Rev Immunol* **11**, 702-711, doi:10.1038/nri3064 (2011).

381 Neri, D. & Bicknell, R. Tumour vascular targeting. *Nat Rev Cancer* **5**, 436-446, doi:10.1038/nrc1627 (2005).

382 Schoonjans, R. *et al.* Fab chains as an efficient heterodimerization scaffold for the production of recombinant bispecific and trispecific antibody derivatives. *J Immunol* **165**, 7050-7057, doi:10.4049/jimmunol.165.12.7050 (2000).

383 Chen, W. *et al.* Improving the CH1-CK heterodimerization and pharmacokinetics of 4Dm2m, a novel potent CD4-antibody fusion protein against HIV-1. *MAbs* **8**, 761-774, doi:10.1080/19420862.2016.1160180 (2016).

384 Kochenderfer, J. N. *et al.* Construction and preclinical evaluation of an anti-CD19 chimeric antigen receptor. *J Immunother* **32**, 689-702, doi:10.1097/CJI.0b013e3181ac6138 (2009).

385 Brogdon, J. L., Leitenberg, D. & Bottomly, K. The potency of TCR signaling differentially regulates NFATc/p activity and early IL-4 transcription in naive CD4+ T cells. *J Immunol* **168**, 3825-3832, doi:10.4049/jimmunol.168.8.3825 (2002).

386 Hooijberg, E., Bakker, A. Q., Ruizendaal, J. J. & Spits, H. NFAT-controlled expression of GFP permits visualization and isolation of antigen-stimulated primary human T cells. *Blood* **96**, 459-466 (2000).

387 Jutz, S. *et al.* Assessment of costimulation and coinhibition in a triple parameter T cell reporter line: Simultaneous measurement of NF-kappaB, NFAT and AP-1. *J Immunol Methods* **430**, 10-20, doi:10.1016/j.jim.2016.01.007 (2016).

388 Root, A. R. *et al.* Development of PF-06671008, a Highly Potent Anti-P-cadherin/Anti-CD3 Bispecific DART Molecule with Extended Half-Life for the Treatment of Cancer. *Antibodies (Basel)* **5**, doi:10.3390/antib5010006 (2016).

389 Liddy, N. *et al.* Monoclonal TCR-redirected tumor cell killing. *Nature medicine* **18**, 980-987, doi:10.1038/nm.2764 (2012).

390 Hemmer, B., Stefanova, I., Vergelli, M., Germain, R. N. & Martin, R. Relationships among TCR ligand potency, thresholds for effector function elicitation, and the quality of early signaling events in human T cells. *J Immunol* **160**, 5807-5814 (1998).

391 Valitutti, S., Muller, S., Dessing, M. & Lanzavecchia, A. Different responses are elicited in cytotoxic T lymphocytes by different levels of T cell receptor occupancy. *J Exp Med* **183**, 1917-1921, doi:10.1084/jem.183.4.1917 (1996).

392 Itoh, Y. & Germain, R. N. Single cell analysis reveals regulated hierarchical T cell antigen receptor signaling thresholds and intraclonal heterogeneity for individual cytokine responses of CD4+ T cells. *J Exp Med* **186**, 757-766, doi:10.1084/jem.186.5.757 (1997).

393 Ellerman, D. Bispecific T-cell engagers: Towards understanding variables influencing the in vitro potency and tumor selectivity and their modulation to enhance their efficacy and safety. *Methods* **154**, 102-117, doi:10.1016/j.ymeth.2018.10.026 (2019).

394 Stone, J. D., Aggen, D. H., Schietinger, A., Schreiber, H. & Kranz, D. M. A sensitivity scale for targeting T cells with chimeric antigen receptors (CARs) and bispecific T-cell Engagers (BiTEs). *Oncoimmunology* **1**, 863-873, doi:10.4161/onci.20592 (2012).

395 Eyquem, J. *et al.* Targeting a CAR to the TRAC locus with CRISPR/Cas9 enhances tumour rejection. *Nature* **543**, 113-117, doi:10.1038/nature21405 (2017).

396 Georgiadis, C. *et al.* Long Terminal Repeat CRISPR-CAR-Coupled "Universal" T Cells Mediate Potent Anti-leukemic Effects. *Mol Ther* **26**, 1215-1227, doi:10.1016/j.ymthe.2018.02.025 (2018).

397 Jung, I. Y. & Lee, J. Unleashing the Therapeutic Potential of CAR-T Cell Therapy Using Gene-Editing Technologies. *Mol Cells* **41**, 717-723, doi:10.14348/molcells.2018.0242 (2018).

398 Zhu, M. *et al.* Blinatumomab, a Bispecific T-cell Engager (BiTE((R))) for CD-19 Targeted Cancer Immunotherapy: Clinical Pharmacology and Its Implications. *Clin Pharmacokinet* **55**, 1271-1288, doi:10.1007/s40262-016-0405-4 (2016).

399 Diaconu, I. *et al.* Inducible Caspase-9 Selectively Modulates the Toxicities of CD19-Specific Chimeric Antigen Receptor-Modified T Cells. *Mol Ther* **25**, 580-592, doi:10.1016/j.ymthe.2017.01.011 (2017).

400 Ma, J. S. *et al.* Versatile strategy for controlling the specificity and activity of engineered T cells. *Proc Natl Acad Sci U S A* **113**, E450-458, doi:10.1073/pnas.1524193113 (2016).

401 Ajina, A. & Maher, J. Strategies to Address Chimeric Antigen Receptor Tonic Signaling. *Mol Cancer Ther* **17**, 1795-1815, doi:10.1158/1535-7163.MCT-17-1097 (2018).

402   Alonso-Camino, V., Sanchez-Martin, D., Compte, M., Sanz, L. & Alvarez-Vallina, L. Lymphocyte display: a novel antibody selection platform based on T cell activation. *PLoS One* **4**, e7174, doi:10.1371/journal.pone.0007174 (2009).

403   Alonso-Camino, V. *et al.* CARbodies: Human Antibodies Against Cell Surface Tumor Antigens Selected From Repertoires Displayed on T Cell Chimeric Antigen Receptors. *Mol Ther Nucleic Acids* **2**, e93, doi:10.1038/mtna.2013.19 (2013).

404   Rydzek, J. *et al.* Chimeric Antigen Receptor Library Screening Using a Novel NF-kappaB/NFAT Reporter Cell Platform. *Mol Ther* **27**, 287-299, doi:10.1016/j.ymthe.2018.11.015 (2019).

405   Li, Q. & Verma, I. M. NF-kappaB regulation in the immune system. *Nat Rev Immunol* **2**, 725-734, doi:10.1038/nri910 (2002).

406   Gioia, L., Siddique, A., Head, S. R., Salomon, D. R. & Su, A. I. A genome-wide survey of mutations in the Jurkat cell line. *BMC Genomics* **19**, 334, doi:10.1186/s12864-018-4718-6 (2018).

407   Reeves, J. P. & Epstein, S. L. Recombinant human CD4 elicits antibody responses different in epitope specificity from those that cellular CD4 elicits. *Mol Immunol* **30**, 765-773, doi:10.1016/0161-5890(93)90148-5 (1993).

408   Keller, T. *et al.* Selection of scFv Antibody Fragments Binding to Human Blood versus Lymphatic Endothelial Surface Antigens by Direct Cell Phage Display. *PLoS One* **10**, e0127169, doi:10.1371/journal.pone.0127169 (2015).

409   Asgarov, K. *et al.* A new anti-mesothelin antibody targets selectively the membrane-associated form. *MAbs* **9**, 567-577, doi:10.1080/19420862.2017.1288770 (2017).

410   Barboni, E. *et al.* The glycophosphatidylinositol anchor affects the conformation of Thy-1 protein. *J Cell Sci* **108 (Pt 2)**, 487-497 (1995).

411   Hale, G. Synthetic peptide mimotope of the CAMPATH-1 (CD52) antigen, a small glycosylphosphatidylinositol-anchored glycoprotein. *Immunotechnology* **1**, 175-187, doi:10.1016/1380-2933(95)00017-8 (1995).

412   Zhang, Y. & Pastan, I. High shed antigen levels within tumors: an additional barrier to immunoconjugate therapy. *Clin Cancer Res* **14**, 7981-7986, doi:10.1158/1078-0432.CCR-08-0324 (2008).

413   Zhao, Z. *et al.* Structural Design of Engineered Costimulation Determines Tumor Rejection Kinetics and Persistence of CAR T Cells. *Cancer Cell* **28**, 415-428, doi:10.1016/j.ccell.2015.09.004 (2015).

414   Zhu, J. Mammalian cell protein expression for biopharmaceutical production. *Biotechnol Adv* **30**, 1158-1170, doi:10.1016/j.biotechadv.2011.08.022 (2012).

415   Li, J. *et al.* CD3 bispecific antibody-induced cytokine release is dispensable for cytotoxic T cell activity. *Sci Transl Med* **11**, doi:10.1126/scitranslmed.aax8861 (2019).

416   D'Souza, W. N. & Lefrancois, L. IL-2 is not required for the initiation of CD8 T cell cycling but sustains expansion. *J Immunol* **171**, 5727-5735, doi:10.4049/jimmunol.171.11.5727 (2003).

417   Dooms, H., Kahn, E., Knoechel, B. & Abbas, A. K. IL-2 induces a competitive survival advantage in T lymphocytes. *J Immunol* **172**, 5973-5979, doi:10.4049/jimmunol.172.10.5973 (2004).

418   Au-Yeung, B. B. *et al.* IL-2 Modulates the TCR Signaling Threshold for CD8 but Not CD4 T Cell Proliferation on a Single-Cell Level. *J Immunol* **198**, 2445-2456, doi:10.4049/jimmunol.1601453 (2017).

419   Au-Yeung, B. B. *et al.* A sharp T-cell antigen receptor signaling threshold for T-cell proliferation. *Proc Natl Acad Sci U S A* **111**, E3679-3688, doi:10.1073/pnas.1413726111 (2014).

420   Skokos, D. *et al.* A class of costimulatory CD28-bispecific antibodies that enhance the antitumor activity of CD3-bispecific antibodies. *Sci Transl Med* **12**, doi:10.1126/scitranslmed.aaw7888 (2020).

421   Robert, B. *et al.* Tumor targeting with newly designed biparatopic antibodies directed against two different epitopes of the carcinoembryonic antigen (CEA). *Int J Cancer* **81**, 285-291, doi:10.1002/(sici)1097-0215(19990412)81:2<285::aid-ijc19>3.0.co;2-t (1999).

422   DaSilva, J. O. *et al.* A biparatopic antibody that modulates MET trafficking exhibits enhanced efficacy compared to parental antibodies in MET-driven tumor models. *Clin Cancer Res*, doi:10.1158/1078-0432.CCR-19-2428 (2019).

423   Li, J. Y. *et al.* A Biparatopic HER2-Targeting Antibody-Drug Conjugate Induces Tumor Regression in Primary Models Refractory to or Ineligible for HER2-Targeted Therapy. *Cancer Cell* **29**, 117-129, doi:10.1016/j.ccell.2015.12.008 (2016).

424   Liu, J. *et al.* Bp-Bs, a Novel T-cell Engaging Bispecific Antibody with Biparatopic Her2 Binding, Has Potent Anti-tumor Activities. *Mol Ther Oncolytics* **14**, 66-73, doi:10.1016/j.omto.2019.03.009 (2019).

425   Moynihan, K. D. *et al.* Eradication of large established tumors in mice by combination immunotherapy that engages innate and adaptive immune responses. *Nature medicine* **22**, 1402-1410, doi:10.1038/nm.4200 (2016).

Julie Katrin FIERLE

PERSONAL INFORMATION

Address	Avenue de la Dôle 2
	CH-1005 Lausanne
Phone	+41 76 561 9103
E-Mail	julie.fierle@gmail.com

EDUCATION

PhD in Cancer and Immunology (10/2015 – present)
Ludwig Institute for Cancer Research at the University of Lausanne (UNIL), Switzerland

Master of Science in Molecular Medicine (10/2012 – 07/2015)
Albert-Ludwigs-University, Freiburg, Germany

Bachelor of Science in Molecular Medicine (10/2009 – 09/2012)
Albert-Ludwigs-University, Freiburg, Germany

RESEARCH EXPERIENCE

Since 10/2015
Doctoral assistant (PhD) at the Ludwig Institute for Cancer Research/UNIL, Lausanne, Switzerland
Advisors: Prof. George Coukos and Dr. Steven Dunn

- *De novo* discovery of scFv antibodies by phage display
- Engineering, purification and biophysical characterization of various bispecific antibody formats – protein purification (HPLC) – SPR – ELISA and FACS binding assays
- Design and generation of DNA libraries – sequence analysis – molecular biology and PCR/RT-PCR
- Developing and conducting functional T cell activation assays – cytotoxicity assays – multichromatic flow cytometry
- Design and testing of chimeric antigen receptors in primary T cells – lentiviral transduction
- Design and realization of a scientific project; project management
- Data analysis, scientific writing and presentation of scientific data

06/2014 – 04/2015
Intern/Master's project at The Scripps Research Institute, La Jolla, CA, USA
Advisor: Prof. Brunhilde Felding

- Developing and conducting cell-based and biochemical assays for the analysis of ERα functions in breast cancer cell lines
- Proliferation assays – RNA extraction and RT-qPCR – SDS-PAGE and Western Blotting
- Conducting *in vitro* metabolic assays – high-resolution respirometry
- Analysis and presentation of scientific data; scientific reading and project planning

10/2012 – 03/2013
Intern at Roche Diagnostics GmbH, Department Antibody Development, Penzberg, Germany
Advisor: Dr. Michael Gerg

- Development and characterization of antibodies for use in diagnostic assays
- Application and optimization of a recombinant antibody isolation technology (B cell PCR)
- PCR and molecular biology techniques – various ELISA formats for antibody evaluation
- Experience with high-throughput discovery using laboratory automation

04/2012 – 08/2012
Intern/Bachelor's project at the Institute for Neurosciences, INSERM, Montpellier, France
<u>Advisor:</u> Prof. Cédric Raoul

- Isolation of CD8+ T-lymphocytes from murine models of amyotrophic lateral sclerosis (ALS)
- Establishing co-cultures of fetal motoneurons and CD8+ T-lymphocytes – developing and conducting assays measuring neuronal survival and neurite outgrowth – immunocytochemistry

SCIENTIFIC CONFERENCES AND PRESENTATIONS

"A novel tri-valent T cell engager targeting tumor endothelial marker 1 (TEM1, Endosialin) efficiently recruits human T cells to kill endogenous tumor cells." – CICON19, Paris, France – *poster presentation*

"Engineering novel antibody-based therapeutics for targeting of tumor endothelial marker 1 (TEM1)." – CIMT 2018, Mainz, Germany – *poster presentation*

ISREC Faculty and Staff Retreat 2015 and 2019 – *poster presentation*

Protein & Antibody Engineering Summit (PEGS) Europe 2017

PUBLICATIONS AND PATENTS

J.K. Fierle, J. Abram-Saliba, et al., "Integrating SpyCatcher/SpyTag covalent fusion technology into phage display workflows for rapid antibody discovery." *Sci. Rep.* 2019, <u>DOI: 10.1038/s41598-019-49233-7</u>.

E. Coque, C. Salsac, […], **J. K. Fierle**, et al., "Cytotoxic CD8+ T lymphocytes expressing ALS-causing SOD1 mutant selectively trigger death of spinal motoneurons." *PNAS* 2019, <u>DOI: 10.1073/pnas.1815961116</u>.

S. M. Dunn, **J. K. Fierle** and G. Coukos, "Anti-TEM1 Antibodies." Provisional U.S. Patent Application No. 62/855,559, filed on 31 May 2019

ADDITIONAL EXPERIENCE AND LANGUAGES

Coordinator (2019) and Vice-president (2020) of the BioScience Network Lausanne (<u>BSNL</u>)
A joint association of EPFL and UNIL aiming to foster connection between academia, industry and society

- Organization of the Life Science Career Day (~350 participants; 22 companies) in 2019 and 2020, in collaboration with the School of Biology and Medicine, UNIL
- Key tasks: project coordination, recruitment of sponsors (15'500 CHF raised in 2019) and communication with team members and sponsors

Languages

German (native speaker)

English (fluent)

French (fluent)